National Chiao Tung University

Department of Materials Science and Engineering

PhD Thesis

Synthesis and Study of Novel Chemosensing Probes for Selective Detection of Metal Ions and Ru-Based Supramolecular Dendrimers for Solar Cell Applications

對金屬離子選擇性檢測之新穎化學感側探針與含 Ru 樹枝狀超分子做為太陽能應用之合成及研究

Rudrakanta Satapathy (盧達侃)

Advisor: Prof. Hong-Cheu Lin, PhD. (林宏州 教授)

May, 2012

Synthesis and Study of Novel Chemosensing Probes for Selective Detection of Metal Ions and Ru-Based Supramolecular Dendrimers for Solar Cell Applications

對金屬離子選擇性檢測之新穎化學感側探針與含 Ru 樹枝狀超分子做為太陽能應用之合成及研究

Rudrakanta Satapathy (盧達侃)

Advisor: Prof. Hong-Cheu Lin, PhD. (林宏州 教授)

Abstract

The main objective of this dissertation is to synthesize novel chemosensing binding probe for selective detection of metal ions. In the introduction of the thesis we have described about several chemosensing mechanisms and the advantages of polymeric cheosensors over small molecular analogue. Several sensing probes have been developed for selective sensing of Pb^{2+}, Hg^{2+}, and Zn^{2+}. Here we have developed novel thieno-benzo-imidazole based small molecules for the sensing of toxic metal ion Pb^{2+} in aqueous solutions. Again, we discussed about thieno-imidazole based homopolymer for the colorimetric detection of Hg^{2+} and fluorometric detection of Zn^{2+}. Furthermore, we discussed about the amendment of sensitivity of chemosensing polymers upon variation of their attached imidazole based pendants. In addition to these novel chemosensing moieties, we synthesized mono, bis, and tris Ru containing thiophene dendrimers for the application in photovoltaic cell.

In the first chapter we synthesized two novel dithieno-benzo-imidazole-based compounds (**M2** and **A2**), which showed remarkable sensitivities towards Pb^{2+} by 12-fold enahancement and 10-fold decay of fluorescence, respectively, in aqueous solutions. Substituent effects of different dithieno-benzo-imidazole-based moieties (**M1**, **M2**, **A1**, and **A2**) on the quantum yields, fluorescence lifetimes and sensitivities to Pb^{2+} along with the reversibilities by S^{2-} were investigated.

In the second chapter we synthesized novel thieno-imidazole-based polymer **P**, which showed both colorimetric, and ratiometric detections of Hg^{2+} as well as fluorometric detection of Zn^{2+} via fluorescence turn-on response with augmented lifetime. Its model polymer **M** did not show any such sensing capability under similar conditions, which further confirmed the unique sensitivity of **P** towards Hg^{2+} and Zn^{2+} via the chelation of metal ions to both 'S' and 'N' hetero-atoms.

In the third chapter three novel electron donor-acceptor conjugated polymers (**P1**-**P3**) with various imidazole pendants were synthesized, and their excellent photo-physical along with electrochemical properties led them to become suitable transduction materials for chemosensing applications. Herein, polymers (**P1**-**P3**) showed remarkable sensing capabilities towards H^+ and Fe^{2+} in semi-aqueous solutions. Upon titration with H^+, polymers **P1** and **P2** showed hypsochromic shifts of absorption and PL maxima with enhanced fluorescence intensities. However, **P3** showed diminished abosorption as well as fluorescence intensities under similar conditions due to static quenchning. The anomalous behaviour of **P3** compared with **P1** and **P2** was clarified by the electronic distributions via computational analysis. Furthermore, **P3** ($Ksv= 1.03 \times 10^7$) showed the best sensing ability towards Fe^{2+} compared with **P1** ($Ksv= 2.01 \times 10^6$) and **P2** ($Ksv= 4.12 \times 10^6$) due to its improved molecular wire effect. Correspondingly, fluorescence lifetime of P3 was decreased intensively (almost 11 times) than polymers **P1** (4.6 times) and **P2** (6.2 times) in the presence of Fe^{2+}. By means of fluorescence on-off-on tactics, the chemosensing reversibilities in protonation-deprotonation and metallation-demetallation were achieved by triethylamine (TEA) and disodium salt of ethylenediaminetetraacetic acid (Na_2-EDTA)/phenanthroline, respectively, as the suitable counter ligands. ^{1}H NMR titrations revealed the unique behaviour of P3 compared with **P1** and **P2**. To the best of our knowledge, no reports of Fe^{2+} sensors were provided by solo imidazole receptors conjugated to the main chain polymer with diverse sensitivity pattern depending on their attached substituents.

In the fourth chapter mono (**G1RuG1**, **G2RuG2**, **G3RuG3**), bis (**BT2RuG1**, **BT2RuG2**, **BT2RuG3**) and tris (**TPA3RuG1**, **TPA3RuG2**, **TPA3RuG3**) 'Ru' containing supramolecular thiophene dendrimers were constructed. Their photophysical, electrochemical and thermal properties were investigated. Due to the donor-acceptor, benzothiadiazole-hexyl thiophene cored architecture in bis 'Ru' containing thiophene dendrimers, these showed higher photovoltaic efficiency than other two series. Tris 'Ru' containing architecture with terthiophene-triphenylamine core, showed moderate photovoltaic performance due to their star shaped branched structure. Among the three generations (G1-G3) of bis 'Ru' containing dendritic series, **BT2RuG3** showed the highest solar cell efficiency 0.77% without the aid of any additives or anealing conditions. This solar cell efficiency value is the highest among all metal containing dendritic supramolecule reported so far.

Thus in the conclusion, novel chemosensing probes for the selective and sensitive detection of metal ions has been developed. Amendments of sensitivity pattern upon the variation of substituents were discussed. Synthesis and photovoltaic properties of metal containing thiophene dendrimers were described.

摘要

本論文的主要目的是合成新型化學感測器結合探測金屬離子的選擇性檢測。在本論文中，我們介紹了幾個化學感測機制及分析高分子勝過相似結構小分子的原因。針對感測Pb^{2+} 和Hg^{2+}，Zn^{2+} 的幾個化學感測器探針已由此研究開發出來。同時，我們已開發出在水溶液中針對有毒鉛離子金屬進行感測的新型噻吩苯並咪唑小分子。再者，我們討論了有關噻吩並咪唑基於比色法檢測Hg^{2+} 和Zn^{2+} 的螢光檢測聚合物。此外，我們探討論改變咪唑基之附屬側鏈結構後聚合物化學感測的靈敏度。除了這些新型化學感測分子外，我們合成了含單，雙和三**Ru**金屬的噻吩樹枝狀高分子並應用在光伏電池中。

在第一章中，我們合成了兩種新型dithieno-苯並咪唑基化合物（**M2** 和**A2**），這裡顯示在水溶液中針對Pb^{2+} 各別具有 **12** 倍的螢光強度增加和 **10** 倍的螢光衰變。不同**dithieno-**苯並咪唑基（**M1**，**M2**，**A1** 和**A2**）的量子產率，螢光壽命和靈敏度的取代基效應，針對**S2-**進行了調查，其對Pb2 +檢測是具有可逆性的。

我們在第二章中，合成出新的噻吩-咪唑基的聚合物**P**，這裡顯示透過色度和比例檢測，對Hg^{2+} 以及Zn^{2+} 的螢光檢測螢光的開啟響應增強其生存週期。它的比較聚合物**M**中沒有表現出任何類似的條件下，這進一步證實了在"S"和"N"雜原子通過金屬離子螯合的情況下，**P**對Hg^{2+} 和Zn^{2+} 具有檢測之能力。

在第三章合成出三種新型電子給體－受體與各種咪唑垂吊基的共軛聚合物（**P1-P3**），其優異的光、物理與電化學性能，使他們成為良好的傳導材料及化學感測的應用。此外，聚合物（**P1-P3** 的）對H^+ 和Fe^{2+} 的半水溶性液體表現出其具有明顯的感測能力。當滴定與H^+，聚合物**P1** 和**P2** 螢光強度增強，吸收和**PL**有極大變化。然而，**P3**的顯示吸收度減少以及螢光強度下降，這是由於其具有靜態烍滅的情況發生。通過理論計算分析，**P3** 電子分佈的異常行為與**P1** 和**P2** 的結果不同。此外，與**P1**（**KSV =** $2.01×10^6$）和**P2**（**KSV =** $4.12×10^6$）相比，**P3**（**KSV =** $1.03×10^7$）表現出最好的Fe^{2+} 感應能力，此乃由於其提昇的分子導線效應。相對地，在Fe^{2+}存在的條件下，**P3** 的螢光壽命降低程度（將近 **11** 倍）比聚合物**P1**（**4.6** 倍）和**P2**（**6.2** 倍）有更大的下降。通過螢光 **on-off-on** 機制，在質子－質子和金屬化及去金屬化的化學感測中，分別得到了具可逆性的三乙胺（**TEA**）和乙二胺四乙酸二鈉（**NA2-EDTA**）/鄰菲羅啉來做為適合的配位基。氫核磁共振滴定透露**P3** 與**P1-P2** 的差異行為。據我們所知，之前並沒有運用由咪唑受體共軛主鏈聚合物做為Fe^{2+} 的感測器，且取決於其不同取代基會具有不同的敏感性。

在第四章，含單（**G1RuG1**，**G2RuG2**，**G3RuG3**），二（**BT2RuG1**，**BT2RuG2**，**BT2RuG3**）和三（**TPA3RuG1**，**TPA3RuG2**，**TPA3RuG3**）"**Ru**"超分子噻吩樹枝狀結構。進行了他們的光物理，電化學性能和熱性能研究。由於給體－受體，苯並噻二唑－己基噻吩芯雙"釘噻吩樹枝狀的結構，這些表現比其他兩個系列高出更多的光伏效率。三 **Ru** 含噻吩三苯核心的架構，由於他們的星型分支結構顯示中等的光伏性能。在三代雙 **Ru** 含樹突狀系列（**G1-G2**），在無任何添加劑或退火條件援助的情況下，**BT2RuG3** 顯示最高的太陽能電池的效率 **0.77**％。這種太陽能電池的效率值是在迄今所有含樹枝狀超分子金屬報告中最高的。

因此，得出結論為新型化學感測探針的金屬離子的高選擇性和高靈敏度的檢測已被開發出來。之後，針對取代基的變化靈敏度模型進行了討論。並對金屬含有噻吩的樹枝狀高分子合成及其光電特性也進行了描述。

Acknowledgement

Table of Contents

List of Figures and Schemes

List of Tables

Om Jay Sriram

Dedicated to my beloved Parents

"In the path of life certain stage comes when it seems all the doors to go forward are closed.

Remain honest and pure both in mind and duty with trust in almighty. Time will reward you."

Chapter 1

1.1 Introduction:

Owing to their demand in analytical, biomedical, biotechnological, and nanotechnological applications, great effort has recently been devoted to the design and construction of molecular sensory systems.[1-6] A sensor is defined by the Oxford dictionary as "device which detects or measures a physical property and records, indicates, or otherwise responds to it." A sensor achieves this goal by responding to an external stimulus and converting it into a signal which can be measured or recorded. A chemical sensor is a device that qualitatively or quantitatively detects the presence of specific chemical substances, a class of chemicals or a specific chemical reaction.

Detecting cations is of great interest to many scientists, including chemists, biologists, clinical biochemists and environmentalists. Among the numerous analytical methods that are available for the detection of cations, flame photometry, atomic absorption spectrometry, ion sensitive electrodes, electron microprobe analysis, neutron activation analysis, etc., are expensive, often require samples of large size and do not allow continuous monitoring. In contrast, the methods based on fluorescent sensors[1,6] offer distinct advantages in terms of sensitivity, selectivity, response time, local observation (e.g. by fluorescence imaging spectroscopy). Moreover, remote sensing is possible by using optical fibres with a molecular sensor immobilized at the tip. Therefore, considerable efforts are being made to develop selective fluorescent sensors for cation detection.

Generally, a sensor device contains three elements: a receptor, a signal transducer and a read-out (Figure 1.1). The receptor should have the ability to discriminate and bind a specific target substance known as the analyte. Successful, selective receptor–analyte complex formation depends on the size, shape and binding energy of the receptor and analyte molecules. Signal transduction is the process through which an interaction of receptor with

1

analyte yields a measurable form of energy change and is converted to a signal change that can be read and quantified. The read-out domain is the part responsible for reporting the binding event. Some parameters that define a sensor's performances are selectivity, sensitivity, stability, reproducibility, and cost.
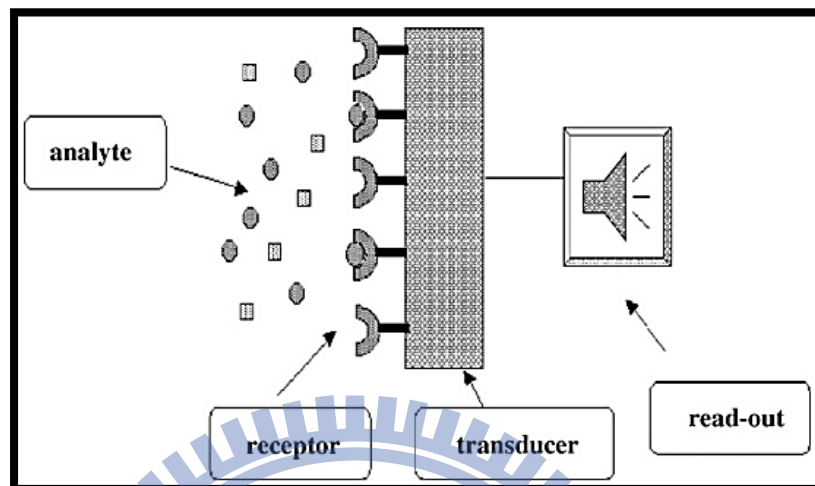
Figure 1.1. Schematic illustration of a sensor device (especially a chemical sensor device).

Chemical sensors are generally understood to be devices that transform chemical information into analytically useful signals. The term chemosensor has been defined as a molecule of abiotic origin that signals the target presence of matter or energy. The three elements of a sensor device are not necessarily independent and physically separated into the three components. Sometimes, one part of the molecule can act as a combination of two or more elements. Fluorescence is the emission of photons following relaxation from an excited electronic state to the ground state. Chemosensors based on fluorescence signal changes are commonly referred to as fluorescent chemosensors. Fluorescent chemosensors are gaining increased attention due to their high sensitivity and ease of measurement. Fluorescent chemosensors capable of selectively recognizing guest species are receiving considerable attention in supramolecular chemistry because of their potential applications in environmental detection, molecular catalysis, and biological fluorescence imaging, etc.[7,8] On account of their simplicity, high selectivity and sensitivity, together with the advantages of spatial

and temporal resolution, fluorescent chemosensors can be conveniently used as a tool to analyze and measure the amount of guest species as well as sense biologically important species in vitro and in vivo to clarify their function in living systems.[9,10] Fluorescent chemosensors that recognize guest species are currently of critical importance for the development of supramolecular chemistry. Such fluorescent sensors consists of a fluorophore linked to an ionophore and is thus called a fluoroionophore (Figure 1.2). In the design of such sensors, attention should be paid to both recognition and signaling moieties. The signaling moiety acts as a signal transducer, i.e. it converts the information (recognition event) into an optical signal expressed as the changes in the photophysical characteristics of the fluorophore. These changes are due to the perturbation (by the bound cation) of photoinduced processes such as electron transfer, charge transfer, energy transfer, excimer or exciplex formation or disappearance, etc. These aspects are relevant to the field of photophysics.
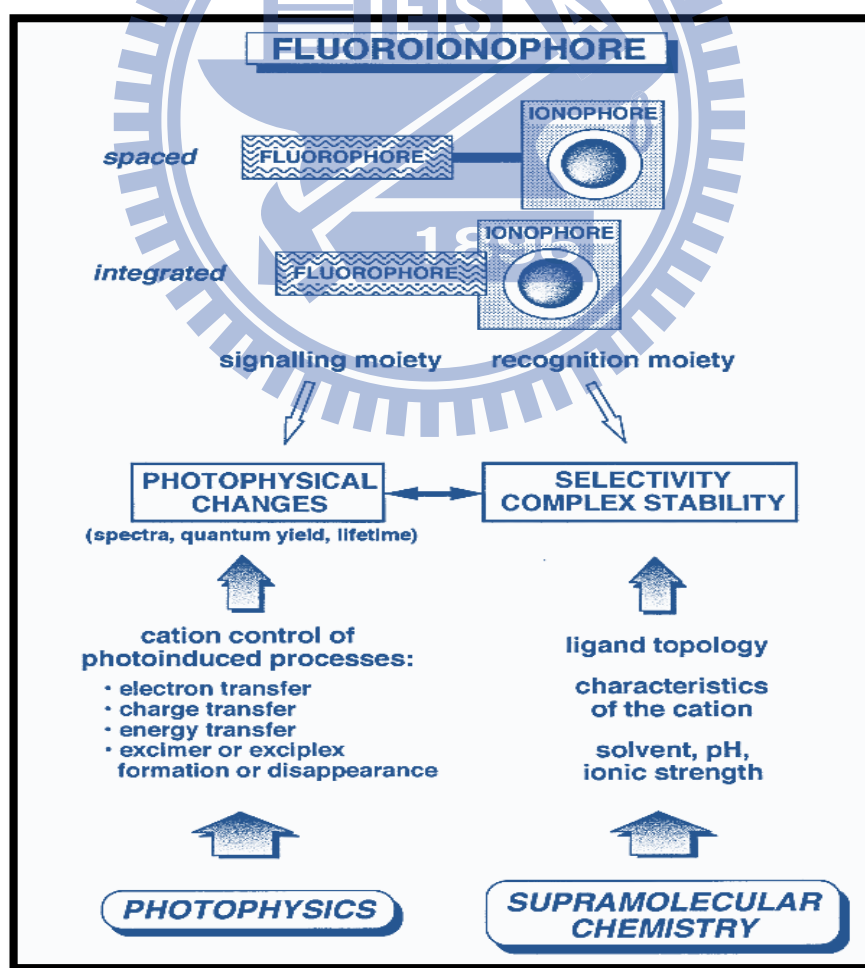
Figure 1.2. Main aspects of fluorescent molecular sensors for cation recognition.

A fluorescent chemosensor is a molecular system for which the physicochemical properties change upon interaction with a chemical species so that a change in fluorescence is produced. The construction of a fluorescent chemosensor usually involves two integrated components. One is a signaling fluorophore and another is a guest receptor that possesses a recognition capability, both are connected by a spacer to form a so called fluorophore–spacer–receptor scaffold.[11] Therefore, an ideal fluorescent chemosensor must meet two basic requirements: firstly, the receptor must have the strongest affinity with the relevant target (binding-selectivity). Secondly, on the basis of good binding-selectivity, the fluorescence signal should avoid environmental interference (signal-selectivity), such as photo bleaching, sensor molecule concentration, the environment around the sensor molecule (pH, polarity, temperature, and so forth), and stability under illumination. When a guest species is bound to the receptor, the photophysical characteristics of the fluorophore, such as fluorescence intensity, emission wavelength and fluorescence lifetime, will change via different mechanisms, and such a change provides a signal that indicates guest binding. In most cases, the spacer is not responsible for signal transduction. The read-out of a fluorescent chemosensor usually is measured as a change in fluorescence intensity, intensity decay lifetime, or a shift of the emission wavelength. An important feature of the fluorescent chemosensors is that signal transduction of the analytes binding event into the readout can happen in a very short time and without any other assistance. This makes real-time and real-space detection of the analyte possible as well as imaging associated with analyte distribution. As chemosensors are applied in food analysis, process control, environmental monitoring, medical diagnosis, and many other disciplines, a thorough understanding of the available constructions at the molecular level can help elucidate and improve the design of fluorescent chemosensors to develop sophisticated sensing systems.[12-14]

1.2 Mechanisms of analyte detection:

There are several mechanisms of fluorescence sensing. Photoinduced electron transfer (PET) and electronic energy transfer (EET) are mechanisms that have been extensively studied and widely used in the design of the chemosensors. Both mechanisms result in changes in fluorescence intensity. This review will be focused on the detection of cations by either mechanism. These sensing mechanisms are applicable to a broad array of analytes as has been reviewed previously. [1,2,15]

1.2.1. Photoinduced electron transfer (PET):

PET is a deactivation process involving an internal red-ox reaction between the excited state of the fluorophore and another species able to donate or to accept an electron. A fundamental point explaining this process is to consider that in the excited state the properties of the species are quite different compared with those of the ground-state. In particular, due to its higher energy content, an excited state is both a stronger reducing and oxidant than the corresponding ground state. The presence of a coordinated metal ion lowers the energy of the lone pair involved in the coordination preventing the PET, thus causing the switch-ON of the fluorescence. PET strongly depends on the solvent polarity which affects the oxidation potential of the lone pairs of the coordinating moiety. Higher solvent polarity makes easier the electron transfer; as a consequence, the PET-mediated quenching effect of the fluorescence occurs more quickly in high-polar environments.[16] PET type fluorescent response does not cause any spectroscopic shifts in the emission band upon complexation of metal ions. Photoinduced electron transfer sensors can be classified into two categories: fluorescence "turn-on" or fluorescence "turn-off" upon binding cations. For fluorescence "turn-on" sensors, the receptors usually contain a relatively high-energy non-bonding electron pair. PET takes place from a lone pair of the coordinating atoms (e.g. N, O, S, P) to the HOMO of the excited fluorophore. Thus, in the absence of analytes, these electron pairs quench the emission by rapid intramolecular electron transfer from the receptor to the excited

fluorophore, as shown in Figure 1.3. When this electron pair coordinates to Lewis acid cations in solution, the HOMO of the receptor is lowered. This decreases the driving force for the PET process effectively stopping the quenching event and turning on the fluorescence of the chromophore.

In some cases, the receptor takes part only indirectly in the photophysical process. If the energy level of the cation LUMO is between the energy levels of the fluorophore HOMO and LUMO, the binding of the cations by the receptor provides a non-radiative path to dissipate the excitation energy, resulting in a quenching of the fluorescence of the chemosensor (Figure 1.4).

The difference between these two mechanisms is that the PET process takes place either before or after the cation binding. For the "turn-on" sensor, the PET process is participated in by the HOMO, LUMO of the fluorophore and the HOMO of the receptor before cation binding. For the "turn-off" sensor, the PET process involves the HOMO, LUMO of the fluorophore and the LUMO of the cation after complex formation.
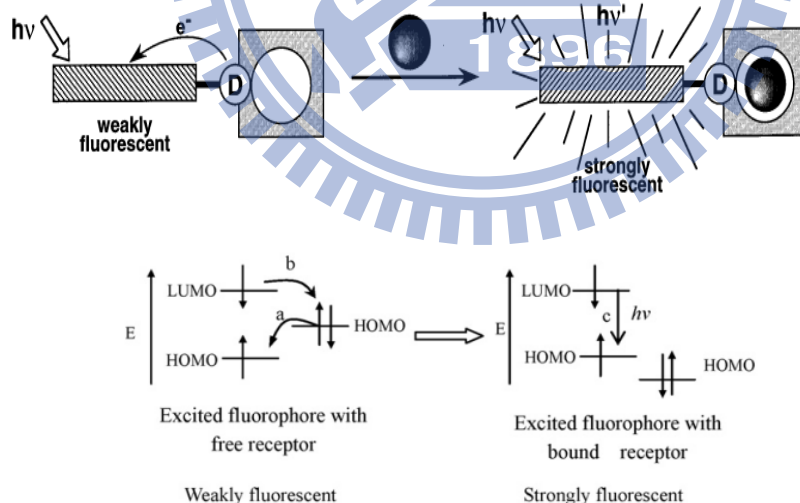
Figure 1.3. Orbital energy diagrams for fluorescence "turn-on" PET sensors before and after binding cation and (a) forward electron transfer; (b) backward electron transfer; (c) fluorescence emission processes.
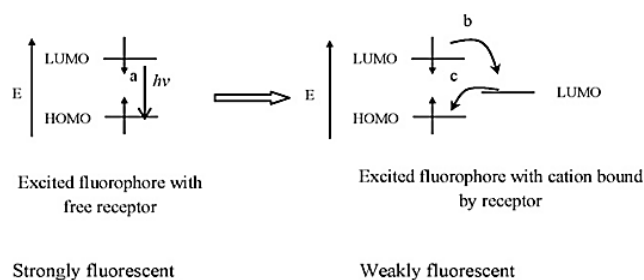
Figure 1.4. Orbital energy diagrams for fluorescent "turn-off" PET sensors before and after binding cation and (a) fluorescence emission; (b) forward electron transfer; (c) backward electron transfer processes.

1.2.2. Electronic energy transfer (EET):

Electronic energy transfer is another mechanism for the fluorescence quenching upon binding cations. There are two kinds of EET mechanisms: the double electron exchange (Dexter) energy transfer and the dipole–dipole coupling (Förster) energy transfer.[17,18] In the organic fluorophore–cation system, usually the Dexter energy transfer dominates as shown in Figure 1.5. In this case, the fluorophore goes back to its ground state by non-radiative decay. The Dexter energy transfer requires close contact between the fluorophore and the cations and also direct orbital overlap. This type of fluorescence quenching not only requires the appropriate relative energy levels between fluorophore and cation, but also requires some specific characteristics of the spacer, such as flexibility and a shorter distance between the donor and acceptor. The Förster energy transfer mechanism involves the long range coupling of dipoles, allowing for an exchange of excitation energy through space, i.e. without a path of direct orbital overlap. These two mechanisms of energy transfer are differentiated primarily in their dependence on the distance between the donor and acceptor states. The Förster mechanism is more likely to occur at extremely short and extremely long distances. For most chemosensory systems where conjugation is involved, the Dexter mechanism of direct orbital overlap is expected to be dominant.[18-20]
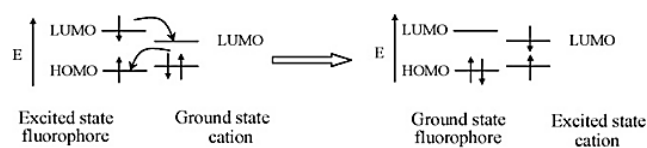
Figure 1.5. Orbital energy diagrams for double exchange transfer between the excited fluorophore to the cation bound by receptor followed by cation return to the ground state by non-radiative decay.

1.2.3. Photoinduced Charge Transfer (PCT):

When a fluorophore contains an electron-donating group (often an amino group) conjugated to an electron-withdrawing group, it undergoes intramolecular charge transfer from the donor to the acceptor upon excitation by light. The consequent change in dipole moment results in a Stokes shift that depends on the microenvironment of the fluorophore; polarity probes have been designed on this basis.[25] It can thus be anticipated that cations in close interaction with the donor or the acceptor moiety will change the photophysical properties of the fluorophore because the complexed cation affects the efficiency of intramolecular charge transfer.[22-24] When a group (like an amino group) playing the role of an electron donor within the fluorophore interacts with a cation, the latter reduces the electron-donating character of this group; owing to the resulting reduction of conjugation, a blue shift of the absorption spectrum is expected together with a decrease of the extinction coefficient. Conversely, a cation interacting with the acceptor group enhances the electron-withdrawing character of this group; the absorption spectrum is thus red-shifted and the molar absorption coefficient is increased. The fluorescence spectra are in principle shifted in the same direction as those of the absorption spectra. In addition to these shifts, changes in

8

quantum yields and lifetimes are often observed. All these photophysical effects are obviously dependent on the charge and the size of the cation, and selectivity of these effects are expected. The photophysical changes upon cation binding can also be described in terms of charge dipole interaction.[26] Let us consider only the case where the dipole moment in the excited state is larger than that in the ground state. Then, when the cation interacts with the donor group, the excited state is more strongly destabilized by the cation than the ground state, and a blue shift of the absorption and emission spectra is expected (however the fluorescence spectrum undergoes only a slight blue shift in most cases; this important observation will be discussed below). Conversely, when the cation interacts with the acceptor group, the excited state is more stabilized by the cation than the ground state, and this leads to a red shift of the absorption and emission spectra (Figure 1.6).
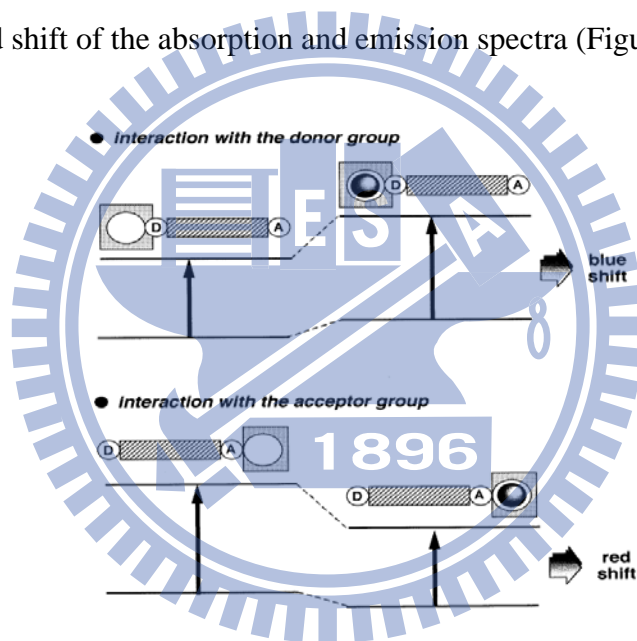
Figure 1.6. Spectral displacements of PCT sensors resulting from interaction of a bound cation with an electron-donating or electron-withdrawing group.

1.2.4. Fluorescence Resonance Energy Transfer (FRET):

FRET is a distance dependent interaction between the electronic excited state of a fluorophore and another fluorophore in which the excitation is transferred from a donor molecule to an acceptor molecule without emission of photons; if FRET takes place exciting a fluorophore, the emission of another fluorophore is detected. FRET needs of some essential

conditions: donor and acceptor molecules must be in close proximity (typically 10–100 ˚A); the absorption spectrum of the acceptor must overlap the fluorescence emission spectrum of the donor; donor and acceptor transition dipoles orientation must be approximately parallel. The efficiency of FRET is dependent on the inverse sixth power of the intermolecular separation. The presence of a metal ion forces the two fluorophores to move close or far each other. In the first case, exciting the free fluorophore A (Figure 1.7) the emission spectra of A is detected because FRET is prevented due the great distance between the two fluorophores. By coordination of the metal ion, the distance between the two fluorophores decreases switching on the FRET, thus exciting the fluorophore A the emission spectra of B can be detected.
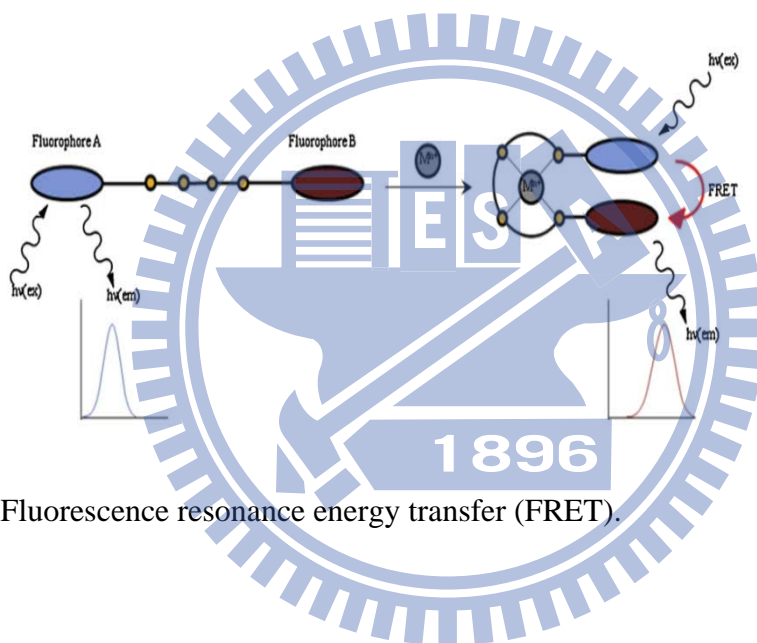
Figure 1.7. Fluorescence resonance energy transfer (FRET).

1.2.5 Excimer or exciplex formation:

 In the case in which the interaction between excited and ground-state components in a metal sensor is sufficiently strong, new chemical species called excimers or exciplexes are formed. Excimer and exciplex formation is a reversible process and both can be luminescent chemical entities. The emission of an excimer or exciplex is always at lower energy compared with the monomer emission, and usually the corresponding band is rather weak and broad. Once again, the presence of metal ions strongly encourages or disrupts excimer or exciplex affecting the emission spectra (Figure 1.8). Often, the ratio between the emission intensity of monomer

and excimer gives a quantitative measure of the amount of metal ion present in solution. Sensors based on this concept are called "ratiometric sensors".
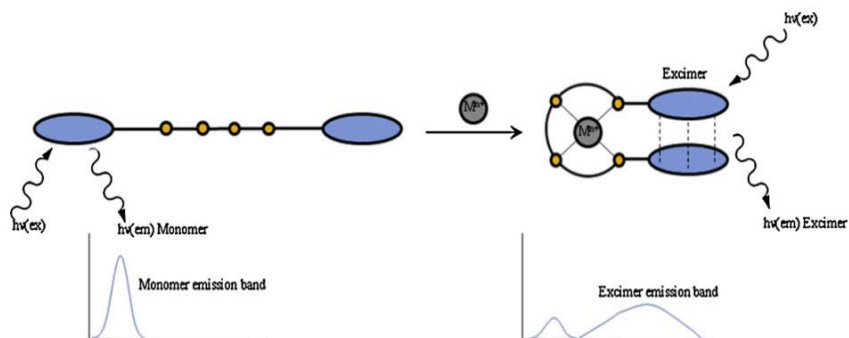
Figure 1.8. Excimer or exciplex formation.

1.2.6 Irreversible reaction-based sensors (chemodosimeters):

Chemodosimeters are mainly used to obtain OFF-ON sensors for those metal ions usually quenching the fluorescence (e.g. Cu (II)). They are non-emissive molecules converted in emissive ones via irreversible chemical reaction promoted by the metal ion (Figure 1.9). Many of these sensors suffer several issues, often they only act in organic solvents or require specific conditions as high temperature.
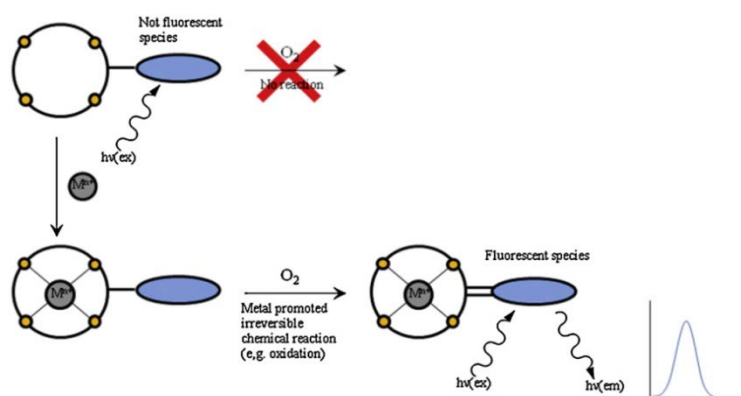
Figure1.9. Irreversible reaction-based sensors.

1.2.7. Metal-to-ligand charge transfer (MLCT):

Metal-to-ligand charge-transfer (MLCT) complexes arise from transfer of electrons from molecular orbitals with metal like character to those with ligand like character. This is most commonly observed in complexes with ligands having low-lying π^* orbitals especially aromatic ligands. The transition will occur at low energy if the metal ion has a low oxidation number for its d orbitals will relatively be high in energy. Examples of such ligands taking part in MLCT include 2,2';6',2"-terpyridine (tpy), 2,2'-bipyridine (bipy), 1,10-phenanthroline (phen), CO, CN$^-$ and SCN$^-$. For examole, Terpyridine-containing tetraphenylethenes (TPEs) can work as "turn-off" fluorescent chemosensors for metal ions and display different fluorescence responses to various metal ions. A characteristic red shift in the emission spectra is observed in the presence of Zn^{2+}, which facilitates the discrimination of Zn^{2+} from other metal ions. Because of the MLCT process, terpyridine-substituted TPEs display an obvious magenta color upon selectively binding with Fe^{2+}, allowing a rapid identification of Fe^{2+} in the aqueous media by naked eyes (Figure 1.10).[27]
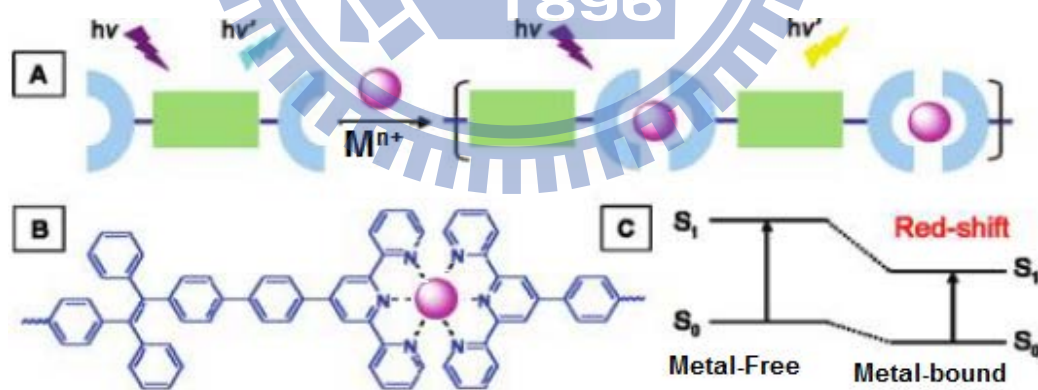
Figure 1.10. (A) Possible stoichiometry of metal-tpy complex. (B) Structure of metal-bound TPE2TPy. (C) Proposed mechanism for the spectral red-shift of TPE2TPy upon binding to metal ion (Zn^{2+}).

1.2.8. Paramagnetic fluorescence quenching:

In a wide variety of metal complexes the formally forbidden intersystem crossing (isc) become faster due to the presence of a paramagnetic atom (the metal ion) in the proximity of the fluorophore (Figure 1.11). This phenomenon is called paramagnetic effect, and it is the principal cause of the fluorescence quenching by the d^9 Cu (II) ion. Metal complexes containing this metal ion undergo isc by excitation, from S1 to T1 state of the fluorophore that is deactivated by bimolecular non-radiative processes. For this reason classical probes for Cu (II) and other strongly paramagnetic metal ions such as Fe (III), Cr (III), Co (II) are usually based on the quenching of the fluorescence.
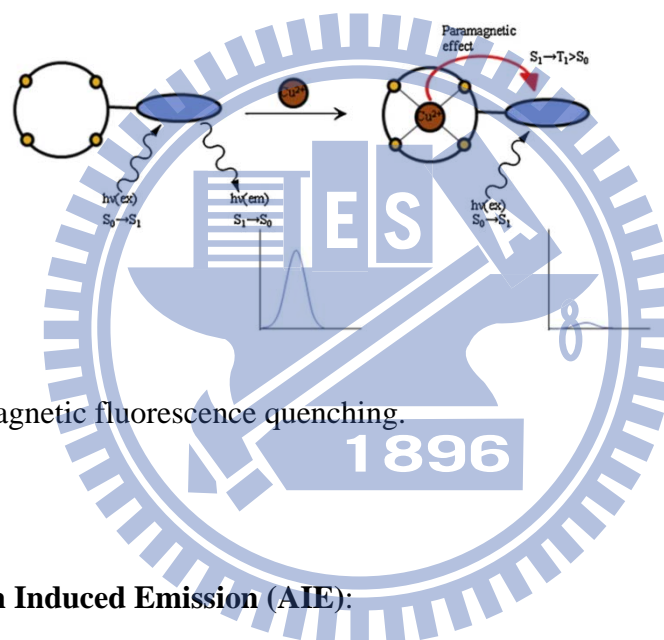
Figure 1.11 Paramagnetic fluorescence quenching.

1.2.9. Aggregation Induced Emission (AIE):

This is mainly attributed to the conformational restriction of intramolecular rotation comprising aggregation-induced emission. In general, Luminescence is often weakened or quenched at high concentrations, a phenomenon widely known as ''concentration quenching''.[28] A main cause for the quenching process is mechanistically associated with the ''formation of aggregates'',[28,29] which is probably why the concentration quenching effect has frequently been referred to as ''aggregation-caused quenching'' (ACQ). Because of the ACQ effect, the application of many organic fluorophores in organic light-emitting diodes (OLEDs) and as sensing materials (chemosensors, biosensors) has been greatly limited. To

overcome the ACQ effect, branched chains, bulky cyclic species and dendritic wedges have been covalently attached to the fluorophores to suppress the formation of aggregates. However, some organic molecules that are almost nonfluorescent in solution were shown to become strongly fluorescent upon aggregation, which is an abnormal behavior. In 2001, Tang *et al*. discovered this "abnormal" system, in which luminogen aggregation plays a constructive, instead of destructive, role in the light-emitting process (Figure 1.12a).[30] Hexylphenylsilole (HPS) dissolved in its good solvent is nonemissive. Addition of large amounts of water into the solution causes the silole molecules to aggregate and induces them to emit efficiently. This was coined as "aggregation-induced emission" (AIE) for this novel phenomenon, because the nonluminescent silole molecules are induced to emit by aggregation. Thus, the restriction of intramolecular rotation of the peripheral phenyl rings in the aggregate is the main cause for the AIE effect. Recently, metal (Al^{3+}) induced aggregation induced emission has been proposed for chemosensing application (Figure 1.12b).[31]
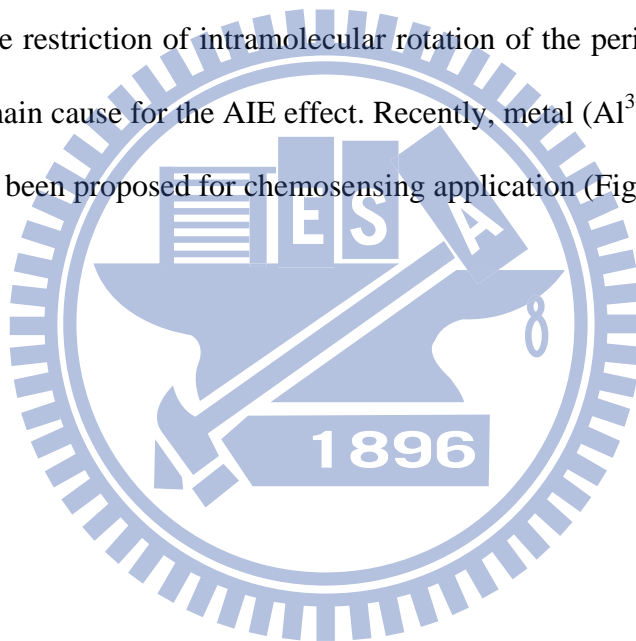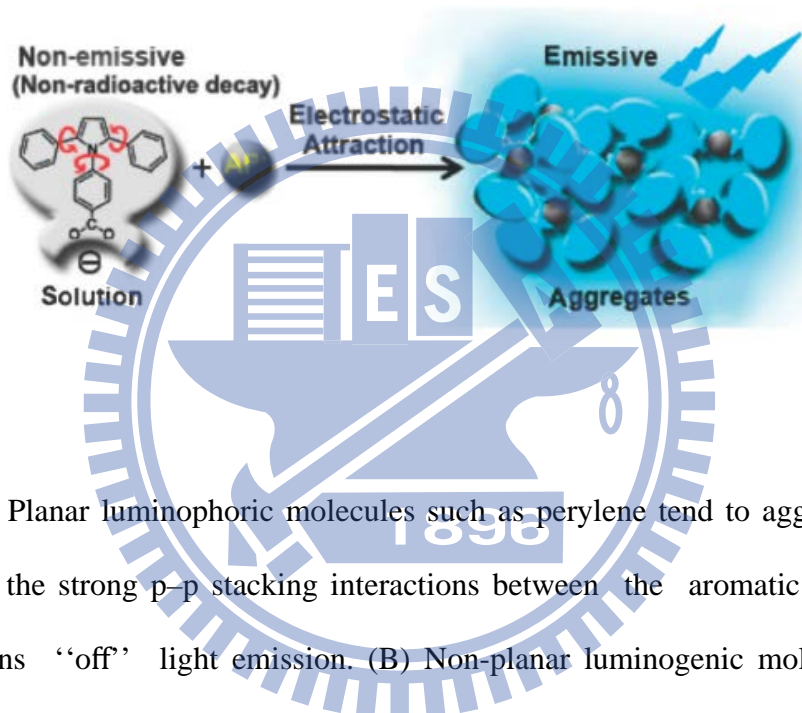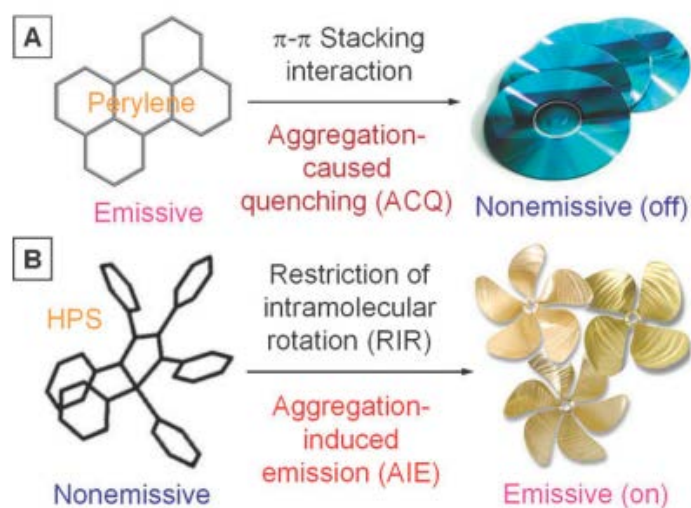
Figure 1.12 (a) Planar luminophoric molecules such as perylene tend to aggregate as discs pile up, due to the strong p–p stacking interactions between the aromatic rings, which commonly turns ''off'' light emission. (B) Non-planar luminogenic molecules such as hexaphenyl-silole (HPS) behave oppositely, with their light emissions turned ''on'' by aggregate formation, due to the restriction of the intramolecular rotation (RIR) of the multiple phenyl rotors against the silole stator in the aggregate state. (b) Example of sensing process based on AIE mechanism.

15

1.3 Literature Survey:

1.3.1 Pb^{2+} Sensors:

1.3.1.1:

Phenanthroline-based colorimetric sensors **1** and **2** have been designed, synthesized, and compared with phenanthrene-based receptor **3** for sensing of Pb^{2+} by color change. Receptor **1** imparts color change (from yellow to red) selectively with Pb^{2+} in acetonitrile/water (9:1) as well as in methanol/water (9:1) when in the presence of other metal ions studied (Li^+, Na^+, K^+, Ca^{2+}, Mg^{2+}, Ba^{2+}, Fe^{3+}, Co^{2+}, Ni^{2+}, Cu^{2+}, Zn^{2+}, Cd^{2+}, Hg^{2+}, and Mn^{2+} as their perchlorate salts). Receptor **1** also shows fluorescence enhancement upon addition of lead perchlorate in acetonitrile/water (9:1) solvent possibly due to the chelation enhanced fluorescence (CHEF) effect (See Figure 1.13). However, the binding behavior of **2** with Pb^{2+} is found to be less effective compared to that of receptor **1**.[32]
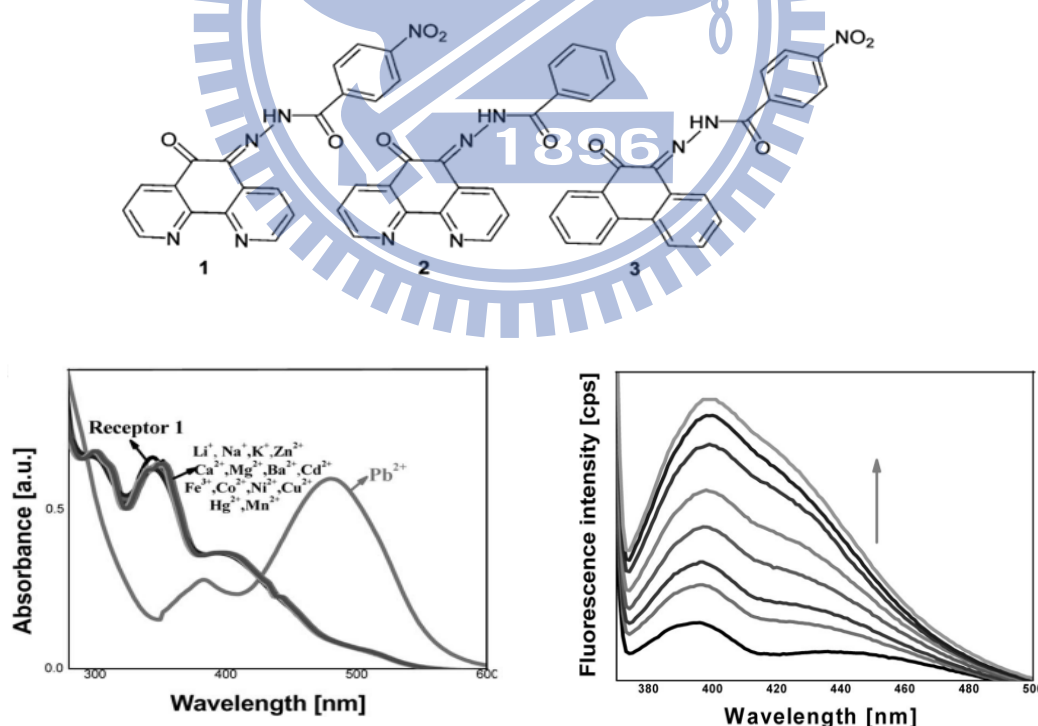
Figure 1.13. UV/Vis spectra of receptor **1** with the addition of different metal ions (left); Fluorescence spectra of receptor **1** the addition of increasing amounts of Pb^{2+} [0, 0.5, 1, 1.5, 2, 3, 5, and 7 equiv.] (right).

1.3.1.2:

A novel organic–inorganic fluorescent material as chemosensor containing 2-substitute imidazole-[4,5-f]-1,10-phenanthroline derivative was prepared by sol–gel reaction, and the binding ability of hybrid material with metal ions was evaluated, and the results indicated that the hybrid material can selectively recognize Pb^{2+} (Figure 1.14). By examining the ability of hybrid material to adsorb Pb^{2+} in solid liquid phase, 98.3% of Pb^{2+} was adsorbed onto the surface of hybrid material, and the hybrid material can be repeatedly utilized with suitable treatment, where the "off-on-off" process was due to the pH modulation of the phenanthroline ligand. The combination of well-defined inorganic matrix and functionalized organic receptor can play a pivotal role in the development of a novel generation of functionalized composites.[33]
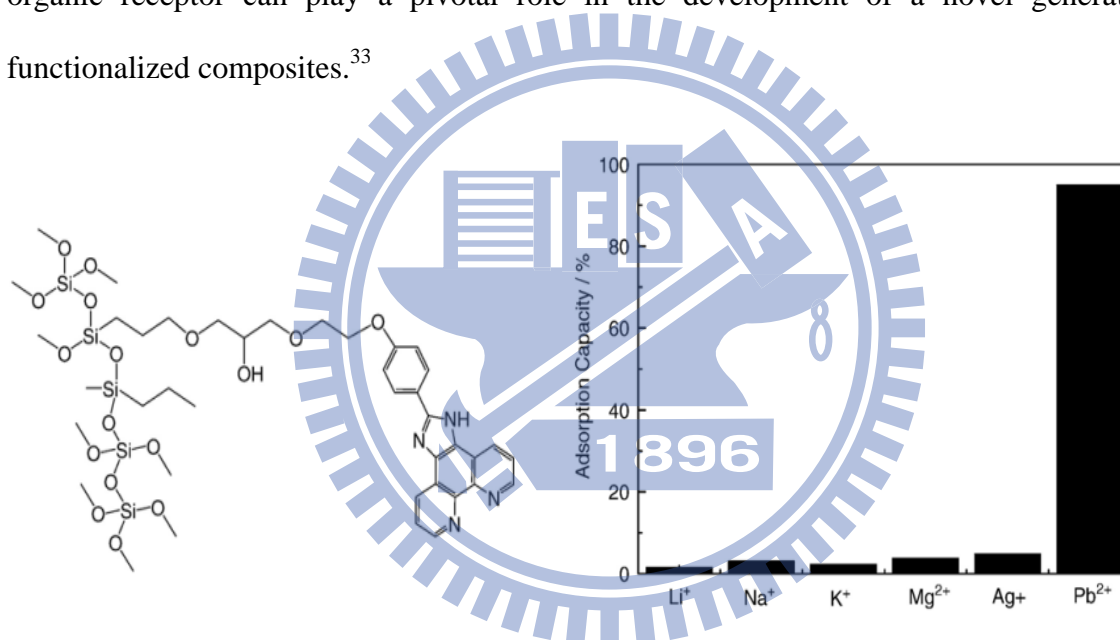
Figure 1.14. Organic–inorganic hybrid material containing 1,10-phenanthroline (left); Adsorption capacity (%) of hybrid material upon the addition of metal ions (right).

1.3.1.3:

The ferrocene-imidazopyrene dyad, bearing the imidazole ring as the only receptor site, acts as a redox and optical molecular sensor for ion pairs, exhibiting an easily detectable signal change in the redox potential of the ferrocene/ferrocinium redox couple and in the emission spectrum. Perturbation of the emission spectrum follows the order $Pb^{2+} > Hg^{2+} > Zn^{2+}$ for

cations and $H_2PO_4^-$ > AcO^- for anions (Figure 1.15). ie. The ferrocene-imidazopyrene dyad **3** behaves as a host-separated ion pair receptor. A salient feature of this simple receptor is the presence of only one receptor site, the imidazole ring, which is able simultaneously to recognize an anion and a cation through variation of the oxidation potential of the ferrocene/ferrocinium redox couple and a remarkable perturbation of the emission spectrum.[34]
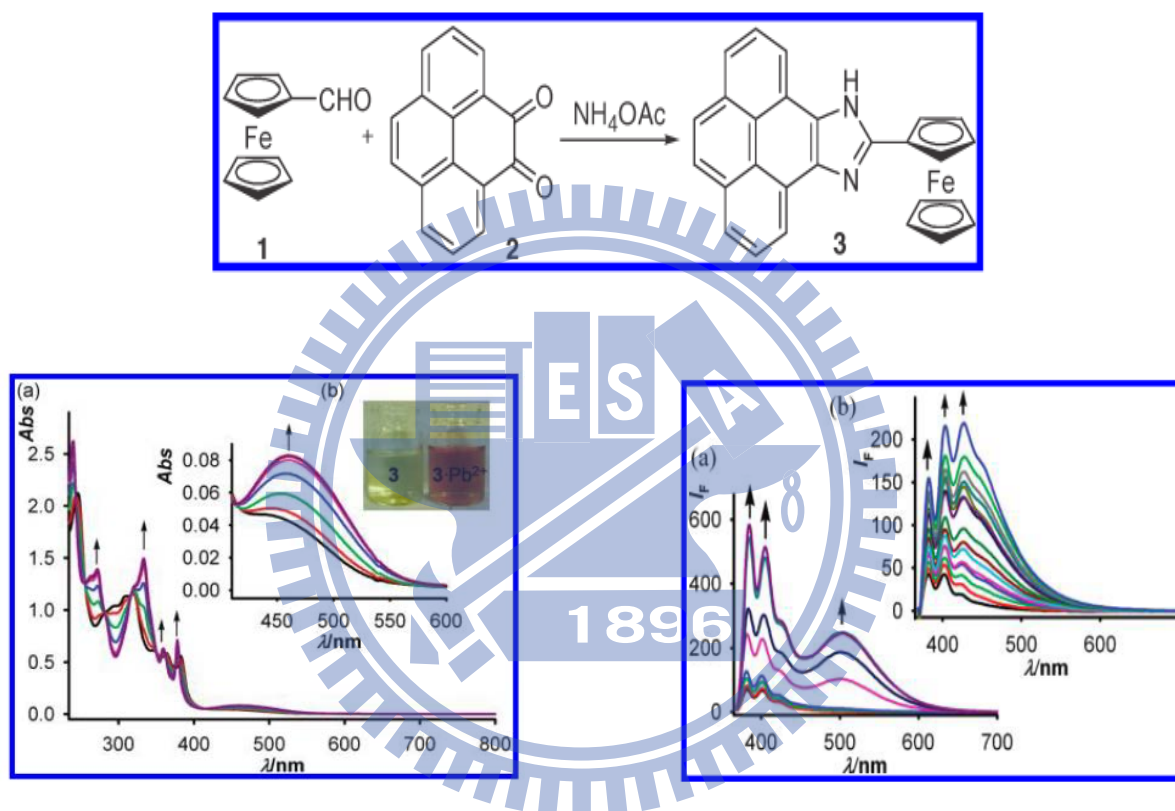
Figure 1.15. (Left): (a) Changes in the absorption spectra of **3** (black) (5 x 10^{-5} M) in CH_3CN upon addition of increasing amounts of $Pb(ClO_4)_2$, until 1 equiv (purple). (b) Visual features observed by passing from 3 to the complex 3**.**Pb^{2+}. (Right): Changes in the fluorescence emission spectra of **3** (black) (c = 1 x 10^{-5} M in CH_3CN) upon addition of increasing amounts of (a) $Pb(ClO_4)_2$ until 0.5 equiv (purple) and (b) [(n- Bu)$_4$ N]H_2PO_4 until 2 equiv (blue).

1.3.1.4:

Among Ferrocene-imidazoquinoxaline dyads **6a** and **6b**, showed selective sensitivity towards Pb^{2+} and Hg^{2+} respectively (Figure 1.16) Dyad **6a** behaves as a highly selective redox, chromogenic and fluorescent chemosensor molecule for Pb^{2+} cations in CH_3CN solutions; the oxidation redox peak is anodically shifted ($\Delta E_{1/2} = 110$ mV); in the absorption spectrum a new low-energy band appeared at $\lambda = 463$ nm, and the emission band is red-shifted ($\Delta\lambda = 31$ nm) along with an important chelation-enhanced fluorescence factor (CHEF = 276), upon complexation with this metal cation. The dyad **6b**, bearing two additional pyridine rings as substituents, has shown its ability for sensing Hg^{2+} cations through three different channels: the oxidation peak is anodically higher shifted ($\Delta E_{1/2} = 300$ mV), a new low-energy band appears in the absorption spectrum at $\lambda = 483$ nm, and the emission band was also red-shifted ($\Delta\lambda = 28$ nm) and underwent an important chelation-enhanced fluorescent factor (CHEF = 227). The changes in their absorption spectra are accompanied by color changes from yellow to orange which allow their potential use for the "naked eye" detection of these metal cations. Linear sweep voltammetry revealed that Cu^{2+} cations induced oxidation of the ferrocene unit in both dyads, which is accompanied by an important increase of the emission band.[35]

.

6a: X=CH
6b: X=N
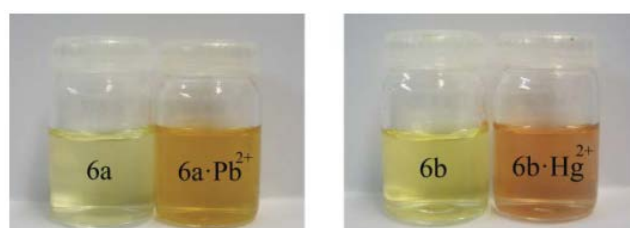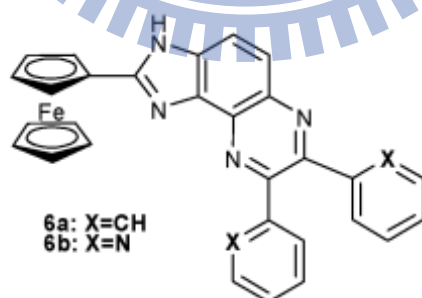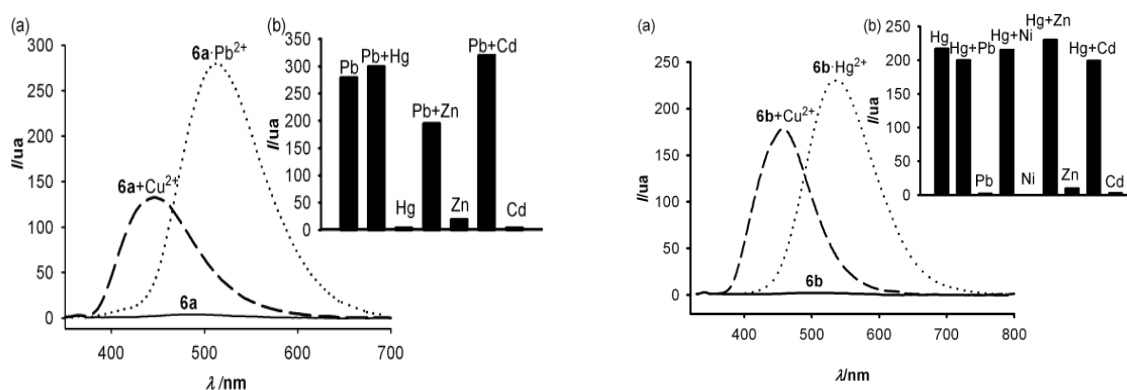
Figure 1.16 (Left): (a) Changes in the fluorescence spectra of **6a** (1 x 10^{-5} M) in CH_3CN upon addition of Pb^{2+} (dotted line) and Cu^{2+} (dashed line) metal cations (λ_{exc} = 330 nm). (b) Fluorescence emission intensity of **6a** upon addition of 0.5 equivalents of Pb^{2+} in the presence of 0.5 equivalents of interference metal ions in CH_3CN. (Right): Changes in the fluorescence spectra of **6b** (1 x 10^{-5} M) in CH_3CN upon addition of Hg^{2+} (dotted line) and Cu^{2+} (dashed line) metal cations (λ_{exc} = 310 nm). (b) Fluorescence emission intensity of **6b** upon addition of 0.5 equivalents of Hg^{2+} in the presence of 0.5 equivalents of interference metal ions in CH_3CN.

1.3.1.5:

Ferrocene–imidazophenazine dyads **4** and **7** showed selective sensing towards Pb^{2+} and Hg^{2+} respectivily (Figure 1.17). Dyad **4** behaves as a highly selective chemosensor molecule for Pb^{2+} cations in CH_3-CN/H_2O (9:1). The emission spectrum (λ_{exc} = 317 nm) undergoes an important chelation-enhanced fluorescence effect (CHEF = 47) in the presence of Pb^{2+} cations. A new low-energy band appeared at 502 nm, in its UV/vis spectrun, and the oxidation redox peak is anodically shifted ($\Delta E_{1/2}$ = 230 mV). The presence of Hg^{2+} cations also induced a perturbation of the redox potencial although in less extension than those found with Pb^{2+} cations. Dyad **7**, bearing two fused pyridine rings, has shown its ability for sensing Hg^{2+} cations selectively through three channels: electrochemical, optical, and fluorescent; the

oxidation redox peak is anodically shifted ($\Delta E_{1/2}$ = 200 mV), a new low-energy band of the absorption spectrum appeared at 485 nm, and the emission spectrum (λ_{exc} = 340 nm) is red-shifted by 32 nm accompanied by a remarkable chelation-enhanced fluorescent effect (CHEF = 165). Linear sweep voltammetry revealed that Cu^{2+} cations induced oxidation of the ferrocene unit in both dyads. ^{1}H NMR studies have been carried out to obtain information about the molecular sites which are involved in the binding process.[36]
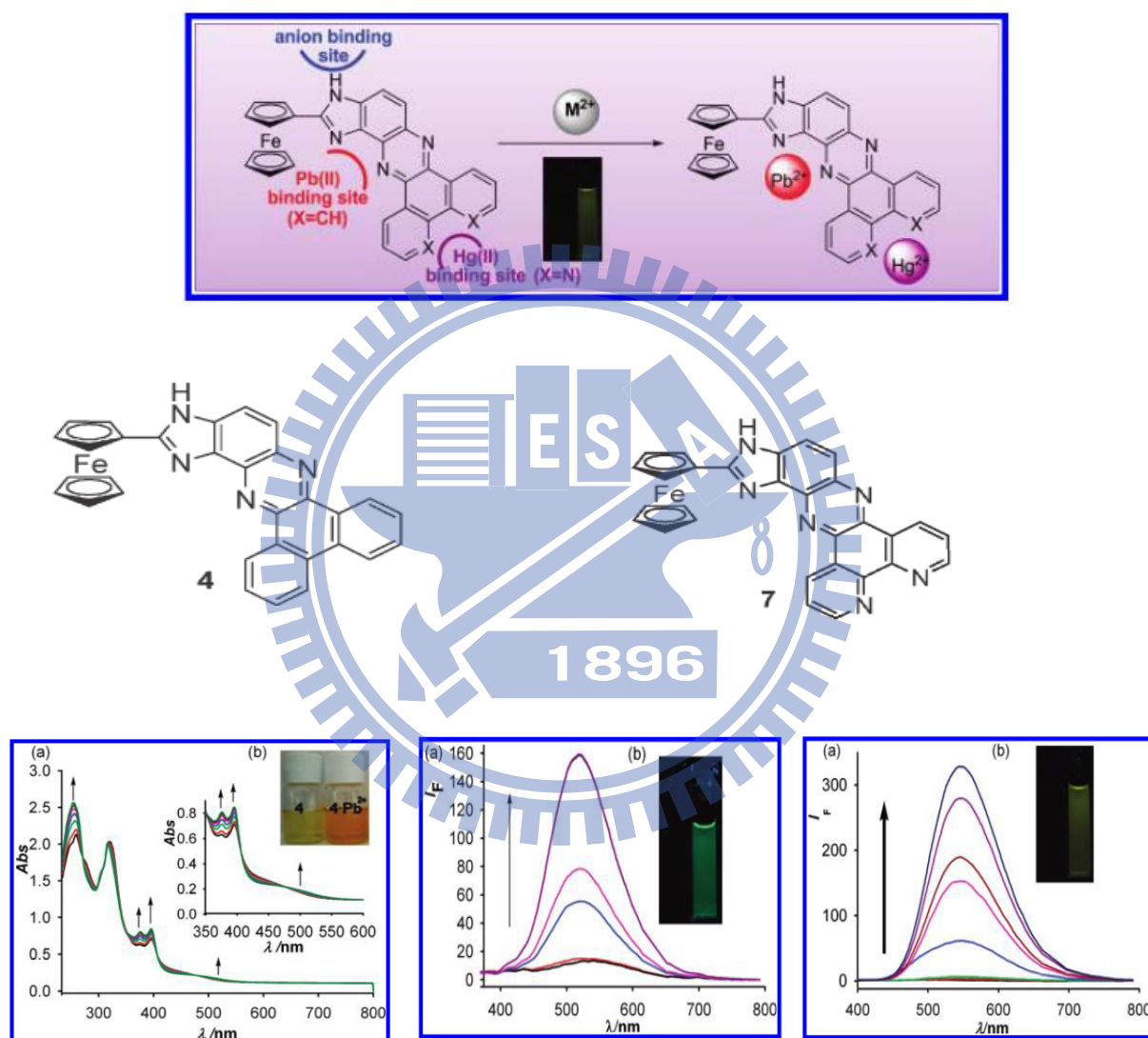
Figure 1.17. (Left): Changes in the absorption spectra of **4** upon addition of increasing amounts of $Pb(ClO_4)_2$. (Middle): Changes in the fluorescence emission spectrum of **4** upon addition of $Pb(ClO_4)_2$. (Right): Changes in the fluorescence emission spectrum of **7** upon titration with $Hg(OTf)_2$.

1.3.1.6:

A new pyrene-based sensor that functions as a fluorescent probe for Pb^{2+} sensing with high selectivity (Figure 1.18) . **LFS-1** coordinates Pb^{2+} with 1:1 complex stoichiometries. **LFS-1** displayed significant pyrene excimer emission as well as the quenching of monomer in the presence of Pb^{2+}. In contrast to **LFS-1**, **LFS-2** showed fluorescence quenching upon addition to Pb^{2+} but without emission of the pyrene excimer, indicating distinct mechanisms underlying fluorescence quenching and the formation of the pyrene dimer necessary for excimer formation. These measurements emphasize a requirement for sufficient flexibility in the probe scaffold in the rational design of fluorescent sensors requiring pyrene–pyrene interactions.[37]
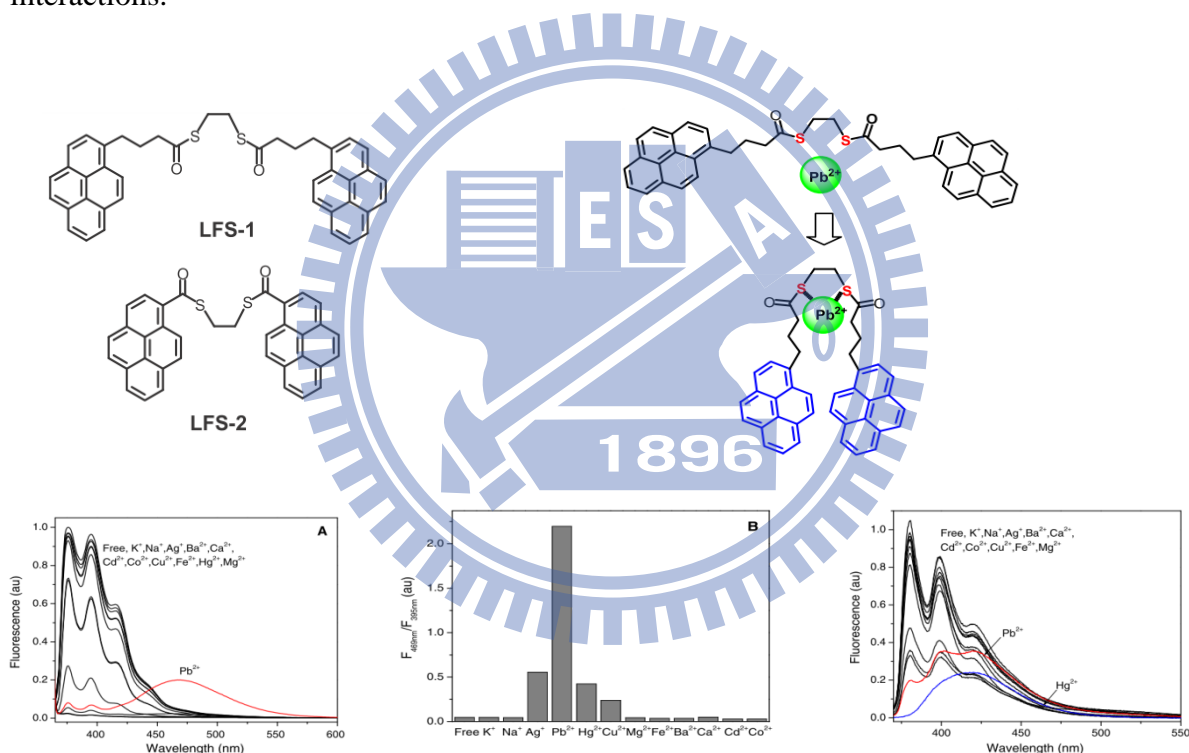
Figure 1.18. (Left and Middle): Selective association between **LFS-1** and Pb^{2+}. (Left): Fluorescence emission spectra of **LFS-1** (1.0 μM) upon addition of different metal ions (100 equiv) in 10 mM HEPES buffer (containing 10% DMSO at pH 7.4) (λ_{ex} = 355 nm). (Middle): The gray bars represent the ratio of excimer emission fluorescence at 469 nm to monomer emission at 395 nm (I_{469} /I_{395}) in presence of indicated cations. (Right): Selective fluorescence quenching of **LFS-2** upon metal binding with no excimer formation. Fluorescence emission spectra of **LFS-2** (1.0 μM) upon addition of different metal ions (100 equiv) in 1.0 mM HEPES buffer (containing 10% DMSO at pH 7.4) (λ_{ex} = 355 nm).

1.3.2: Colorimetric Hg^{2+} Sensors:

1.3.2.1:

Two new highly selective colorimetric chemosensors for Hg^{2+}, based on azobenzene and highly selective Hg^{2+}-promoted deprotection of adithioacetal have been designed and synthesized. In the presence of as little as 20 µM Hg^{2+}, the sensors change their color from light yellow to deep red, which can easily be observed by the naked eye. The underlying signaling mechanism is intramolecular charge transfer (Figure 1.19) . The sensors have good selectivity for Hg^{2+} with respect to several common alkali, alkaline earth, and transition metal ions. Furthermore, they can be used for in-the-field measurements by virtue of a dipstick approach without any additional equipment.[38]
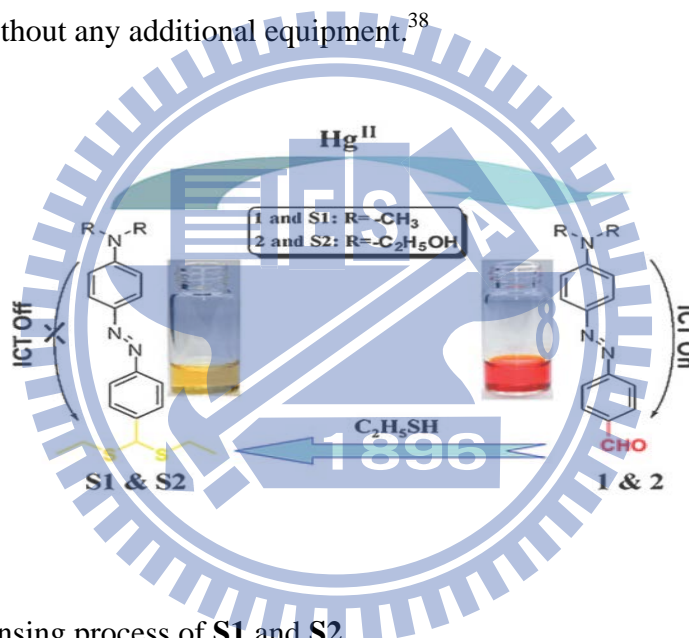
Figure 1.19. Hg^{2+}-sensing process of **S1** and **S2**.

1.3.2.2:

A chiral conjugated polymer sensor with incorporated (R,R)-salen and perylenyl moieties in the main chain backbone was obtained by the polymerization of 1,7-bis((3-formyl-4-hydroxyphenyl) ethynyl)perylene-3,4:9,10-tetracarboxylic tetrabutylate (**M-1**) with (R,R)-1,2-diaminocyclohexane (**M-2**) via a nucleophilic addition–elimination reaction. The polymer sensor can emit the fluorescence situated at 635 nm due to the introduction of a strong fluorophore perylenyl group. Compared with the other cations (including Na^{+}, K^{+}, Ca^{2+}, Ag^{+},

Ni^{2+}, Cd^{2+}, Pb^{2+}, Cr^{3+}, Al^{3+}, Fe^{3+}, Co^{2+}, Zn^{2+}), only Hg^{2+} can lead to the most pronounced response of the polymer sensor, which is as high as a 26-fold fluorescence enhancement without interference from other metal ions. More importantly, the fluorescent color of the polymer sensor displays an obvious change from red to bright yellow upon addition of Hg^{2+}, which could be easily detected by the naked eye (Figure 1.20). The results indicate that the polymer sensor with incorporated (R,R)-salen and perylenyl moieties can be favorably utilized for the development of a potential sensor for Hg^{2+} detection.[39]
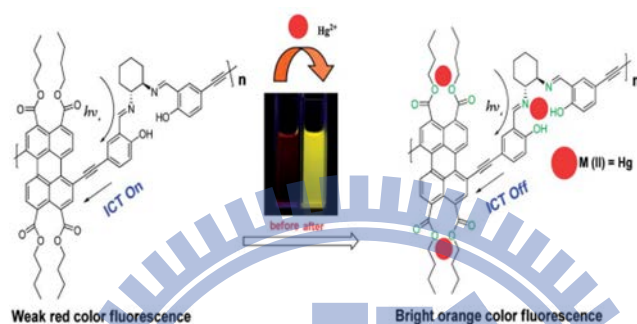
Figure 1.20. Hg^{2+} induced ICT ON–OFF.

1.3.2.3:

The synthesis and sensing characteristics of a new class of colorimetric and fluorometric dual-modal probe **DMS1** for mercury ion was outlined. Judicious placement of two dithia-dioxa-aza macrocycles on the BODIPY chromophore generates this interesting molecule. A highly Hg^{2+}-selective fluorescence enhancing property (>7-fold) in conjunction with a visible colorimetric change from purple to red-pink can be observed, leading to potential fabrication of both "naked-eye" and ratiometric fluorescent detection of Hg^{2+}(Figure 1.21).[40]
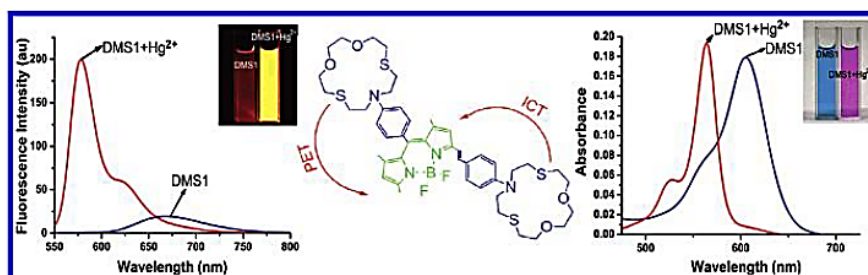
Figure. 1.21. Hg^{2+} induced absorption and fluorescence sensing of **DMS1**.

1.3.2.4:

The synthesis and characterization of ferrocene (Fc) derivatives 4-[2,5-diferrocenyl-4-(4-pyridyl)imidazolidin-1-yl-methyl]pyridine (**1**), ferrocenylmethylenepyridin-3-ylmethylamine (**2**), N,N′-bis(ferrocenylmethylene)-2,4,6-trimethylbenzene-1,3-diamine (**3**), and 6-ferrocenyl-5,6-dihydro[4,5]imidazo[1,2-c]-quinazoline (**4**) have been described. Structures of **1**, **2**, and **4** have been determined by single-crystal X-ray diffraction analyses. At 25 °C, **1−3** are nonfluorescent, while **4** displays moderate fluorescence and chromogenic, fluorogenic, and electrochemical sensing selectively toward Hg^{2+} and Pb^{2+} ions. Association constants (K_a) for Hg^{2+} and Pb^{2+} have been determined by the Benesi−Hildebrand method. Job's plot analysis supported 1:1 and 1:2 stoichiometries for Hg^{2+} and Pb^{2+} ions. Cyclic voltammograms of **1−4** exhibited reversible waves corresponding to a ferrocene/ferrocenium couple. The wave associated with **4** (+0.0263 V) exhibited positive ($\Delta E_{pa} = 0.136$ V) and negative ($\Delta E_{pa} = 0.025$ V) shifts in the presence of Hg^{2+} and Pb^{2+} ions, respectively (Figure 1.22). The mode of interaction between metal ions and **4** has been supported by ^{1}H NMR and mass spectrometry studies and verified by theoretical studies. It presents the first report dealing with ferrocene-substituted quinazoline as a multichannel chemosensor for Hg^{2+}/Pb^{2+} ions.[41]
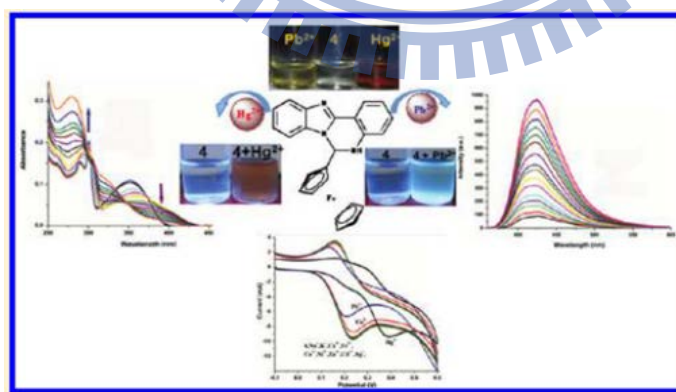
Figure 1.22. Hg^{2+} and Pb^{2+} sensing by **4**.

1.3.3: Zn senssors:

1.3.3.1:

A new zinc (II) complex with a two-dipicolylamine-substituted 1,8-naphthalimide for recognition of pyrophosphate with ratiometrical fluorescence changes in aqueous solution has been synthesized and characterized. Its biological application to monitor the intracellular pyrophosphate (**PPi**) was successfully demonstrated by the observation that the fluorescence of **1** was enhanced by the presence of the Zn^{2+} ion and was quenched by addition of **PPi** (Figure 1.23).[42]
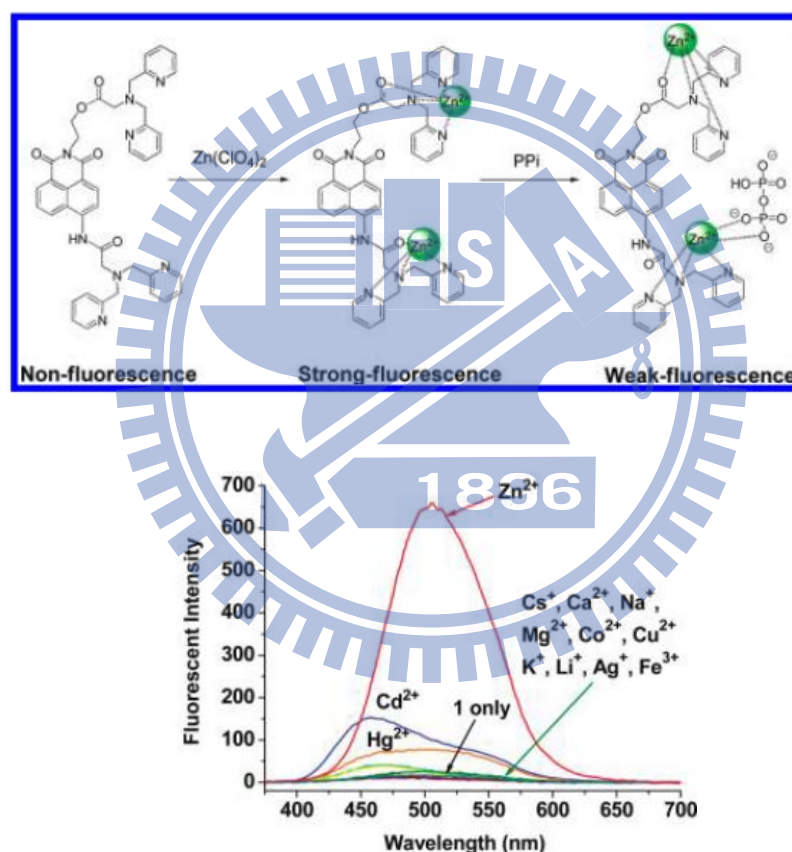
Figure 1.23. Zn^{2+} sensing pattern of **1**.

1.3.3.2:

A C_3-symmetric Schiff-base example of the new simple, low cost, highly water soluble, and sensitive turn-on fluorescent Zn^{2+} chemosensor **L** was described. The sensor was successfully

applied to the detection of intracellular Zn^{2+}. Moreover, the sensor could also serve as a potential recyclable component in sensing materials. Notably, the color change is so obvious that all of the recycling process can be seen clearly by the naked eye (Figure 1.24).[43]
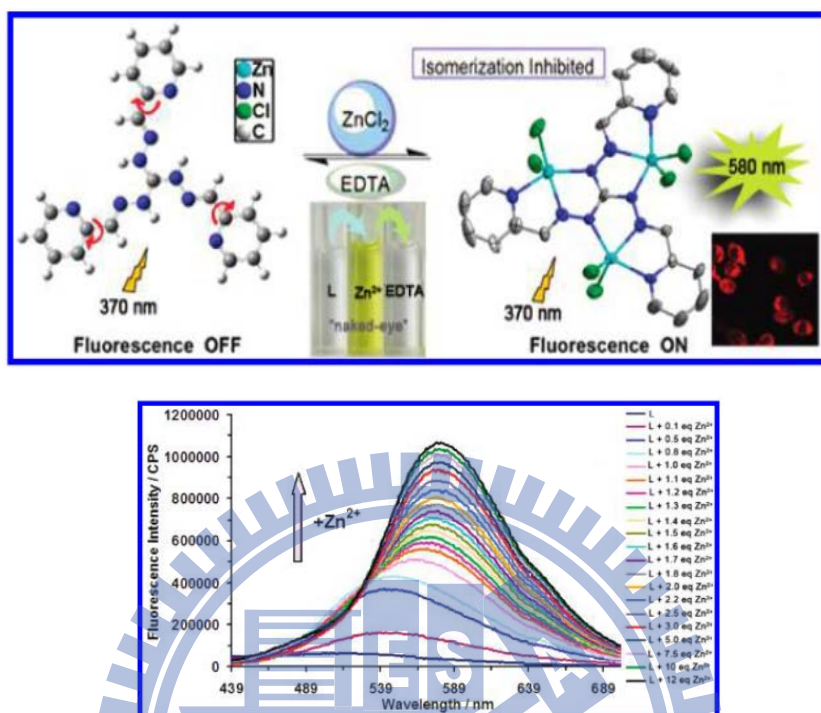
Figure 1.24. Zn^{2+} sensing by C3-symmetric Schiff-base **L**.

1.3.3.3:

New ratiometric two-photon fluorescent probe **6MPVQ** was developed from 6-substituted quinoline for biological Zn^{2+} detection. They show large red shifts and good ratiometric responses upon Zn^{2+} binding (Figure 1.25). They also exhibit high ion selectivities and large two-photon absorption cross sections at nearly 720 nm. Because the new probes are cell-permeable, they can be used to detect intracellular zinc flux under two-photon excitation.[44]
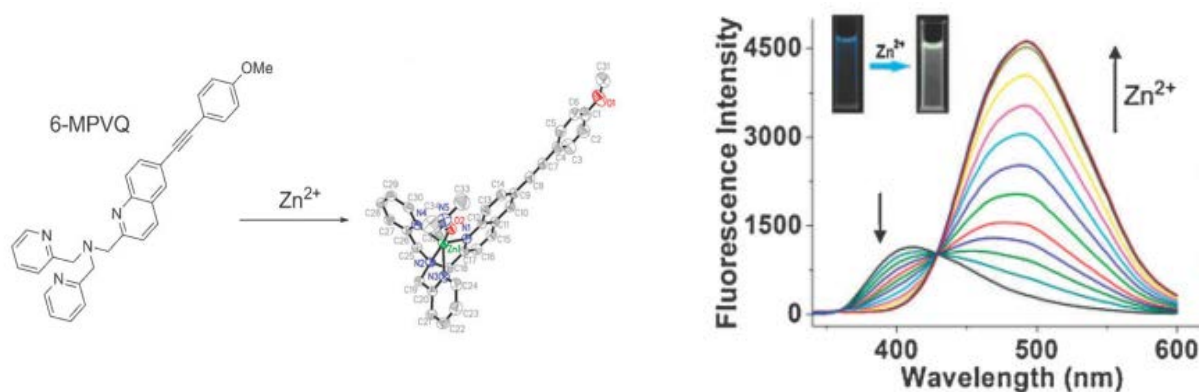
Figure 1.25. **6-MPVQ** for Zn^{2+} detection.

1.3.4: Advantages of conjugated polymer sensor over small molecular sensors.

The concept of a molecular wire has been discussed for over 30 years since it was first discovered that conjugated polymers could be prepared as electrical conductors.[45,46] In conjugated polymers, each carbon atom along the backbone has sp or sp^2 hybridization. The remaining p orbitals, with one unpaired π electron each is placed side by side to form π bonds. Since the orbitals of successive carbon atoms along the backbone overlap, the π electrons are delocalized along the polymer backbone. This electronic delocalisation provides a pathway for electron or hole mobility along the backbone of the polymer chain. Recently, there has been renewed interest in the developing of conjugated polymer molecular wires for their applications in organic light emitting diodes,[47-51] photovoltaics,[52-55] actuators,[56] batteries,[57-59] and field-effect transistors.[60] This wide range of applications is the result of the unique metallic and semiconducting properties inherent to many of these conjugated polymer systems. An interesting recent extension of these materials has been their subsequent application to fluorescent sensors.[61-65] Numerous studies have been made on the properties and applications of conjugated polymers such as poly(acetylene)poly(p- phenylenevinylene) (PPV),[66-68] poly(p-phenyleneethylene) (PPE)[61,62] and polythiophene (PT).[69-70] Several groups

28

have investigated the structure–property relationships of poly[p-(phenyleneethynylene)-alt-(thienyleneethynylene)] (PPETE).[71,72] The PPETE structure has been found to be highly luminescent and also have very good possibility. They deviate slightly from the PPE rigid-rod structure due to the inclusion of the five-member thiophene ring, but still have a relatively high degree of π electron delocalisation.[71,72]

Small molecules as fluorescence sensors have been extensively studied in the past several decades. Recently, conjugated polymer chemosensors have been used with great success for detection of a range of analytes from biomolecules to explosives. Conjugated polymers, or molecular wires, have several advantages over small molecules for sensing applications due to enhancements associated with electronic communication between receptors along the polymer backbone, processibility and ease of structural modification. Conjugated polymer sensors have been classified based on various transduction principles such as conductometry, potentiometry, chemical field-effect transistor (CHEMFET) and fluorescence.[63,73,74] Here we will focus our discussion on conjugated polymers as fluorescence chemosensors. In some cases, conjugated polymer fluorescence shows a direct response to an external analyte and the conjugated polymers can be used directly as fluoescent sensors. The combination of the sensitivity of fluorescence and unique properties of conjugated polymers provides new opportunities for sensory system development. One type of conjugated polymer fluorescent sensor is based on the conformational change of conjugated backbone driven by interaction with the analyte. For instance, the fluorescence of poly[3-oligo(oxyethylene)-4-methythiophene] changes in the presence of alkali metals and the intensity of fluorescence is a function of the concentration of alkali metal cations.[75] Another type of conjugated polymer sensor involves the introduction of molecular recognition units (receptors) on the polymer. The receptors can be either in the polymer backbone or as pendants. An elegant example of the former is the polymer synthesized by Wang and Wasielewski.[76] A bipyridyl group with a dihedral angle of 20° was introduced into the polymer backbone. Chelation to transition metal ions increases the planarity of the bipyridyl site and the conjugation length. Hence the

conformational change can be monitored by UV–vis and fluorescence spectroscopy. Polymers offer a great deal of flexibility in their synthesis and utility. Assembling the receptor pendants through the conjugated polymer backbone is another excellent approach to amplifying the fluorescent signals.[62,77,78] As illustrated in Figure 1.26, the receptors are connected by the conjugated polymer-'molecular wire'. Analyte binding produces energy trap sites for the fluorescent excitons. Due to the facile energy migration, in which excitons diffuse along the conjugated polymer backbone, the emission intensity of conjugated polymers decreases dramatically.[62] By utilizing the collective properties of the molecular wire configuration containing multiple receptors, one can achieve enhanced sensitivity of polymer fluorescent sensors relative to small molecule sensors. This concept was first advanced and demonstrated by Swager's group.[77-78] They assembled the cyclophane-based receptors onto a para poly(phenyleneethynylene) backbone and this polymer showed a 65-fold fluorescence enhancement in sensitivity to paraquat, compared to a model fluorescent chemosensor containing only one receptor. This signal amplification creates a chemosensor that is significantly more sensitive to analytes than its single molecule counterparts. The phenomenon of energy transfer enhancement essentially allows one binding event to quench the fluorescence of multiple fluorescence sensor sites on the chain. In this review we are going to focus on the research carried out in our lab using conjugated polymers as the backbone combined with different receptors as transition metal ion chemosensors. All the photophysical measurements of the polymer and including the titration with metal cations were carried out in tetrahydrofuran (THF). The THF solvent was an ideal carrier based on the high solubility of the polymer and its miscibility with H_2O, which was the target medium for cation detection in the environment.
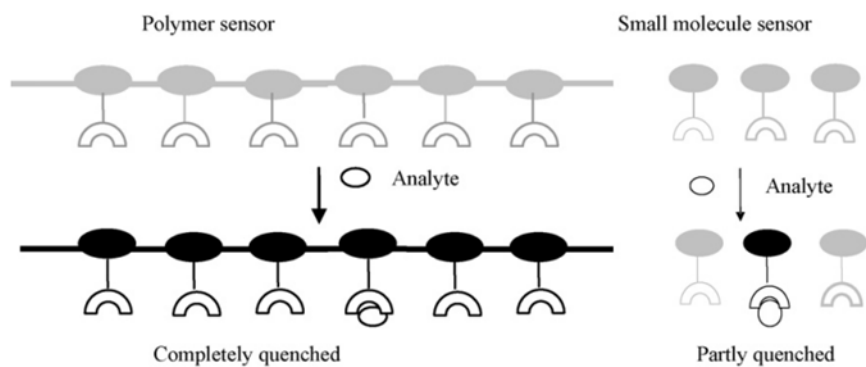
Fig 1.26. This schematic representation demonstrates sensory signal amplification using the molecular wire approach.

Chapter 2

Novel dithieno-benzo-imidazole-based Pb^{2+} sensors: substituent effects on sensitivity and reversibility.

2.1 Introduction:

Owing to the biological, medicinal, oceanographic and environmental toxicity of cations, numerous analytical methods, such as neutron activation analysis, ion sensitivity (to electrodes), flame photometry, atomic absorption spectrometry, electron microprobe analysis and inductively coupled plasma-mass spectroscopy, were developed for their detections.[79] The drawbacks of these detection methods are due to their expensiveness, time consuming, difficulties in continuous monitoring and requirements of large size samples. On the contrary, the methods based on fluorescent sensors offer diverse advantages in terms of sensitivity, selectivity, response time, local observation (e.g., fluorescence imaging spectroscopy).[1,15,80] Lead being a poisonous neurotoxin substance damages the nervous system. Excessive lead also causes cardiovascular, reproductive and developmental disorders in mammals and brain disorder.[81] Thus, development of selective and sensitive methods for the detection of lead ions is an extensive awareness for chemists. For instance, fluorescence turn-on sensing mechanisms could be explained in terms of intramolecular charge transfer (ICT)[2] and/or chelation[82] effects, and the aggregation induced by quenchers is one of the rudimentary reasons for fluorescence turn-off.[82]

Recently various probes, such as cyclen,[83a] imidazoquinoxaline,[35] imidazopyrene,[34] imidazophenazine,[36] rhodamine[83b] and calixarene[83c] have been successfully reported for selective sensing of Pb^{2+}. To the best of our knowledge, thieno-imidazole-based sensors have not been reported so far. Therefore, two novel dithieno-benzo-imidazole-based compounds **M2** and **A2** were synthesized to find the effects of chelation by 'N' and 'S' linkages on

selectivity and sensitivity towards target metal ions. Figure 2.1 shows the fluorescence off-on-off and on-off-off mechanisms for **M2** and **A2**, respectively, towards Pb^{2+} and S^{2-}.
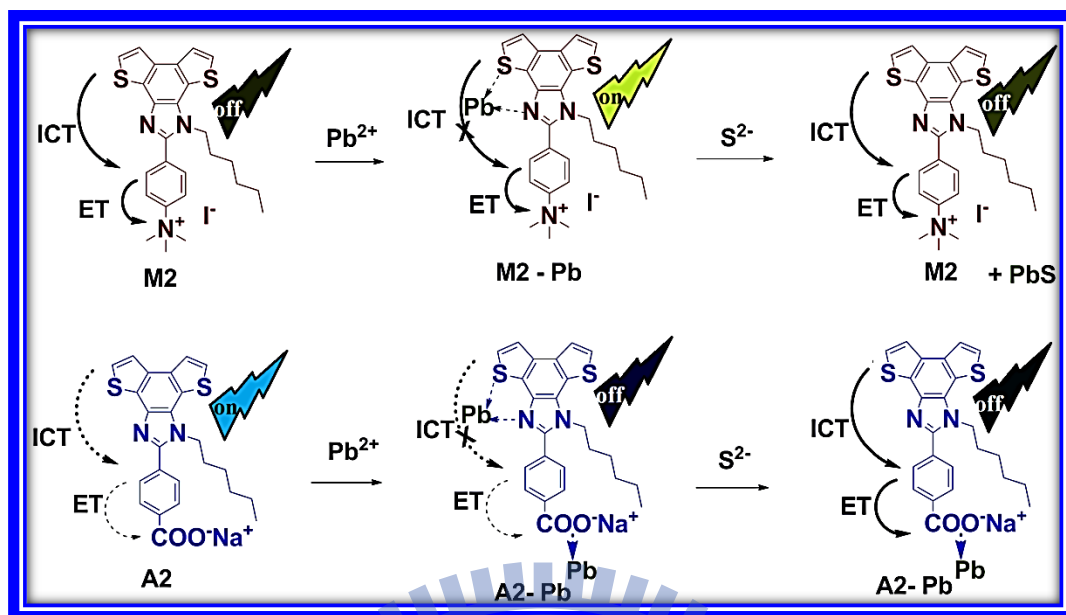
Figure 2.1. Schematic representation of the fluorescence off-on-off and on-off-off mechanisms of **M2** and **A2**, respectively, towards Pb^{2+} and S^{2-}.

2.2 Experimental Section:

2.2.1 Reagents, measurements and characterizations: All chemicals and solvents were reagent grades and purchased from ACROS, Aldrich, TCI, Fluka, TEDIA, and Lancaster Chemical Co. THF was distilled over sodium/benzophenone to keep anhydrous before use. After distillation over CaH_2, DMF was purified by refluxing with calcium hydride and then distilled. The solvents were degassed by nitrogen 1 h prior to use before reaction. ^{1}H-NMR and ^{13}C-NMR spectra were recorded on a Bruker DX-300 (300 MHz for ^{1}H and 75 MHz for ^{13}C) spectrometer using $CDCl_3$, D-THF and D_6-DMSO solvents. Elemental analyses were performed on HERAEUS CHN-OS RAPID elemental analyser. A solution of **M1, M2**, and **A2** (1.4×10^{-5} mol/L) were prepared in DMSO and hepes-buffered water (v/v = 1/1) (pH = 7.0). A solution of **A1** (1.4×10^{-3} mol/L) was prepared in THF. This stock solution was further

diluted by THF and hepes-buffered water (v/v = 1/1) to afford a final concentration of sample solution 1.4×10^{-5} mol/L (pH = 7.0). The solutions of metal ions (1.4×10^{-3} mol/L) were prepared in DI water. The solutions of **M1**, **M2**, **A1** and **A2** (3.0 mL) were placed in a quartz cell (10.0 mm width) and the fluorescence as well as absorption spectra were recorded. Metal ion sensing were carried out by taking following metal ions as their nitrate salts ($NaNO_3$, KNO_3, $Mg(NO_3)_2 \cdot 6H_2O$, $Ca(NO_3)_2 \cdot 4H_2O$, $Ba(NO_3) \cdot XH_2O$, $AgNO_3$, $Co(NO_3)_2 \cdot 6H_2O$, $Ni(NO_3)_2 \cdot 6H_2O$, $Zn(NO_3)_2 \cdot 6H_2O$, $Cu(NO_3)_2 \cdot 3H_2O$, $Pb(NO_3)_2$. Reversibility test has been performed by taking the sodium salts of desired anions. Anion sensing of compound **4** has been tested by taking tetrabutylammonium salts of desired anions.

2.2.2 Synthesis:

Synthetic procedures of **M1**, **M2**, **A1** and **A2** were depicted in Scheme 2.1. The easiest way to prepare 3,3'-bithiophene was from 3-bromothiophene by treating with n-BuLi and Cu powder. 3,3'-Bithiophene acylated by oxalic acid without the aid of any Lewis acid to yield compound **3**, which was coupled with 4-nitrobenzaldehyde in the presence of ammonium acetate in acetic acid to get compound **4**. N-alkylation of compound **4** produced compound **5**. **M1** was prepared by reduction of compound **5** by Pd/C and hydrazine. Finally, N-methylation of **M1** acquired **M2**. Furthermore, compound **3** was coupled with 4-cyanobenzaldehyde to get compound **6**. N-alkylation of compound **7** afforded **A1**. Further hydrolysis of **A1** by aqueous sodium hydroxide yielded **A2**. According to Scheme 2.2, a phenathrene-benzo-imidazole analogue **M** without a 'S' linkage was synthesized to compare its sensitivity with **M2** (with a 'S' linkage).
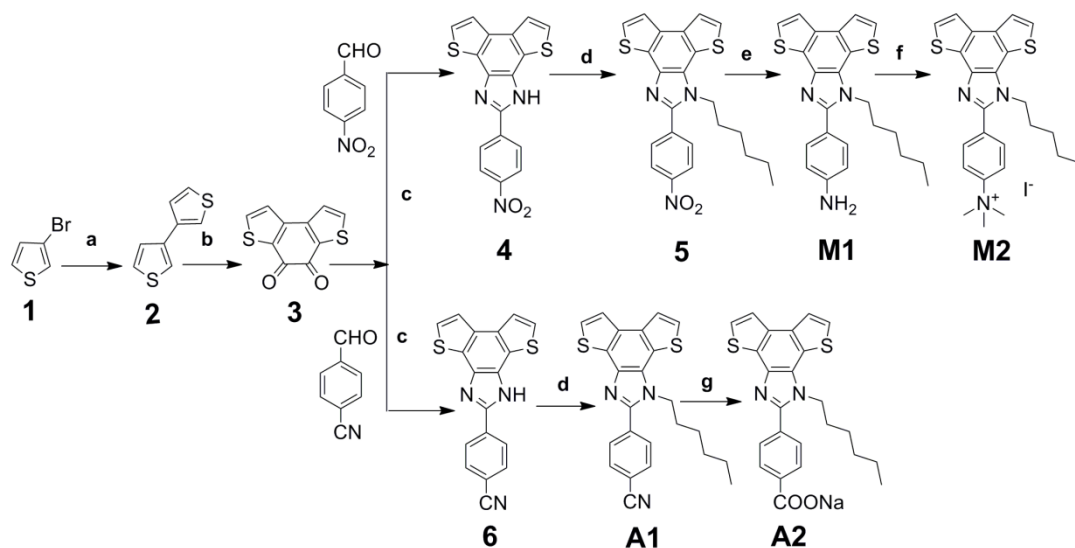
Scheme 2.1 *Reagents and conditions*: (a) n BuLi, THF, -78 °C to -60 °C, CuCl$_2$, -60 °C to rt, 18 h, 77.9%; (b) CO$_2$Cl$_2$, 1,2-DCE, 90 °C, 4days, 64.65%; (c) NH$_4$OAc, AcOH, 100 °C, overnight; (d) 1-iodohexane, K$_2$CO$_3$, DMF, 95 °C, overnight, (5 = 80.4%, **A1** = 82.4%); (e) Pd/C, NH$_2$-NH$_2$.H$_2$O, reflux, 4 h, 89.9%; (f) iodomethane, THF, reflux, 72 h, 61.3%; (g) aq. NaOH, EtOH, 2 h, 94%.
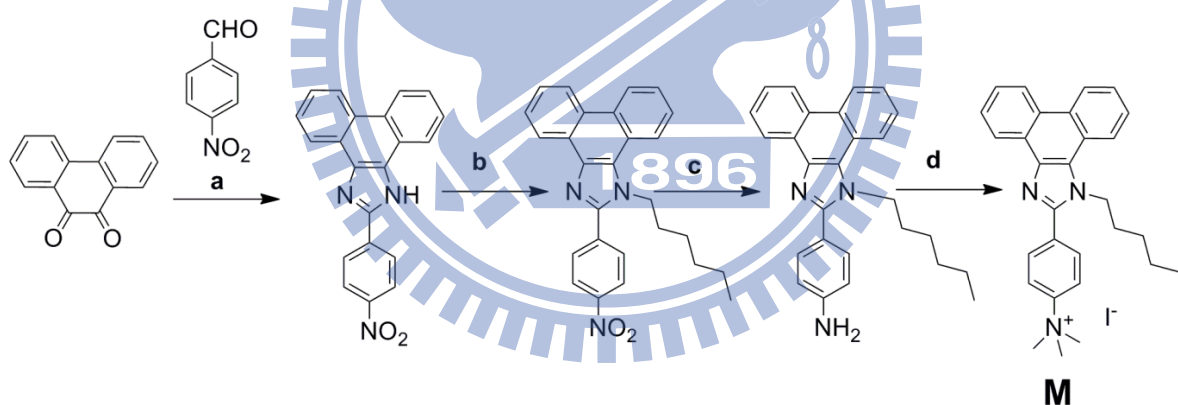
Scheme 2.2 *Reagents and conditions*: (a) NH$_4$OAc, AcOH, 100°C, overnight; (b) 1-iodohexane, K$_2$CO$_3$, DMF, 95°C, overnight, (81.3%); (c) Pd/C, hydrazine monohydrate, reflux, 4 h, 88.1%; (d) iodomethane, THF, reflux, 2 h, 91.3%.

2.2.3 Synthetic procedures

3,3'Bithiophene (2):

 3-Bromothiophene (0.122 mole, 20 gm) was dissolved in 100 mL anhydrous diethyl ether. The solution was cooled to -78 $^\circ$C. To it, 2.5 molar of n-BuLi in hexane (0.122 mole, 48.8 mL) was added dropwise for 40 mins under N_2. The reaction was allowed to stir for 10 mins at -78 $^\circ$C and 20 mins at -60 $^\circ$C. Then, $CuCl_2$ (0.130 mole, 17.42 gm) was added in one portion at -60 $^\circ$C. The reaction was carefully maintained at -60 $^\circ$C for another 1 h. Then, the reaction mixture was slowly warmed to room temperature and continued stirring for another 18 h at room temperature. The reaction mixture was quenched by 30 mL water and filtered to remove inorganic impurity. The organic phase was collected and dried in $MgSO_4$. Solvent was removed by rotary evaporation. The crude product was purified by silica gel column chromatography using hexane as an eluent. Product was obtained as white solids (7.9 gm, 77.9%). ^{1}H NMR (300 MHz, $CDCl_3$): δ (ppm) 7.38 (m, 2H), 7.35 (m, 4H). ^{13}C NMR (75 MHz, $CDCl_3$): δ (ppm) 137.0, 126.1, 125.8, 119.6; EI-MS (m/z): Calcd for $C_8H_6S_2$, 165.99; Found 166 (M^+). ^{1}H and ^{13}C NMR spectra were in agreement with the reported literature.[84]

Benzo[1,2-b:4,3-b$^/$]dithiophene-4,5-quinone (3):

3,3' Bithiophene (7 gm, 42.10 mmole) was dissolved in 100 mL of 1,2- dichloroethane. To it oxalyl chloride (3 mL, 34.94 mmole) was added slowly, and the solution was turned to orange. The reaction mix was allowed to stir at 90 $^\circ$C for 4 days. The reaction mix was cooled and kept at 0 $^\circ$C overnight. Then, the mixture was filtered. Residue product was washed thoroughly by hexane. After drying, the product obtained was red solids (6 gm, 64.65%). ^{1}H NMR (300 MHz, $CDCl_3$): δ (ppm) 7.83 (d, 2H, 4.8 Hz), 7.29 (d, 2H, 4.8 Hz). ^{1}H NMR (D_6-DMSO): δ 8.23 (d, 2H, 4.8 Hz), 7.69 (d, 2H, 4.8 Hz). ^{13}C NMR (75 MHz, $CDCl_3$): δ (ppm) 173.5, 142.1, 138.2, 134.9, 124.5. EI-MS (m/z): Calcd for $C_{10}H_4O_2S_2$, 219.97; Found 220 (M^+). ^{1}H and ^{13}C NMR spectra were in agreement with the reported literature.[85]

2-(4-Nitrophenyl)-1H-dithieno[2',3':3,4;3'',2'':5,6]benzo[1,2-d]imidazole (4):

A mixture of 4-nitrobenzaldehyde (2.8 gm, 18.52 mmole), benzo[1,2-b:4,3-b']dithiophene-4,5-quinone (3.7 gm, 16.84 mmole), ammonium acetate (40.64 gm, 527.8 mmole) and acetic acid (150 mL) was heated to 100 °C overnight. The green solution was cooled to room temperature, and 50 mL water was added to stir for 15 mins at room temperature. The solution was filtered in a Buchner funnel. The red residue was washed thoroughly in water and hexane, dried and taken to the next step without further purification. ^{1}H NMR (D$_6$-DMSO, 300 MHz) δ ppm 13.98 (s, 1H), 8.44 (d, 2H, 9Hz), 8.36 (d, 4H, 8.7Hz), 8.02 (d, 1H, 5.1 Hz), 7.81 (d, 1H, 5.1 Hz). EI-MS (m/z): Calcd for C$_{17}$H$_9$N$_3$O$_2$S$_2$, 351.01; Found 351 (M$^+$).

1-Hexyl-2-(4-nitrophenyl)-1H-dithieno[2',3':3,4;3'',2'':5,6]benzo[1,2-d]imidazole (5):

To a solution of **4** (4.8 gm, 13.65 mmole) in DMF (50 mL), K$_2$CO$_3$ (4.54 gm, 32.89 mmole) was added and heated to 95 °C for 3 h and then cooled to room temperature. To it, 1-iodohexane (2.61 mL, 3.76 gm, 17.73 mmole) was added slowly. Reaction mixture was heated to 95 °C overnight. After cooling to room temperature the reaction mixture was poured in 300 mL water. Organic phase was extracted by ethyl acetate via repeated washing in water and dried over MgSO$_4$. Then, the solvent was removed under rotary evaporation. A crude product was purified by silica gel column chromatography (EA: Hexane = 5: 95) to give yellow solids (4.79 gm, 80.4%). ^{1}H NMR (CDCl$_3$, 300 MHz) δ ppm 8.42 (d, 2H, 6.9 Hz,), 8.01 (d, 2H, 6.9 Hz,), 7.89 (d, 1H, 5.4 Hz), 7.81 (d, 2H, 5.4 Hz), 7.59 (d, 2H, 5.4 Hz), 7.55 (d, 2H, 5.2 Hz) 4.54 (t, 2H, 7.9 Hz), 1.94 (m, 2H), 1.34-1.24 (m, 6H), 0.84 (t, 3H, 6.6 Hz). ^{13}C NMR (CDCl$_3$, 75 MHz): δ ppm 149.45, 148.52, 137.15, 137.05, 136.11, 133.50, 132.46, 130.68, 129.39, 128.49, 124.95, 124.38, 123.57, 122.98, 121.15, 47.12, 31.51, 31.37, 26.57, 22.88, 14.31. EI-MS (m/z): Calcd for C$_{23}$H$_{21}$N$_3$O$_2$S$_2$, 435.11; Found 435 (M$^+$). Anal. Calcd. for C$_{23}$H$_{21}$N$_3$O$_2$S$_2$: C, 63.42; H, 4.86; N, 9.65. Found: C, 63.39; H, 4.83; N, 9.63.

4-(1-Hexyl-1H-dithieno[2',3':3,4;3'',2'':5,6]benzo[1,2-d]imidazol-2-yl)aniline (M1):

A mixture of **5** (2.8 gm, 6.42 mmole) and 50 mg Pd/C (10 %) was dissolved in ethanol and heated to reflux for 20 mins. To it 4.5 mL hydrazine monohydrate was added slowly. The solution mixture was further refluxed for 4 h and filtered. The filtrate was dried and the product was recrystallized to get gray solids (2.33 gm, 89.9%). ^{1}H NMR (D$_6$-DMSO, 300MHz) δ ppm 8.09 (d, 1H, 5.4 Hz), 8.02 (d, 1H, 5.4 Hz), 7.86 (d, 1H, 5.4 Hz), 7.75 (d, 1H, 5.4 Hz), 7.48 (d, 2H, 8.1 Hz), 6.73 (d, 2H, 8.4 Hz), 5.60 (s, broad, 2H) 4.48 (t, 2H, 6.9 Hz), 1.80 (m, 2H), 1.21-1.16 (m, 6H), 0.77 (t, 3H, 6.3 Hz). ^{13}C NMR (D$_6$-DMSO, 75 MHz) δ ppm 154.29, 151.60, 137.15, 136.05, 133.08, 132.47, 131.65, 129.86, 129.18, 128.38, 125.65, 124.78, 121.88, 118.18, 114.96, 47.23, 31.99, 31.88, 26.91, 26.37, 15.20. EI-MS (m/z): Calcd for C$_{23}$H$_{23}$N$_3$S$_2$, 405.13; Found 405 (M$^+$). Anal. Calcd. for C$_{23}$H$_{23}$N$_3$S$_2$: C, 68.11; H, 5.72; N, 10.36. Found C, 68.16; H, 5.77; N, 10.33.

4-(1-Hexyl-1H-dithieno[2',3':3,4;3'',2'':5,6]benzo[1,2-d]imidazol-2-yl)-N,N,N-trimethylbenzenaminium iodide (M2):

M1 (1.7 gm, 4.19 mmole) was dissolved in THF. To it an excess of iodomethane (3 mL) was added dropwise and stirred at 50 °C for 24 h. Further, 2 mL of iodomethane was added and the reaction was continued for 48 h at 50 °C. The reaction was monitored by ESI-MS. The mixture was cooled, filtered, washed with hexane and recrystallized with THF-Et$_2$O to get white solids (1.47 gm, 61.3%). ^{1}H NMR (D$_6$-DMSO, 300MHz) δ ppm 8.32 (d, 2H, 4.5 Hz), 8.21 (d, 2H, 7.5 Hz), 7.67 (d, 1H, 9 Hz), 7.50 (d, 1 H, 8.4 Hz), 7.02 (d, 1H, 9.3 Hz), 6.85 (d, 1H, 8.4 Hz), 4.50 (t, 2H, 6.8 Hz), 3.07 (s, 9 H), 1.78-1.72 (m, 2H), 1.21-1.13 (m, 6H), 0.78 (3H, t, 6.4 Hz). ^{13}C NMR (D$_6$-DMSO, 75 MHz) δ ppm 153.71, 150.16, 137.11, 136.45, 135.31, 133.11, 132.79, 132.60, 131.25, 129.58, 129.35, 127.32, 126.14, 124.47, 124.31, 122.02, 121.12, 54.61, 48.21, 31.56, 31.12, 26.07, 22.69, 14.62. EI-MS (m/z): Calcd for C$_{23}$H$_{30}$IN$_3$S$_2$, 575.09; Found 575 (M$^+$). Anal. Calcd. for C$_{23}$H$_{30}$IN$_3$S$_2$: C, 54.26; H, 5.25; N, 7.30. Found: C, 54.39; H, 5.19; N, 7.28.

4-(1H-Dithieno[2',3':3,4;3'',2'':5,6]benzo[1,2-d]imidazol-2-yl)benzonitrile (6):

A mixture of 4-cyanobenzaldehyde (3.2 gm, 24.40 mmole), benzo[1,2-b:4,3-b$^/$]dithiophene-4,5-quinone (4.88 gm , 22.18 mmole), ammonium acetate (51.28 gm, 665.40 mmole) and acetic acid (150 mL) was heated to 100 $^\circ$C overnight. The solution was cooled to room temperature, and 50 mL water was added to stir for 15 mins at room temperature. The solution was filtered in a Buchner funnel. The green residue was washed thoroughly in water and hexane, dried and taken to the next step without further purification. ^{1}H NMR (D$_6$-DMSO, 300MHz) δ ppm 13.92 (s, 1H), 8.42 (d, 2H, 8.4 Hz), 8.05 (m, 4H), 7.87 (d, 1H, 5.1 Hz), 7.80 (d, 1H, 5.1 Hz). EI-MS (m/z): Calcd for C$_{18}$H$_9$N$_3$S$_2$, 331.02; Found 331 (M[+]).

4-(1-Hexyl-1H-dithieno[2',3':3,4;3'',2'':5,6]benzo[1,2-d]imidazol-2-yl)benzonitrile (A1):

To a solution of **6** (5.2 gm, 15.69 mmole) in DMF 50 mL, K$_2$CO$_3$ (5.22 gm, 37.81 mmole) was added and heated to 95°C for 3 h, and then cooled to room temperature. To it 1-iodohexane (3.0 mL, 4.32 gm, 20.39 mmole) was added slowly. Reaction mixture was heated to 95 $^\circ$C overnight. After cooling to room temperature, the reaction mixture was poured in 300 mL water. Organic phase was extracted by ethyl acetate via repeated washing in water. Dried over MgSO$_4$, solvent was removed under rotary evaporation. Crude product was purified by silica gel column chromatography (EA:Hexane = 5:95) to give yellow solids (5.37 gm, 82.4%). ^{1}H NMR (CDCl$_3$, 300 MHz) δ ppm 7.94 (d, 2H, 8.4 Hz), 7.88-7.79 (m, 4H), 7.58 (d, 2H, 5.4 Hz), 7.55 (d, 2H, 5.4 Hz) 4.51 (t, 2H, 7.8 Hz), 1.91 (m, 2H), 1.32-1.23 (m, 6H), 0.84 (t, 3H, 6.6 Hz). ^{13}C NMR (CDCl$_3$, 75 MHz): δ ppm 149.38, 136.02, 135.26, 133.38, 132.90, 132.38, 130.43, 129.36, 128.34, 127.98, 124.87, 124.26, 123.54, 122.97, 121.17, 118.77, 113.48, 47.00, 31.48, 31.37, 26.54, 22.87, 14.32. EI-MS (m/z): Calcd for C$_{24}$H$_{21}$N$_3$S$_2$, 415.12; Found 415 (M[+]). Anal. Calcd. for C$_{24}$H$_{21}$N$_3$S$_2$: C, 69.36; H, 5.09; N, 10.11. Found: C, 69.35; H, 5.07; N, 10.12.

Sodium 4-(1-hexyl-1H-dithieno[2',3':3,4;3'',2'':5,6]benzo[1,2-d]imidazol-2-yl)benzoate (A2):

A1 (1.6 gm, 3.85 mmole) was dissolved in ethanol and aqueous NaOH (2 mL, 3 M) was added. The mixture was refluxed for 2 h. After cooling in freezer, the sodium salt was precipitated out. The resulting solution was filtered and the precipitate was dried to afford **A2** as green solids (1.64 gm, 94%). ^{1}H NMR (D$_6$-DMSO, 300 MHz) δ ppm 8.15-8.12 (m, 3H), 8.06 (d, 1H, 5.4 Hz), 7.97-7.91 (m, 3H), 7.80 (d, 1H, 5.4 Hz), 4.55 (t, 2H, 7.2 Hz), 1.80 (m, 2H), 1.27-1.19 (m, 6H), 0.77 (t, 3H, 7.3 Hz). ^{13}C NMR (D$_6$-DMSO, 300 MHz) δ ppm 170.78, 152.22, 136.49, 135.62, 134.19, 133.22, 131.41, 131.19, 130.61, 129.91, 129.71, 129.20, 126.89, 126.50, 125.15, 122.17, 47.57, 32.15, 32.17, 26.31, 23.27, 14.96. EI-MS (m/z): Calcd for C$_{24}$H$_{21}$N$_2$NaO$_2$S$_2$, 456.09; Found 456 (M$^+$). Anal. Calcd. for C$_{24}$H$_{21}$N$_2$NaO$_2$S$_2$: C, 63.14; H, 4.64; N, 6.14. Found: C, 62.44; H, 4.96; N, 5.94.

2-(4-Nitrophenyl)-1H-phenanthro[9,10-d]imidazole:

A mixture of 4-nitrobenzaldehyde (2.1 gm, 13.89 mmole), phenanthrene-9,10-dione (2.7 gm, 12.98 mmole), ammonium acetate (30.01 gm, 389.4 mmole) and acetic acid (150 mL) was heated to 100 $^\circ$C overnight. The green solution was cooled to room temperature, and 50 mL water was added to stir for 15 mins at room temperature. The solution was filtered in a Buchner funnel. The red residue was washed thoroughly in water and hexane, dried and taken to the next step without further purification. ^{1}H NMR (D$_6$-DMSO, 300 MHz) δ ppm 13.78 (s, 1H), 8.87 (d, 2H, 8.1 Hz), 8.58 (d, 2H, 8.4 Hz), 8.55 (d, 2H, 9 Hz), 8.45 (d, 2H, 9 Hz), 7.76 (t, 2H, 7.2 Hz), 7.67 (t, 2H, 7.2 Hz). EI-MS (m/z): Calcd for C$_{21}$H$_{13}$N$_3$O$_2$, 339.10; Found 339 (M$^+$).

1-Hexyl-2-(4-nitrophenyl)-1H-phenanthro[9,10-d]imidazole:

To a solution of 2-(4-nitrophenyl)-1H-phenanthro[9,10-d]imidazole (4.05 gm, 11.93 mmole) in DMF 50 mL, K$_2$CO$_3$ (5.11 gm, 36.98 mmole) was added and heated to 95 $^\circ$C for 3 h. Then,

it was cooled to room temperature, and 1-iodohexane (2.29 mL, 3.28 gm, 15.50 mmole) was added slowly. Reaction mixture was heated to 95 °C overnight. After cooling to room temperature, the reaction mixture was poured into 300 mL water. Organic phase was extracted by ethyl acetate via repeated washing in water. Dried over $MgSO_4$, the solvent was removed under rotary evaporation. Crude product was purified by silica gel column chromatography (EA: Hexane = 5: 95) to give golden yellow solids (4.1 gm, 81.3%). ^1H NMR (CDCl$_3$, 300 MHz) δ ppm 8.84 (d, 1H, 7.6 Hz), 8.76-8.69 (m, 2H), 8.44 (d, 2H, 8.8 Hz), 8.24 (d, 1H, 7.5 Hz), 7.99 (d, 2H, 8.7 Hz), 7.71-7.64 (m, 4H), 4.64 (t, 2H, 7.5 Hz), 1.97-1.92 (m, 2H), 1.24-1.18 (m, 6H), 0.79 (t, 3H, 6.6 Hz). ^{13}C NMR (CDCl$_3$, 75 MHz) δ ppm 150.32, 148.38, 138.78, 137.60, 131.11, 129.79, 128.61, 127.78, 127.40, 127.28, 127.16, 126.24, 125.62, 124.85, 124.23, 123.44, 122.80, 121.15, 47.56, 31.30, 30.57, 26.26, 22.69, 14.16. EI-MS (m/z): Calcd for $C_{27}H_{25}N_3O_2$, 423.19; Found 423 (M$^+$). Anal. Calcd. for $C_{27}H_{25}N_3O_2$: C, 76.57; H, 5.95; N, 9.92. Found: C, 76.51; H, 5.91; N, 9.88.

4-(1-Hexyl-1H-phenanthro[9,10-d]imidazol-2-yl)aniline:

A mixture of 1-hexyl-2-(4-nitrophenyl)-1H-phenanthro[9,10-d]imidazole (2.2 gm, 5.19 mmole) and 47 mg Pd/C (10 %) was dissolved in ethanol and heated to reflux for 20 mins. To it 4.4 mL hydrazine monohydrate was added slowly. The solution mixture was further refluxed for 4 h and filtered. The filtrate was dried and the product was recrystallized to get gray solids (1.79gm, 88.1%). ^1H NMR (D$_6$-DMSO, 300MHz) δ ppm 8.90 (d, 1H, 8.1 Hz), 8.79 (d, 1H, 8.1 Hz), 8.56 (d, 1H, 7.8 Hz), 8.31 (d, 1H, 7.8 Hz), 7.70-7.57 (m, 4H), 7.39 (d, 2H, 8.4 Hz), 6.74 (d, 2H, 8.4 Hz), 5.55 (s, broad, 2H), 4.58 (t, 2H, 6.7 Hz), 1.74-1.68 (m, 2H), 1.05-0.99 (m, 6H), 0.66 (t, 3H, 6.6 Hz). ^{13}C NMR (D$_6$-DMSO, 75 MHz) δ ppm 154.72, 150.72, 145.67, 137.88, 131.52, 128.71, 127.99, 126.21, 126.15, 125.51, 125.24, 124.28, 123.81, 122.76, 121.69, 118.16, 114.34, 46.97, 31.13, 30.26, 25.92, 22.66, 14.47. EI-MS (m/z): Calcd for $C_{27}H_{27}N3$, 393.22; Found 393 (M$^+$). Anal. Calcd. for $C_{27}H_{27}N3$: C, 82.41; H, 6.92; N, 10.68. Found: C, 82.47; H, 6.88; N, 10.75.

4-(1-Hexyl-1H-phenanthro[9,10-d]imidazol-2-yl)-N,N,N-trimethylbenzenaminium iodide:

4-(1-Hexyl-1H-phenanthro[9,10-d]imidazol-2-yl)aniline (1.2 gm, 3.04 mmole) was dissolved in THF. To it an excess of iodomethane (2.5 mL) was added dropwise and stirred at 50 °C for 24 h. Further, 2mL of iodomethane was added and the reaction was continued for 48 h. at 50°C. The reaction was monitored by ESI-MS. The mixture was cooled, filtered, washed with hexane and recrystallized with THF-Et_2O to get white solids (0.94 gm, 55.2 %). ^{1}H NMR (D_6-DMSO, 300MHz) δ ppm 9.01 (d, 1H, 8.6 Hz), 8.94 (d, 1H, 7.8 Hz), 8.56 (d, 1H, 7.5 Hz), 8.46 (d, 1H, 7.6 Hz), 7.87-6.75 (m, 5H), 7.71 (d, 1H, 8.6 Hz), 7.05 (d, 1H, 8.9 Hz), 6.90 (d, 1H, 8.7 Hz), 4.72 (t, 2H, 6.6 Hz), 3.09 (s, 9 H), 1.77-1.71 (m, 2H), 1.37-1.08 (m, 6H), 0.72 (3H, t, 6.3 Hz). ^{13}C NMR (D_6-DMSO, 75 MHz) δ ppm 153.39, 150.68, 145.84, 139.47, 132.98, 132.57, 129.39, 129.28, 129.15, 128.83, 128.04, 125.66, 125.24, 125.01, 122.86, 122.73, 121.58, 121.17, 57.86, 48.29, 31.48, 31.14, 25.96, 22.67, 14.50. EI-MS (m/z): Calcd for $C_{30}H_{34}IN_3$, 563.18; Found 563 (M+). Anal. Calcd. for $C_{30}H_{34}IN_3$: C, 63.94; H, 6.08; I, 22.52; N, 7.46. Found: C, 63.22; H, 6.78; N, 7.85.
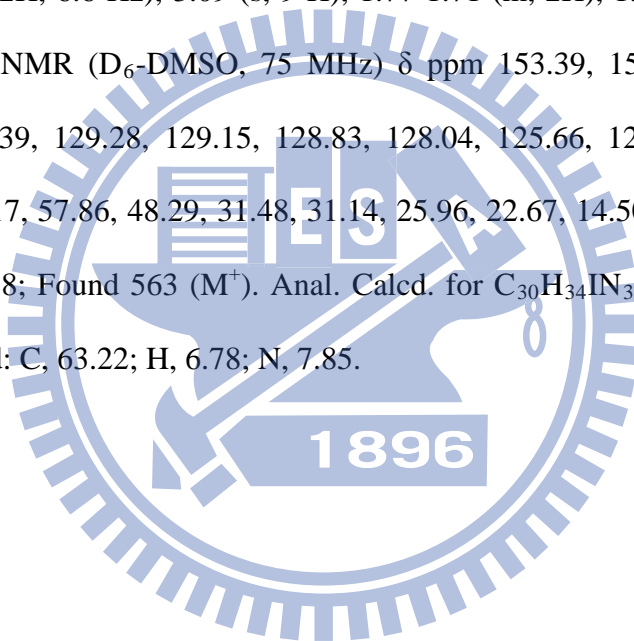
2.3 Results and Discussion

As shown in Table 2.1, the quantum yields of **M1**, **M2**, **A1** and **A2** are compared. A strong ICT occurred in **M2** due to the further electron transfer (ET) via negative inductive effect (-I effect) by the electron withdrawing quartenary ammonium salt group, reduced the quantum yield of **M2**. Unlike **M2**, back- ward ET took place in **M1** due to the positive mesomeric effect (+M effect) caused by the lone-pair of electrons on electron-donating NH_2 group and thus the ICT effect was minimized.[82c] This in turn increased the quantum yield of **M1** (0.42) significantly compared with **M2** (0.04). The electron cloud shifting can been further explained by the computational analysis (Figure 2.2). Furthermore, ICT was moderate in case of **A1** and **A2**. The COONa group in **A2** made it a weaker electron-withdrawing group than the cyanide group in **A1** due to the delocalization of electrons in the acetate group. Thus, ICT was more prominent in **A1** than **A2**. As a result, the quantum yield of **A2** (0.26) was higher than **A1** (0.16). The values of fluorescence lifetime (τ) for all compounds obtained from time-resolved fluorescence spectroscopy folowed the trend of **M1**> **A2**> **A1**> **M2** (see Table 2.1), which is in similar aggrement with the trend of the quantum yields. Thus, both fluorescence quantum yields and lifetimes are dependent on the intramolecular ICT occurring in the compounds.
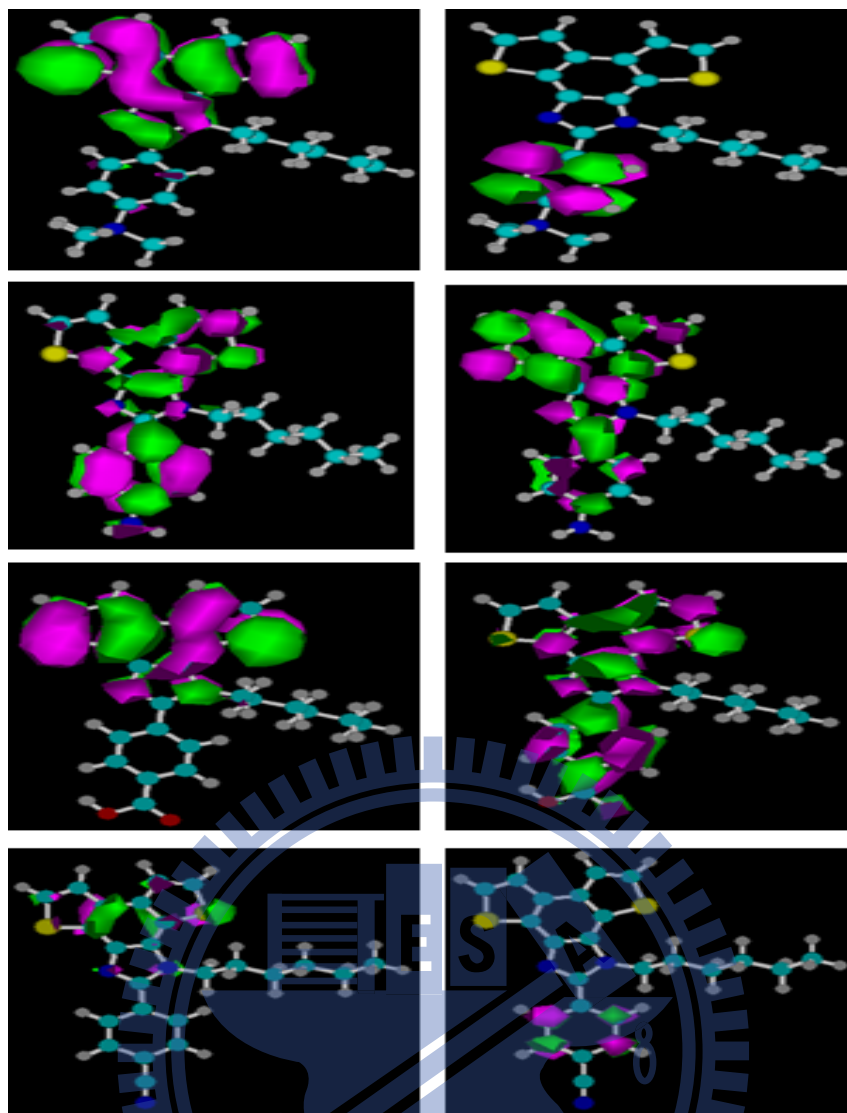
Figure 2.2 Computational analysis showing coagulation of HOMO electron clouds in the electron donating part and coagulation of LUMO electron clouds in the electron withdrawing part favouring the direction of electron flow in **M2, M1, A2** and **A1**.

Table 2.1 Photophysical properties of **M1, M2, A1** and **A2**

Compound	Φ^a	Fluorescence response[b] to Pb^{2+}	Recovery by S^{2-}	τ (ns)[c]
M1	0.42	Turn Off (1.8-fold)	No	1.85
M2	0.04	Turn On (12-fold)	Yes	0.62
A1	0.16	Turn On (5.2-fold)	Yes	0.98
A2	0.26	Turn Off (10-fold)	No	1.57

[a] quantum yields of **M1, M2, A2** (in DMSO) and **A1** (in THF), 9-10 DPA in THF as a standard ($\Phi = 0.9$); [b] **M1, M2, A2** (in DMSO/H_2O=1/1) and **A1** (in THF/H_2O=1/1); [c] fluorescence lifetimes.

44

Aqueous solutions of various metal ions, such as Na^+, K^+, Mg^{2+}, Ca^{2+}, Ba^{2+}, Ag^+, Co^{2+}, Ni^{2+}, Zn^{2+}, Cu^{2+}, Fe^{2+}, Pb^{2+} and Hg^{2+} were added to the stock solutions of **M2** and **A2**. Their effects on fluorescence signals of **M2** and **A2** (for both single and dual metal systems) were depicted in Figs. 2.3 and 2.4, respectively. Trivial fluorescent changes of **M2** were observed as other metal ions (Na^+, K^+, Mg^{2+}, Ca^{2+}, Ba^{2+}, Co^{2+}, Ni^{2+}, Zn^{2+}, Cu^{2+}, Fe^{2+} and Hg^{2+}) were added. While a noteworthy enhancement of fluorescence intensity (ca. 12-fold) in **M2** was observed in the presence of Pb^{2+} (Figure 2.5a). Whereas, **A2** showed a quenching of fluorescence (ca. 10-fold) in the presence of Pb^{2+} (Figure 2.5b). In case of **M2**, the ICT effect was further enhanced by the ET effect due to a strong electron-withdrawing quaternary ammonium salt group which in turn minimized the quantum yield of **M2**. Furthermore, upon the addition of Pb^{2+}, both obstruction of ICT and chelation-induced fluorescence enhanced the fluorescence intensity of **M2** (chelation enhanced fluorescence factor, CHEF=12),[36] and two new peaks at 403 and 451 nm appeared consequently.
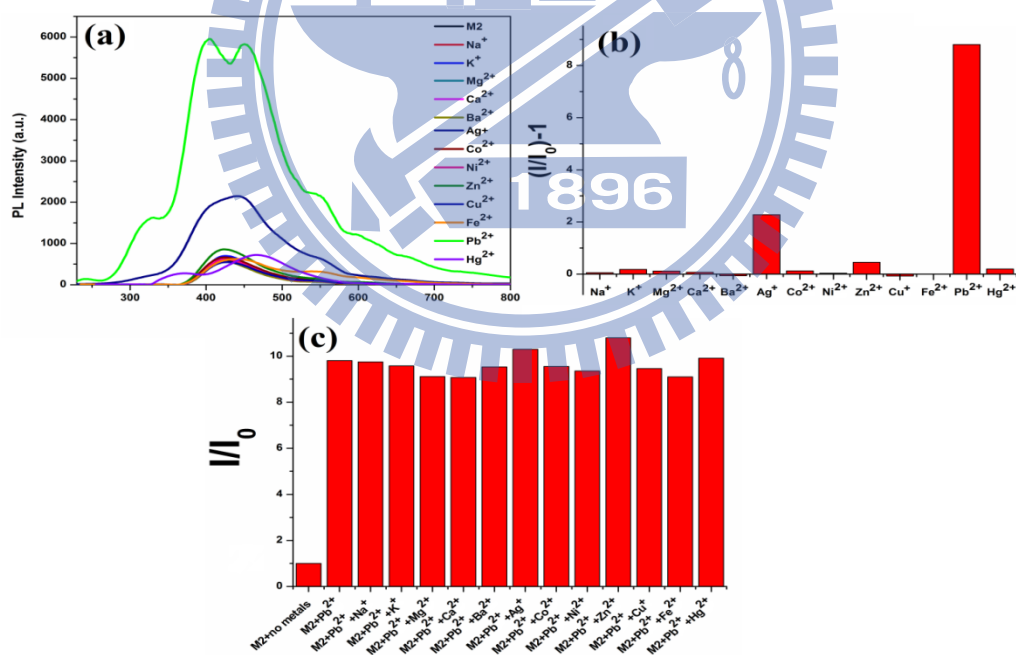
Figure 2.3 (a) Fluorescence emission spectra of **M2** (λ_{ex} = 240 nm) upon the addition of various metal ions. The concentration of **M2** (1.4×10^{-5} M) in DMSO/H_2O (1:1), metal ions added (1.5×10^{-3} M) in H_2O. (b) Histogram representing the fluorescence spectral responses of **M2** upon the addition of different metal ions. (c) Histogram representing the emission profiles of **M2** in presence of Pb^{2+} and equivalent amount of other background metal ions (Dual metal system).
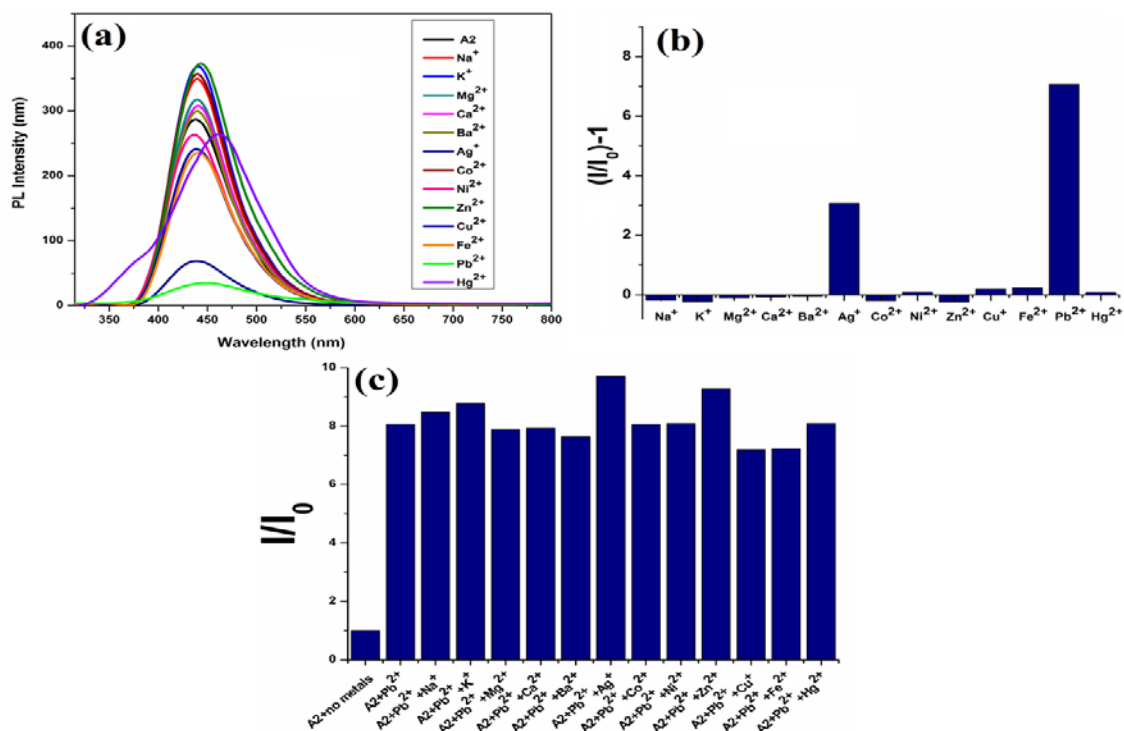
Figure 2.4 (a) Fluorescence emission spectra of **A2** (λ_{ex} = 265 nm) upon the addition of various metal ions. The concentration of **A2** (1.4×10^{-5} M) DMSO/H$_2$O (1:1), metal ions added (1.5×10^{-3} M) in H$_2$O. (b) Histogram representing the fluorescence spectral responses of **M2** upon the addition of different metal ions. (c) Histogram representing the emission profiles of **A2** in presence of Pb^{2+} and equivalent amount of other background metal ions (Dual metal system).
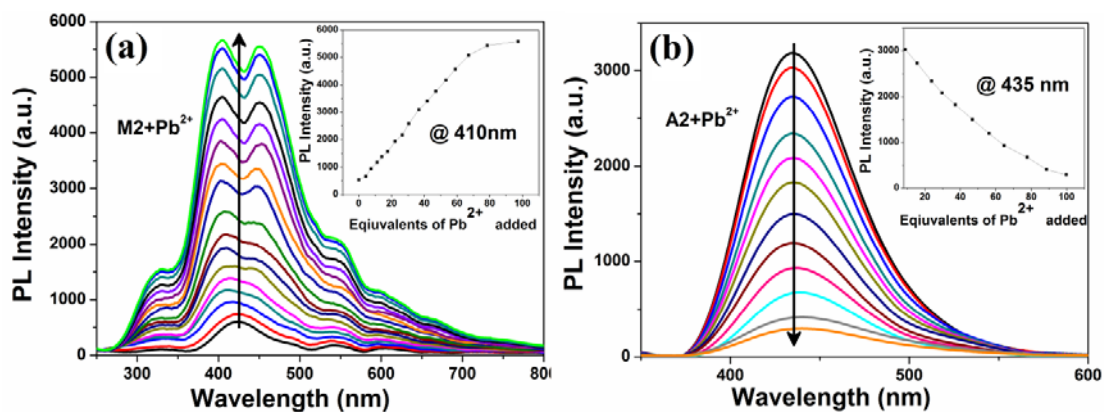
Figure 2.5 Fluorescence spectral changes of (a) **M2** (1.4×10^{-5} M) in DMSO/H_2O (1:1) (λ_{ex} = 240 nm) and (b) **A2** (1.4×10^{-5} M) in DMSO/H_2O (1:1) (λ_{ex} = 265 nm) upon titration of Pb^{2+} (0 - 1.5×10^{-3} M). Insets show PL speactral responses of (a) **M2** and (b) **A2** as a function of Pb^{2+}.

^{1}H NMR titrations with 0-1 equiv. of Pb^{2+} showed significant up-field shifts of peaks correspoding to **M2** (Figure 2.6). Absorption spectral titration of **M2** upon the addition of Pb^{2+} was depicted in figure 2.7. Job's plot for **M2** by taking the variation of the absorption at 406 nm as a function of [Pb^{2+}]/[**M2**] showed 1:1 stoichiometry and the detection limit was obtained to be 9.48 μM (Figure 2.8). Again, based on the time-resolved-fluorescence spectra (Figure 2.9a), the fluorescence lifetime of **M2** (0.62 ns) was elevated to 1.86 ns upon the addition of Pb^{2+}, which supports the turn-on mechanism. For model compound **M** (where the binding site is only the 'N' atom on imidazole ring), the ^{1}H NMR and the PL titrations did not show any significant changes even at higher concentrations of Pb^{2+} (Figure 2.10 a & b). Thus, it may be concluded that the coordination of Pb^{2+} with both 'S' and 'N' atoms occurred in dithieno-benzo-imidazole moiety of **M2**, which was the key binding site causing chelation-induced fluorescence enhancement.
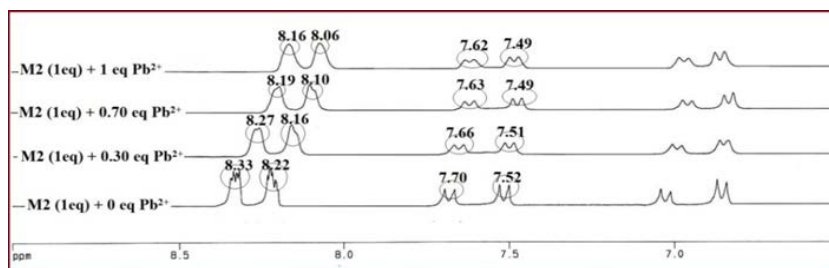
Figure 2.6 ^{1}H NMR titration of **M2** upon the addition of 0-1 equiv. of Pb^{2+}.
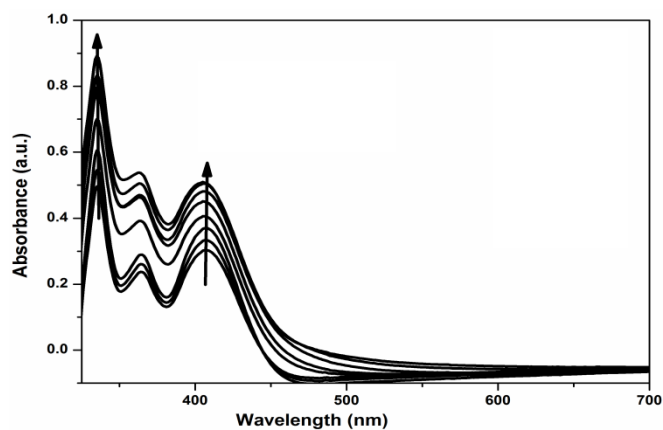
Figure 2.7 Absorption spectral titration of **M2** upon the addition of Pb^{2+} metal ions. The concentration of **M2** (1.4×10^{-5} M) DMSO/H_2O (1:1), Pb^{2+} ions added (1.5×10^{-5} M) in H_2O.
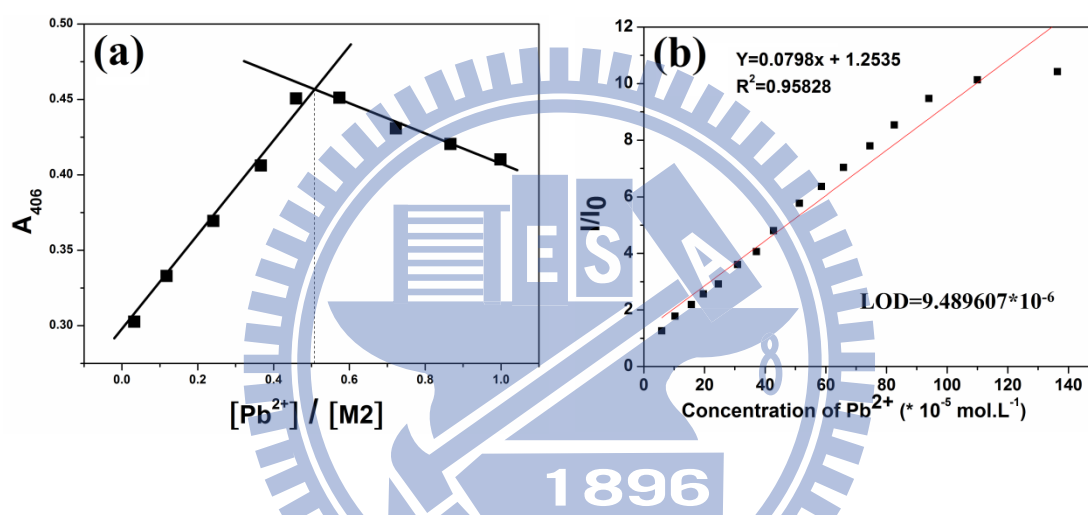
Figure 2.8 (a) Job's Plot for **M2** by plotting the variation of the absorption at 406 nm as a function of $[Pb^{2+}]/[$**M2**$]$. Total concentration of **M2**+Pb^{2+} was kept constant at 14 μM. (b) Calculation of detection limit from the linear fit equation and standard deviation.
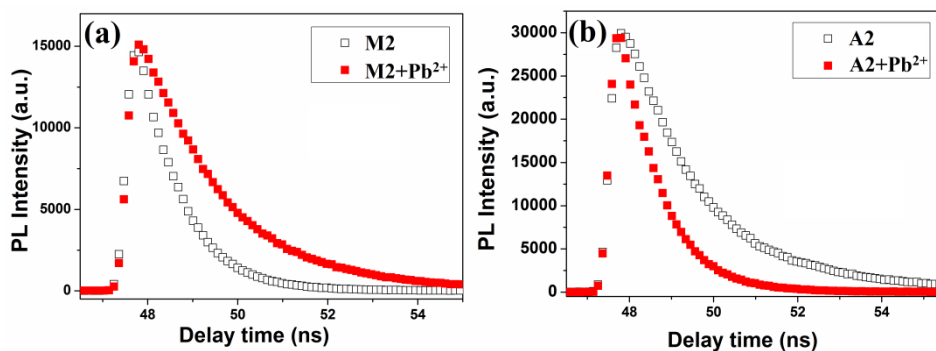
Figure 2.9 (a) Time-resolved fluorescence spectra of **M2** (empty circle), and **M2**+Pb^{2+} (solid circle); (b) **A2** (empty square) and **A2**+Pb^{2+} (solid square).
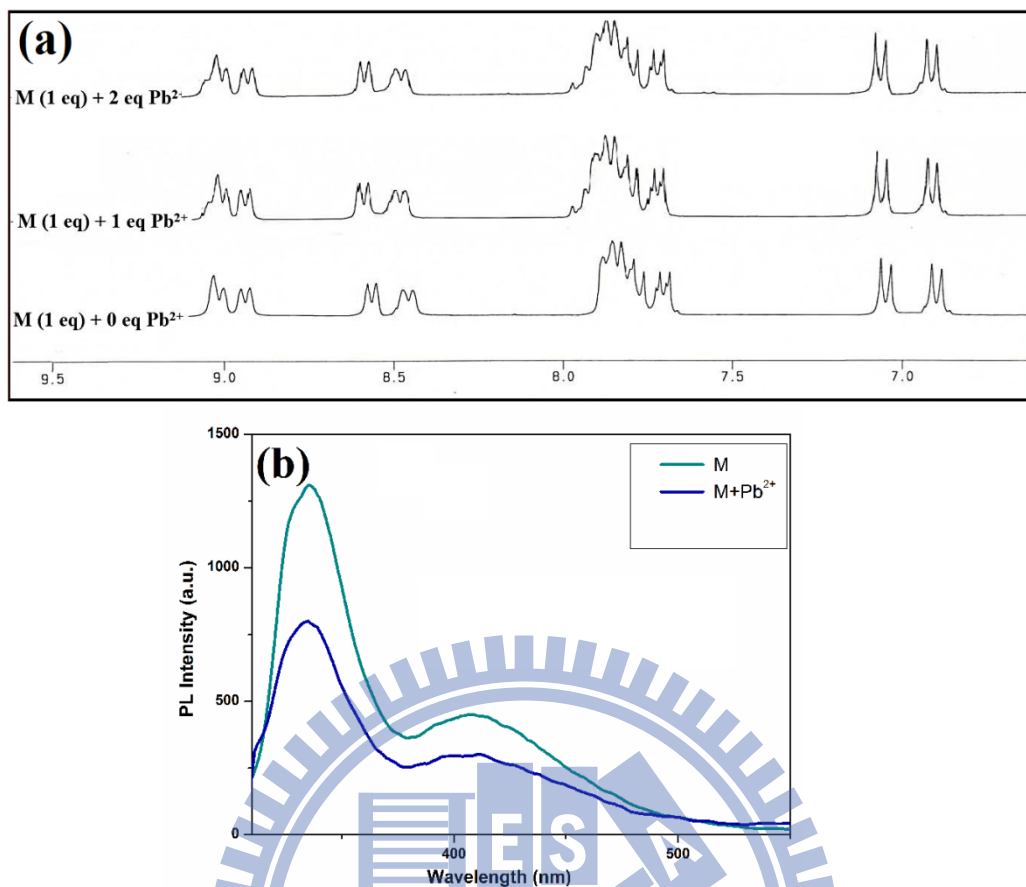
Figure 2.10 (a) ^{1}H NMR titration of **M** upon the addition of 0-2 equiv. of Pb^{2+}.(b) Fluorescence spectral changes of **M** (1.4×10^{-5} M) in DMSO/H_2O (1:1) (λ_{ex} = 290 nm) upon the addition of Pb^{2+} (1.5×10^{-3} M) in H_2O.

However, the CHEF values could be amended by the effective ICT in molecules due to their various substituents. For instance, the ICT effect on **A2** was enhanced owing to the auxiliary electron withdrawing by the COONa group. Thus, upon complexation of Pb^{2+} with **A2**, the fluorescence was expected to be enhanced due to the obstruction of original ICT. Surprisingly, the fluorescence intensity was quenched upon the addition of Pb^{2+} (Figure 2.5b), which might be attributed to the binding of the metal ions to the COO^- groups. Thus the quencher induced aggregation plays a major role while competing with obstruct of ICT causing quenching of fluorescence. Stern-Volmer plot for the fluorescence quenching of A2 indicated the binding constant of Pb^{2+} for **A2** would decrease upon increasing temperature which indicated the static quenching mechanism (Figure 2.11).[86] Furthermore, from Figure

2.9b, fluorescence lifetime of **A2** (1.57 ns) was decayed to 0.81 ns upon the addition of Pb^{2+} which was a further evidence for above quenching mechanism. As shown in Table 1 and Figure 2.12a, **A1** showed a turn-on response during sensing of Pb^{2+} similar to **M2**. However, the sensitivity of **A1** (CHEF = 5.2) was lower than that of **M2** (CHEF = 12). This is due to stronger electron
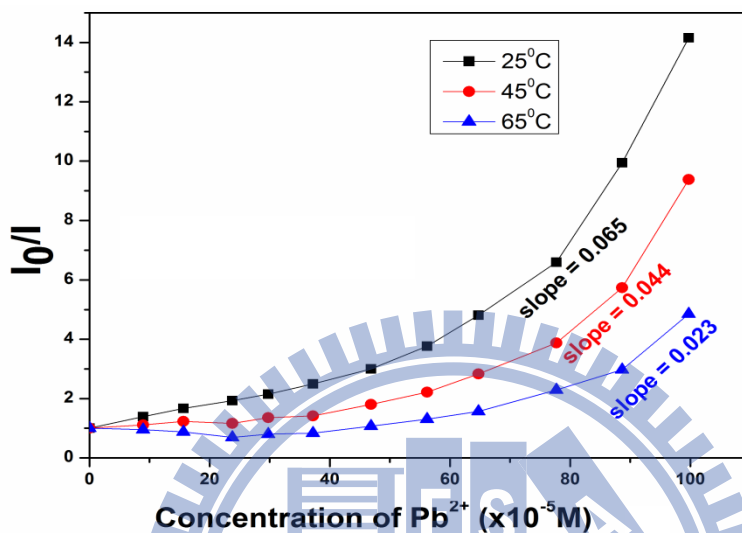
Figure 2.11 Stern-Volmer plots for the fluorescence quenching of **A2** by Pb^{2+} at 25°C, 45°C and 65°C.
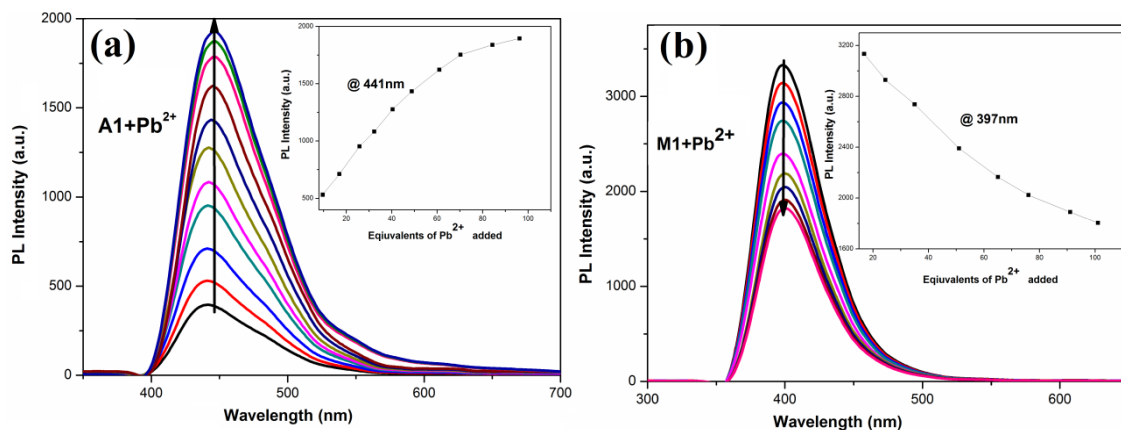
Figure 2.12 Fluorescence spectral changes of (a) **A1** (1.4×10^{-5} M) in THF/H_2O (1:1) (λ_{ex} = 240 nm) and (b) **M1** (1.4×0^{-5} M) in DMSO/H_2O (1:1) (λ_{ex} = 245 nm) upon titration with Pb^{2+} (0 - 1.5×10^{-3} M) in H_2O.

Upon complexation of Pb^{2+} with **M1**, the fluorescence intensity was quenched upon the addition of Pb^{2+}. This can be attributed to the amine group coordinated with the Pb^{2+} ions to cause further electron-withdrawal and thus to quench the fluorescence. Binding of amine group with metal ions was confirmed by proton NMR titrations (Figure 2.13). Upon the addition of 10 equivs. of Pb^{2+}, the amine peak at 5.6 ppm was completely disappeared. Peaks at 6.72, 7.48, 7.75 and 7.85 ppm in **M1** were shifted to 6.78, 7.55, 7.73 and 7.91 ppm, respectively. Similar to **A2**, upon binding to Pb^{2+}, although ICT was obstructed for **M1**, the quencher-induced aggregation played a major role to cause the fluorescence quenching.
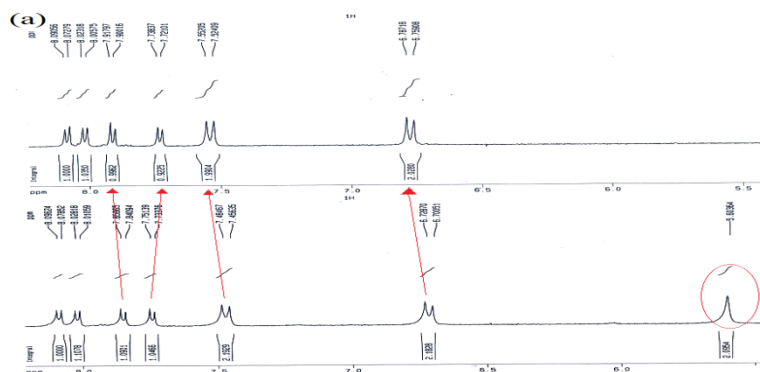
Figure 2.13 ^{1}H NMR spectra of **M1** in D_6-DMSO/D_2O=1/1 before (down) and after (up) the addition of 10 equiv. of Pb^{2+} in D_2O.

The reversibility of PL for **M2** upon binding to Pb^{2+} was investigated by further addition of different anions, for example Cl^-, HCO_3^-, HSO_3^-, HSO_4^-, I^-, NO_3^-, OH^-, PO_4^{3-}, $S_2O_3^{2-}$, SCN^- and S^{2-} (Figure 2.14). Among all these anions, the enhanced PL of **M2-**Pb complex was mainly annihilated upon the addition of diminutive amount of S^{2-} (0.1 equiv. w.r.t the concentration of **M2**). A similar result has been obtained for **A1-**Pb complex upon the addition of S^{2-}. Fluorescence titrations, by the addition of successive aliquots of S^{2-} to the solutions of **M2**-Pb and **A1**-Pb are illustrated in Figure 2.15a and 2.16a, respectively. To confirm the sensitivity of S^{2-} towards **M2**-Pb and **A1**-Pb complex, fluorescence signal response of solo **M2** and **A1** towards S^{2-} in the absence of Pb^{2+}, were conducted. As shown in Figs. S17a-b, very irrelevant changes in the fluorescence of **M2** and **A1** were observed upon the addition of even higher concentration of S^{2-} (10 equiv. w.r.t. stock solutions of **M2** and **A1**). This experiment confirmed the sensitivity of S^{2-} towards Pb^{2+} only in their metal-ligand complex state. Similarly, the effect of S^{2-} on **M1**-Pb and **A2**-Pb were tested as depicted in Figure 2.16b and Figure 2.15b, respectively. It was found that the fluorescences of the mixtures were further quenched upon the addition of S^{2-}. This can be attributed to the stronger binding of the NH_2 (in **M1**) and COONa groups (in **A2**) to metal ions which could not be cleaved by S^{2-}. The ICT was restored (in **M1/A2**) due to the breakage of imidazole 'N' and 'S' linkage with Pb^{2+}. Moreover, the additional enhancement of ICT, due to the auxiliary binding of metal ions to amine/COONa caused sheer quenching of fluorescence.
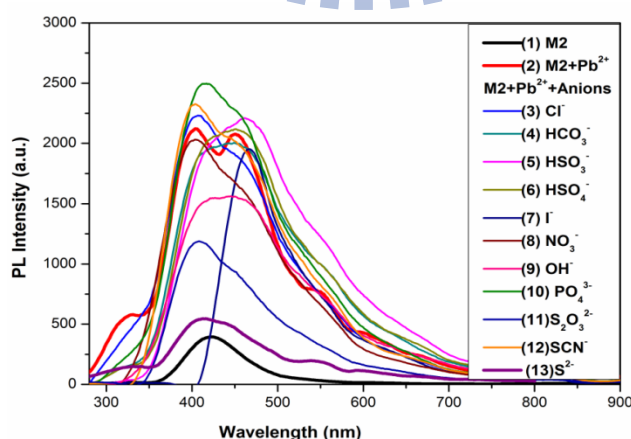
Figure 2.14 Fluorescence spectral response of **M2** (1.4×10^{-5} M) in DMSO/H_2O (1:1) (λ_{ex} = 240 nm) upon the addition of S^{2-} (1.4×10^{-6} M) and other anions (1.4×10^{-4} M) in the presence of Pb^{2+} (1.5×10^{-3} M).
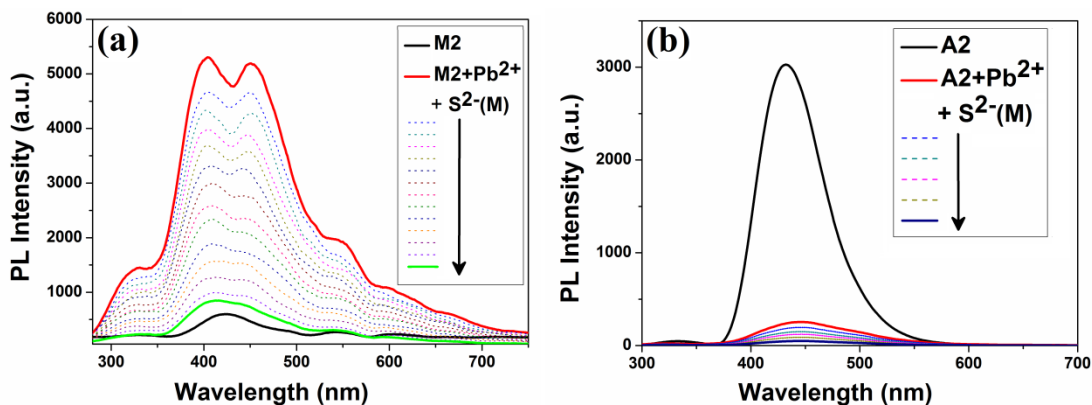
Figure 2.15 Fluoroscence recovery responses of **M2**-Pb and **A2**-Pb upon titration with 0-0.1 equiv. of S^{2-} (i.e., 0-1.4 x10^{-6} M) w.r.t the concetration of **M2/A2** (1.4x10^{-5} M) (λ_{ex} **M2** = 240 nm/**A2** = 265 nm).
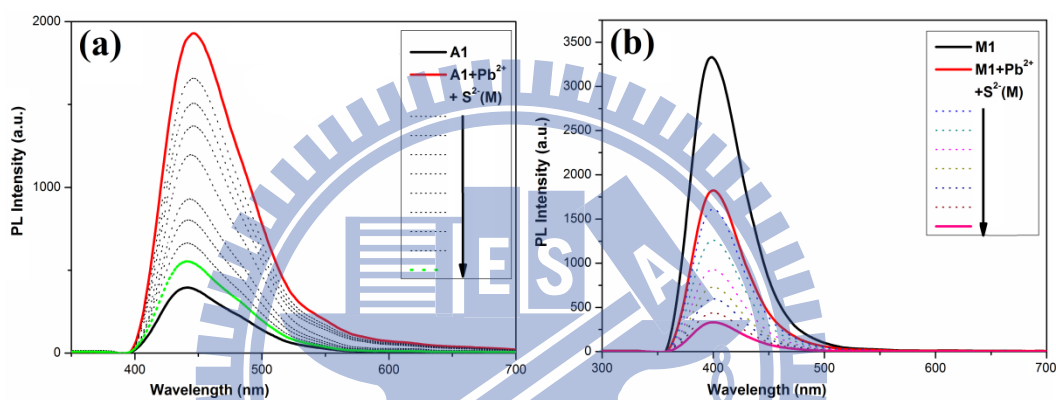
Figure 2.16 Fluorescence spectral response of (a) **A1** (1.4×10^{-5} M) in THF/H$_2$O (1:1) (λ_{ex} = 240 nm)and (b) **M1** (1.4×10^{-5} M) in DMSO/H$_2$O (1:1) (λ_{ex} = 245 nm) upon titration with S^{2-} (0 - 1.4×10^{-6} M) in the presence of Pb^{2+} (1.5×10^{-3} M).
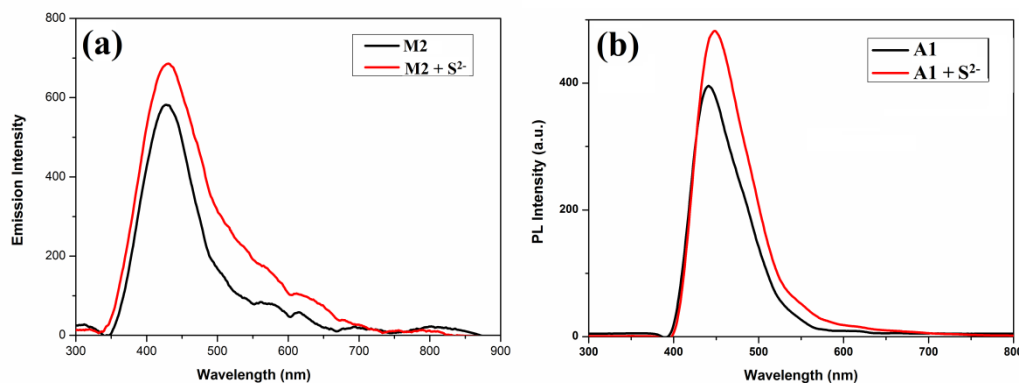
Figure 2.17 Fluorescence spectral response of (a) **M2** (1.4×10^{-5} M) in DMSO/H$_2$O (1:1) (λ_{ex} = 240 nm) and (b) **A1** (1.4×10^{-5} M) in THF/H$_2$O (1:1) (λ_{ex} = 240 nm) upon the addition of S^{2-} (1.4×10^{-5} M) in H$_2$O.

Again we observed compund **4** showed the best colorimetric and ratiometric sensing ability by F⁻ via changing the color of the solution from light yellow to dark pink and shifting of absorption maxima up to 85 nm (from 410 to 495 nm) upon the addition of 1 equiv. of F⁻ ion with respect to **4** (Figure 2.18).
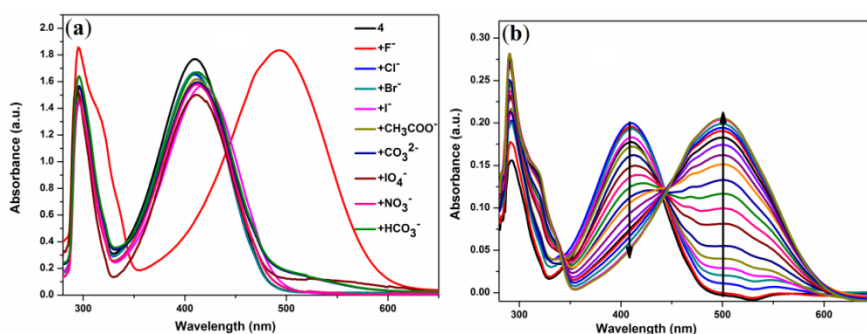
Figure 2.18 Absorption spectral response of **4** (1.4×10^{-5} M) (a) upon the addition of 1 equiv. of different anions (b) titration of **4** upon the sequential addition of F⁻ ions (0-1 equiv. w.r.t. **4**).

2.4 Conclusion:

In conclusion, two novel dithieno-benzo-imidazole-based compounds **M2** and **A2** showed remarkable sensitivity towards Pb^{2+} over the other metal ions. In case of **M2**, the fluorescence was almost 12-fold enhanced. However, the fluorescence of **A2** was quenched almost 10-fold upon titration with Pb^{2+}. Model compound phenathrene-benzo-imidazole-based **M** has almost no momentous effects during sensing of Pb^{2+}, which indicated the unique sensitivity of dithieno-benzo-imidazole-based **M2** and **A2** towards Pb^{2+} via chelation with 'S' and 'N' atoms. The quantum yields and fluorescence lifetime values followed the trend of **M1**> **A2**> **A1**> **M2**, which was in consistent with their intramolecular ICT fashion. In case of **M2** and **A1**, the obstruction of ICT induced the enhancement of fluorescence owing to the binding of thieno-imidazole unit with Pb^{2+}. However, the quencher induced aggregation played a major role in the fluorescence quenching for **A2** and **M1** due to the auxiliary binding of NH_2 and COONa with Pb^{2+}. Compared with other anions, trace amounts of S^{2-} induced reversible binding effects of Pb^{2+} with both **M2** and **A1**. Nevertheless, the reversible binding effects of Pb^{2+} by adding S^{2-} were not observed for **M1** and **A2** due to stronger binding of Pb^{2+} with NH_2 and COONa groups, respectively.

Chapter 3

Novel Thieno-Imidazole-Based Probe for Colorimetric Detection of Hg^{2+} and Fluorescence Turn-on Response of Zn^{2+}

3.1 Introduction:

Owing to the ghastly immunotoxic, genotoxic, neurotoxic, malnutrition, digestive disorder effects, mercury is considered to be a highly dangerous element in the environment, which can be easily bio-accumulated.[87] Zinc being a pervasive second most essential transition element in the human body after iron is involved in numerous biological processes, such as cellular metabolism, neurotransmission, signal transduction, gene expression, apoptosis, as well as pathological processes in many diseases (including Alzheimer's disease, epilepsy, ischemic stroke, and so forth).[88] It is thus imperative to develop analytic and detective methods for sensitive sensing of Zn^{2+} and Hg^{2+}. Unlike other biological transition metal ions, such as Fe^{2+}, Mn^{2+}, and Cu^{2+} ions, both Zn^{2+} and Hg^{2+} ions are spectroscopic or magnetic neutral and thus do not give any signals due to their $3d^{10} 4s^0$ (Zn^{2+}) and $5d^{10} 6s^0$ (Hg^{2+}) electronic configurations. Thus common analytic techniques, such as Mossbauer, nuclear magnetic resonance (NMR), and electron paramagnetic resonance (EPR), are thus inapt to detect this archetypal metal ion in biological systems. Furthermore, fluorescence offers significant advantages over other methods for these metal ions detection because of simplicity, non-destructive character, high sensitivity, and instantaneous response.[8,15,89] Consequently, non-invasive fluorescence technique emanates as a mode of choice for metal ion imagining.[4,90]

The furthermost advantage of fluorescence "turn-on" sensors related to "turn-off" sensors is the ease of detecting low-concentration contrast relative to a "dark" background which reduces the possibility of false positive signals and enhances the sensitivity, as demonstrated by numerous studies.[91] The intramolecular charge transfer (ICT) based fluorescence mechanisms has been widely used to illustrate fluorescence turn-on and turn-off behaviours for various sensory materials.[92] Furthermore, ratiometric fluorescent probes have immense significance because they permit signal ratio corresponding to more than one wavelength and provide built-in correction for environmental effects.[93] The perceived naked eye color change would be beneficial for instantaneous visual sensing.

Numerous probes have been reported for sensing of Hg^{2+}, for example, bis(N-methylindolyl)methane,[94a] aminoacid,[94b,c] indole,[94d] sulfonamide,[94e] triazole-based dansyl,[94f] methionine,[94g] and rhodamine.[94h] Likewise several probes have been designed for Zn^{2+} sensing, such as dipicolylamine,[42,9a] DPA,[9b] TPEN,[9c] and Schiff base derivatives.[9d] Since sulphur atom is considered as a ''soft'' donor atom, which can act as a chelating agent and also increase the sensor's affinity and selectivity for binding transition metal cations.

Herein, we synthesized thieno-imidazole-based polymer **P** (Scheme 3.1), with neighbouring nitrogen and sulphur hetero-atoms as chelating sites for metal ions. This was found to be a suitable design for colorimetric detection of Hg^{2+} and fluorometric detection of Zn^{2+}.
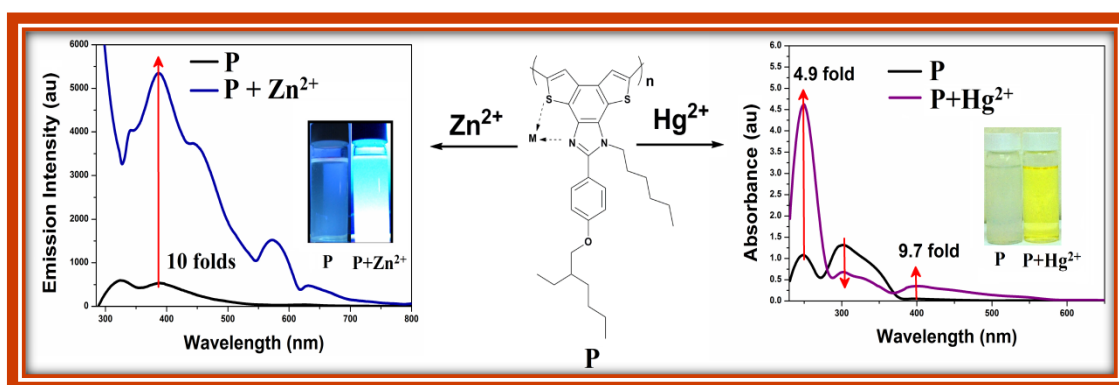
Figure 3.1 Overview of the sensing pattern for **P**.

3.2 Experimental Section:

3.2.1 Reagents, Measurements, and Characterizations. All chemicals and solvents were reagent grades and purchased from Aldrich, ACROS, TCI, Fluka, TEDIA, and Lancaster Chemical Co. THF was distilled over sodium/benzophenone to keep anhydrous before use. DMF was purified by refluxing with calcium hydride and then distilled. The solvents were degassed by nitrogen 1 h prior to use before reaction. ^{1}H-NMR and ^{13}C-NMR spectra were recorded on a Bruker DX-300 (300 MHz for ^{1}H and 75 MHz for ^{13}C) spectrometer using CDCl$_3$, THF-d$_8$ and DMSO-d$_6$ solvents. Elemental analyses were performed on HERAEUS CHN-OS RAPID elemental analyser. Solutions of **P** and **M** (1.1×10^{-3} mol/L) were prepared in THF. This stock solution was further diluted by water (v/v = 1/1) to afford a final concentration of sample solution 1.1×10^{-5} mol/L. The solutions of metal ions (1.1×10^{-3} mol/L) were prepared in distilled water. The solutions of **P** and **M** (3.0 mL) were placed in a quartz cell (10.0 mm width) and the fluorescence as well as absorption spectra were recorded.

3.2.2 Synthesis:

  Syntheis of thieno-imidazole-based polymer **P** was depicted in Scheme 3.1. 3,3'-Bithiopene was prepared from 3-bromothiophene by treating with n-BuLi and CuCl$_2$, which was further acylated without any lewis acid to produce compound **3**. Then, it was coupled with 4-((2-ethylhexyl)oxy)benzaldehyde by refluxing in the presence of acetic acid and NH$_4$OAc to get compound **4**. N-alkylation of **4** by hexyliodide and K$_2$CO$_3$ yielded compound **5**, which was brominated by NBS to get monomer **6**. Finally, grignard polymerization of monomer **6** by CH$_3$MgBr and NiDPPCl$_2$ produced polymer **P**. To compare the selectivity of polymer **P** towards metal ions, model polymer **M** (where only single-nitrogen atom in the imidazole ring is available for binding) was synthesized. Synthesis of model polymer **M** was depicted in Scheme 3.2.
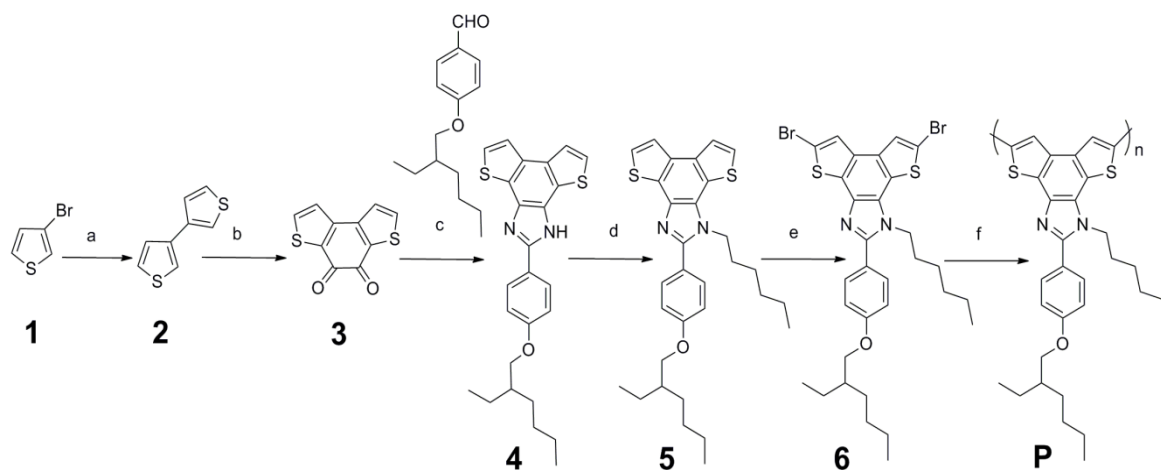
Scheme 3.1 *Reagents and conditions*: (a) n-BuLi, THF, -78 °C to -60 °C, CuCl$_2$, -60 °C to rt, 18 h, 77.9%; (b) oxalyl chloride, 1,2-DCE, 90 °C, 4 days, 64.65%; (c) NH$_4$OAc, AcOH, 100 °C, overnight; (d) 1-iodohexane, K$_2$CO$_3$, DMF, 95 °C, overnight, 88.4%; (e) NBS, THF, 95.4%; (f) n-BuMgCl, THF, 2h, Ni(dppp)Cl$_2$, 20 h, 75%.
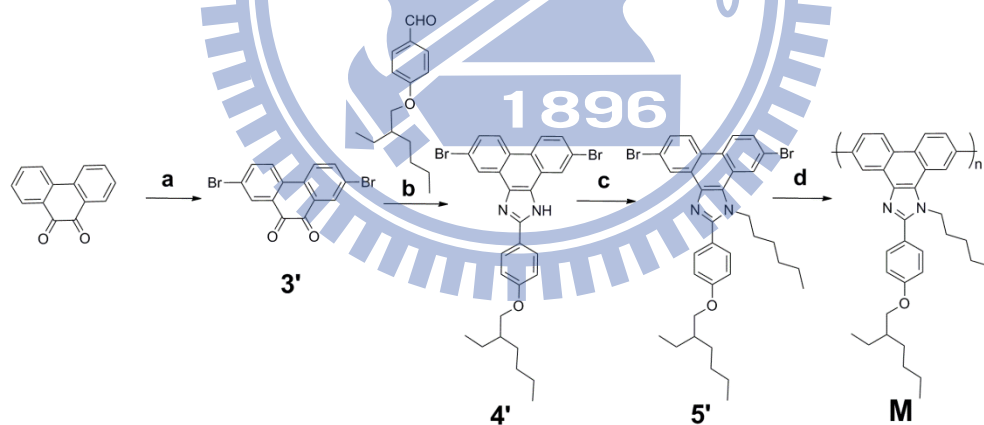
Scheme 3.2 *Reagents and conditions*: (a) NBS, conc. H$_2$SO$_4$, 3 h, rt, 76.1%; (b) NH$_4$OAc, AcOH, 100 °C, overnight; (c) 1-iodohexane, K$_2$CO$_3$, DMF, 95 °C, overnight, 85.2%; (d) n-BuMgCl, THF, 2 h, Ni(dppp)Cl$_2$, 28 h, 65.1%.

3.2.3 Synthetic Procedures:

3,3'-Bithiophene (2):

3-Bromothiophene (20 g, 0.122 mol) was dissolved in anhydrous diethyl ether (100 mL). The solution was cooled to -78 ^{o}C. To it 2.5 M n-BuLi in hexane (48.8 mL, 0.122 mol) was added dropwise for 40 mins under N_2. The reaction was allowed to stir for 10 mins at -78 ^{o}C and 20 mins at -60 ^{o}C. Then $CuCl_2$ (17.42 g, 0.130 mol) was added in one portion at -60 ^{o}C. The reaction was carefully maintained at -60 ^{o}C for another 1 hour. Then the reaction mixture was slowly warmed to room temperature and continued stirring for another 18 hours at room temperature. The reaction mixture was quenched by water (30 mL) and filtered to remove inorganic impurity. The organic phase was collected and dried in $MgSO_4$. Solvent was removed by rotary evaporation. The crude product was purified by silica gel column chromatography using hexane as eluent. The Product was obtained as white solids (7.9 g, 77.9%). ^{1}H NMR (300 MHz, $CDCl_3$): δ (ppm) 7.38 (m, 2H), 7.35 (m, 4H). ^{13}C NMR (75 MHz, $CDCl_3$): δ (ppm) 137.0, 126.1, 125.8, 119.6; EI-MS (m/z): Calcd for $C_8H_6S_2$, 165.99; Found 166 (M$^+$). ^{1}H and ^{13}C NMR were in agreement with the reported lit.[84]

Benzo[1,2-b:4,3-b$^/$]dithiophene-4,5-quinone (3):

3,3' Bithiophene (7 g, 42.10 mmol) was dissolved in of 1,2-dichloroethane (100 mL). To it oxalyl chloride (3 mL, 34.94 mmol) was added slowly. The solution was turned orange. The reaction mix was allowed to stir at 90 ^{o}C for 4 days. The reaction mix was cooled and kept at 0 ^{o}C overnight. Then the mixture was filtered. Residue product was washed thoroughly by hexane. After drying, the product obtained was red solids (6 g, 64.65%). ^{1}H NMR (300 MHz, $CDCl_3$): δ (ppm) 7.83 (d, 2H, 4.8 Hz), 7.29 (d, 2H, 4.8 Hz). ^{1}H NMR (DMSO-d$_6$): δ 8.23 (d, 2H, 4.8 Hz), 7.69 (d, 2H, 4.8 Hz). ^{13}C NMR (300 MHz, $CDCl_3$): δ (ppm) 173.5, 142.1, 138.2,

134.9, 124.5. EI-MS (m/z): Calcd for $C_{10}H_4O_2S_2$, 219.97; Found 220 (M^+). ^1H and ^{13}C NMR were in agreement with the reported lit.[85]

2-(4-((2-Ethylhexyl)oxy)phenyl)-1H-dithieno[2',3':3,4;3'',2'':5,6]benzo[1,2-d]imidazole (4):

A mixture of 4-((2-ethylhexyl)oxy) benzaldehyde[96] (4.1 g, 21.36 mmol), benzo[1,2-b:4,3-b$^/$]dithiophene-4,5-quinone (4.4 g, 19.97 mmol), ammonium acetate (38.44 g, 499.25 mmol) and acetic acid (150 mL) was heated to 100 ^{o}C for overnight. The solution was cooled to room temperature, water (50 mL) was added to it and stirred for 15 mins in rt. The solution was filtered in a Buchner funnel. The green residue was washed thoroughly in water and hexane, dried and taken to the next step without further purification. ^1H NMR (DMSO-d_6, 300MHz) δ ppm 13.44 (s, 1H), 8.13 (d, 2H, 8.4 Hz), 7.99 (d, 2H, 9.1 Hz), 7.75 (d, 2H, 4.8 Hz), 7.14 (d, 2H, 8.7 Hz), 3.95 (d, 2H, 5.7 Hz), 2.07 (m, 1H), 1.71-1.69 (m, 2H), 1.48-1.21 (m, 6H), 0.93-0.83 (m, 6H). ^{13}C NMR (300 MHz, D6-DMSO): δ 160.94, 150.55, 136.54, 134.51, 132.58, 131.80, 129.55, 128.67, 128.15, 127.05, 125.60, 124.74, 124.32, 123.24, 121.90, 115.76, 70.99, 47.40, 30.78, 29.31, 24.17, 23.39, 14.83, 11.80. EI-MS (m/z): Calcd for $C_{25}H_{26}N_2OS_2$, 434.15; found 434 (M^+).

2-(4-((2-Ethylhexyl)oxy)phenyl)-1-hexyl-1H-dithieno[2',3':3,4;3'',2'':5,6]benzo[1,2-d]imidazole (5):

To a solution of **4** (4.05 g, 9.31 mmol) in DMF (50 mL), K_2CO_3 (3.08 g, 22.34 mmol) was added and heated to 95 ^{o}C for 2 hours. Then cooled to room temperature. To it 1-iodohexane (1.8 mL, 2.58 g, 12.19 mmol) was added slowly. Reaction mixture was heated to 95 ^{o}C overnight. After cooling to room temperature the reaction mixture was poured in water (300 mL). Organic phase was extracted by ethyl acetate via repeated washing in water. Dried over MgSO$_4$, solvent was removed under rotary evaporation. Crude product was purified by silica gel column chromatography (Hexane as eluent) to give a brown solid (4.27 g, 88.4%). ^1H NMR (CDCl$_3$, 300 MHz): δ ppm 7.86 (d, 1H, 5.4 Hz), 7.79 (d, 1H, 5.4 Hz), 7.69 (d, 2H, 8.7

Hz), 7.50 (t, 2H, 5.4 Hz), 7.07 (d, 2H, 8.7 Hz), 4.36(t, 2H, 7.9 Hz), 3.94 (d, 2H, 5.7 Hz), 2.04 (m, 1H), 1.84-1.45 (m, 4H,), 1.35-1.23 (m, 12H), 0.98-0.83 (m, 9H). ^{13}C NMR (300 MHz, CDCl$_3$): δ 171.52, 160.88, 152.48, 135.70, 132.56, 131.89, 131.30, 129.30, 127.72, 124.26, 123.35, 123.29, 122.85, 122.77, 121.30, 115.12, 71.04, 46.63, 39.75, 32.22, 32.00, 29.50, 29.45, 26.43, 23.06, 22.99, 22.89, 14.56, 14.50, 11.50. EI-MS (m/z): Calcd for C$_{31}$H$_{38}$N$_2$OS$_2$, 518.24; Found 518 (M$^+$). Anal. Calcd for C$_{31}$H$_{38}$N$_2$OS$_2$: C, 71.77; H, 7.38; N, 5.40; Found: C, 72.05; H, 7.15; N, 5.13.

5,8-Dibromo-2-(4-((2-ethylhexyl)oxy)phenyl)-1-hexyl-1H-dithieno[2',3':3,4;3'',2'':5,6]benzo[1,2-d]imidazole (6):

Compound **5** (3.5 g, 7.44 mmol) was taken in THF (40 mL). To it N-bromosuccinamide (2.71 g, 15.26 mmol) was added portion wise in 10 mins intervals with continuous stirring at room temperature. Completion of reaction was monitored via TLC. After completion of the reaction, the reaction mixture was evaporated under rotary evaporation and purified by silca gel column chromatography (Hexane as eluent) to give a brown solid (4.80 g, 95.4%). ^{1}H NMR (CDCl$_3$, 300 MHz): 7.65 (d, 2H, 8.6 Hz), 7.64 (s, 1H), 7.58 (s, 1H), 7.05 (d, 2H, 8.7 Hz), 4.33 (t, 2H, 7.8 Hz), 3.93 (d, 2H, 5.7 Hz), 2.07 (m, 1H), 1.84 (m, 2H), 1.47 (m, 2H), 1.36-1.23 (m, 12H), 0.98-0.84 (m, 9H). ^{13}C NMR (300 MHz, CDCl$_3$): δ 160.63, 152.57, 134.15, 130.75, 130.44, 129.97, 129.83, 126.42, 125.38, 124.86, 121.76, 121.59, 114.75, 112.70, 111.59, 70.60, 46.19, 39.20, 31.04, 30.95, 30.38, 28.98, 25.43, 23.72, 22.95, 22.36, 14.01, 13.81, 11.02. HRMS (ESI-TOF) Calcd for C$_{31}$H$_{36}$Br$_2$N$_2$OS$_2$, 674.0615; Found 674.0611 (M$^+$). Anal. Calcd for C$_{31}$H$_{36}$Br$_2$N$_2$OS$_2$: C, 55.03; H, 5.36; N, 4.14; Found: C, 55.44; H, 5.05; N, 4.46.

Preparation of polymer P:

n-Butylmagnesium chloride (0.3 mL, 2.0 M in THF, 0.60 mmol) was added drop-wise to a solution of **6** (410 mg, 0.60 mmol) in dry THF (10 mL) under a nitrogen atmosphere. The mixture was heated under reflux for 2 hours, then transferred to a flask containing

Ni(dppp)Cl$_2$ (3.2 mg, 0.006 mmol). The solution was heated under reflux for 20 hours. The solution was precipitated into methanol and purified by Soxhlet extraction using hexanes, methanol, and chloroform. The chloroform fraction was concentrated to afford the polymer as a brown solid (236 mg, 75%). ^{1}H NMR (CDCl$_3$, 300 MHz): δ 7.71 (br, 2H), 7.65 (br, 2H), 7.06 (br, 2H), 4.38 (br, 2H), 3.93 (br, 2H), 2.00 (br, 1H), 1.87-1.25 (br, 16H), 0.95-0.85 (m, 9H). GPC: Mw =13657, PDI = 1.1.

2,7-Dibromophenanthrene-9,10-dione (3'):

Phenanthrene-9,10-dione (2.5 g, 12.0 mmol) was dissolved in 98% H$_2$SO$_4$ (20 mL) and to it NBS (4.48 g, 25.21 mmol) was added with continuous stirring. The stirring was continued at room temperature for 3 hours. The reaction mixture was poured into a tub containing crushed ice and left for 1 hour with stirring. The orange product was filtered off and washed thoroughly with water. The product was finally recrystallized in DMSO[97] to yield orange solids (3.34 g, 76.1%). M.p. 331 ^{o}C (by DSC). ^{1}H NMR (CDCl$_3$, 300 MHz): δ 8.20 (d, 2H, 8.1 Hz), 8.05 (d, 2H, 1.8 Hz), 7.94 (dd, 2H, 8.1, 1.8 Hz). EI-MS (m/z): Calcd for C$_{14}$H$_6$Br$_2$O$_2$, 363.87; Found 364 (M$^+$).

5,10-Dibromo-2-(4-((2-ethylhexyl)oxy)phenyl)-1H-phenanthro[9,10-d]imidazole (4'):

A mixture of 4-((2-ethylhexyl)oxy) benzaldehyde (2.1 g, 8.97 mmol), 2,7-dibromophenanthrene-9,10-dione (3.1 g, 8.46 mmol), ammonium acetate (16.9 g, 219.96 mmol) and acetic acid (80 mL) was heated to 100 ^{o}C overnight. The solution was cooled to room temperature. Water (50 mL) was added to it and stirred for 15 mins in rt. The solution was filtered in a Buchner funnel. The gray residue was washed thoroughly in water and hexane, dried and taken to the next step without further purification. ^{1}H NMR (DMSO-d$_6$, 300 MHz): δ 13.13 (s, 1H), 8.57 (s, 2H), 8.45 (d, 2H, 8.8 Hz), 8.14 (d, 2H, 8.3 Hz), 7.51 (t, 2H, 8.4 Hz), 7.04 (d, 2H, 8.3 Hz), 3.81 (d, 2H, 4.0 Hz), 1.90 (m, 1H), 1.59-1.52 (m, 2H),

1.42-1.20 (m, 6H), 0.85-0.78 (m, 6H). EI-MS (m/z): Calcd for $C_{29}H_{28}Br_2N_2O$, 578.06; Found 578 (M^+).

5,10-Dibromo-2-(4-((2-ethylhexyl)oxy)phenyl)-1-hexyl-1H-phenanthro[9,10-d]imidazole (5'):

To a solution of 5,10-dibromo-2-(4-((2-ethylhexyl)oxy)phenyl)-1H-phenanthro[9,10-d]imidazole (4.2 g, 7.23 mmol) in DMF (50 mL), K_2CO_3 (3.08 g, 17.35 mmol) was added and heated to 95 ^{o}C for 2 hours. Then cooled to room temperature. To it 1-iodohexane (1.5 mL, 2.14 g, 10.12 mmol) was added slowly. Reaction mixture was heated to 95 ^{o}C overnight. After cooling to room temperature the reaction mixture was poured in water (300 mL). Organic phase was extracted by ethyl acetate via repeated washing in water. Dried over $MgSO_4$, solvent was removed under rotary evaporation. Crude product was purified by silica gel column chromatography (Hexane as eluent) to give a light yellow liquid (4.09 g, 85.2%). ^{1}H NMR (CDCl$_3$, 300 MHz): δ ppm 8.93 (d, 1H, 2.07 Hz), 8.61 (d, 1H, 9.01 Hz), 8.47 (d, 1H, 8.91 Hz), 8.35 (d, 1H, 1.83 Hz), 7.70-7.61 (m, 4H), 7.09 (d, 2H, 8.66 Hz), 4.51 (t, 2H, 6.13 Hz), 3.95 (d, 2H, 5.79 Hz), 1.93-1.68 (m, 3H), 1.66-1.58 (m, 2H), 1.38-1.27 (m, 12H), 0.96-0.86 (m, 9H). ^{13}C NMR (300 MHz, CDCl$_3$): δ 160.53, 155.32, 131.05, 128.41, 127.31, 126.62, 125.80, 125.51, 125.00, 125.42, 124.39, 124.33, 123.07, 122.32, 122.76, 121.80, 121.04, 114.67, 70.56, 46.57, 39.22, 31.30, 28.99, 25.27, 22.96, 22.41, 13.87, 13.80, 11.01. HRMS (ESI-TOF) Calcd for $C_{35}H_{40}Br_2N_2O$, 662. 1504; Found 662.1555 (M^+). Anal. Calcd for $C_{35}H_{40}Br_2N_2O$: C, 63.26; H, 6.07; N, 4.22; Found: C, 63.53; H, 6.41; N, 4.01.

Preparation of polymer M:

n-Butylmagnesium chloride (0.39 mL, 2.0 M in THF, 0.78 mmol) was added drop-wise to a solution of **6** (520 mg, 0.78 mmol) in dry THF (10 mL) under a nitrogen atmosphere. The mixture was heated under reflux for 3 hours, then transferred to a flask containing Ni(dppp)Cl$_2$ (4.16 mg, 0.0078 mmol). The solution was heated under reflux for 20 hours. The solution was precipitated into methanol and purified by Soxhlet extraction using hexanes,

methanol, and chloroform. The chloroform fraction was concentrated to afford the polymer as a brown solid (254 mg, 65.1%). ^{1}H NMR (CDCl$_3$, 300 MHz): δ 8.99 (br, 2H), 8.61-8.25 (br, 4H), 7.57 (br, 2H), 7.07 (br, 2H), 4.34 (br, 2H), 3.92 (br, 2H), 2.01 (br, 1H), 1.78-1.31(m, 16H), 0.97-0.84 (m, 9H). GPC: Mw =15107, PDI = 1.24.

3.3 Result and Discussion:

To verify the sensing abilities of metal ions, polymer **P** was titrated over a wide range of metal ions, such as Na$^+$, K$^+$, Ba^{2+}, Ca^{2+}, Ni^{2+}, Cu$^+$, Co^{2+}, Ag$^+$, Zn^{2+}, and Hg^{2+} (Figure 3.1). Originally, two absorption maxima at 248 and 303 nm appeared in polymer **P**. Upon the sequential addition of Hg^{2+}, a significant change in absorption pattern was observed. As shown in Figure 3.2a, the final intensities of peak at 248 nm increased ca. 4.9 folds and peak at 303 nm decreased ca. 50%. Furthermore, a new peak appeared at 395 nm and increased almost 9.7 folds. Two clear isosbestic points at 281 and 367 nm were obtained upon titration with Hg^{2+}. The intensities at 305 and 248 nm (Figure 3.2b) as well as 395 and 305 nm (Figure 3.2c) were compared, which showed the intensity changes almost linearly with the concentration of Hg^{2+}. The color of polymer solution changed from colorless to yellow which could be easily detected by the naked eye. However, other metal ions could not show such alteration in absorption pattern. Job's plot was plotted to find the stoichiometry during the binding of Hg^{2+} (Figure 3.3).
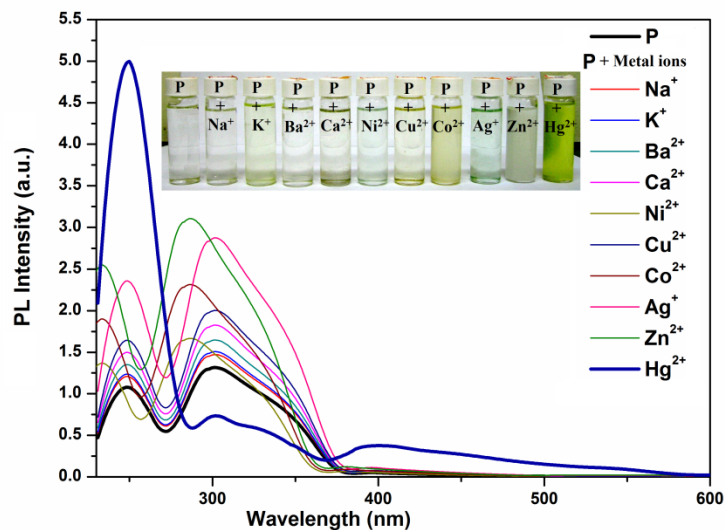
Figure 3.1 Absorption spectral response of polymer **P** $(1.1 \times 10^{-5}$ M) in THF/H$_2$O:(1/1) acquired by the sequential addition of 0-10 equiv of different metal ions. Inset: Photographs of solution of polymer **P** upon the addition of various metal ions.
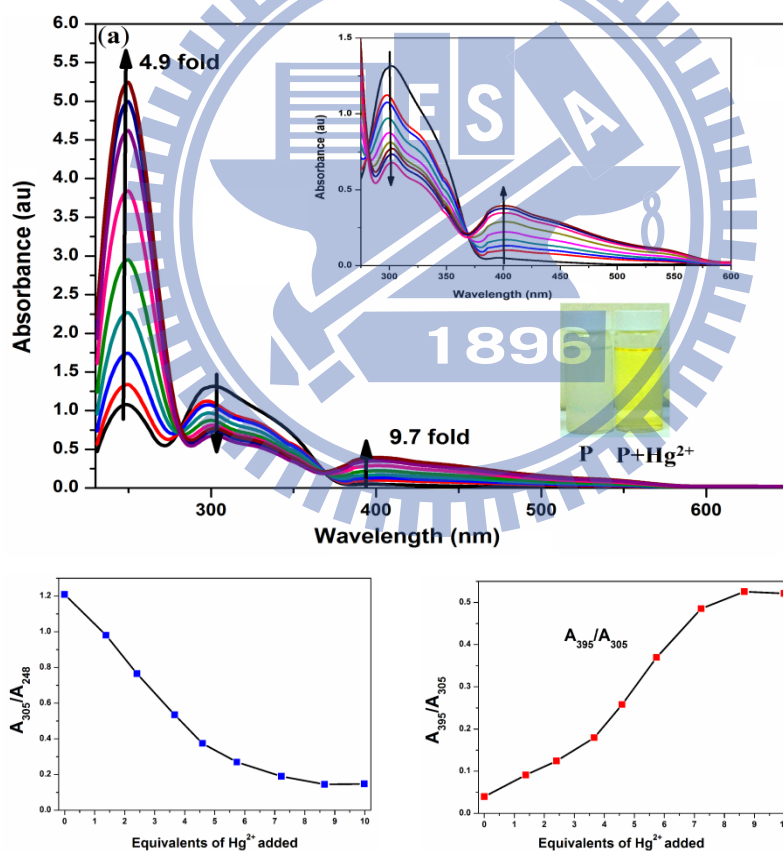
Figure 3.2 (a) Absorption spectral changes of **P** $(1.1 \times 10^{-5}$ M) in THF/H$_2$O (1:1) upon titration with $(0-1.1 \times 10^{-4}$ M) of Hg^{2+}. Upper inset: absorption pattern from 275 to 600 nm. Lower inset: color change upon the addition of Hg^{2+} (b) Absorption spectral ratio A$_{305}$/A$_{248}$ and (c) Absorption spectral ratio A$_{395}$/A$_{205}$ as a function of equiv of Hg^{2+} added.
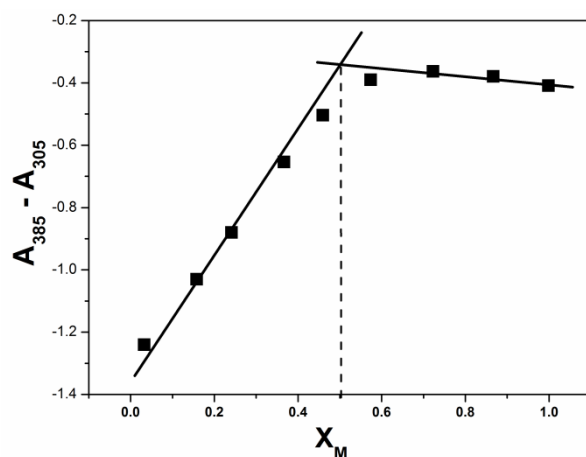
Figure 3.3 Job's plot for polymer **P** plotting the variation of the difference in absorption (A_{385}-A_{305}) as a function of molar ratio X_M = [Hg^{2+}]/{[Hg^{2+}]+ [P] showed 1:1 stoichiometry.

The variation of absorption intensities at 385 and 305 nm (A_{385}-A_{305}) as a function of molar ratio X_M = [Hg^{2+}]/{[Hg^{2+}] + [**P**]} showed 1:1 stoichiometry. ^{1}H NMR titration was further conducted to elucidate the binding mode, and the NMR titration spectra of monomer **6** (in d-THF) upon the addition of 0-1.1 equiv of Hg^{2+} (in D$_2$O) are depicted in Figure 3.4. Notable down-field shifts of peaks corresponding to the aromatic protons of monomer **6** were observed upon the gradual addition of Hg^{2+}. However, no further changes in ^{1}H NMR signals were observed at higher equiv of Hg^{2+}. This result is consistent with 1:1 binding stoichiometry of Hg^{2+} with polymer **P**. However, no further changes in ^{1}H NMR signals were observed at higher equiv of Hg^{2+}. This result is consistent with 1:1 binding stoichiometry of Hg^{2+} with polymer **P**. The binding constant for binding of Hg^{2+} was calculated to be 0.74 × 10^5 from Figure 3.5.
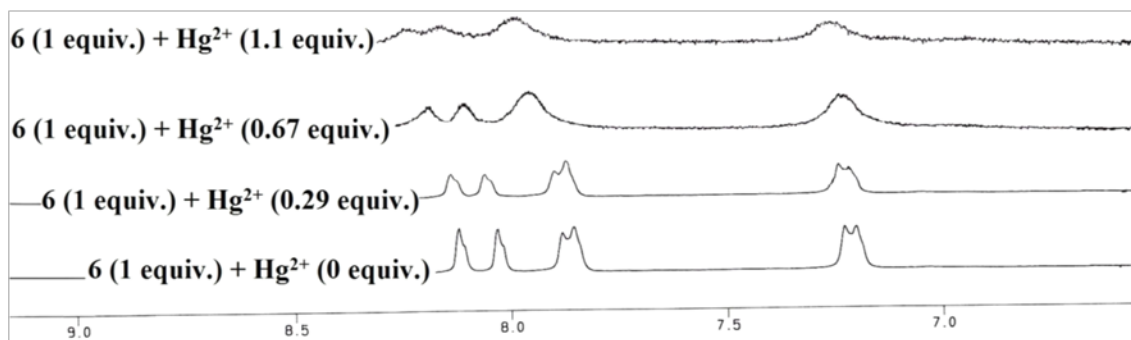
Figure 3.4 ^{1}H NMR spectra (aromatic region) of monomer **6** upon the addition of 0-1.1 equiv of Hg^{2+} w.r.t. [**6**].
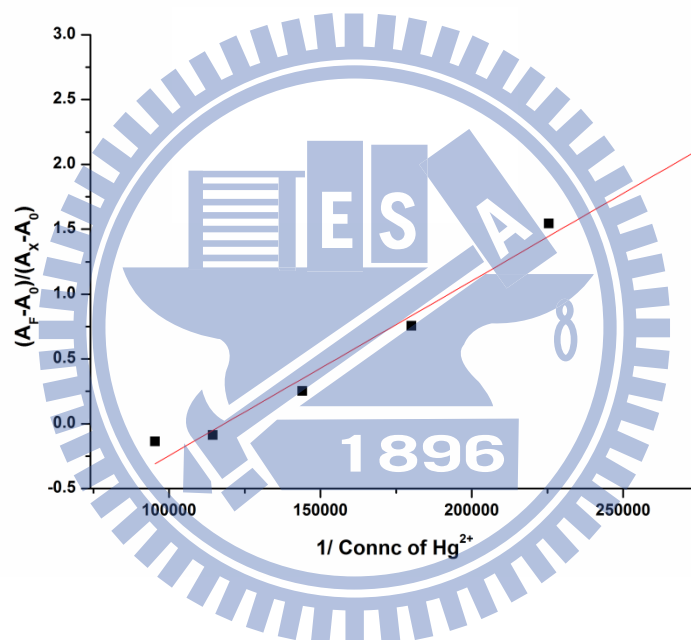
Figure 3.5 Calculation of binding constant for Hg^{2+} with polymer **P** from the plot (A$_F$-A$_0$)/(A$_X$-A$_0$)Vs 1/ [Hg^{2+}].

(The binding constant for the P-Hg complex was determined from the absorbance intensities recorded at different Hg^{2+} following the modified Benesi-Hildebrand equation 1/ΔA = 1/ΔA$_{max}$ + (1/k[C]) (1/ΔA$_{max}$).[98] Here ΔA = A$_x$ - A$_0$ and ΔA$_{max}$ = A$_F$ - A$_0$ where A$_0$, A$_x$ and A$_F$ are the intensities of the P-Hg complex at 395 nm considered in the absence of Hg^{2+}, at a certain concentration of Hg^{2+} and at a concentration of complete interaction respectively; k is the binding constant and [C] is the concentration of Hg^{2+}).

Model polymer **M** (where the binding site is only nitrogen hetero-atom in the imidazole ring) showed two absorption maxima at 267 and 290 nm. Polymer **M** was titrated with Hg^{2+} under the similar condition as that of polymer **P**. However, unlike polymer **P**, no additional peak appeared and the absorption pattern was not changed substantially (Figure 3.6). This may be attributed to the susceptibility of Hg^{2+} to be bound between 'S' and 'N' of thieno-imidazole unit in polymer **P**. Thus, it is concluded that the thieno-imidazole-based probe is a suitable design for the colorimetric detection of Hg^{2+}.
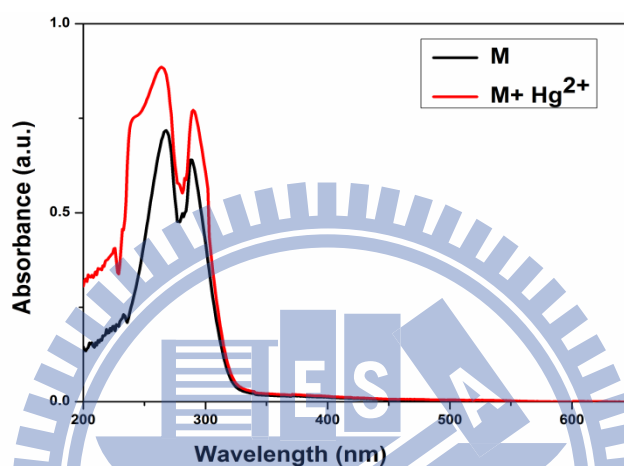
Figure 3.6 Absorption spectral response of polymer **M** (1.1×10^{-5} M) in THF/H_2O: (1/1) acquired by the addition of 10 equiv of Hg^{2+}.

Similarly, the fluorescence patterns of polymer **P** upon the addition of various metal ions under similar conditions are depicted in Figure 3.7 and their histograms are shown in Figure 3.8. As observed in Figure 3.9, upon the addition of Zn^{2+}, the fluorescence intensity increased ca. 10 folds, which was the most significant change in fluorescence signals compared with the other metal ions. The lone-pair electrons in the thieno-imidazole receptor undergo rapid electron transfer which causes the week fluorescence of **P**. In the presence of suitable cationic analytes (here Zn^{2+}), the non-bonding electrons get coordinated and thus the ICT effect is inhibited which resulted in the strong fluorescence of **P**. Thus, in the presence of Zn^{2+}, it showed a remarkable increase in the intensity of the emission band with a chelation enhanced fluorescence factor (CHEF) = 10.5. Again, it resulted in a 14.3-fold enhancement of the quantum yield for polymer **P** (from $\Phi = 0.03$ to $\Phi = 0.43$). From the fluorescence binding

isotherm, the association constant was calculated to be $K_a = 5.14 \times 10^6$ M^{-1}. To find the interference of other back ground cations, we conducted the titrations by taking dual metal system (Figure 3.10). The enhanced fluorescence of polymer **P** in the presence of Zn^{2+} was not substantially perturbed by the background cations. To get insight into the binding of Zn^{2+} with the repeating unit of **P**, ^{1}H NMR titration was carried out by the gradual addition of Zn^{2+}(in D$_2$O) to monomer **6** (in *d*-THF). As shown in Figure 3.11, a momentous up-field shift of peaks corresponding to the aromatic protons of monomer **6** was observed upon the sequential addition of Hg^{2+} (0-1.1 equiv).
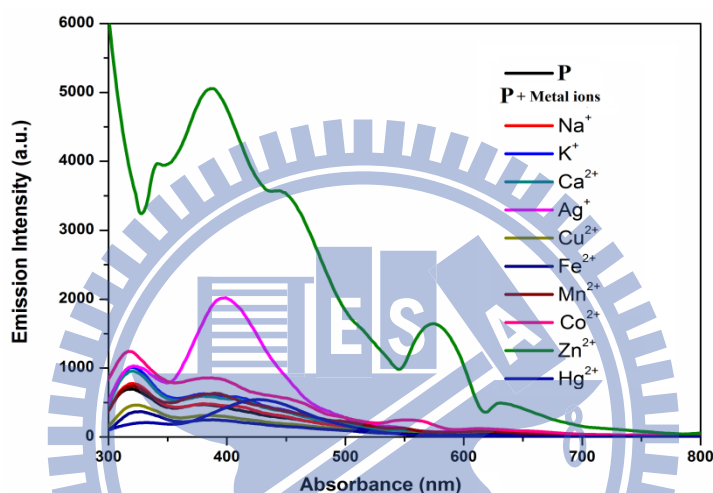
Figure 3.7 Fluorescence spectral response of polymer **P** (1.1×10^{-5} M) in THF/H$_2$O:(1/1) acquired by the addition of 0-10 equiv of different metal ions.
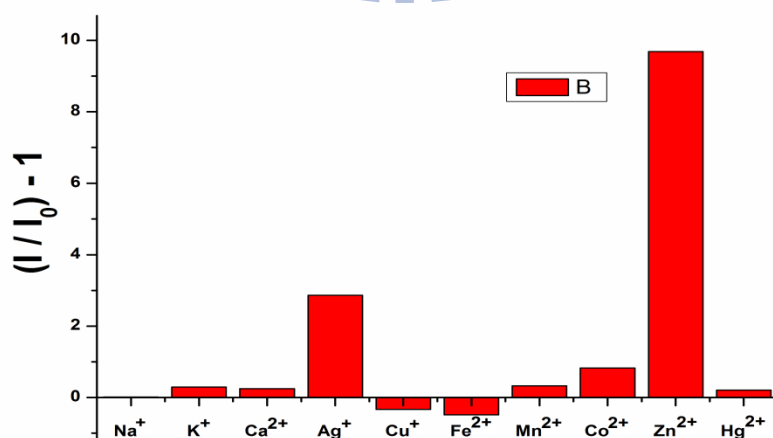
Figure 3.8 Histograms representing the fluorescence spectral responses of polymer **P** upon the addition of 10 equiv of different metal ions.
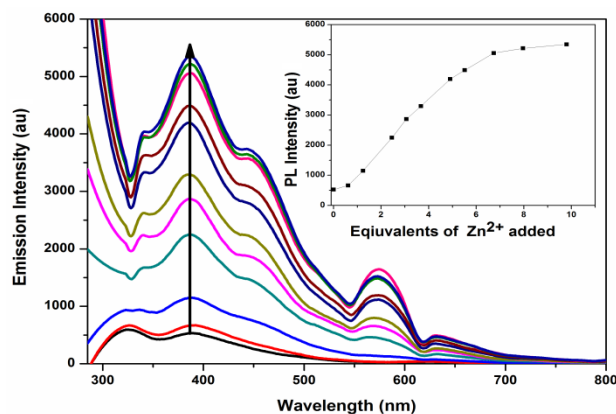
Figure 3.9 Fluorescence spectral response of P (1.1×10^{-5} M) in THF/H$_2$O:(1/1) acquired by the sequential addition of 0-10 equiv of Zn^{2+}. Inset: Intensity of P as a function of equiv of Zn^{2+} added.
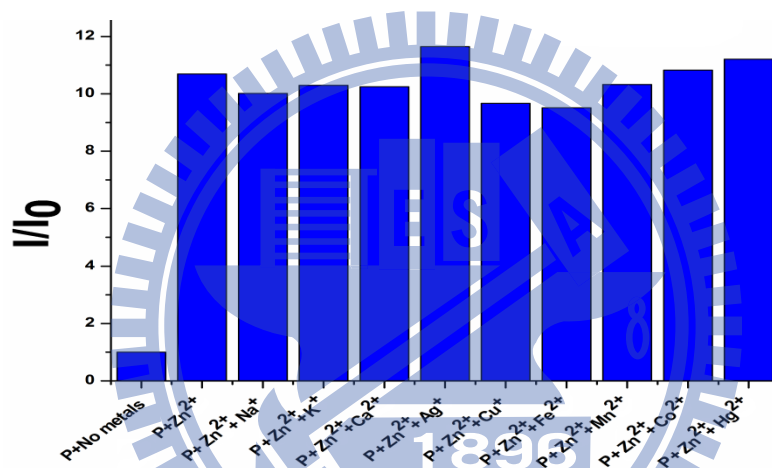
Figure 3.10 Fluorescence emission response profiles (I/I$_0$) of polymer **P** in THF/H$_2$O:(1/1). The polymer concentration (1.1×10^{-5} M), [Zn^{2+}] = 1.1×10^{-4} M and in the presence of other metal ions = 1.1×10^{-4} M. (Dual metal system).
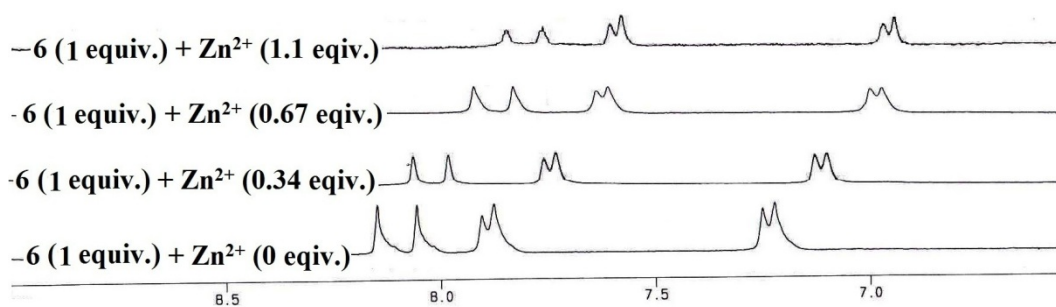
Figure 3.11. ^{1}H NMR spectra (aromatic region) of monomer **6** upon the addition of 0-1.1 equiv of Zn^{2+} w.r.t. [**6**].

70

Fluorometric titration of Zn^{2+} was conducted for model polymer **M** to investigate the effect of Zn^{2+}. Model polymer **M** did not show any significant fluorescence enhancement in the presence of Zn^{2+} under similar conditions (see Figure 3.12). As shown in Table 3.1, the quantum yield of **M** revealed only 2.25-fold increase (from $\Phi = 0.04$ to $\Phi = 0.09$), and correspondingly the CHEF was increased just up to 2.2 times. Furthermore, the association constant of polymer **P** with Zn^{2+} was calculated as 5.14×10^6 which is almost 3.8×10^3 times higher than that of polymer **M**. To elucidate the effect of polymerization, we further carried out the fluorescence titration of compound **5** with Zn^{2+}. Upon the addition of equivalent amounts of Zn^{2+}, the fluorescence intensities of compound **5** were sequentially increased merely up to 4 times (Figure 3.13). Thus, in contrast to the small molecular analogue **5** (CHEF = 3.8), the increased sensitivity of polymer **P** (CHEF = 10.5) is due to the molecular ion effect with a larger number of binding sites in polymer **P**.
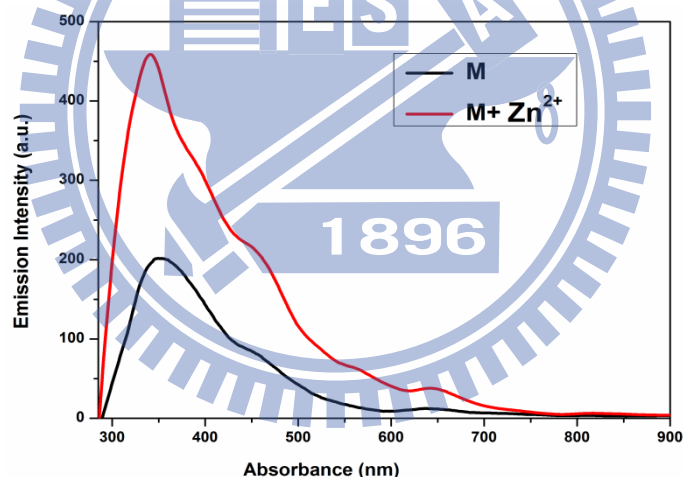
Figure 3.12. Fluorescence spectral response of polymer **P** (1.1×10^{-5} M) in THF/H$_2$O:(1/1) acquired by the addition of 10 equiv of Zn^{2+}.

Table 3.1 Quantum Yields, Fluorescence Lifetimes, Association Constants, and CHEF Values of Polymers **P** and **M** upon the Addition of Zn^{2+}.

	Φ^a	Lifetime[b]	$K_a{}^c$	CHEF[d]
P	0.03	0.49	NA	NA
P+Zn²⁺	0.43	2.96	5.14×10^6	10.5
M	0.04	0.34	NA	NA
M+Zn²⁺	0.09	0.37	1.35×10^3	2.26

[a] Quantum yields calculated using tryptophan (in H_2O) as a standard. [b] Obtained from time resolved fluorescence measurements. [c] Association constants calculated from the slopes of binding isotherms. [d] CHEF is defined as I/I_0, where I is the maximum emission intensity of the receptor-metal complex and I_0 is the maximum emission intensity of the free receptor.
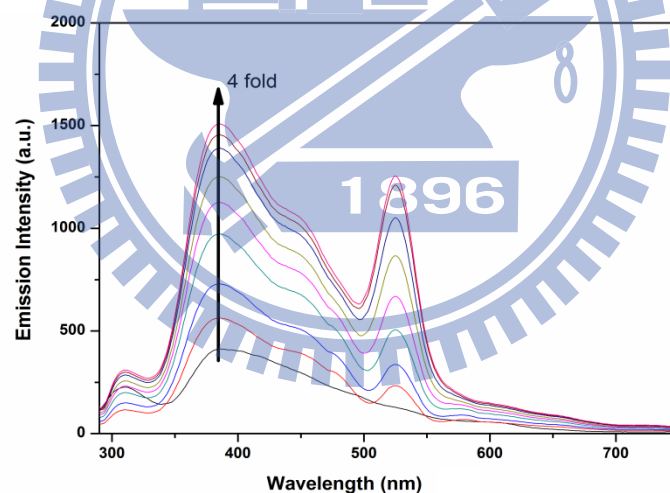
Figure 3.13 Fluorescence spectral response of monomer **5** (1.1×10^{-5} M) in THF/H_2O:(1/1) acquired by the sequential addition of 0-10 equiv of Zn^{2+}.

Time resolved fluorescence measurements were performed for both polymer **P** and its Zn^{2+}-complex probed at 390 nm (excited at 375 nm), as shown in Figure 3.14. In the absence of Zn^{2+}, a single exponential fitting for the fluorescence lifetime of polymer **P** was estimated as 0.49 ns, which corresponded to the lifetime of the S1 state. Upon the addition of Zn^{2+}, the

fluorescence lifetime corresponding to the S1 state was elevated to 2.96 ns. No remarkable change in fluorescence life time of model polymer **M** was observed under similar conditions (see Table 3.1 and Figure 3.15).
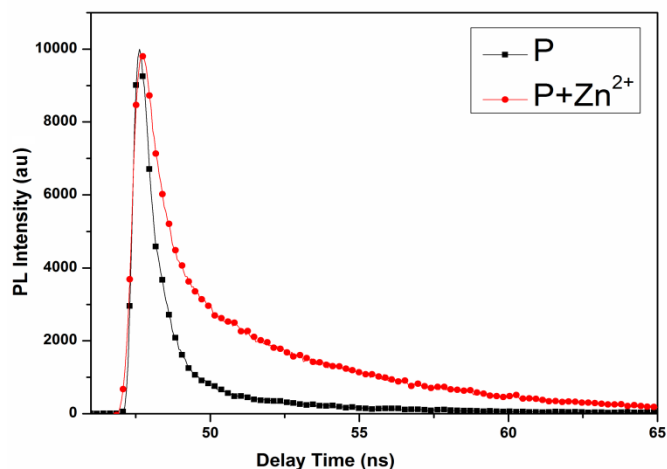
Figure 3.14. Time resolved fluorescence spectral responses for polymer **P** before and after the addition of Zn^{2+}.
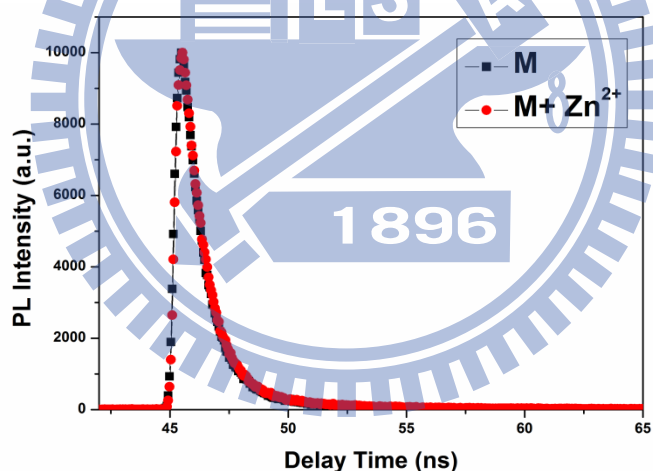
Figure 3.15 Time resolved fluorescence spectral responses for polymer **M** before and after the addition of Zn^{2+}.

Upon the progressive addition of Zn^{2+}, two oxidation peaks Ox_1 and Ox_2 of polymer **P** were anodically shifted and disappeared, respectively (see Figure 3.16), and the half-wave oxidation potential ($E_{1/2}$) of Ox_1 (appeared at 1520 mV originally) was shifted to 1200 mV with $\Delta E_{1/2} = 320$ mV. This indicated a less favourable oxidation process for polymer **P** due to

the presence of close proximity of a positively charged Zn cation center. Furthermore, the HOMO level of polymer **P** was lowered (from -5.36 to -5.56) and its LUMO level was increased (from -3.92 to -3.42) after complexation with Zn^{2+}. Thus, the obstruction of the reductive as well as oxidative ICT caused the enhancement of the fluorescent intensity.
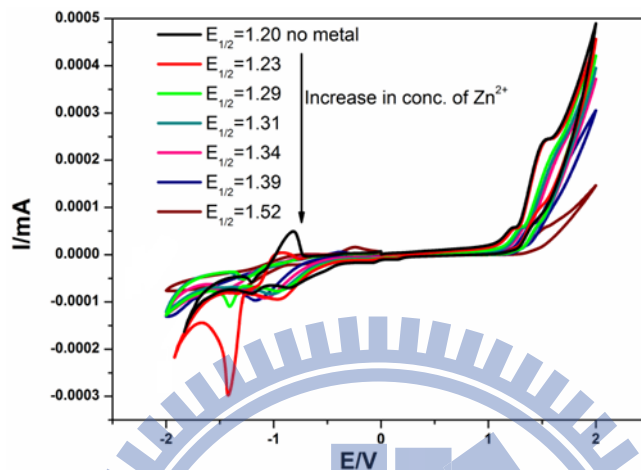
Figure 3.16 Evolution of cyclic voltametry of polymer **P** in THF/$[(n\text{-}Bu)_4]PF_6$ scanned at 0.1 V s^{-1} in the presence of increasing amounts of Zn^{2+}.

To check the affinities of different anions towards a **P**-Zn complex, we added various anions, such as F$^-$, Cl$^-$, Br$^-$, I$^-$, S^{2-}, NO$_3^-$, Ac$^-$, PO$_4^{3-}$, and SCN$^-$ to the solution of **P**-Zn complex. Surprisingly, unlike other anions, upon the addition of I$^-$, the color of the solution changed from colorless to yellow (Figure 3.17a). The progressive appearance of a new peak at 375 nm observed upon the sequential addition of I$^-$ (Figure 3.17b). Thus, **P**-Zn complex is susceptible for the colorimetric detection of I$^-$ ions. Reversible association of Zn^{2+} with polymer **P** was achieved by the addition of Na$_2$-EDTA as a suitable counter ligand (Figure 3.18). Therefore, the on-off-on fluorescence etiquette was successfully achieved via the alternate addition of Zn^{2+} and Na$_2$-EDTA for 5 successive cycles (Figure 3.19).
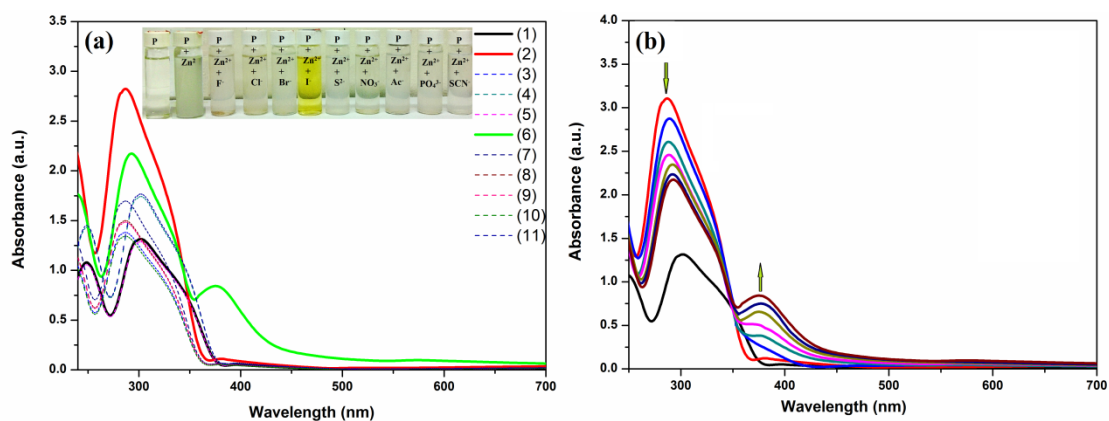
Figure 3.17 Absorption spectral response of (1) polymer **P** (1.1×10^{-5} M) and (2) **P**+Zn^{2+} (1.1×10^{-5} M) in THF/H$_2$O:(1/1) upon the further addition of (a): (3) F$^-$, (4) Cl$^-$, (5) Br$^-$, (6) I$^-$, (7) S^{2-}, (8) NO$_3^-$, (9) Ac$^-$, (10) PO$_4^{3-}$, and (11) SCN$^-$. (Each anion 1 equiv w.r.t. concentration of polymer **P**) (b) Progressive change in the absorption pattern of polymer **P** upon the sequential addition of I$^-$ (0-1 equiv w.r.t. polymer **P**).
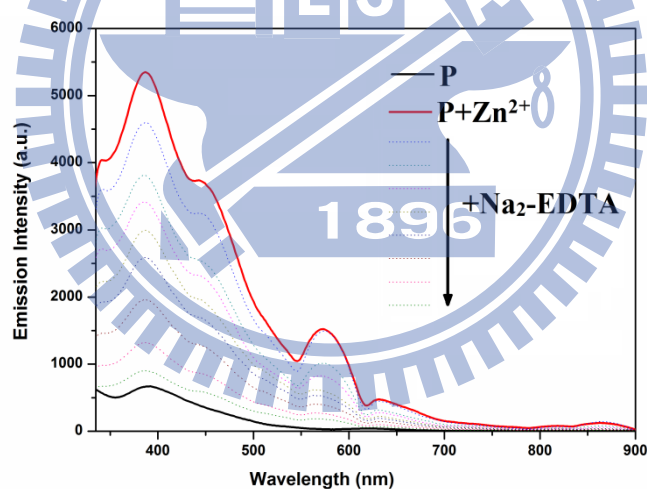
Figure 3.18 Fluorescence spectral response of polymer **P**+Zn^{2+} (1.1×10^{-5} M) in THF/H$_2$O, upon the sequential addition of Na$_2$-EDTA, showing retrieval of original fluorescence of polymer **P** due to the reversible association of Zn^{2+} with polymer **P**.
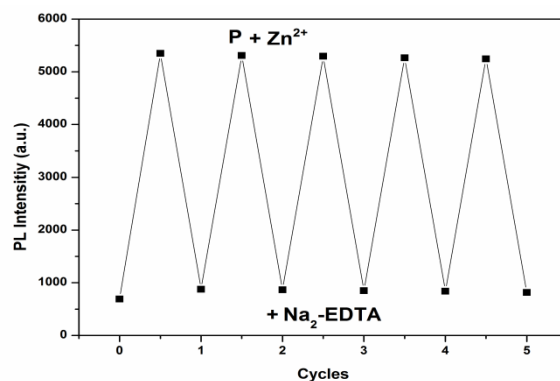
Figure 3.19 Reversible association of Zn^{2+} with polymer **P** for 5 successive cycles achieved by the alternate addition of Zn^{2+} and Na_2-EDTA.

3.4 Conclusion:

In summary, the naked-eye detection of Hg^{2+} was achieved by polymer **P** with a thieno-imidazole backbone. Furthermore, polymer **P** showed a fluorescence turn-on response with an enhanced fluorescence lifetime in the presence of Zn^{2+}. Its model polymer **M** could not show any such remarkable sensitivity towards Hg^{2+} and Zn^{2+}, which confirmed the unique sensitivity of **P** via the chelation of metal ions to both 'S' and 'N' hetero-atoms. Moreover, the colorimetric detection of I^- was selectively accomplished by **P**-Zn complex over other anions.

Chapter 4

Synthesis and Characterization of Reversible Chemosensory Polymers: Amendment of Sensitivity via Novel Imidazole Pendants

4.1 Introduction:

The molecular design for sensors is a predominant cornerstone because of the tremendous demands in analytical, biomedical, biotechnological, and nanotechnological applications.[99] The success of fluorescence sensors can be explained by their potentials of specific sensitivity, selectivity, and real-time screening for various moieties.[100] Rigid and ladder type low bandgap conjugated polymers can provide excellent redox and optoelectronic properties, such as broad and long wavelength light absorption, luminescence intensity, and carrier mobility, which lead to their potential applications in optoelectronics, microelectronics, light emitting diodes, photovoltaics, and field-effect transistors.[101] Some interesting recent extensions of these materials were done by their subsequent applications to fluorescence and biological sensors.[63,102] Conjugated polymers (as molecular wires) have enormous advantages over small molecules for sensing applications due to the facile excitons and energy migrations along conjugated polymer backbones, which led to the enhancement of electronic communications between receptors and polymers.[63,102] Conjugated polymers are attractive to act as semi-conductive "molecular wires" owing to their π-electron resonances via conjugations between donor-acceptor repeat units. This provides the polymers to be utilized as one of the most vital classes of sensing materials for their high sensitivities derived from molecular wire effects.[63,103] Furthermore, conjugated polymer sensors have brought

promising attentions, because their emission intensities, absorbances, charge transports, conductivities, and exciton migrations can be easily perturbed by external chemical species, such as acids, bases, and ions, leading to substantial changes in measurable signals.[99,104,105] The incorporation of sensitive and selective functionalities (as probes) towards both protons and metal ions, with notorious fluorophores into conjugated polymers yielded new materials suitable for chemosensory applications.[104] Thus, the synthesis of soluble and stable fluorescent conjugated polymers were emerged as improved selective recognition and transduction materials for chemical and biological sensing purposes.[106-108] A key feature for the sensing applications involved reversibilities within certain ranges of recognition processes.[105] The imidazole-based ligand was selected on the worth of its reversible fluorescence (on-off-on) by protonation/deprotonation with the aid of acid/base as well as metallation/demetallation in the presence of metal ion/suitable counter ligands, respectively, which can induce a large energy perturbation.[104]

Fe^{2+} is the most copious transition metal ions in biological systems that play significant roles in metabolic processes.[105] Fe^{2+} ions are requisite for most organisms, but both deficiency and overload of Fe^{2+} can cause various syndromes with iron trafficking, storage, and balance.[106] For example, Fe^{2+} deficiency leads to anemia and breathing problems excess iron in the body causes DNA, liver and kidney damage (hemochromatosis).[107] Introduction of specific probes, such as epoxy, bipyridine, terpyridine, quinoline, dipyrrolylquinoxaline, and imidazole, sulphate to the backbones or side chains of conjugated polymers has been successfully employed for the metal ion detection owing to the characteristic metal-to-ligand charge transfer.[108] However, to the best of our knowledge, there are no researches for Fe^{2+} sensors with a solo imidazole receptor conjugated to main chain polymer backbone. Herein, we report three imidazole-based polymers which showed remarkable sensing capabilities towards Fe^{2+}.

On the other hand, fluoride anion is of particular interest among halide anions owing to its association with preventing dental caries, as well as the treatments for osteoporosis, anesthetics, hypnotics, psychiatric drugs, and nerve gases, which is also concerned in the analysis of drinking water and the refinement of uranium used in nuclear weapon manufacture.[109a-d] The detection of fluoride is often interfered by the other halides.[109e,f] So fluoride detection over the other halides has also become objective of many researchers.[109g-j]

Thus, according to these concepts in view, herein we synthesized three novel imidazole-based conjugated fluorescent polymers (**P1**-**P3**). The photo-physical and electrochemical properties showed the polymers to act as excellent energy transfer materials with remarkable stabilities to be used as chemosenors. Compared with **P1** and **P2**, polymer **P3** showed a different spectral change during pH sensing probably due to its distinct electronic distribution. All polymers showed reversibilities in pH sensing upon the addition of TFA as the source of protonation and TEA as the counter ligand for deprotonation. Furthermore, the quenched fluorescence of polymers **P1**-**P3** regained their original fluorescence intensities upon the addition of counter ligands, so reversible sensing capabilities of polymers (**P1**-**P3**) towards Fe^{2+} ions were achieved via the addition of suitable counter ligands (Na_2-EDTA/phenanthroline). Furthermore, all monomer precursors (**1B**-**4B**) also showed distinct sensitivities towards fluoride ions over the other halides.

4.2 Experimental Section:

4.2.1 Reagents, Measurements, **and Characterizations**: All chemicals and solvents were reagent grades and purchased from ACROS, Aldrich, TCI, Fluka, TEDIA, and Lancaster Chemical Co. Toluene was distilled over sodium/benzophenone to keep anhydrous before use. Chloroform ($CHCl_3$) and DMF were distilled over CaH_2 was purified by refluxing with calcium hydride and then distilled. The solvents were degassed by nitrogen 1 hour prior to use when necessary.

^{1}H-NMR and ^{13}C-NMR spectra were recorded on a Bruker DX-(300 MHz for ^{1}H and 75 MHz for ^{13}C respectively) spectrometer using CDCl$_3$, DMSO-D$_6$ solvent. Elemental analyses were performed on a HERAEUS CHN-OS RAPID elemental analyzer. Thermogravimetric analyses (TGA) were conducted with a TA Instrument Q500 at a heating rate of 10 °C/min under nitrogen. The molecular weights of polymers were measured by gel permeation chromatography (GPC) using Waters 1515 separation module where polystyrene was used as a standard with tetrahydrofuran (THF) as an eluant. UV-visible absorption spectra were recorded in dilute THF solutions (10^{-5} M) and on solid films (spin-coated on glass substrates from THF solutions with a concentration of 10 mg/ml) on a HP G1103A. Cyclic voltammetry (CV) measurements were performed using a BAS 100 electrochemical analyzer with a standard three-electrode electrochemical cell in a 0.1-M solution of tetrabutylammonium hexafluorophosphate (TBA)PF$_6$ in acetonitrile at room temperature with a scanning rate of 100 mV/s. During the CV measurements, the solutions were purged with nitrogen for 30 s. In each case, a carbon working electrode coated with a thin layer of polymers, a platinum wire as the counter electrode and a silver wire as the quasi-reference electrode were used and Ag/AgCl (3 M KCl) electrode was served as a reference electrode for all potentials quoted herein. The redox couple of ferrocene/ferrocenium ion (Fc/Fc$^+$) was used as an external standard. The corresponding HOMO and LUMO levels were calculated using $E_{ox/onset}$ and $E_{red/onset}$ for experiments in solid films of polymers, which were performed by drop casting films with the similar thickness from chloroform solutions (ca. 5mg/mL). The onset potentials were determined from the intersections of two tangents drawn at the rising and background currents of cyclic voltammetry (CV) measurements. The pH sensing properties were performed in THF/H$_2$O (1/1) solutions via the addition of TFA as proton source and TEA for reversibility test. Similarly, metal sensing properties were performed via the addition of metal ions into the polymer solutions in THF/H$_2$O (1/1). Reversibility in metal ions sensing were tested using disodium salt of ethylene diamine tetra acetic acid (Na2-EDTA) or phenanthroline.

4.2.2 Synthesis: Herein, four imidazole-based monomers (**M1-M4**) were synthesized according to Scheme 4.2. Benzo[1,2-b:4,3-b']dithiophene-4,5-quinine (**1A**) was prepared via two steps involving the preparation of 3,3'-bithiophene and followed by acylation of oxalyl chloride without any lewis acid. The best way for preparing 3,3'-bithophene was observed by treating 3-bromothiophene with n-BuLi and subsequent oxidative coupling using commercial grade $CuCl_2$ with 77.9% yield (Scheme 4.1). Furthermore, 1,10-phenanthroline-5,6-dione (**4-A**) was prepared by treating 1,10-phenanthroline with H_2SO_4, HNO_3, and KBr.[110] Phenanthrene-9,10-dione (**2A**) and acenaphthylene-1,2-dione (**3A**) were obtained from commercial sources. Imidazole derivatives (**1B-4B**) were obtained by cyclisation of 3-thiophenecarboxaldehyde with corresponding diketo compounds (**1A-4A**) using NH_4OAc in acetic acid. All imidazole derivatives (**1B-4B**) were directly employed without further purification. Monomers (**M1-M4**) were prepared by N-alkylation of **1B-4B** using K_2CO_3 as base and alkyl iodide in DMF via subsequent purification in column chromatography with good yields. To the best of our knowledge, all these monomers were synthesized for the first time in this report. Finally, Suzuki polymerization of monomers **M1-M4** with diboronic ester of benzothiadiazole afforded respective polymers **P1-P4** (Scheme 4.2). It is noteworthy to mention that except **P4**, all polymers were soluble in common organic solvents, such as DCM, $CHCl_3$, THF, and ODCB. However, the molecular weight of polymer **P3** (Mw=4614) is higher than polymer **P1** (Mw=5755) and **P2** (Mw=13718) due to good solubility of acenaphthene-imidazole units.(in **P3**) rather than benzodithiophene units (in **P1**) and phenanthrene units (in **P2**). Further characterisations of polymers **P1**-**P3** were carried out in semi-aqueous solutions of THF/H_2O (1/1).
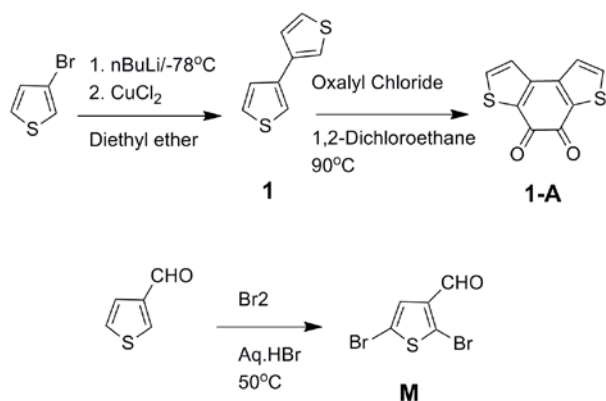
Scheme 4.1: Synthetic procedures of **1-A** and **M**.
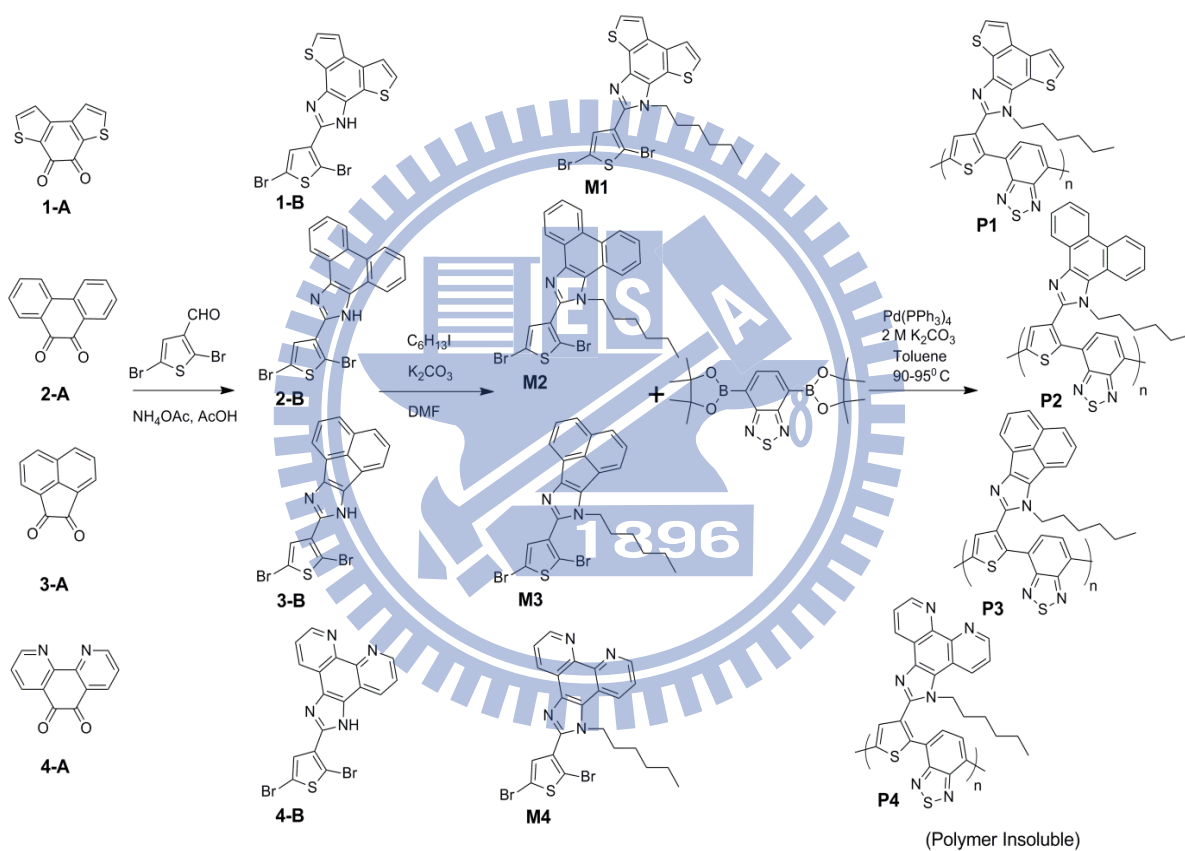
Scheme 4.2. Synthetic routes of Monomers and Polymers.

4.2.3 Synthetic procedure:

3,3'-Bithiophene (1): 3-Bromothiophene (0.122 mole, 20 gm) was dissolved in 100 ml anhydrous diethyl ether. The solution was cooled to -78 °C. To it, 2.5 molar n-BuLi in hexane (0.122 mole, 48.8 ml) was added dropwise for 40 mins under N_2. The reaction was

allowed to stir for 10 mins at -78 °C and 20 mins at -60°C. Then CuCl$_2$ (0.130 mole, 17.42 gm) was added in one portion at -60°C. The reaction was carefully maintained at -60 °C for another 1 hour. Then, the reaction mixture was slowly warmed up to room temperature and continued stirring for another 18 hours at room temperature. The reaction mixture was quenched by 30 ml water and filtered to remove inorganic impurity. The organic phase was collected and dried in MgSO$_4$. Solvent was removed by rotary evaporation. The crude product was purified by silica gel column chromatography using hexane as an eluant. Product was obtained as a white solid (7.9 gm, 77.9%). ^{1}H NMR (300 MHz, CDCl$_3$): δ (ppm) 7.38 (m, 2H), 7.35 (m, 4H). ^{13}C NMR (75 MHz, CDCl$_3$): δ (ppm) 137.0, 126.1, 125.8, 119.6 EI-MS (m/z): Calcd for C$_8$H$_6$S$_2$, 165.99 found 166 (M$^+$). ^{1}H and ^{13}C NMR spectra were in agreement with the reported literature.[84]

2,5-Dibromothiophene-3-carbaldehyde: A mixture of bromine (4.90 ml, 15.30 gm, 95.76 mmole) and 15 ml of aqueous HBr was added dropwise to a mixture of thiophene-3-carboxaldehyde (4 ml, 5.12 gm, 45.65 mmole), 20 ml of 48% aqueous HBr, and 20 ml of diethyl ether in an ice cold condition. After addition was completed the reaction mixture was heated to 50°C. Reaction was allowed to continue for overnight. The reaction mixture was quenched by adding 50 ml of aqueous NaHSO$_3$ solution. The organic phase was extracted by ethyl acetate, washed with brine, and dried over MgSO$_4$. After removal of solvent under reduced pressure the crude product was purified by column chromatography (EA: hexane = 5:95) to give a light yellow solid (11.3 gm, 91.72%). ^{1}H NMR (300 MHz, CDCl$_3$): δ (ppm) 9.80 (s, 1H), 7.34 (s, 1H). ^{13}C NMR (75 MHz, CDCl$_3$): δ (ppm) 183.0, 139.2, 128.6, 124.2, 113.2. EI-MS (m/z): Calcd for C$_5$H$_2$Br$_2$OS, 169.82 Found: 169 (M$^+$). ^{1}H and ^{13}C NMR spectra were in agreement with the reported literature.[111]

Benzo[1,2-b:4,3-b']dithiophene-4,5-quinone (1-A): 3,3'-Bithiophene (7 gm, 42.10 mmole) was dissolved in 100 ml of 1,2-dichloroethane. To it, oxalyl chloride (3 ml, 34.94 mmole) was added slowly. The solution was turned orange. The reaction mix was allowed to stir at 90

°C for 4 days. The reaction mix was cooled and kept at 0 °C overnight. Then the mixture was filtered. Residue product was washed thoroughly by hexane. After drying, the product obtained was a red solid (6 gm, 64.65%). ^{1}H NMR (300 MHz, CDCl$_3$): δ (ppm) 7.83 (d, 2H, 4.8 Hz), 7.29 (d, 2H, 4.8 Hz). ^{1}H NMR (DMSO-D6): δ 8.23 (d, 2H, 4.8 Hz), 7.69 (d, 2H, 4.8 Hz). ^{13}C NMR (75 MHz, CDCl$_3$): δ (ppm) 173.5, 142.1, 138.2, 134.9, 124.5. EI-MS (m/z): Calcd for $C_{10}H_4O_2S_2$, 219.97 Found: 220 (M$^+$). ^{1}H and ^{13}C NMR spectra were in agreement with the reported literature.[85]

1,10-Phenanthroline-5,6-dione (4-A): 1,10-Phenanthroline (4.6 gm, 25.52 mmole) and KBr (4.6 gm, 38.65 mmole) were taken together. To it, a cooled mixture of 35 ml conc. H$_2$SO$_4$ and 30 ml conc. HNO$_3$ was added dropwise in an ice cold condition. The mixture was stirred for 3 hours at 130 °C. Then, the solution was transferred to a beaker containing ice and carefully neutralised by NaOH. The product was extracted by DCM, dried over MgSO$_4$ and solvent was removed under rota vapour to give a yellow solid (5.19 gm, 98.1%). ^{1}H NMR (300 MHz, CDCl$_3$): δ (ppm) 9.10 (dd, 2H, 6.1 Hz, 1.5 Hz), 8.49 (dd, 2H, 7.8 Hz, 1.5 Hz) 7.57 (m, 2H). ^{13}C NMR (75 MHz, CDCl$_3$): δ (ppm) 125.4 128.1 137.1 153.4 156.0 178.8. EI-MS (m/z): Calcd for $C_{12}H_6BrN_2O_2$, 210.04 Found: 210.0 (M$^+$). ^{1}H and ^{13}C NMR spectra were in agreement with the reported literature.[112]

2-(2,5-Dibromothiophen-3-yl)-1H-dithieno[2',3':3,43'',2'':5,6]benzo[1,2-d]imidazole (1-B): A mixture of 2,5-dibromothiophene-3-carbaldehyde (2.94 gm, 10.88 mmole), benzo[1,2-b:4,3-b$^{/}$]dithiophene-4,5-quinone (2 gm, 9.08 mmole), ammonium acetate (21 gm, 272.44 mmole), and acetic acid (100 ml) was heated to 100 °C overnight. The green solution was cooled to room temperature. 30 ml water was added to it and stirred for 15 mins at RT. The solution was filtered in a Buchner funnel. The green residue was washed thoroughly in water and hexane, dried, and taken to the next step without further purification. Mp = 290-293 °C ^{1}H NMR (300 MHz, CDCl$_3$): δ (ppm) 12.11 (s, 1H, broad), 7.92 (s, 1H), 7.80 (d, 2H,

4.8Hz). ^{1}H NMR (300 MHz, DMSO-D6) : δ 13.53 (s, 1H), 8.03 (t, 2H, 6Hz), 7.82 (d, 2H, 6Hz), 7.76 (1H, d, 6Hz). EI-MS (m/z): Calcd for $C_{15}H_6Br_2N_2S_3$, 469.80 Found: 469 (M$^+$).

2-(2,5-Dibromothiophen-3-yl)-1-hexyl-1H-dithieno[2',3':3,43'',2'':5,6]benzo[1,2-d]imidazole (M1): To a solution of **1-B** (5.1 gm, 10.84 mmole) in DMF 30 ml, K_2CO_3 (3.52 gm, 25.51 mmole) was added and heated to 95°C for 3 hours. Then, it was cooled to room temperature. To it, 1-iodohexane (2.07 ml, 2.98 gm, 14.09 mmole) was added slowly. Reaction mixture was heated to 95 °C overnight. After cooling to room temperature the reaction mixture was poured in 300 ml water. Organic phase was extracted by ethyl acetate via repeated washing in water, dried over $MgSO_4$, and solvent was removed under rotary evaporation. Crude product was purified by silica gel column chromatography (EA: hexane = 5: 95) to give a yellow solid (4.15 gm, 80.44%). Mp = 139-142°C ^{1}H NMR (300 MHz, CDCl$_3$): δ (ppm) 7.87 (d, 1H, 5.1 MHz), 7.80 (d, 1H, 5.1 MHz), 7.57 (d, 1H, 5.4 MHz), 7.54 (d, 1H, 6.3 MHz), 7.19 (s, 1H), 4.42 (t, 2H, 7.2 Hz), 1.83-1.77(m, 2H), 1.25-1.22 (m, 6H), 0.85(t, 6.7Hz) . ^{13}C NMR (75 MHz, CDCl3) : δ (ppm) 144.54, 135.92, 133.16, 132.84, 132.40, 132.17, 129.43, 127.30, 124.72, 123.99, 123.42, 122.84, 121.24, 114.72, 112.85, 46.79, 31.54, 26.45, 22.84, 14.36. EIMS (m/z): Calcd for $C_{21}H_{18}Br_2N_2S_3$, 553.90 Found: 554 (M$^+$). Anal. Calcd. for $C_{21}H_{18}Br_2N_2S_3$: C, 45.50 H, 3.27 N, 5.05. Found: C, 45.48 H, 3.76 N, 5.22.

2-(2,5-Dibromothiophen-3-yl)-1H-phenanthro[9,10-d]imidazole (2-B): A mixture of 2,5-dibromothiophene-3-carbaldehyde (4 gm, 14.81 mmole), phenanthrene-9,10-dione (3.08 gm,14.81 mmole), ammonium acetate (34.24 gm, 444.3 mmole), and acetic acid (150 ml) was heated to 100 °C overnight. The yellow solution was cooled to room temperature. 40 ml water was added to it and stirred for 15 mins at RT. The solution was filtered in a Buchner funnel. The off-white residue was washed thoroughly in water and hexane, dried and taken to the next step without further purification. Mp = 195-199 °C. ^{1}H NMR (300 MHz, CDCl$_3$): δ

(ppm) 8.72 (d, 2H, 7.8 Hz), 8.32(s, 1H, broad), 7.90 (s, 1H), 7.71-7.61 (m, 4H). EI-MS (m/z): Calcd. for $C_{19}H_{10}Br_2N_2S$, 457.89 Found: 457 (M^+).

2-(2,5-Dibromothiophen-3-yl)-1-hexyl-1H-phenanthro[9,10-d]imidazole (M2): To a solution of **2-A** (6.5 gm, 14.18 mmole) in DMF 40 ml, K_2CO_3 (5.87 gm, 42.54 mmole) was added and heated to 95°C for 3 hours. Then, it was cooled to room temperature. To it, 1-iodohexane (2.71 ml, 3.90 gm, 18.43 mmole) was added slowly. Reaction mixture was heated to 95 °C overnight. After cooling to room temperature, the reaction mixture was poured in 300 ml water. Organic phase was extracted by ethyl acetate via repeated washing in water, dried over $MgSO_4$, and solvent was removed under rotary evaporation. The crude product was purified by silica gel column chromatography (EA: hexane=5:95) to give a white powder (6.41 gm, 83.4%). Mp = 135-138 °C. ^{1}H NMR (300 MHz, CDCl$_3$): δ (ppm) 8.85 (d, 1H, 7.8 Hz), 8.75(d, 1H, 7.8 Hz), 8.70 (d, 1H, 8.1 Hz), 8.27 (d, 1H, 8.1 Hz), 7.72-7.62 (m, 4H), 7.21 (s, 1H), 4.52 (t, 2H, 7.35 Hz), 1.90-1.85 (m, 2H), 1.25-1.18 (m, 6H), 0.82 (t, 7.2Hz). ^{13}C NMR (75 MHz, CDCl3) : δ (ppm) 145.16, 138.69, 133.43, 132.71, 129.70, 128.58, 127.80, 127.66, 127.28, 126.32, 126.12, 125.52, 124.86, 123.64, 123.49, 122.97, 121.30, 114.93, 112.87, 47.46, 31.49, 30.41, 26.42, 22.86, 14.40. EI-MS (m/z): Calcd for $C_{25}H_{22}Br_2N_2S$, 541.98 Found: 542 (M^+). Anal. Calcd. for $C_{25}H_{22}Br_2N_2S$: C, 55.37 H, 4.09 N, 5.17. Found: C, 55.48 H, 4.30 N, 5.25.

8-(2,5-Dibromothiophen-3-yl)-7H-acenaphtho[1,2-d]imidazole (3-B): A mixture of 2,5-dibromothiophene-3-carbaldehyde (5 gm, 18.51 mmole) , acenaphthylene-1,2-dione i.e. 3-A (3.37 gm, 18.51 mmole), ammonium acetate (42.80 gm, 555.3 mmole), and acetic acid (150 ml) was heated to 100 °C for 2 hours. The red solution was cooled to room temperature. 15ml water was added to it and stirred for 10 mins at RT. The solution was filtered in a Buchner funnel. The off-white residue was washed thoroughly in water and hexane, dried and taken to the next step without further purification. Mp =205-208 °C. ^{1}H NMR (300 MHz, CDCl$_3$): δ

(ppm) 7.77 (d, 2H, 2.4 Hz), 7.74 (s, 2H), 7.72 (s, 2H), 7.52 (t, 2H, 7.65 Hz). EI-MS (m/z): Calcd. for $C_{17}H_8Br_2N_2S$, 431.88 Found: 431 (M^+).

8-(2,5-Dibromothiophen-3-yl)-7-hexyl-7H-acenaphtho[1,2-d]imidazole (M3): To a solution of **3-B** (4.9 gm, 11.33 mmole) in acetone 50 ml, K_2CO_3 (4.69 gm, 33.99 mmole), and 1-iodohexane (2.1 ml, 3.12 gm, 14.72 mmole) was added. Reaction mixture was heated to 55 °C overnight. After cooling to room temperature the reaction mixture was filtered in a celite bed and washed with acetone. Filtrate was concentrated under rotary evaporation. Crude product was purified by silica gel column chromatography using hexane as an eluant to give a dark brown dense liquid (5.03 gm, 86.06%). Mp =41-43 °C. ^{1}H NMR (300 MHz, CDCl$_3$): δ (ppm) 7.86 (d, 1H, 6.9 Hz), 7.71 (t, 2H, 9.3 Hz), 7.55-7.50 (m, 3H), 7.12 (s, 1H), 4.16 (t, 2H, 7.2 Hz), 1.90-1.85 (m, 2H), 1.24-1.21 (m, 6H), 0.83 (t, 7.05 Hz). ^{13}C NMR (75 MHz, CDCl$_3$): δ (ppm) 148.71, 144.07, 137.18, 133.34, 132.43, 132.05, 131.21, 129.98, 128.34, 127.52, 127.43, 127.35, 126.80, 120.92, 119.36, 114.00, 112.45, 47.20, 31.52, 30.39, 26.53, 23.11, 14.54. EI-MS (m/z): Calcd. for $C_{23}H_{20}Br_2N_2S$, 515.97 Found: 516 (M^+). Anal. Calcd. for $C_{23}H_{20}Br_2N_2S$: C, 53.51 H, 3.90 N, 5.43. Found: C, 53.71 H, 3.98 N, 5.39.

4,7-Bis(4,4,5,5-tetramethyl-1,3,2-dioxaborolan-2-yl)benzo[c][1,2,5]thiadiazole: Synthesis was done by following literature[5] procedure. Mp = 208.0-210.5 °C. ^{1}H NMR (300 MHz, CDCl$_3$): δ (ppm) 8.11 (s, 2H), 1.42 (s, 24H). ^{13}C NMR (75 MHz, CDCl3): δ (ppm) 157.1, 137.6, 84.4, 25.1. Anal. Calcd. for $C_{18}H_{26}B_2N_2O_4S$: C 55.71, H 6.73, N 7.22 Found: C 55.48, H 6.57, N 7.10.

General Polymerization Procedure:

All polymerization steps were carried out through the palladium (0)-catalyzed Suzuki coupling reactions. In a 50 ml flame dried two-neck flask, 1 equiv of 4,7-bis(4,4,5,5-tetramethyl-1,3,2-dioxaborolan-2-yl)benzo[c][1,2,5]thiadiazole, 1 equiv of (5a-5c), and Pd(PPh$_3$)$_4$ (1.5 mol %) were taken and degassed with N$_2$ three times. It was dissolved in a

mixture of toluene ([monomer] = 0.5 M) and aqueous 2 M K_2CO_3 (2:3). The solution was vigorously stirred at 90-95 °C for 3 days under N_2 atmosphere. After reaction completion, an excess of bromobenzene was added to the reaction. After 1 h, an excess of phenylboronic acid was added and the reaction refluxed overnight to complete the end-capping reaction. The polymer was precipitated in methanol/water (10:1), filtered through 0.45 µm nylon filter and washed on Soxhlet apparatus using hexane, acetone, and chloroform. The chloroform fraction was reduced to 40-50 ml under reduced pressure, precipitated in methanol/water (10:1, 500 ml), filtered through 0.45 µm nylon filter, and finally air-dried overnight.

P1: Following the general polymerization procedure, **P1** obtained as a black powder. Yield: 74%. GPC: Mw: 4614 PDI: 1.14 ^{1}H NMR (300 MHz, CDCl$_3$): δ (ppm) 8.51 (broad), 8.06 (broad), 7.86-7.77 (broad), 7.74-7.67 (broad), 6.97(s), 4.13 (broad), 1.87-1.80 (broad), 1.25-1.02 (broad), 0.76-0.64 (broad). Anal. Calcd for $(C_{27}H_{20}N_4S_4)_n$: C, 61.33 H, 3.81 N, 10.60 Found: C, 61.94 H, 4.09 N, 10.39.

P2: Following the general polymerization procedure, **P2** was obtained as a black powder. Yield: 76%. GPC: Mw: 5755 PDI: 1.23 ^{1}H NMR (300 MHz, CDCl$_3$): δ (ppm) 8.78 (broad), 8.29 (broad), 8.07-7.99 (broad), 7.62-7.35 (broad), 4.17 (broad), 1.87-1.83 (broad), 1.25-1.00 (broad), 0.75-0.70 (broad). Anal. Calcd. for $(C_{31}H_{24}N_4S_2)_n$: C, 72.06 H, 4.68 N, 10.84. Found: C, 72.51 H, 4.92 N, 10.39.

P3: Following the general polymerization procedure, P3 obtained black powder. Yield: 77%. GPC: Mw: 13718 PDI: 1.16 ^{1}H NMR (300 MHz, CDCl$_3$): δ (ppm) 8.62 (broad), 8.23 (broad), 8.12-7.88 (broad), 7.78-7.64 (broad), 7.56-7.47 (broad), 7.05 (s), 4.18 (broad), 1.95-1.83 (broad), 1.27-1.03 (broad), 0.89-0.69 (broad). Anal. Calcd for $(C_{29}H_{22}N_4S_2)_n$: C, 71.28 H, 4.13 N, 11.47 Found: C, 71.77 H, 4.30 N, 11.19.

4.3 Results and Discussion:

4.3.1 Photo-physical characterization: The normalised absorption and emission spectra of polymers in both solutions and solid films were shown in Figure 4.1 and their characteristic optical data were summarized in Table 4.1. All these polymers exhibited two distinct broad absorption peaks, in which the high energy sharp peaks at 300-400 nm were attributed to ð-ð* transitions and low energy broad bands 500-650 nm were ascribed to localized intramolecular charge transfers between electron donors and acceptors, respectively, in the polymer backbones. Significant bathochromic shifts of the absorptions as well as photoluminescence (PL) emissions of all polymers in solid films were due to the interchain aggregations of rigid planar segments in the polymer backbones.[113a-c] The shoulders of PL spectra in Figure S1b) may be ascribed to the increased vibronic coupling associated with the molecular rigidities in solid films. The noticeably larger values of strokes shifts of all polymers signify the differences in geometrical structures in the ground states and excited states. This further signifies prominent excited state intermolecular charge transfer occurring in the chromophores which is essential for chemosensory applications.[113d,e] The optical bandgaps (~1.85 ev) of these polymers (**P1**-**P3**) were found to be smaller than P3HT (~1.90 eV)14g due to the combination of electron donor and acceptor moieties. In addition, the bandgaps of **P1**-**P3** were also smaller than the analogous polymer PT2BT (1.97 ev) containing bithiophene (as donor) and benzothiadiazole (as acceptor) units,[113h] which implies that in contrast to the bithiophene unit in PT2BT, the 3-thiophene-imidazole unit (with a stronger electron donating capability) induced more effective conjugations between donor and acceptor segments in polymers **P1**-**P3**. Therefore, polymers **P1**-**P3** could be concluded to have good electronic communications between receptors in the backbones of polymers via facile migrations of excitons during the sensing processes.[113i]

Table 4.1. Photo-Physical, Electrochemical, and Thermal Properties of **P1**, **P2**, and **P3**

Polymer	solution[a]			film[b]				energy levels			T_g (°C)
	$\lambda_{max,abs}$ (nm)	Stokes shift[g] (nm)	$\lambda_{max,abs}$ (nm)	$\lambda_{max,em}$ (nm)	Stokes shift[g] (nm)	$E_{onset,abs}$ (nm)	$E_{g,opt}$[e] (eV)	$E_{onset,ox}$[d] (V)/ HOMO (eV)	$E_{onset,red}$[d] (V) /LUMO (eV)	$E_{g,el}$[f] (eV)	
P1	305 515	119	325 535	(659)[c] 684	149	664	1.86	1.05/ -5.40	-0.86/ - 3.49	1.91	234
P2	301 521	119	329 539	(684)[c] 711	172	676	1.83	1.02/ -5.37	-0.87/ - 3.48	1.89	274
P3	319 470	224	327 497	(683)[c] 709	212	662	1.87	1.06/ -5.41	-0.86/ - 3.49	1.92	249

[a] In THF solutions; [b] Spin coated from THF solutions on glass surface; [c] Shoulder peak; [d] $E_{HOMO}/E_{LUMO} = [-(E_{onset} - E_{onset} (FC/FC^+ \text{ vs } Ag/Ag^+)) - 4.8]$; [e] Optical bandgap $E_{g,op} = 1240/\lambda_{edge}$; [f] Electrochemical bandgap $E_{g,el} = E_{onset/ox} - E_{onset/red}$; [g] Stroke shift = $\lambda_{em} - \lambda_{abs}$.
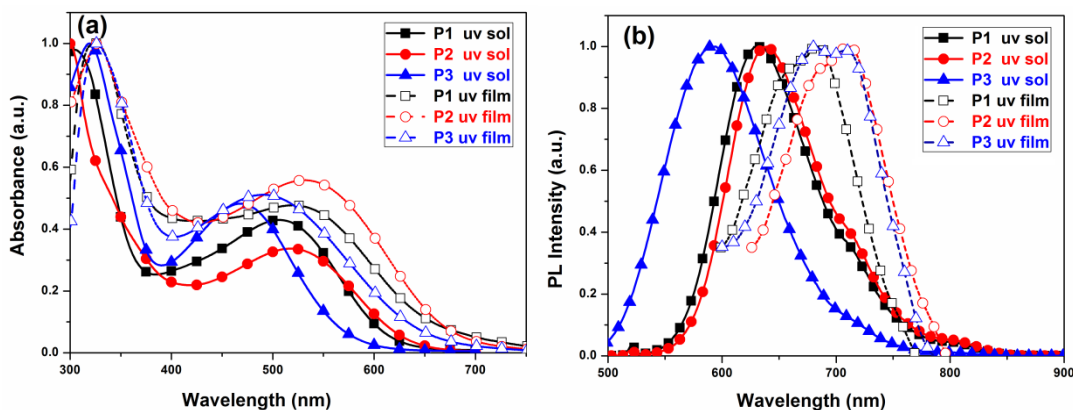
Figure 4.1. Normalized (a) UV absorption and (b) photoluminescence spectra of **P1**, **P2**, and **P3** in THF solutions and solid films.

4.3.2 Electrochemical characterization: The cyclic voltamograms of the polymers in solid films were shown in Figure 4.2 and their related data were summarized in Table 4.1. All polymers possessed reversible or quasi-reversible n-doping/dedoping (reduction/reoxidation) processes at negative potentials, which indicated good structural stability in the charged states. Furthermore, the highest occupied molecular orbital (HOMO) levels of polymers **P1**-**P3** (ca. -5.4 eV) were lower than -5.2 eV which showed their good air stability.[114c] Finally, in addition to structural stability, the low values of HOMO levels (ca. -5.4 eV) in polymers P1-P3 facilitated them to act as good electron-donor candidates for sensory applications.[114]
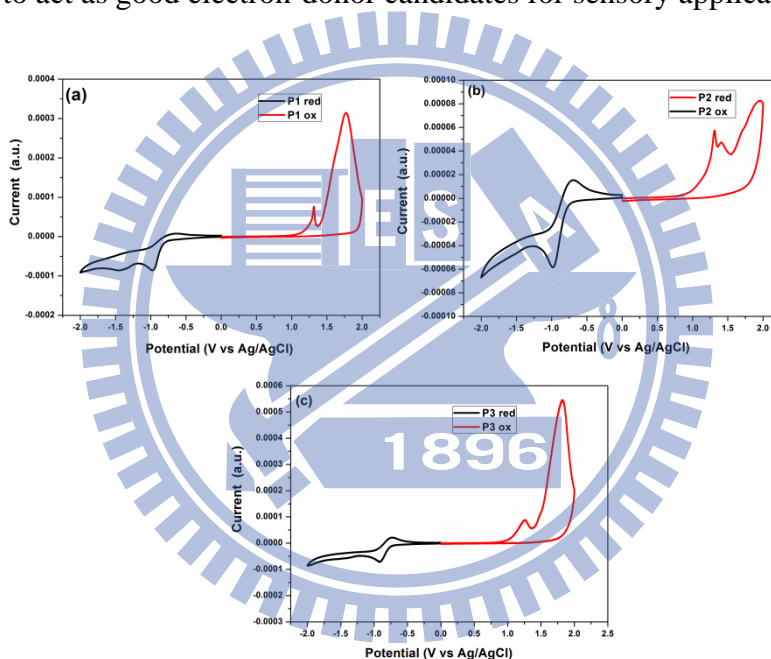
Figure 4.2 Cyclic voltamograms of polymers (a) **P1**, (b) **P2**, and (c) **P3** in solid films at a scan rate of 100 mVs^{-1}.

4.3.3 pH sensing and reversibility: The pH sensing properties of these polymers were investigated by UV-vis and PL titrations. As shown in Figure 4.3 (a), upon increasing [H$^+$] by the addition of trifluoroacetic acid (TFA), a hypsochromic shift in the absorption maximum as well as the onset occurred with the concomitant decrease in the absorption intensity of **P1**. Polymer **P2** showed a similar pH sensing response (Figure 4.3b) probably due to a similar

electronic distribution. At higher [H⁺], the imidazole units got protonated which hindered the effective charge transfer from benzodithiophene and pheanthrene units to the backbones of **P1** and **P2**, respectively. The excited state was more strongly destabilized than the ground state, due to the protonation of donor imidazole units, thus hypsochromic shifts of the absorption and emission spectra were observed.[15] PL spectra of **P1** and **P2** in Figures 4.4 (a) and (b), respectively, showed significant blue shifts with enhanced intensities upon increasing [H⁺]. Photoinduced electron transport (PET)[115a] from the imidazole units to polymer backbones of **P1** and **P2** cause week fluorescence. However, the protonation of imidazole diminished PET effects at higher [H⁺] which in turn restored the fluorescence originating from the imidazole unit and hence the fluorescence was enhanced.[1,115b] Due to the different electronic distribution of five-membered anti-aromatic (acenaphthylene) rings in **P3**, it showed a different pH response from **P1** and **P2** containing six-membered aromatic rings (benzodithiophene and phenanthrene, respectively). In contrast to **P1** and **P2**, upon increasing [H⁺], the absorption intensities of **P3** (Figure 4.3c) decreased without prominent blue shifts of absorption maxima. Sequentially, a new shoulder at 360-400 nm appeared at medium [H⁺] ($2 \times 10^{-6} \sim 2.1 \times 10^{-3}$ M). Surprisingly, unlike **P1** and **P2**, the fluroscence intensities of **P3** decreased as [H+] increased (Figure 4c), which could be possibly attributed to static quenching.[16e-g] The static quenching was further confirmed by Stern-Volmer plot for fluorescence quenching of **P3** upon titration with [H⁺] at various temperatures (Figure 4.4 d), which revealed that the binding constant of quencher [H⁺] for **P3** was reduced upon increasing temperature. Furthermore, all polymers recovered most of their original absorption and fluorescence by the addition of triethylamine (TEA) due to the deprotonation of

imidazolium salt. Consequently, the mutation of both UV-vis and PL spectra upon the addition of TFA and TEA clearly indicates that all polymers (**P1**-**P3**) are promising reversible pH sensing materials in terms of both absorption and fluorescence ratiometries.

Figure 4.3. UV-vis absorption spectra of (a) **P1**, (b) **P2**, and (c) **P3** in THF/H$_2$O=1/1 (1.4 × 10^{-5} M) at various concentrations of trifluoroacetic acid (TFA) and the final neutralizations with triethylamine (TEA).
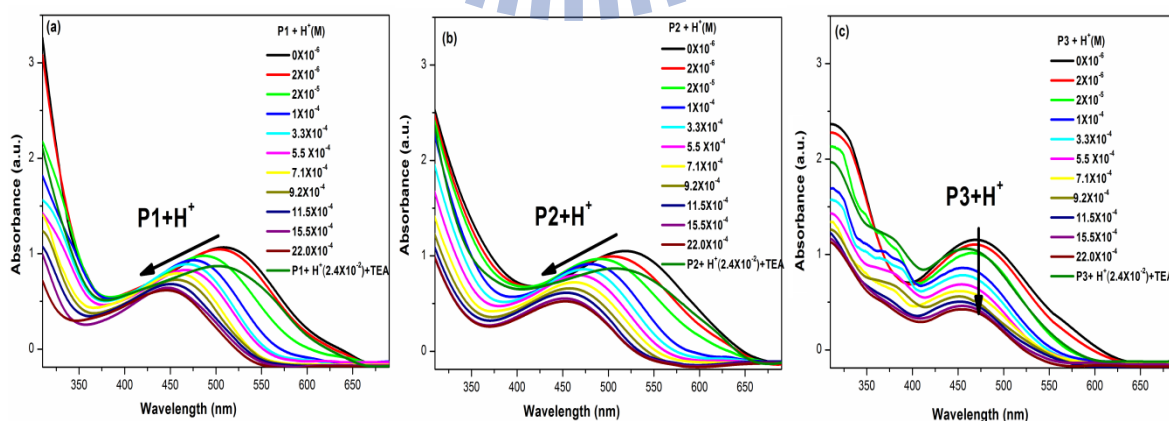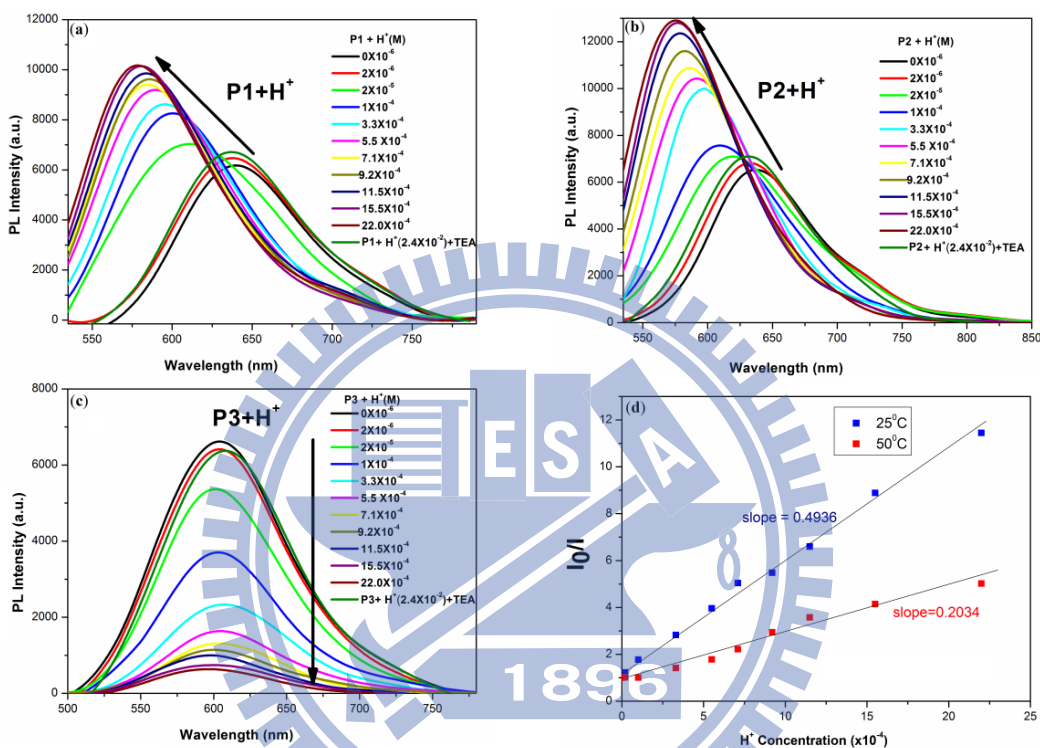
Figure 4.4 PL spectra of (a) **P1**, (b) **P2**, and (c) **P3** in THF/H2O=1/1 (1.4 × 10-5 M) at various concentrations of trifluoroacetic acid (TFA) and the final neutralizations with

triethylamine (TEA). (d) Stern-Volmer plots for the fluorescence quenching of **P3** by H$^+$ at 25°C and 50°C.

We further investigate the sensing mechanism by theoretical calculations based on the computational analysis (see Figure 4.5). The HOMO electron clouds are mostly coagulated over the benzodithiophene units of **P1** and the LUMO electron clouds are coagulated over the benzothiadiazole units. More electron rich centre is induced by the aromaticity of the benzodithiphene unit in **P1** and thus the HOMO electron clouds congregate over the benzodithiphene unit. As a highly electron accepting group, the benzothiadiazole unit gathers most of the LUMO electron clouds. Thus there is an effective intramolecular charge transfer (ICT) occur from the pendant benzodithiophene unit to the polymer backbone through the imidazole linkage. The aromaticity of the phenanthrene ring in **P2** makes it a strong electron-donating unit. The HOMO electron clouds are thus mostly localized over the phenanthrene unit. Similar to **P1**, the LUMO electron clouds of **P2** are mostly coagulated over benzothiadiazole unit. Thus, there is an effective ICT occurs in the polymer backbone of **P2** due to the charge separation states. In both cases of **P1** and **P2** the nitrogen lone pairs of imidazole units belong to HOMO of the respective polymers. Upon titration with H$^+$, the nitrogen lone pairs are co-ordinated with the H$^+$ ions, which cause bonding type interactions and thus to block the original ICT occurring in the polymers. Furthermore, upon complexation with H$^+$, both frontier orbitals (HOMO and LUMO) are located only over the polymer backbones. This could not give a complete charge separation state for an effective ICT process and thus the fluorescence is enhanced in both cases of **P1** and **P2** after their complexation with H$^+$. The antiaromaticity of acenaphthene ring in **P3** causes it a weaker electron rich centre compared with the aromatic benzodithiophene (in **P1**) and phenanthrene (in **P2**) units. Thus, the HOMO electron clouds are not absolutely delocalized over the acenaphthene unit in **P3**. The LUMO electron clouds are localized over the polymer

94

backbone. Unlike **P1** and **P2**, the charge separation states are not well classified in the case of **P3**. However, upon complexation with H^+ ions a well organized charge separation state appears in **P3**. Finally, this causes an effective charge transfer in the polymer backbone, which can be attributed to the plausible quenching mechanism in **P3**.
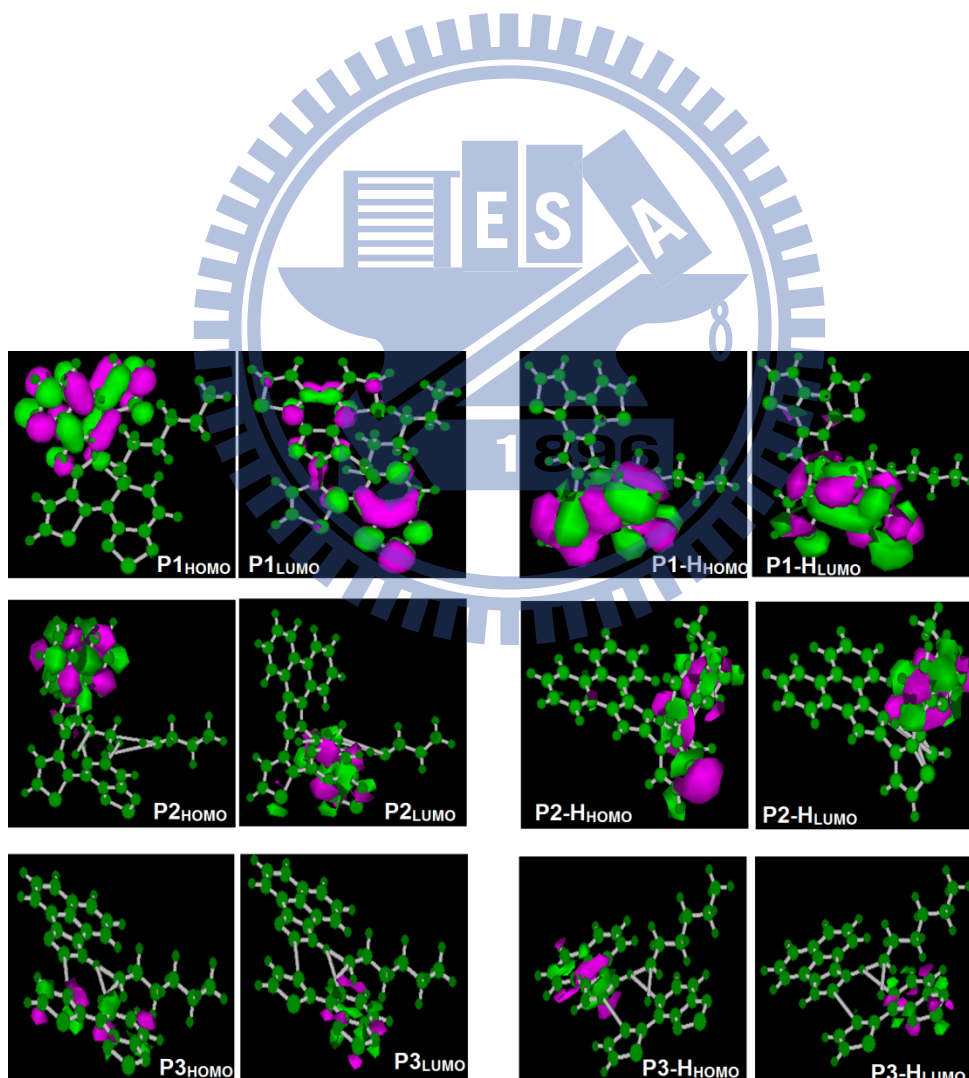
Figure 4.5. Coagulation of electron clouds in HOMO and LUMO of **P1**-**P3** before (left) and after (right) complexation with H^+.

4.3.4 Selectivity, sensitivity, and reversibility in metal ion sensing: The chemosensing properties of fluorescent polymers were investigated for a variety of metal ions, such as Li^+, Na^+, K^+, Ca^{2+}, Ba^{2+}, Mg^{2+}, Zn^{2+}, Co^{2+}, Ni^{2+}, Cd^{2+}, Fe^{2+}, Ag^+, Mn^{2+}, and Cu^{2+} (Figure 4.6). The fluorescence intensities of **P1**-**P3** were slightly altered upon addition of up to 30 equiv. of Li^+, Na^+, K^+, Ca^{2+}, Ba^{2+}, Ni^{2+}, Zn^{2+}, Ag^+, Co^{2+}, Mn^{2+}, and Cu^{2+}. Whereas, Fluorescence intensities of polymers **P1**-**P3** decreased significantly in presence of 10 equiv. of Fe^{2+}. This may be due to higher coordination capabilities of imidazole receptors with Fe^{2+} ions, which can be attributed to energy and/or charge transfer due to the stronger ligand-metal interaction.[115c] The selectivity towards Fe^{2+} was further proven by its interference with other background metal ions. As illustrated in Figure 4.7, the sensitivities of polymers **P1**-**P3** towards Fe^{2+} were not significantly affected by other competitive metal ions. However, **P3** showed the best quenching efficiency than **P1** and **P2**. This could be attributed to a higher molecular weight of **P3** which led to produce a better semiconducting "molecular wire effect" than **P1** and **P2**. The larger number of repeating units in **P3** provided more binding sites and thus to cause sheer fluorescence quenching.
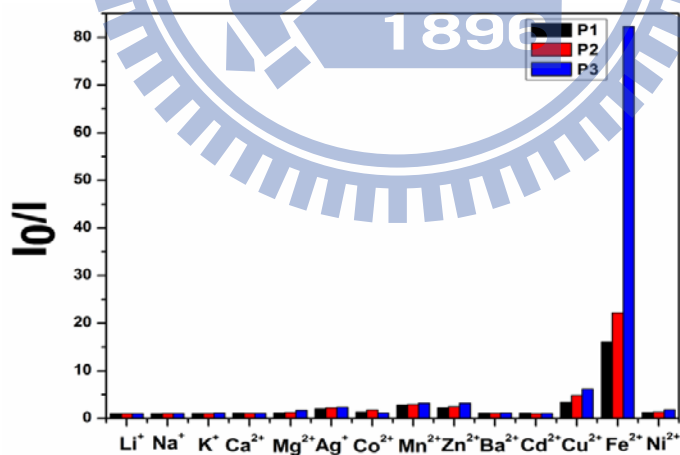
Figure 4.6 Fluorescence emission response profiles (I_0/I) of **P1**, **P2**, and **P3**. The polymer concentration (1.2×10^{-5} M), Fe^{2+} added = 10 eq (1.2×10^{-4} M), other metals ions added = 30eq (3.6×10^{-4} M) (Single metal system).
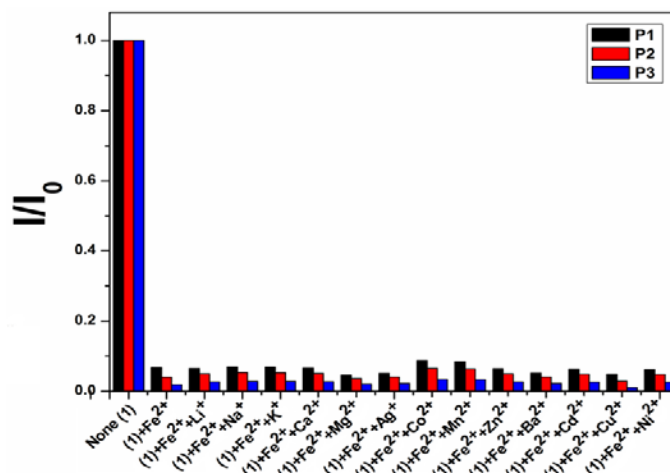
Figure 4.7 Fluorescence emission response profiles (I/I_0) of **P1**, **P2**, and **P3**. The polymer concentration (1.2×10^{-5} M), $[Fe^{2+}] = 1.2 \times 10^{-4}$ M (10 eq) and in the presence of other metal ions $= 1.2 \times 10^{-4}$ M (10 eq) (Dual metal system).

The PL quenching efficiencies (PLQE) and static Stern-Volmer quenching constants (Ksv) were depicted in Table 4.2. Due to the larger molecular wire effect, Ksv of **P3** is ca. 5.1 and 2.5 times higher than **P1** and **P2**, respectively. As depicted in Figure 4.8, sharp decreases of fluorescence intensities in **P1-P3** were observed by the addition of Fe^{2+} up to 1 equiv. molar concentration.

Table 4.2 Photoluminescence quenching efficiency (PLQE) and Stern–Volmer Quenching constants (K_{SV}) of polymers upon the addition of Fe^{2+}

Metal Ion	Polymers	PLQE (%) [a]	K_{sv} [b]
	P1	78.22	2.01×10^6
Fe^{2+}	**P2**	81.57	4.12×10^6
	P3	96.94	1.03×10^7

[a] PLQE = A_0-A/A_0 ; where A_0 = Area under the PL curve without metal ion. A = Area under the PL curve in presence of 10 equiv of metal ions. [b] Stern–Volmer Quenching Constants can be evaluated by the static Stern–Volmer equation I0/I = 1 + KSV [Q] where I0 is the PL

intensity of the polymers (1.2×10^{-5} M) in absence of the quenchers, I is the PL intensity in the presence of each quencher, KSV is the Stern–Volmer quenching constant and [Q] is the quencher concentration.

Table 4.3 Photoluminescence properties of **P1**, **P2**, and **P3** upon titration with Fe^{2+}

Sample	$\lambda_{em}(nm)^a$	$\Phi_{em}{}^b$	τ^c
P1	633	0.82	0.97
P1+Fe^{2+}	628	0.15	0.21
P2	640	0.84	1.12
P2+Fe^{2+}	632	0.11	0.18
P3	661	0.89	1.14
P3+Fe^{2+}	630	0.05	0.10

[a] Emission maxima of Fluorescence spectra obtained by exiting at their absorption maxima. [b] Emission quantum yields measured in THF solutions with reference to Rhodamine 6G for **P1-P3**, respectively. [c] The lifetimes were measured at the emission band maxima.

Fluorescence quantum yields and lifetimes of polymers **P1-P3** before and after the addition of Fe^{2+} are summarized in Table 4.3. Upon the addition of Fe^{2+}, the fluorescence lifetimes of the polymers decreased significantly (see Figure 4.9).[116] In the presence of Fe^{2+}, the fluorescence lifetimes of **P1** and **P2** were decreased almost 4.6 and 6.2 times, respectively. The extensive decrease in the fluorescence lifetime of polymer **P3** (11.4 times) further confirmed the best sensing ability of **P3** due to the stronger molecular wire effect. Stern-Volmer plots for **P1**-**P3** in the presence of Fe^{2+} indicated 1:1 stoichiometry. Fluorescence recovery tests were carried out by two suitable counter ligands disodium salt of ethylenediaminetetraacitic acid (Na$_2$-EDTA) and phenathroline. As illustrated in Figure 4.8, upon the addition of disodium salt of ethylenediaminetetraacitic acid (Na2-EDTA) or

phenathroline in THF to the quenched Fe^{2+}-polymer (**P1**-**P3**) solutions, the florescence intensities were almost 65-85% recovered. This indicates the reversible association of Fe^{2+} with imidazole units, via formation of stable Fe-EDTA complex. Similarly, upon the addition of phenanthroline to the quenched Fe^{2+}-polymers (**P1**-**P3**) solutions, the fluorescence intensities were almost 90% recovered. This suggested that Fe^{2+} coordinates strongly via double coordinating bond with phenantroline in the presence of phenantroline, which casued the polymers to be released from Fe^{2+}. Thus, for the fully quenched Fe^{2+}-polymers (**P1**-**P3**) solutions, phenathroline mediated fluorescence recovery is more prominent than that of EDTA. The photographs of the quenching and recovery in florescence for all polymers (**P1**-**P3**) were also shown in the insets of Figures 4.8.
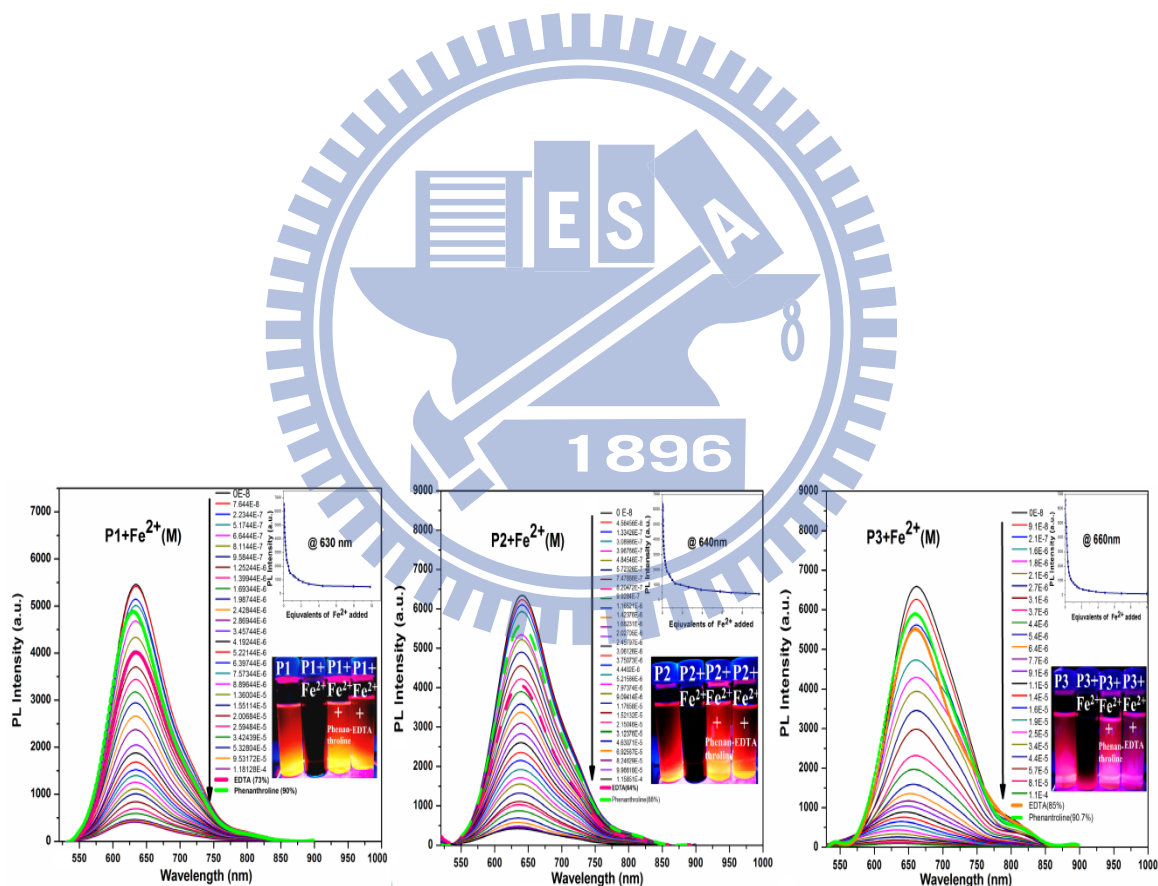
Figure 4.8 Sequential PL quenching of **P1**-**P3** (1.2×10^{-5} M) in THF/H_2O (1/1) acquired by the addition of 0-10 eq of Fe^{2+} and recovery of fluorescence by the addition of Na_2-EDTA and phenantroline. Upper inset PL quenching of **P1** as a function of 0-10 eq [Fe^{2+}]. Lower

inset photographs of fluorescence quenching in polymer solutions upon the addition of Fe^{2+} and regain of original fluorescence upon the addition of phenanthroline or Na_2-EDTA.
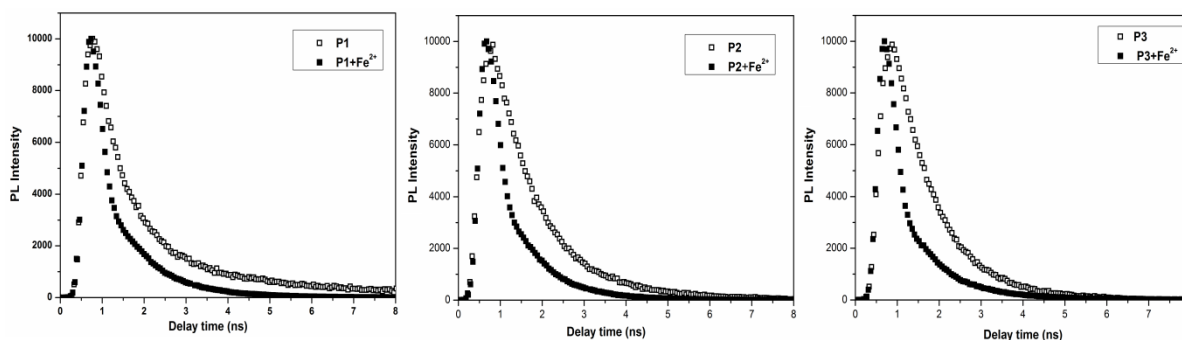
Figure 4.9 Time-resolved fluorescence of polymers **P1-P3**, before (empty circle) and after (solid circle) the addition of Fe^{2+}.

Moreover, the fluorescence on-off-on behaviour was observed for 6 successive cycles (Figure 10).Thus, a remarkable fluorescence on-off-on behaviour was achieved for the polymer solutions, during sensing of Fe^{2+} via reversible binding to imidazole receptors upon the addition of proper counter ligands (such as EDTA and phenathroline) to form more stable complexes. To the best of our knowledge, the phenanthroline ligand intervened efficient fluorescence recovery of imidazole receptors in the presence of metal ions is reported for the first time.
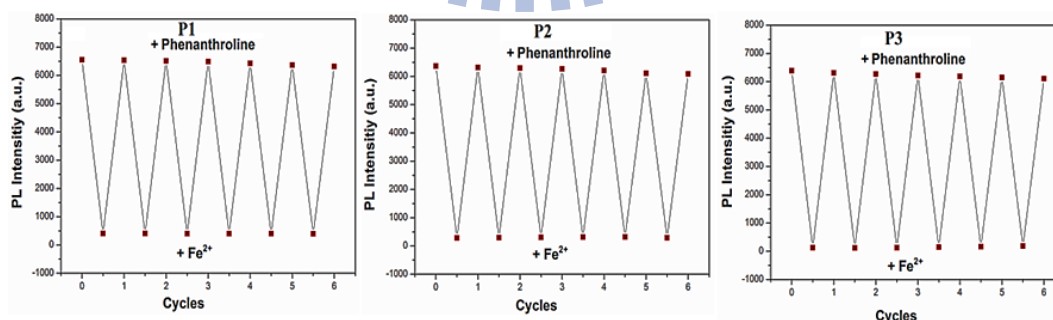
Figure 4.10. The switches of on-off-on fluorescent spectra of **P1**, **P2**, and **P3** for seven successive cycles upon the addition of Fe^{2+} and phenanthroline.

To further elucidate the binding mode, ^{1}H NMR titrations were conducted upon the addition of Fe^{2+} (in D_2O) to **M1**-**M3** (binding probes of **P1**-**P3**, respectively) in d_8-THF (see Figure 11). In **M1**, the aromatic protons were gradually shifted towards up-field upon the sequential addition of Fe^{2+}. The peak corresponding to dibromo thiophene unit was 0.1 ppm up-field shifted (from 7.55 to 7.45 ppm). Likewise, upon the addition of Fe^{2+}, there is notable shift observed in aromatic protons corresponding to **M2**. The proton corresponding to dibromo thiophene was 0.13 ppm up-field shifted (from 7.58 to 7.45 ppm). Unlike **M1** and **M2**, the proton peak corresponding to dibromo-thiophene unit in **M3** was dramatically down-field shifted. The peak of dibromo thiophene in **P3**, originally appeared at 7.42 ppm, was 0.16 ppm down-field shifted to 7.58 ppm. This is probably due to the different electronic distribution in **M3** due to the presence of anti-aromatic acenaphthene moiety (as discussed previously in the computational analysis).
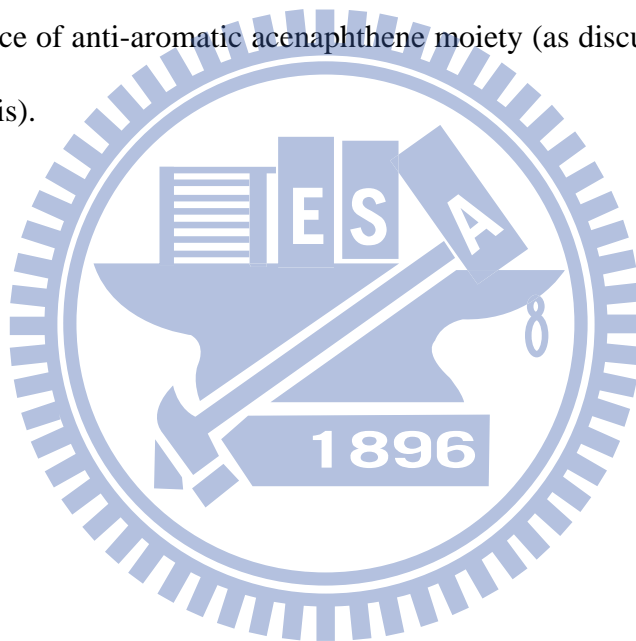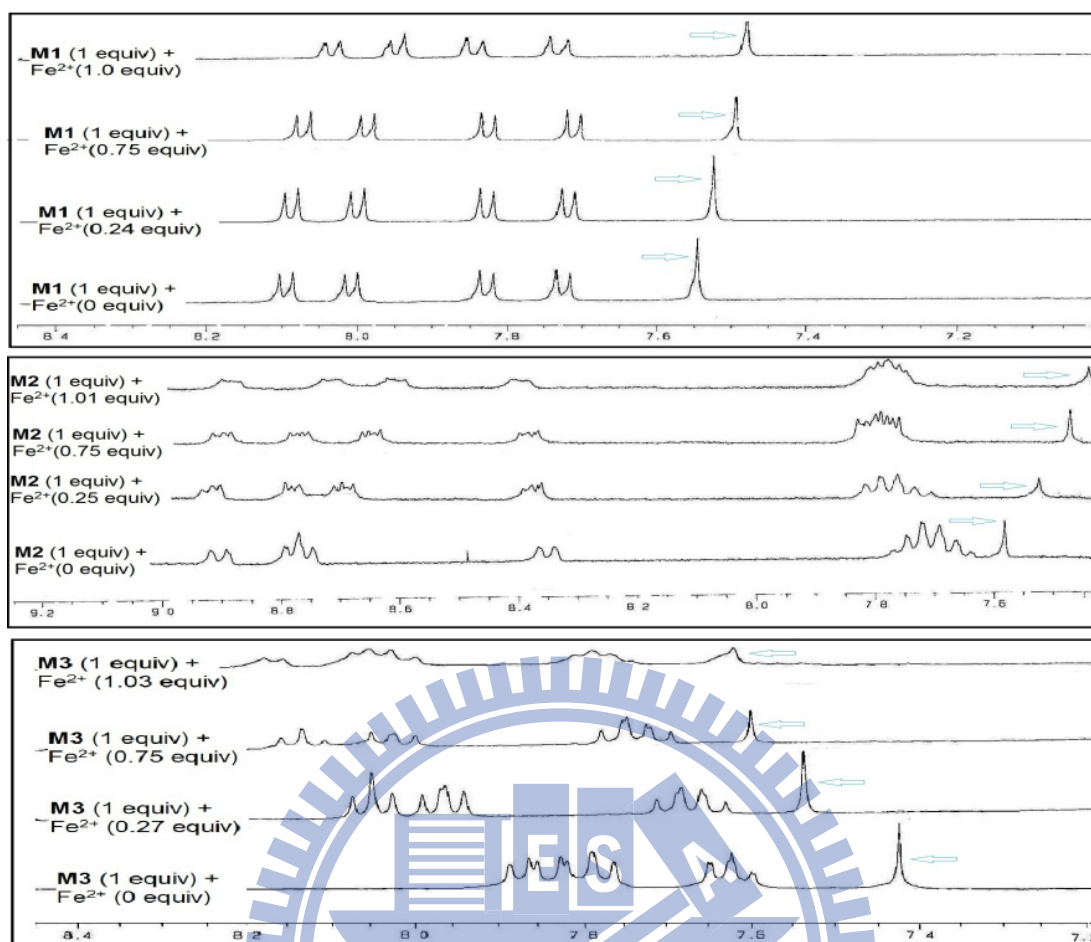
Figure 4.11 ^{1}H NMR titrations of monomers **M1**-**M3** (in d$_8$-THF) upon the sequencial addition of 0-1 equiv of Fe^{2+} (in D$_2$O). (Arrow marks show the shifts of the peak corresponding to the dibromothophene units).

4.3.5 F$^-$ sensing of 1-B, 2-B, 3-B, and 4-B: The precursors of monomers **M1**-**M4** (i.e. imidazole derivatives **1-B**, **2-B**, **3-B** and **4-B** with free NH groups) were investigated for their halide ion sensing capabilities. As shown in Figures 4.12 (a-d), all these imidazole derivatives sensed F$^-$ effectively over other halides (Cl$^-$, Br$^-$ and I$^-$). Upon the addition of F$^-$ to **1-B**, the PL peaks at 500 nm decreased gradually (Figure 4.12e). Again, upon the addition of F$^-$ (approaching 1 equiv.) to **2-B**, the PL peaks at 325 increased and a new peak arised at 430 nm simultaneously (Figure 4.12f). For **3-B**, the PL peaks at 325, 525 and 580 nm decreased

with the addition of F⁻ (Figure 4.12g). However, **4-B** showed the best sensing behavior towards F- ions. The PL peaks of **4-B** at 420 nm decreased gradually and new peaks at 504 nm increased with the concomitant addition of F⁻ (Figure 4.12h).
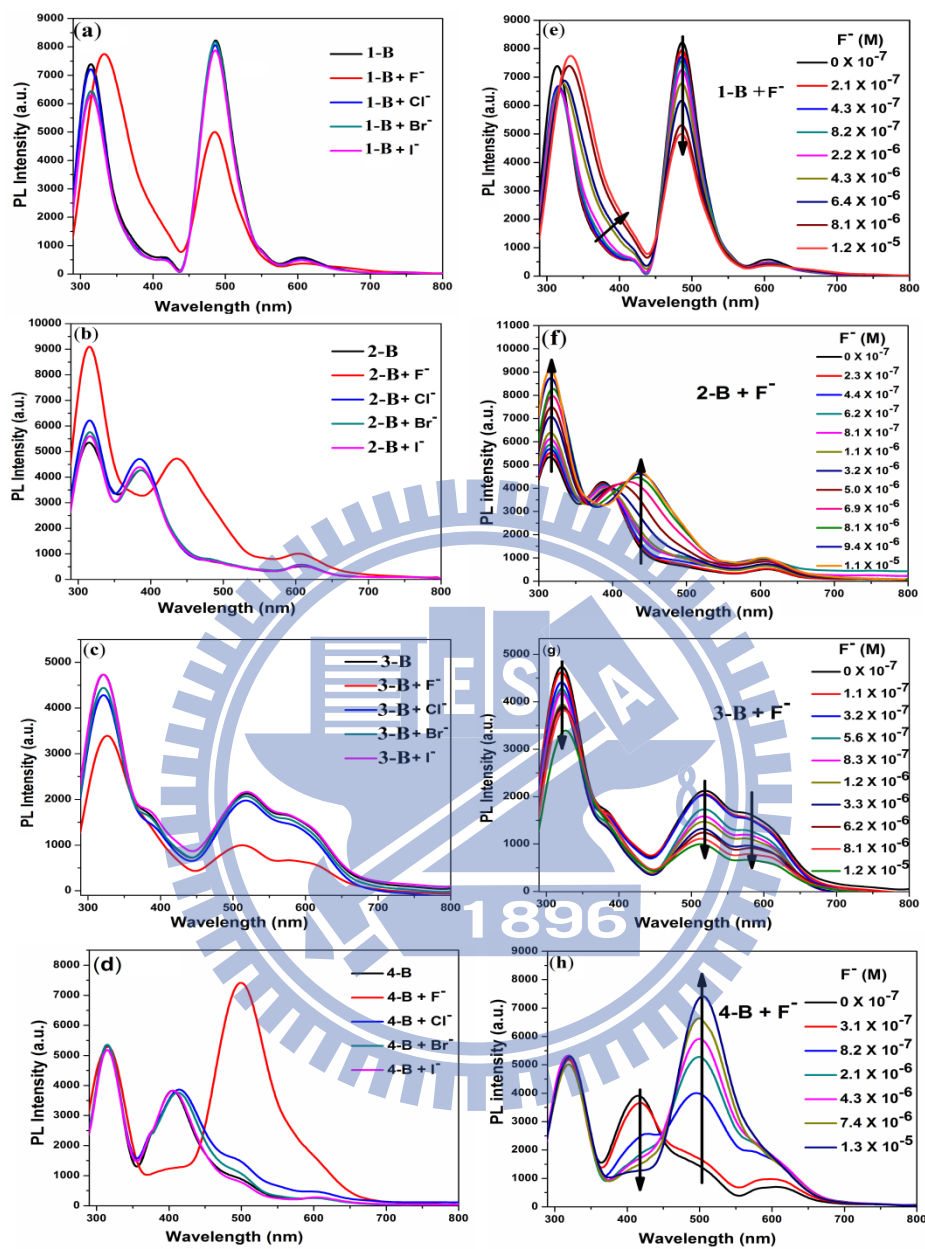
Figure 4.12 (a-d) Fluorescence spectral responses during the addition of different halides (F^-, Cl^-, Br^-, and I^-) to **1-B**, **2-B**, **3-B**, and **4B**; (e-h) Fluorescence spectral changes upon the addition of F^- to **1-B**, **2-B**, **3-B**, and **4B** (each 1.0×10^{-5} M in THF/H$_2$O=1/1).

4.4 Conclusions:

Three novel imidazole-based low bandgap polymers (**P1**-**P3)** were synthesized. Due to their donor-acceptor conjugations, these polymers showed excellent photo-physical and electrochemical properties (such as brilliant fluorescences, low bandgaps, large strokes shifts and low HOMO levels), which led them to be structurally stable semi-conducting molecular wires to act as promising transduction materials for chemosensory applications. Herein, the imidazole-based polymers showed remarkable sensing capabilities towards H^+ and Fe^{2+} in semi-aqueous solutions. However, polymer **P3** showed an unique sensitivity response compared with polymers **P1** and **P2**. Upon titration with H^+, polymer **P3** showed reduced absorption as well as fluorescence intensities due to the static quenchning. Whereas, polymers **P1** and **P2** showed hypsochromic shifts of absorption and PL maxima with enhanced fluorescence intensities under similar conditions. Compared with **P1** and **P2**, the anomalous behaviour of **P3** was proven via the computational analysis representing the electron densities over HOMO and LUMO of **P1**-**P3** before and after the complexation with H^+. Recoveries of their original fluorescence and absorption were achieved by adding TEA. Furthermore, **P3** showed the best sensing ability to Fe^{2+} among **P1**-**P3** due to the larger molecular wire effect. Correspondingly, in the presence of Fe^{2+}, the fluorescence lifetime of **P3** was extensively decreased (almost 11 times) compared with those of polymers **P1** (4.6 times) and **P2** (6.2 times). ^1H NMR titrations with Fe^{2+} revealed the exceptional behaviour of **P3** compared with **P1** and **P2**. Recoveries of quenched fluorescences were achieved by adding Na_2-EDTA/phenanthroline. Thus, imidazole-based polymers can act as efficient chemosensing materials in terms of selectivity, sensitivity and reversibility via the on-off-on fluorescence protocol for future environmental and biological applications.

Chapter 5

5.1 Introduction:

The design of supra molecular assemblies in which the functional properties have the consequence of the tailored structure of the molecules are of growing interest in current research. Especially oligopyridyl ligands and their transition metal complexes have found ample applications as active materials in selfassembled molecular devices, electroluminescent materials and for storage applications in molecular electronics and photonics, luminescent sensors in molecular biology and medical diagnostics, in photocatalysis etc.[117] Directional and effective electron and energy transfer could be achieved by the design of suitable multiple ligands and its complexation with transition metal ions. Among the N-heterocyclic ligands, the remarkably higher affinity of 2,2':6',2"-terpyridine towards transition-metal ions due to $d\pi$-$p\pi^*$ back-bonding of the metal ions to pyridine rings and a chelation effect make them useful for supramolecular construction. Compared with other transition metal ion complexes, due to the high binding strength of RuII to the terpyridine moiety, these complexes show a remarkable stability and can only be cleaved under extreme conditions like low pH value, high temperature, addition of strong competitive ligands.[118] Suitable π-Conjugated substituents at the 4'-position of the 2,2':6',2"-terpyridine unit exhibit intriguing spectroscopic and redox properties which cause effective electronic communication between the metal and π ligand. Furthermore, their photophysical, electrochemical, and magnetic properties are strongly influenced by the nature of the π-Conjugated moiety attached to terpyridine.[119] Furthermore, the electronic communication between the metal-complexed terpyridines with the attached π-Conjugated moiety is another fascinating feature directing their potentials for the design of new supramolecular architecture. Recently, terpyridyl Ru(II) complexes have got interest for the researchers to investigate their photovoltaic cells (PVC) application.[120] Again, dyadic molecules comprised of a 4'-substituted terpyridine complex with ruthenium(II) and terpridine has been studied as specifically active candidates in organic

photovoltaic cells.[121] These systems have got extensive attention due to their very long-lived metal to ligand charge transfer (MLCT) excited states and high molar extinction coefficients in the visible range. In these dyads, the excited state that is generated upon the absorption of light leads to a charge separated state with high efficiency. During the synthesis of dyadic polymer, the polydispersity arising due to chains of various sizes and different molecular weights can extensively amend the carrier mobility when used in OPV devices.[122a,b] Therefore, monodispersed materials are desired for an efficient charge transport and device efficiency in organic photovoltaics applications because of their aptitude to control the morphology of blends.[122c] In this esteem, conjugated dendrimers offer an alternative to the conjugated polymers to be used in organic photovoltaics[122d] because of their following advantages. Dendrimers (1) possess well-defined molecular weight with monodispersity; (2) have shape persistency, which allows them to maintain structure in a solution-processable form; (3) can be synthesized with high purity compared to polymers. (4) an internal local electric field may be created during the charge transfer from the perifery to the core of the dendrimer. In addition, conjugated dendrimers are expected to show a high degree of ordering in OPV devices due to their small size and monodisperse nature. To the best of our knowledge, however, there are only a few reports on the applications of dendrimers in organic solar cells.[123] Due to the three dimensional hyper-branched structure, the branches become denser with increasing distance from the core, which produces shell effect in denrimers.[124] Thus, a high-generation dendrimer has highly dense branches towards the outer surface, which acts as a barrier to restrict the charge transfer between the inner and outer part of the dendrimer. Thiophene dendrimers has recently got promising attention for the application in photovoltaics. Terpyridine cored dendrimers contain metal binding terpyridine site to coordinate metal ions into it.

106

5.2 Experimental section:

5.2.1 Materials and Instrumentation:

All chemicals and solvents were reagent grades and purchased from Aldrich, ACROS, Fluka, TCI, TEDIA, and Lancaster Chemical Co. Toluene, tetrahydrofuran, and diethyl ether were distilled over sodium/benzophenone to keep anhydrous before use. Chloroform ($CHCl_3$) was purified by refluxing with calcium hydride and then distilled. If not otherwise specified, the other solvents were degassed by nitrogen 1 h prior to use. Synthesis of 2-(4-hexylthiophen-2-yl)-4,4,5,5-tetramethyl-1,3,2-dioxaborolane, 4,7-dibromo-2,1,3-benzothiadiazole, were prepared by following the literature procedures.

^{1}H NMR spectra were recorded on a Brocher 300 MHz spectrometer using $CDCl_3$ and DMSO-d_6 solvents. Elemental analyses were performed on a HERAEUS CHN-OS RAPID elemental analyzer. UV-visible absorption were recorded in dilute chloroform solutions (10^{-6} M) on a HP G1103A spectrophotometer. Solid films of UV-vis measurements were spin-coated on quartz substrates from chloroform solutions with a concentration of 10 mg/mL. Cyclic voltammetry (CV) measurements were performed using a BAS 100 electrochemical analyzer with a standard three-electrode electrochemical cell in a 0.1 M tetrabutylammonium hexafluorophosphate (Bu_4NPF_6) solution (in acetonitrile) at room temperature with a scanning rate of 100 mV/s. During the CV measurements, the solutions were purged with nitrogen for 30 s. In each case, a carbon working electrode coated with a thin layer of monomers or polymers, a platinum wire as the counter electrode, and a silver wire as the quasi-reference electrode were used, and Ag/AgCl (3 M KCl) electrode was served as a reference electrode for all potentials quoted herein. The redox couple of ferrocene/ferrocenium ion (Fc/Fc^+) was used as an external standard. The corresponding HOMO and LUMO levels were calculated using $E_{ox/onset}$ and $E_{red/onset}$ for experiments in solid films, which were performed by drop-casting films with the similar thicknesses from THF or DMF solutions (ca. 5 mg/mL).

Mono (**G1RuG1**, **G2RuG2**, **G3RuG3**), bis (**BT2RuG1**, **BT2RuG2**, **BT2RuG3**) and tris (**TPA3RuG1**, **TPA3RuG2**, **TPA3RuG3**) 'Ru' containing supramolecular thiophene dendrimers were constructed. Due to the donor-acceptor, benzothiadiazole-hexyl thiophene cored architecture in bis 'Ru' containing thiophene dendrimers, these showed higher photovoltaic efficiency than other two series. Tris 'Ru' containg architecture with terthiophene-triphenylamine core, showed moderate photovoltaic performance due to their star shaped branched structure.

5.2.2 Synthesis and Structural Characterization:

Shematic representations of one, two and three metal systems are depicted in Figure 5.1. Structure of single, double and triple metal cored thiophene dendrimers has been depicted in Figure 1.Three generations of thiophene dendrimers (**G1**,**G2** and **G3**) has been synthesized by as shown in Scheme 5.1. Stille coupling of $4^{/}$-(2-Bromo-5-thienyl)-$2,2^{/},6^{/},2^{//}$-terpyridine with **G1**-SnBu3, **G2**-SnBu3 and **G3**-SnBu3 produced **G1**-TPY, **G2**-TPY and **G3**-TPY respectively (scheme 5.2). The single metal systems ie. **G1RuG1**, **G2RuG2** and **G3RuG3** were prepared according to scheme 5.3. Core for the two metal systems was prepared by as shown in Scheme 5.4. Synthetic route for the preparation of the core for three metal system was depicted in scheme 5.4. The supramolecular ruthenium cored dendrimer series has got good solubility in common organic solvents such as DCM, THF, EA, DMF, DMA etc. The good solubility of these supramolecular macromolecules led these to have easy processing. The compound structures were confirmed by NMR, UV characterization.

Shematic representation:

One Metal System
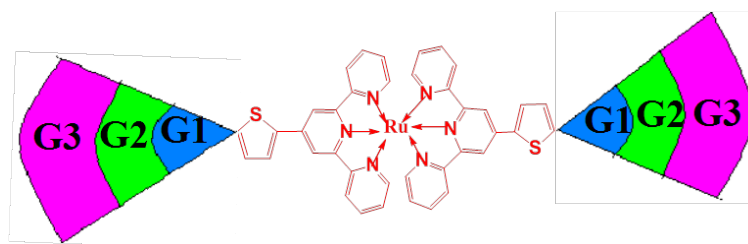
Two Metal System
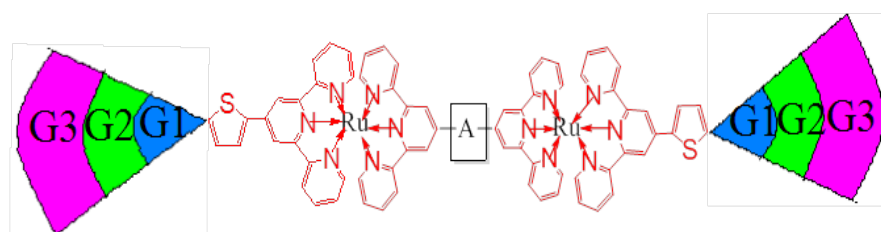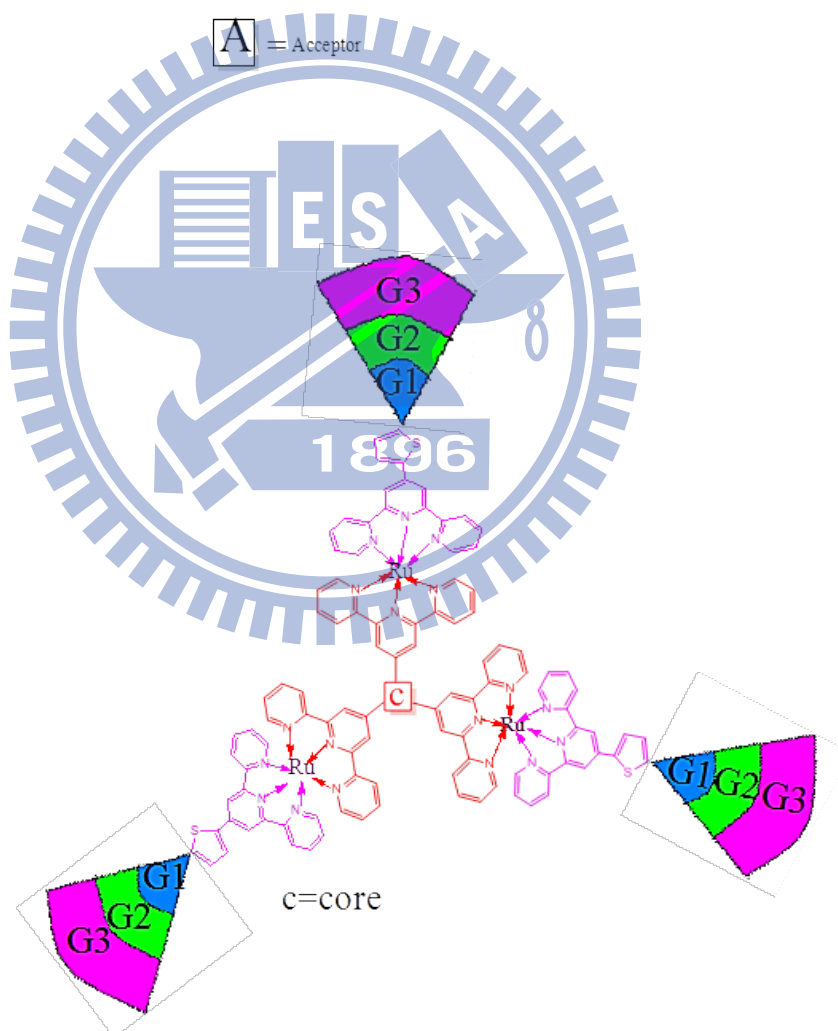
Three Metal System

Figure 5.1 Shematic representations of one, two and three metal systems.
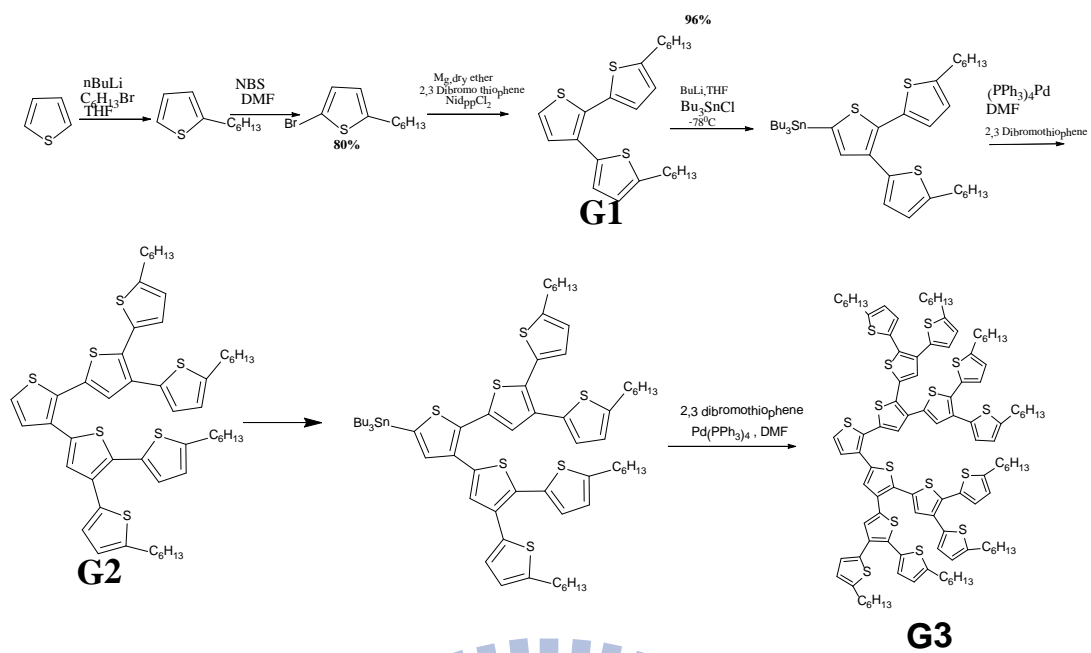
Scheme 5.1 Synthesis of The Dendrimers.
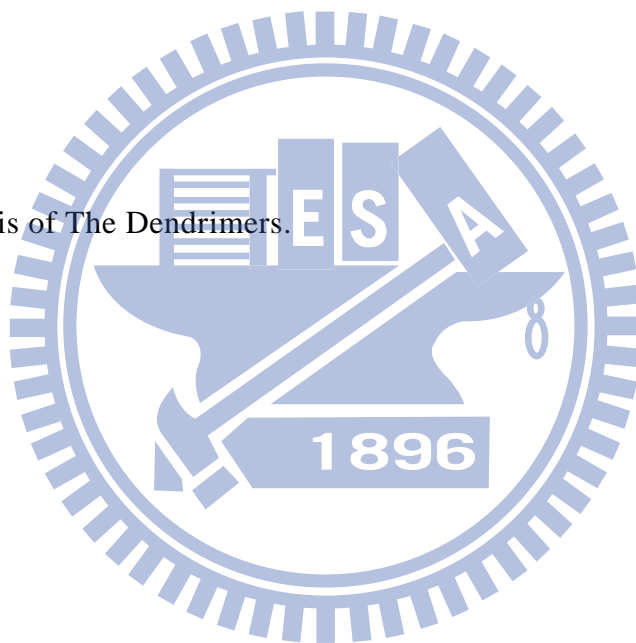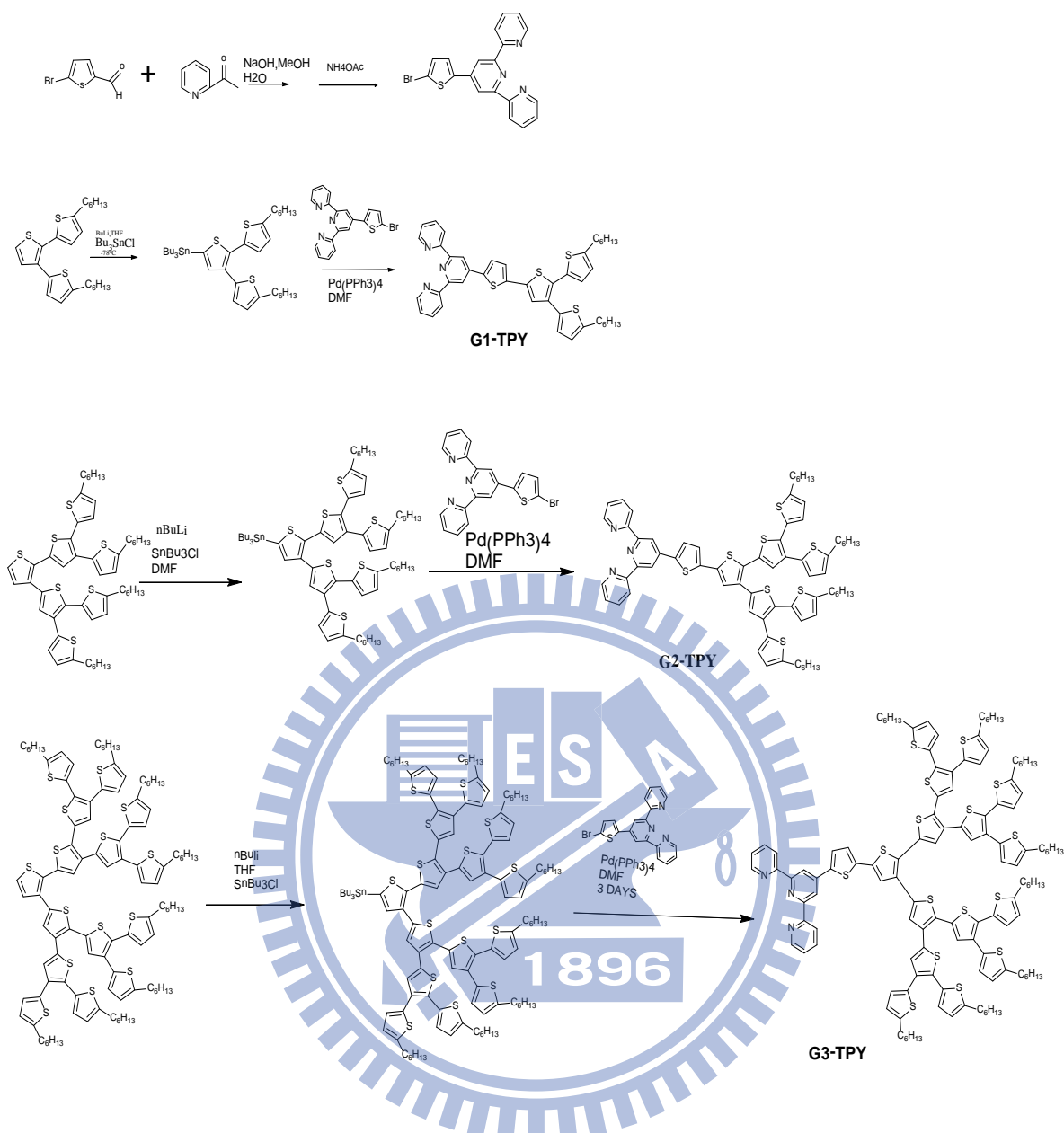
Scheme 5.2 Synthesis of terpyridine derivatives
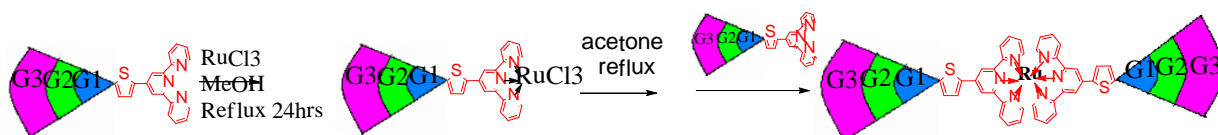
Scheme 5.3 Synthesis of one metal systems
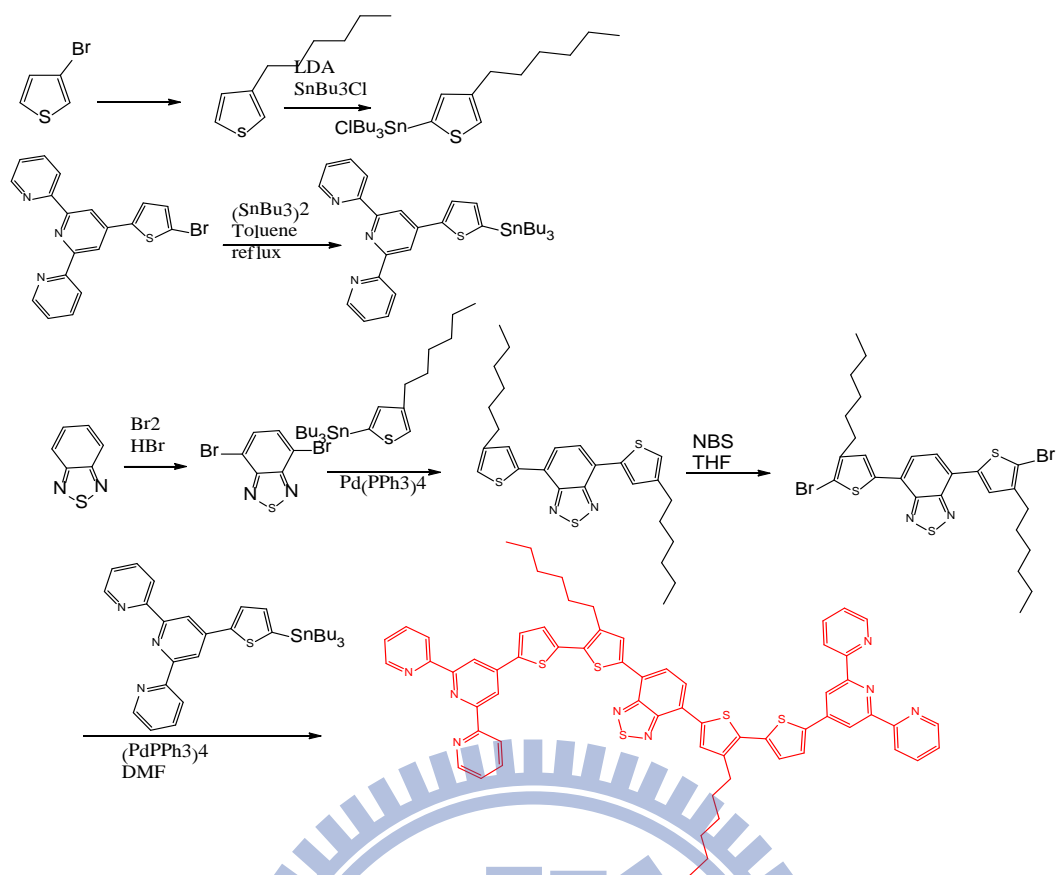
Scheme 5.4 Synthesis of core for two metal systems.
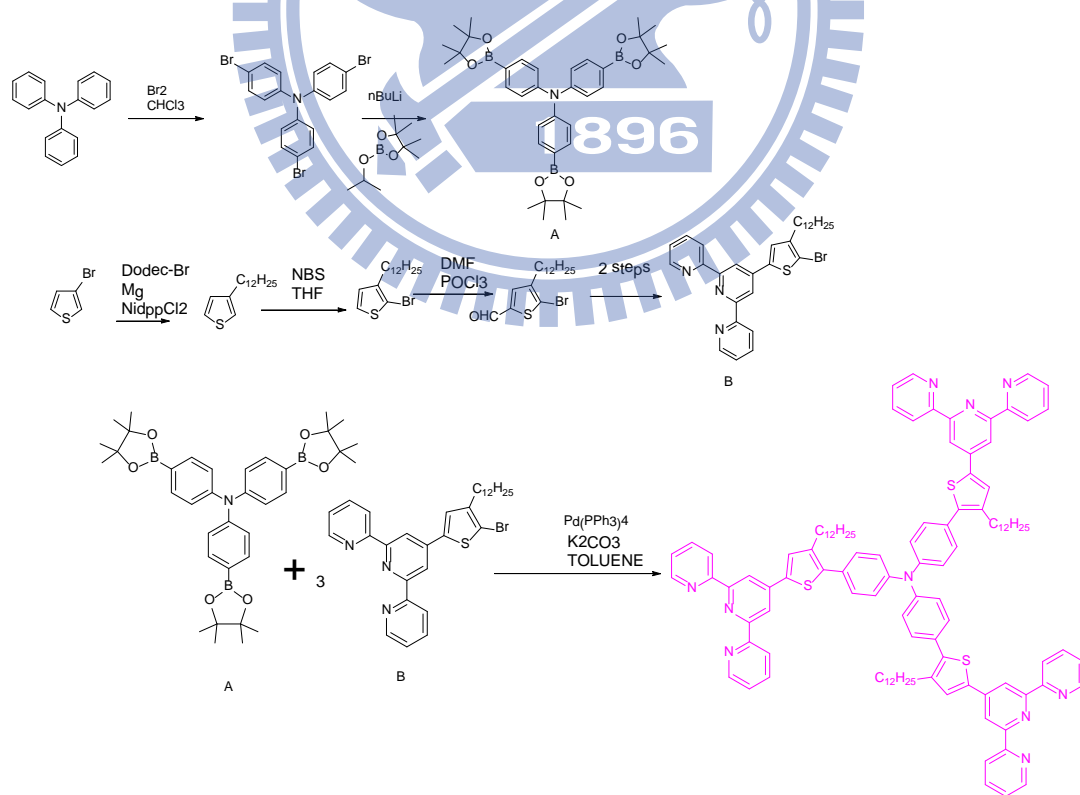
Scheme 5.5 Synthesis of core for three metal systems.

G1RuG1

G2RuG2

G3RuG3
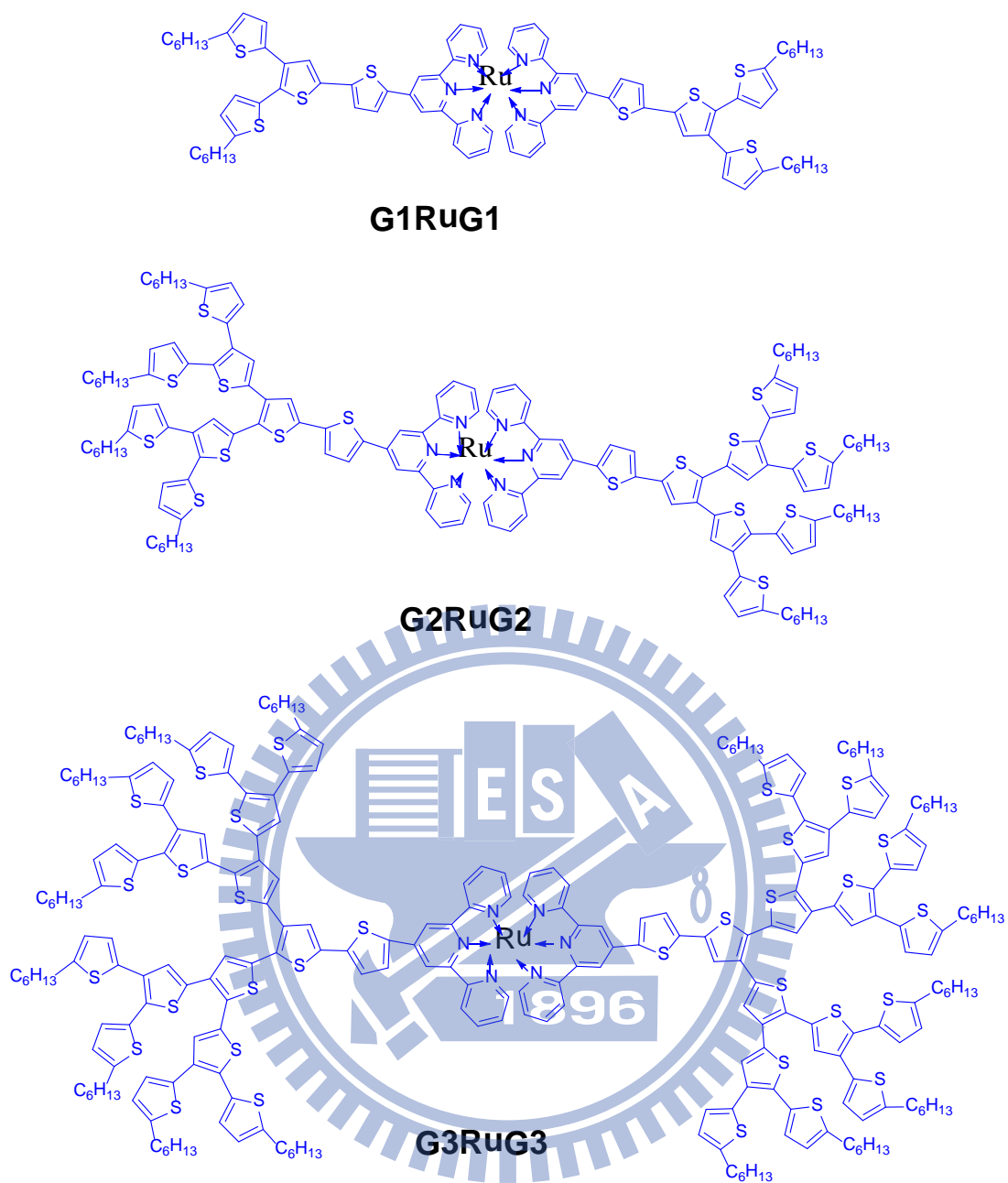
Figure 5.2 Final structures of one metal systems

BT2RuG1

BT2RuG2

BT2RuG3
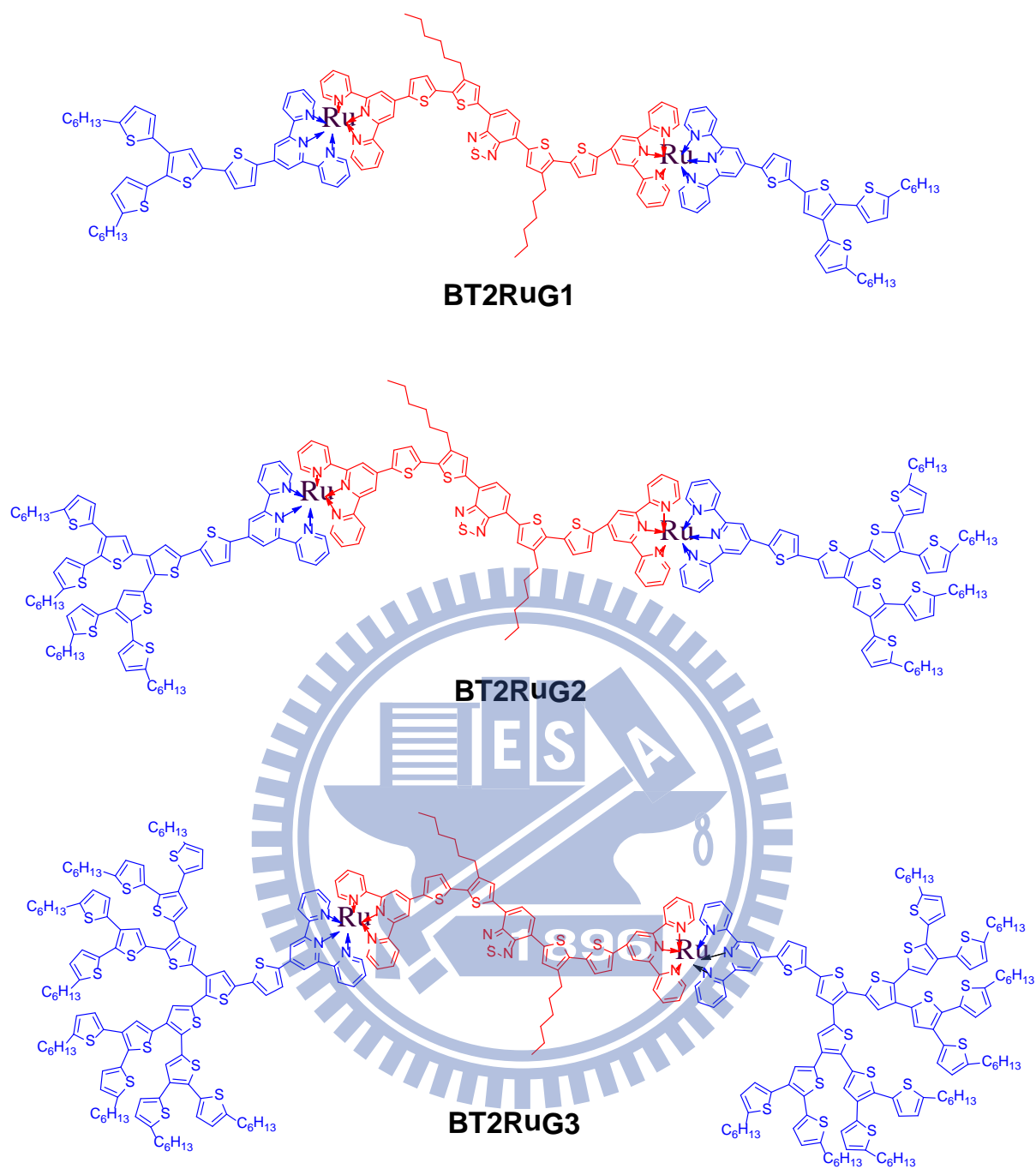
Figure 5.3 Final structures of two metal systems
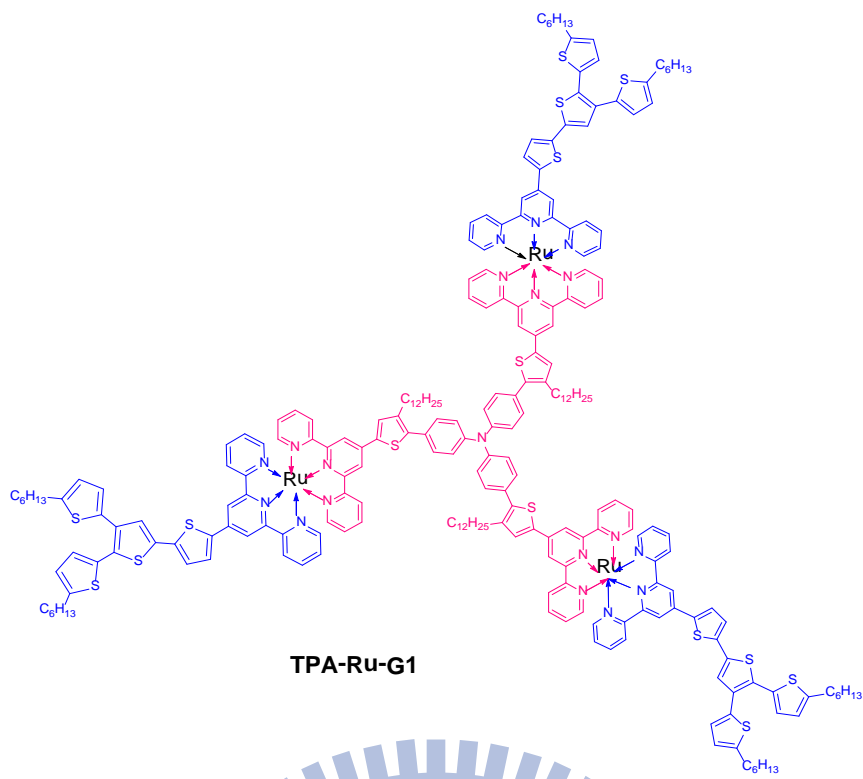
TPA-Ru-G1
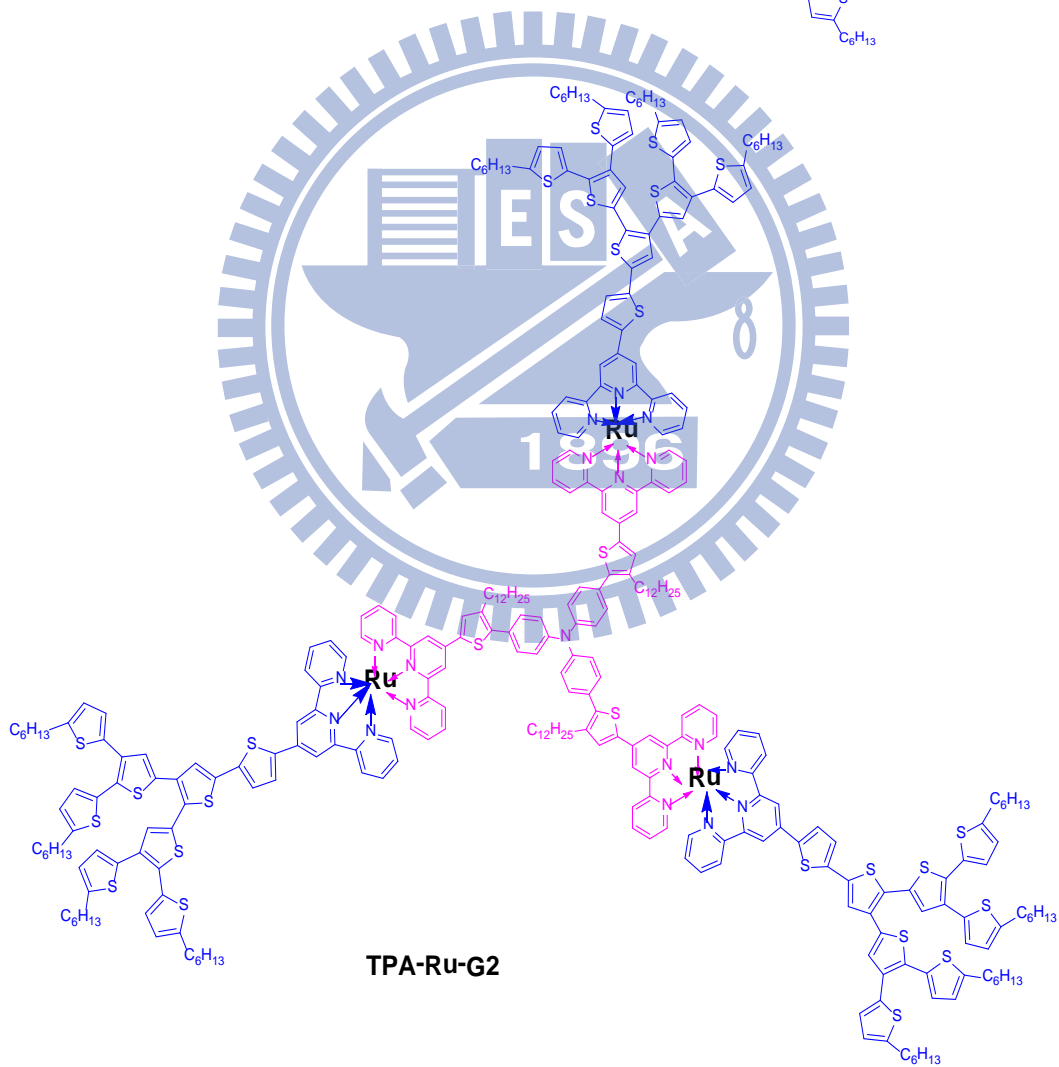
TPA-Ru-G2
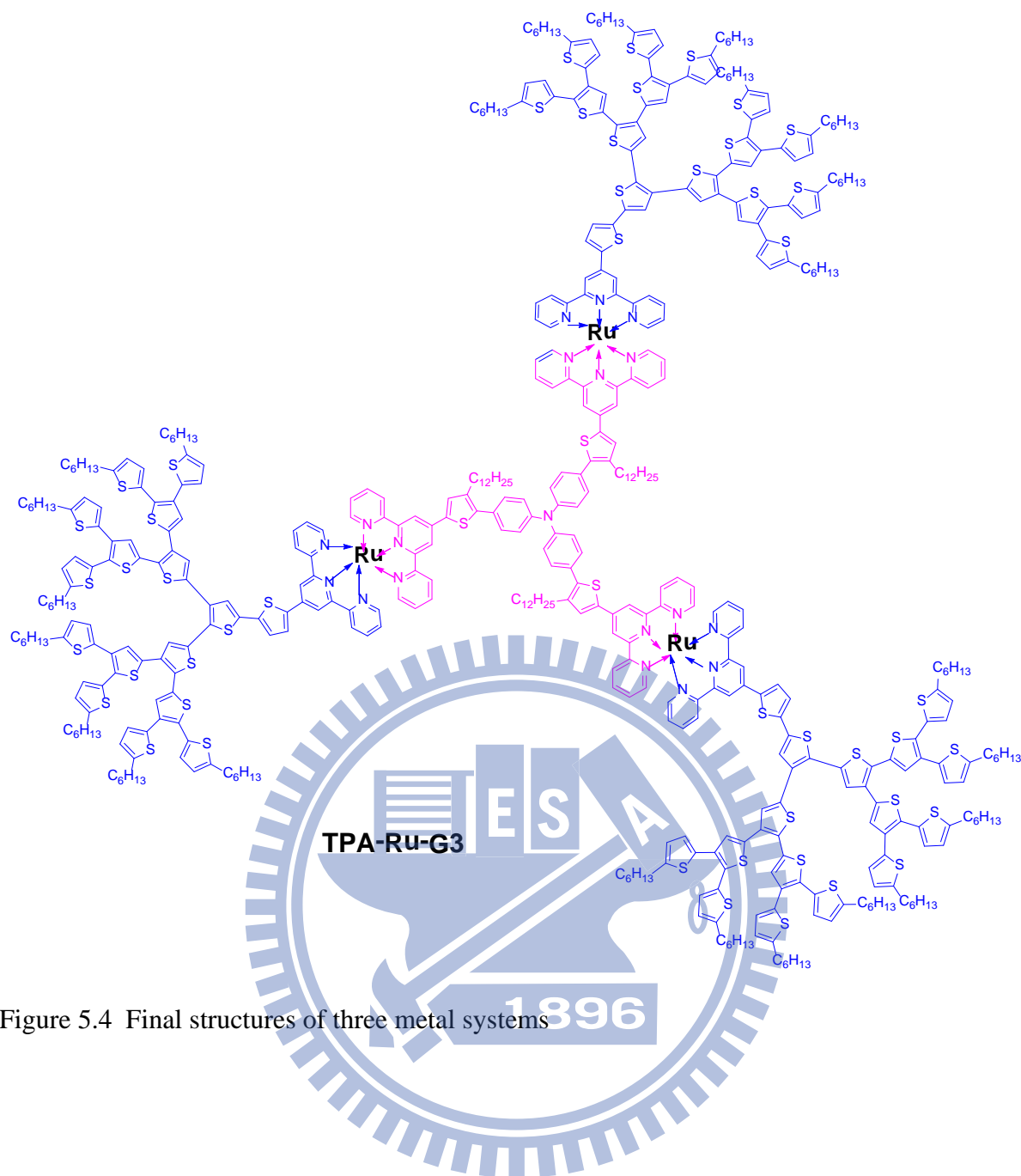
Figure 5.4 Final structures of three metal systems

5.2.3 Synthetic Procedures

G1-SnBu₃: G1 (2.1gm, 5.03 mmole) was dissolved in 25 ml THF and cooled to -78°C. To it 2.5 M n-BuLi in hexane (2.41 ml, 6.04 mmole) was added drop wise.

The reaction was allowed stir at -78°C for 1 hour. To it SnBu3Cl (1.96gm, 1.63ml, 6.03mmole) was added rapidly. The reaction mixture was allowed to warm to room temperature and stirred overnight. The reaction mixture was quenched by addition of 20 ml H₂O and extracted by ethyl acetate via three times water wash. The organic layer was dried

116

over MgSO$_4$, solvent was removed by rotary evaporation to get the crude product as pale-yellow oil. The crude product was used for next step without further purification.

^{1}H NMR (CDCl$_3$, 300 MHz): 7.10 (s, 1H) , 6.91 (d, 1H, 3.3 Hz), 6.87 (d, 1H, 3.6 Hz), 6.66 (d, 2H, 3.3 Hz), 2.77 (m, 4H), 1.64 (m, 4H) , 1.56 (m, 6H), 1.36 (t, 6H, 7.3Hz), 1.30 (m, 12H), 1.11 (t, 6H, 8.3 Hz), 0.90 (m, 15H).

G1-TPY : G1-SnBu3 (3.5 gm,4.95 mmole), Br-th-tpy (1.62 gm,4.13 mmole) and Pd(PPh$_3$)$_4$ (114 mg, 0.099 mmole) was taken in a two neck flask and degassed by nitrogen. 30 ml dry DMF was poured into it and the reaction mixture heated to 90$^°$C

overnight. 100 ml of water was added to it and the reaction mixture was extracted by EA. Organic layer was dried over MgSO4 and the solvent was removed by rota vapour. Crude product was purified by neutral alumina column chromatography using hexane: EA = 15:1 to yield pure compound (2.02 gm, 67.1%). ^{1}H NMR (CDCl$_3$, 300MHz) : 8.75 (d, 2H, 6Hz), 8.67 (s, 2H), 8.65 (d, 2H, 6 Hz), 7.90 (dt, 2H, 9 Hz ,1.2 Hz), 7.71 (1H, 3.9 Hz), 7.38 (2H, 6 Hz), 7.27 (s, 1H), 7.23 (d, 1H, 3 Hz), 6.98 (d, 1H, 3 Hz), 6.92 (d, 1H, 3 Hz), 6.69 (d, 2H, 3 Hz), 2.82 (t, 4H, 7.5 Hz), 1.70-1.61 (m, 4H), 1.39-1.26 (m, 12H), 0.94 (t, 6H, 6.5 Hz) . ^{13}C NMR (CDCl$_3$, 300MHz) : 155.98, 155.88, 149.07, 147.73, 146.41, 142.80, 140.45, 138.32, 136.78, 134.58, 134.28, 132.44, 131.94, 131.11, 127.52, 126.67, 126.57, 126.41, 124.68, 124.23, 124.08, 123.85, 121.24, 116.56, 31.55, 31.52, 31.47, 28.74, 26.81, 22.57, 17.48, 14.07 13.58 Elemental analysis for C$_{43}$H$_{43}$N$_3$S$_4$: Calculated : (%) C, 70.74; H, 5.94; N, 5.76. Found: (%) C, 70.29; H, 5.93; N, 5.90. MS (FAB): m/z 730 (calcd (M)$^+$).

G2-SnBu$_3$: G1 (1.8 gm, 1.97 mmole) was dissolved in 25 ml THF and cooled to -78^{0}C. To it 2.5 M n-BuLi in hexane (0.94 ml, 2.36 mmole) was added drop wise.

The reaction was allowed stir at -78^{0}C for 1 hour. To it SnBu3Cl (0.83 gm, 0.69 ml, 2.56 mmole) was added rapidly. The reaction mixture was allowed to warm to room temperature and stirred overnight. The reaction mixture was quenched by addition of 20 ml H$_2$O and

extracted by ethyl acetate via three times water wash. The organic layer was dried over MgSO$_4$, solvent was removed by rotary evaporation to get the crude product as pale-yellow oil. The crude product was used for next step without further purification. ^{1}H NMR (CDCl$_3$, 300 MHz): 7.19 (s, 1H), 7.18 (s, 1H), 7.15 (s, 1H), 6.93 (t, 2H, 3Hz), 6.87 (d, 2H, 3Hz), 6.65 (m, 4H), 2.76 (t, 8H, 6.9 Hz),1.69-1.57 (m, 14H), 1.36-1.29 (m, 30H), 1.11 (t, 6H, J=8.2 Hz), 0.89 (m, 21H).

G$_2$-TPY: G$_2$-SnBu$_3$ (2.3 gm,1.91 mmole), Br-th-tpy (0.62 gm, 1.59 mmole) and Pd(PPh$_3$)$_4$ (44 mg, 0.038 mmole) was taken in a two neck flask and degassed by nitrogen .25 ml dry DMF was poured into it and the reaction mixture heated to 90$^°$C

overnight. 100 ml of water was added to it and the reaction mixture was extracted by EA. Organic layer was dried over MgSO4 and the solvent was removed by rota vapour. Crude product was purified by neutral alumina column chromatography using (hexane: EA = 20:1) to yield pure compound (1.27 gm, 54.2%).

^{1}H NMR (CDCl$_3$, 300 MHz): 8.75 (d, 2H, 6Hz), 8.67 (s, 2H), 8.65 (d, 2H ,6Hz), 7.90 (dt, 2H, 9 Hz, 1.2 Hz), 7.71 (1H, 3.9 Hz), 7.38 (2H, 6 Hz), 7.27 (s, 1H), 7.23 (d, 1H, 3 Hz), 6.98 (d, 1H, 3 Hz), 6.92 (d, 1H, 3 Hz) 6.69 (d, 2H, 3 Hz), 2.82 (t, 4H, 7.5 Hz), 1.70-1.61 (m, 4H), 1.39-1.26 (m, 12H), 0.94 (t, 6H, 6.5 Hz). ^{13}C NMR (CDCl$_3$, 300 MHz): 155.76 , 155.72 , 148.97, 147.62, 147.41 146.27, 146.09,142.43, 140.79, 137.65, 136.67, 135.61, 134.75, 134.48, 134.39, 132.19, 131.91, 131.87, 131.81, 130.24, 129.70, 127.59, 127.49, 126.51, 126.44, 126.26, 124.19, 124.05, 123.77, 121.16, 116.39, 116.20, 31.61, 31.51, 30.16, 28.82, 28.80, 27.83, 26.86, 25.60, 22.71, 22.63, 14.35, 13.64. Elemental analysis for C$_{71}$H$_{75}$N$_3$S$_8$: Calculated: (%) C, 69.51; H, 6.16; N, 3.42. Found: (%) C, 69.32; H, 6.63; N, 3.41. MS (FAB): m/z 1227 (calcd (m)$^+$).

G$_3$-SnBu$_3$: G$_3$ (1.5 gm, 0.78 mmole) was dissolved in 20 ml THF and cooled to -78$^°$C. To it 2.5 M n-BuLi in hexane (0.37 ml, 0.93 mmole) was added drop wise.

The reaction was allowed stir at -78°C for 1 hour. To it SnBu$_3$Cl (0.33 gm, 0.27 ml, 1.04 mmole) was added rapidly. The reaction mixture was allowed to warm to room temperature and stirred overnight. The reaction mixture was quenched by addition of 20 ml H$_2$O and extracted by ethyl acetate via three times water wash. The organic layer was dried over MgSO$_4$, solvent was removed by rotary evaporation to get the crude product as pale-yellow oil. The crude product was used for next step without further purification.

G$_3$-TPY: G$_2$-SnBu$_3$ (1.7 gm,0.77 mmole), Br-th-tpy (0.25 gm, 0.64 mmole) and Pd(PPh$_3$)$_4$ (17.8 mg, 0.015 mmole) was taken in a two neck flask and degassed by nitrogen .15 ml dry DMF was poured into it and the reaction mixture heated to 90°C

overnight. 100 ml of water was added to it and the reaction mixture was extracted by EA. Organic layer was dried over MgSO4 and the solvent was removed by rota vapor. Crude product was purified by neutral alumina column chromatography using (hexane: EA = 20:1) to yield pure compound (0.82 g , 48.2%). ^{1}H NMR (CDCl3,300MHz): 8.72 (d, 2H, 6Hz), 8.65 (s, 2H), 8.62 (d, 2H, 9Hz),7.77 (t, 2H, 9Hz), 7.59 (d, 3Hz), 7.29-7.24 (m, 7H), 7.18 (s, 1H),7.12 (d, 1H, 2.7Hz), 7.02 (s, 1H),6.97 (m, 4H), 6.91 (m, 4H), 6.65 (m, 8H), 2.74 (t, 16H, 7.4Hz), 1.63 (m, 16H), 1.34 (m, 48H), 0.96 (t, 24H, 5.4Hz). ^{13}C NMR (CDCl$_3$,300 MHz): 155.98, 155.82, 149.06, 147.60, 147.35, 147.29, 146.23, 146.19, 146.06, 146.02, 142.66, 141.13, 137.65, 136.79, 136.11, 135.30,134.76, 134.46, 134.42, 134.36, 133.17, 133.08, 132.95, 132.58, 132.31, 132.21, 132.16, 131.95, 131.86, 131.72, 131.37, 131.31,130.47, 130.39, 130.26, 129.73, 129.59, 127.64, 127.52, 126.66, 126.43, 126.39,126.25, 125.26, 124.10, 123.94, 121.25, 116.65, 31.54,31.46, 30.14, 30.10, 28.77, 22.57, 14.05 .Elemental analysis for C127,H139,N3,S16 : Calculated : (%) C, 68.69; H, 6.31; N, 1.89 . Found: (%) C, 67.86; H, 6.75; N, 1.73. MS (MALDI-TOF): m/z 2220.7 (calcd (M)$^+$) .

G1-TPY-RuCl$_3$: G1-TPY (600 mg, 0.822 mmole) and RuCl$_3$ .xH$_2$O (236.46 mg, 0.906 mmole) were taken in MeOH: THF/ 5:1 under N$_2$ atmosphere. The mixture was refluxed

overnight. The solid residue was filtered, washed in excess methanol and dried to get the product as shiny black solid (746.04 mg, 97%).

G2-TPY-RuCl₃: G1-TPY (500 mg, 0.407 mmole) and RuCl$_3$ .xH$_2$O (117 mg, 0.448 mmole) were taken in MeOH: THF /5:1 (100 ml) under N$_2$ atmosphere. The mixture was refluxed overnight. The solid residue was filtered, washed in excess methanol and dried to get the product as black solid (574.28 mg, 98.5%).

G2-TPY-RuCl₃: G2-TPY (400 mg, 0.18 mmole) and RuCl$_3$ .xH$_2$O (51.15 mg, 0.196 mmole) were taken in MeOH: THF /5:1 (100 ml) under N$_2$ atmosphere. The mixture was refluxed overnight. The solid residue was filtered, washed in excess methanol and dried to get the product as black solid (420.52 mg, 96.4%).

G1RuG1: G1-TPY-RuCl3 (360 mg, 0.385 mmole) and AgBF$_4$ (300 mg, 1.54 mmole) were taken in acetone (60 ml) and refluxed 18 hrs under N$_2$ atmosphere. The solution was filtered to remove AgCl salt. The filtrate was evaporated and to it G1-TPY (280 mg, 0.385 mmole) was added. The mixture was dissolved in 5 ml Dimethyl acetamide and 50 ml of n-BuOH and refluxed for 24 hours. The product was cooled and added drop wise into a beaker containing 500 ml MeOH under stirring. The solid was filtered, washed in MeOH and 5:1 mixture of MeOH: acetone. The residue was dried to get dark red solid (560.04 mg, 93.2%). ^{1}H NMR (DMSO-d6, 300MHz): 9.33 (s, 4H), 9.11 (d, 4H, 8.1 Hz), 8.48 (d, 2H, 3.9 Hz), 8.07 (t, 4H, 7.5 Hz), 7.82 (d, 2H, 3.6 Hz), 7.72 (s, 2H), 7.60 (d, 4H, 6 Hz), 7.28 (t, 4H, 6.2 Hz), 7.12 (d, 4H, 3.6 Hz), 6.87 (d, 2H, 3.6 Hz), 6.85 (d, 2H, 3.3 Hz), 2.78 (t, 8H, 7.5 Hz), 1.60-1.57 (m, 8H), 1.35-1.24 (m, 24H), 0.86 (t, 12H, 6.6 Hz).

G2RuG2: G2-TPY-RuCl3 (340 mg, 0.237 mmole) and AgBF$_4$ (194.67 mg, 0.949 mmole) were taken in acetone (50 ml) and refluxed 20 hrs under N$_2$ atmosphere. The solution was filtered to remove AgCl salt. The filtrate was evaporated and to it G2-TPY (290.3 mg, 0.237 mmole) was added. The mixture was dissolved in 5 ml Dimethyl acetamide and 50 ml of n-BuOH and refluxed for 24 hours. The product was cooled and added drop wise into a beaker

containing 500 ml MeOH under stirring. The solid was filtered, washed in MeOH and 6:1 mixture of MeOH: acetone. The residue was dried to get dark red solid (559.77 mg, 94.1%). ^{1}H NMR (DMSO-d6, 300MHz): 9.35-9.28 (br, 4H), 9.11 (d, 4H, 8.1 Hz), 8.50-8.43 (br, 2H), 8.07 (br, 4H), 7.90-7.83 (br, 4H), 7.58-7.49 (br, 10H), 7.38-7.28 (br, 4H), 7.05-7.02 (br, 8H), 6.82-6.78 (br, 8H), 2.77-2.74 (br, 16H), 1.57-1.55 (br, 16H), 1.27 (br, 48H), 0.85 (br, 24H).

G3RuG3: G3-TPY-RuCl3 (7.2 mg, 0.18 mmole) and AgBF$_4$ (140 mg, 0.721 mmole) were taken in acetone (50 ml) and refluxed 20 hrs under N$_2$ atmosphere. The solution was filtered to remove AgCl salt. The filtrate was evaporated and to it G3-TPY (400 mg, 0.18 mmole) was added. The mixture was dissolved in 5 ml Dimethyl acetamide and 50 ml of n-BuOH and refluxed for 24 hours. The product was cooled and added drop wise into a beaker containing 500 ml MeOH under stirring. The solid was filtered, washed in MeOH and 6:1 mixture of MeOH: acetone. The residue was dried to get dark red solid (749.72 mg, 91.7%). ^{1}H NMR (CDCl$_3$, 300 MHz): 8.85 (br, 4H), 8.70-8.62 (br, 4H), 8.16 (br, 2H), 7.86 (br, 4H), 7.41 (br, 4H), 7.24-7.05 (br, 20H), 6.90-6.82 (br, 16H), 6.61-6.57 (br, 16H), 2.73-2.69 (br, 32H), 1.65-1.58 (br, 32H), 1.26 (br, 96H), 0.85 (br, 48H).

5.3 Results and Discussion:

5.3.1 Optical properties and Electrochemical Properties.

The photophysical properties of the one, two and three Ru containing thiophene dendrimers were investigated by UV-Vis absorption spectroscopy in both dilute solutions (10^{-6}M) and spin coated films on quartz substrates. Their absorption wavelengths (λ_{abs}), optical band gaps (E_g^{opt}), absorption onsets (λ_{onset}) in both solutions and film states were summarized in table 5.1. Figure 5.5 shows the absorption spectra for one metal system (**G1RuG1**, **G2RuG2** and **G3RuG3**) in both solution and film states. The peaks at ~300 nm corresponds to π-π*

transitions of the terpyridine moieties. Peaks at ~400 nm corresponds to the π-π* transitions in the π-conjugated thiophene dendrimers. Peaks at ~550 nm arised due to the MLCT occurring in the occurring in the molecules. Figure 2 shows absorption spectra for two metal system (**BT2RuG1**, **BT2RuG2** and **BT2RuG3**) in both solution and film states. In the film state, the MLCT peaks at ~ 550 nm were significantly shifted bathochromically with the concomitant shift in absorption onsets. Figure 3 depict absorption spectra for three metal system (**TPA3RuG1**, **TPA3RuG2** and **TPA3RuG3**) in both solution and film states. Like the two metal systems, the MLCT peaks at ~550 nm were shifted bathochromically with notable shift in absorption onsets. This corresponds to their strong intramolecular associations and aggregations in the solid films.

Table 5.1: Optical, properties of Supramolecular Ru containing thiophene dendrimers.

COMPOUND	$\lambda_{abs,sol}$ /nm[a]	$\lambda_{abs,film}$ /nm[b]	λ_{onset} /nm	E_g^{opt} / eV[c]
G1RuG1	537	552	665	1.86
G2RuG2	541	543	683	1.81
G3RuG3	545	547	691	1.79
BT2RuG1	534	545	786	1.57
BT2RuG2	537	550	797	1.55
BT2RuG3	540	553	816	1.51
TPA3RuG1	526	536	711	1.74
TPA3RuG2	533	541	750	1.65
TPA3RuG3	535	545	772	1.60

[a] Concentration of 10^{-5} M in chloroform solutions. [b] Spin coated from solutions on quartz substrates. [c] Optical band gaps were estimated from the absorption spectra in films by using the equation $E_g = 1240/\lambda_{edge}$.
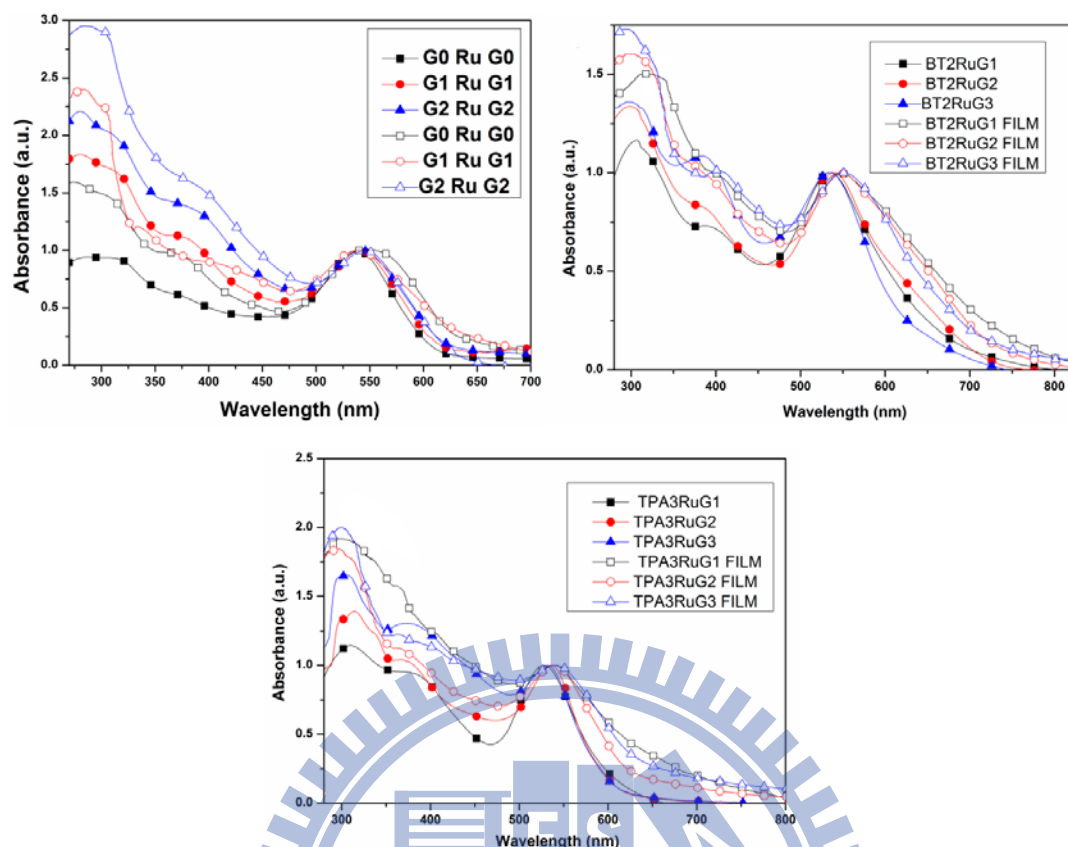
Figure 5.5 UV-Vis absorption spectra of Ru cored supramolecular thiopehene dendrimers in CHCl$_3$ at c=1 x 10^{-5}M (solid symbols) and solid films (hollow symbols).

To study the electronic properties of the three series of metallo-dendrimers, the HOMO and LUMO levels were investigated by the CV measurements in solid films with Ag/AgCl as a reference electrode, calibrated by ferrocene (E$_{1/2(ferrocene)}$ = 0.45 mV vs. Ag/AgCl). The CV voltamograms are depicted in Figure 5.6 and the energy levels are summarized in table 5.2. The HOMO and LUMO levels were estimated by the oxidation and reduction potentials from the reference energy level of ferrocene (4.8 eV below the vacuum level) according to the following equation:[28] E$_{HOMO/LUMO}$ = [(E$_{onset}$ - 0.45) - 4.8] eV. The cyclic voltametric plots were depicted in Figure 5.2 and the results are summarized in Table 5.1. With the increase in generations of the dendrimers, the electron donating ability of the dendrimers increases which result in subsequent increase in HOMO levels in each of the three series. The relatively low band gap of the two metal systems arises due to donor acceptor make up in presence of

benzothiadiazole as acceptor and thiophene dendrimer as donor. Although there is deviation in the optical and electrochemical band gaps, but the trend of the band gaps in the three series are similar.

Table 5.2: Electrochemical properties of Supramolecular Ru containing thiophene dendrimers.[a]

COMPOUND	E_{red}[b]	LUMO[c]/eV	E_{ox}[b]	HOMO[c]/eV	E_g^{el}/eV
G1RuG1	-0.59	-3.75	0.92	-5.27	1.52
G2RuG2	-0.61	-3.74	0.89	-5.24	1.50
G3RuG3	-0.71	-3.64	0.82	-5.17	1.53
BT2RuG1	-0.69	-3.65	0.82	-5.17	1.52
BT2RuG2	-0.70	-3.64	0.79	-5.14	1.50
BT2RuG3	-0.72	-3.62	0.77	-5.12	1.50
TPA3RuG1	-0.69	-3.65	0.86	-5.21	1.56
TPA3RuG2	-0.71	-3.63	0.81	-5.16	1.53
TPA3RuG3	-0.72	-3.62	0.80	-5.15	1.53

[a] Reduction and oxidation potentials measured by cyclic voltammetry in solid films. [b] Onset oxidation and reduction potentials. [c] E_{HOMO} /E_{LUMO}= [-(E_{onset}-0.45)-4.8] eV, where 0.45 V is the value for ferrocene vs. Ag/Ag^+ and 4.8 eV is the energy level of ferrocene below the vacuum.
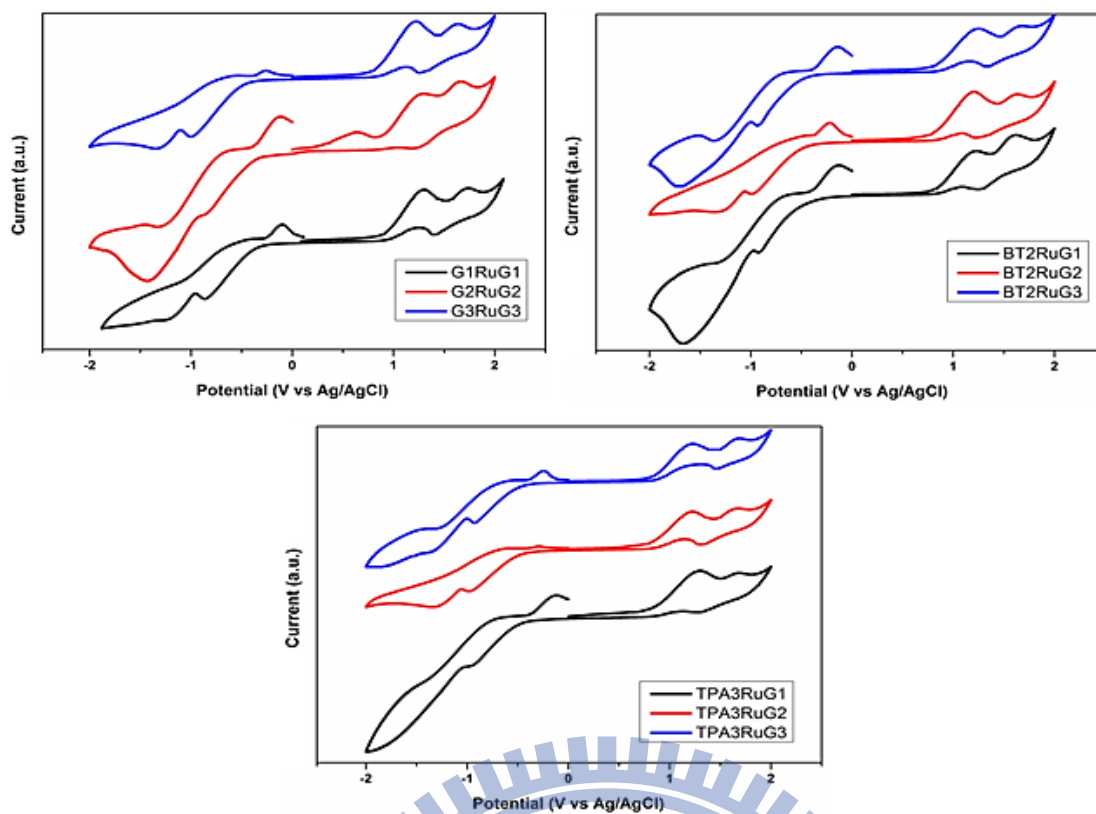
Figure 5.6 CV spectra of Ru cored supramolecular thiopehene dendrimers in solid films.

5.3.2 Photovoltaic Properties:

To investigate the potential use of mono, bis, tris Ru(II)-containing metallo-dendrimers in PVCs, the bulk hetero-junction (BHJ) solar cell devices comprising blends of these compounds as electron donors and ($PC_{70}BM$) as an electron acceptor in their active layer were fabricated with a configuration of ITO/PEDOT : PSS(30 nm)/ "mono, bis, tris Ru(II)-containing metallo-dendrimers" or "mono, bis, tris Ru(II)-containing metallo-dendrimers": $PC_{71}BM$ blend (~80 nm)/Ca(30 nm)/Al(100 nm) and measured under AM 1.5 stimulated solar light. The blended solutions were prepared from compounds and $PC_{71}BM$ in a weight ratio of 1 : 1 (w/w) from chloroform solutions. The current density (J) versus voltage (V) curves of the PVCs are shown in Figure 5.7, where the open circuit voltage (V_{oc}), short circuit current density (J_{sc}), fill factor (FF), and the PCE values are summarized in Table 5.3.
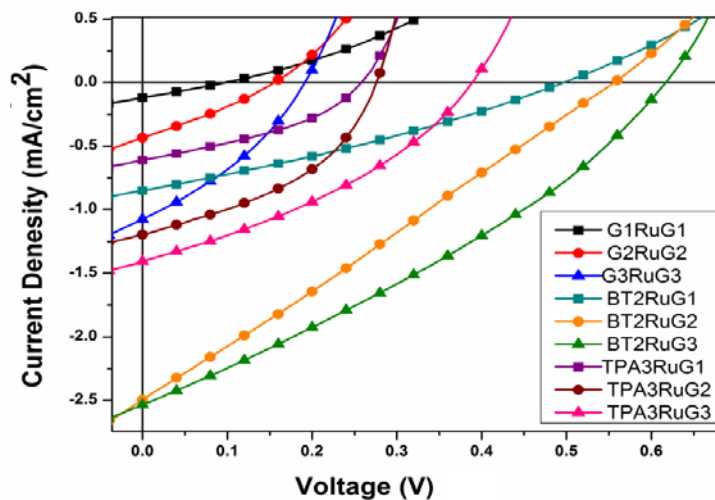
Figure 5.7 Current–voltage curves of BHJ solar cells using blended films of "mono, bis, tris Ru(II)-containing metallo-dendrimers":PC$_{70}$BM (1 : 1 w/w) under the illumination of AM 1.5G, 100 mW cm^{-2}.

Table 5.3 Photovoltaic properties of a BHJ solar cell device with a configuration of ITO/PEDOT:PSS/compound:PC$_{70}$BM/Ca/Al[a]

Active layer Compound:PC$_{70}$BM	V_{oc} /V	J_{sc} /mA cm^{-2}	FF (%)	PCE (%)
G1RuG1	0.10	0.12	25.0	0.003
G2RuG2	0.16	0.44	28.01	0.02
G3RuG3	0.20	1.07	32.4	0.07
BT2RuG1	0.49	0.84	33.78	0.14
BT2RuG2	0.55	2.49	26.34	0.36
BT2RuG3	0.61	2.54	32.67	0.51
TPA3RuG1	0.26	0.61	37.83	0.06
TPA3RuG2	0.28	1.20	41.66	0.14
TPA3RuG3	0.39	1.40	34.79	0.19

[a] Measured under AM 1.5 irradiation, 100 mW cm^{-2}. [b] Active layer with the weight ratio of Compound:PC$_{70}$BM =1 : 1.

The best performance of the photovoltaic cells containing Ru(II)-cored thiophene dendrimers was optimized by fabricating BHJ PSC devices using "Ru(II)-cored thiophene dendrimers" as a donor and $PC_{70}BM$ as an acceptor in weight ratios of 1:2 and 1:3. The J–V curves of the PSC devices based on "Ru(II)-cored thiophene dendrimers":$PC_{70}BM$ in two different blended ratios (1:2 and 1:3) are shown in Figure 5.8, and data are illustrated in Table 5.4. The PSC device based on **BT2RuG3**:$PC_{70}BM$ in 1:3 weight ratio obtained the best PCE value of 0.77% with V_{oc}= 0.69 V, J_{sc}= 3.51 mA/cm^2, and FF= 31.89%.
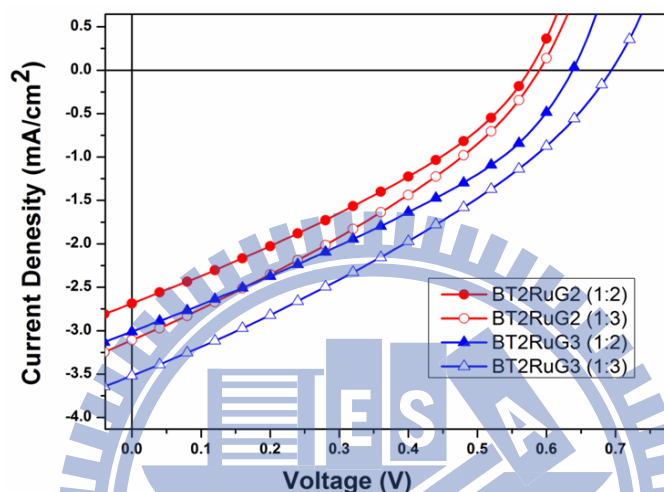
Figure 5.8 Current–voltage curves of BHJ solar cells using blended films of **BT2RuG2** and **BT2RuG3** with $PC_{70}BM$ in two different ratios (1:2 & 1:3) under the illumination of AM 1.5G, 100 mW cm^{-2}.

Table 5.4 Photovoltaic properties of a BHJ solar cell device with a configuration of ITO/PEDOT:PSS/compound:$PC_{70}BM$/Ca/Al[a]

Active layer Compound:$PC_{70}BM$	V_{oc}/V	J_{sc}/mA cm^{-2}	FF (%)	PCE (%)
BT2RuG2:$PC_{70}BM$ (1:2)	0.57	2.69	32.97	0.50
BT2RuG2:$PC_{70}BM$ (1:3)	0.59	3.11	32.41	0.59
BT2RuG3:$PC_{70}BM$ (1:2)	0.63	3.02	34.77	0.66
BT2RuG3:$PC_{70}BM$ (1:3)	0.69	3.51	31.89	0.77

[a] Measured under AM 1.5 irradiation, 100 mW cm^{-2}. [b] Active layer with the weight ratio of Compound:$PC_{70}BM$ =1 : 1.

5.4 Conclusion

Mono (**G1RuG1**, **G2RuG2**, **G3RuG3**), bis (**BT2RuG1**, **BT2RuG2**, **BT2RuG3**) and tris (**TPA3RuG1**, **TPA3RuG2**, **TPA3RuG3**) 'Ru' containing supramolecular thiophene dendrimers were constructed. Their photophysical, electrochemical and thermal properties were investigated. Due to the donor-acceptor, benzothiadiazole-hexyl thiophene cored architecture in bis 'Ru' containg thiophene dendrimers, these showed higher photovoltaic efficiency than other two series. Tris 'Ru' containg architecture with terthiophene-triphenylamine core, showed moderate photovoltaic performance due to their star shaped branched structure. Among the three generations (G1-G3) of bis 'Ru' containing dendritic series, **BT2RuG3** showed the highest solar cell efficiency 0.77% without the aid of any additives or anealing conditions. This solar cell efficiency value is the highest among all metal containg dendritic supramolecule reported so far.

Chapter 6

Two novel dithieno-benzo-imidazole-based compounds (**M2** and **A2**) showed remarkable sensitivities towards Pb^{2+} by 12-fold enahancement and 10-fold decay of fluorescence, respectivily, in aqueous solutions. Substituent effects of different dithieno-benzo-imidazole-based moieties (**M1**, **M2**, **A1** and **A2**) on the quantum yields, fluorescence lifetimes and sensitivities to Pb^{2+} along with the reversibilities by S^{2-} were investigated. Novel thieno-imidazole-based polymer **P** showed both colorimetric and ratiometric detections of Hg^{2+} as well as fluorometric detection of Zn^{2+} via fluorescence turn-on response with augmented lifetime. Its model polymer **M** did not show any such sensing capability under similar conditions, which further confirmed the unique sensitivity of P towards Hg^{2+} and Zn^{2+} via the chelation of metal ions to both 'S' and 'N' hetero-atoms. Three novel Chemosensory Polymers showed different chemosensing sensitivity response towards H^{+} and Fe^{2+} depending on the imidazole pendants. The chemosensing reversibilities were achieved by Na_2-EDTA and phenanthrolinbe as counter ligands. Supramolecular bis Ru containing thiophene dendrimer (**BT2RuG3**) showed a highest solar cell efficiency (0.77%), among all metal containing dendritic supramolecule reported so far.

References

1. (a) de Silva, A. P.; Gunaratne, H. Q. N.; Gunnlaugsson, T.; Huxley, A. J. M.; McCoy, C. P.; Rademacher, J. T.; Rice, T. E. *Chem. Rev*. **1997**, *97*, 1515.

2. Manez, R. M.; Sancenon, F. *Chem. Rev*. **2003**, *103*, 4419.

3. Gunnlaugsson, T.; Glynn, M.; Tocci, G. M.; Kruger, P. E.; Pfeffer, F. M. *Coord. Chem. Rev*. **2006**, *250*, 3094.

4. Jiang, P.; Guo, Z. *Coord. Chem. Rev*. **2004**, *248*, 205.

5. Fabbrizzi, L.; Poggi, A.; *Chem. Soc. Rev*. **1995**, *24*, 197.

6. Czarnik (Ed.), A. W. Fluorescent Chemosensors for Ion and Molecule Recognition, ACS Symposium Series 358, American Chemical Society, Washington, DC, **1993**.

7. Wright A. T.; Anslyn, E. V. *Chem. Soc. Rev*. **2006**, *35*, 14.

8. Yoon, J.; Kim, S. K.; Singh N. J.; Kim, K. S. *Chem. Soc. Rev*. **2006**, *35*, 355.

9. Kobayashi, H.; Ogawa, M.; Alford, R.; Choyke P. L.; Urano, Y. *Chem. Rev*. **2010**, *110*, 2620.

10. Sinkeldam, R. W.; Greco, N. J.; Tor, Y. *Chem. Rev*. **2010**, *110*, 2579.

11. Lodeiro, C.; Capelo, J. L.; Mejuto, J. C.; Oliveira, E.; Santos, H. M.; Pedras B.; Nunez, C. *Chem. Soc. Rev*. **2010**, *39*, 2948.

12. Gunnlaugsson, T.; Glynn, M.; Tocci, G. M.; Kruger, P. E.; Pfeffer, F. M.; *Coord. Chem. Rev*. **2006**, *250*, 3094.

13. Jiang P. J.; Guo, Z. J. *Coord. Chem. Rev*. **2004**, *248*, 205.

14. Bell T. W.; Hext, N. M. *Chem. Soc. Rev*., **2004**, *33*, 589.

15. Valeur, B.; Leray, I. *Coord. Chem. Rev*. **2000**, *205*, 3.

16. (a) Czarnik (Ed.), A. W. Fluorescent Chemosensors for Ion and Molecules Recognition, American Chemical Society, Washington DC, USA, **1993**; (b) Balzani, V.; Campagna (Eds.), S. Photochemistry and Photophysics of Coordination Compounds I, Springer-Verlag, Berlin Heidelberg, Germany, **2007**; (c) Montalti, M.; Credi, A.; Prodi, L.; Gandolfi, M. T. Handbook of Photochemistry, third ed., Taylor & Francis Group, Boca

Raton, USA, **2006**; (d) Geddes, C. D.; Lacowicz, J. R.; Advanced Concepts in Fluorescence Spectroscopy, Small Molecule Sensing, Springer-Sciences, New York, USA, **2005**; (e) Rehm, C. D.; Weller, A. *Isr. J. Chem.* **1970**, *8*, 259.

17. Jiang, P.; Guo, Z. *Coord. Chem. Rev.* **2004**, *248*, 205.

18. Lakowicz, J. R. Principles of Fluorescence Spectroscopy, Kluwer Academic/Plenum, New York, **1999**.

19. Turro, N. J. Modern Molecular Photochemistry, University Science Books Sauslito, California, **1991**.

20. Guillet, J. Polymer Photophysics and Photochemistry, Cambridge University Press, Cambridge, UK, **1985**.

21. Valeur, B. in: S.G. Schulman (Ed.), Molecular Luminescence Spectroscopy, Part 3, Wiley, New York, **1993**, 25.

22. Valeur, B.; Bourson, J.; Pouget, J. in: A.W. Czarnik (Ed.), Fluorescent Chemosensors for Ion and

23. Molecule Recognition, ACS Symposium Series 538, American Chemical Society, Washington, DC, **1993**, 25.

24. Rettig, W.; Lapouyade, R. Probe design and chemical sensing, in: J.R. Lakowicz (Ed.), Topics in Fluorescence Spectroscopy, vol. 4, Plenum, New York, **1994**, 109.

25. Valeur, B.; Badaoui, F.; Bardez, E.; Bourson, J.; Boutin, P.; Chatelain, A.; Devol, I.; Larrey, B.; Lefe`vre, J. P.; Soulet, A. in: J.-P. Desvergne, A.W. Czarnik (Eds.), Chemosensors of Ion and Molecule Recognition, NATO ASI Series, Kluwer, Dordrecht, **1997**, 195.

26. Löhr, H. G.; Vögtle, F. *Acc. Chem. Res.* **1985**, *18*, 65 and Refs. cited therein.

27. Hong, Y.; Chen, S.; Leung, C.W.; Lam, J. W.; Liu, J.; Tseng, N. W.; Kwok, R.T.; Yu, Y.; Wang, Z.; Tang, B.Z. *ACS Appl. Mater. Interfaces*. **2011**, *3*, 341.

28. Photonic Research Systems: http://www.prsbio.com/index.html.

29. Birks, J. B.; Photophysics of Aromatic Molecules, Wiley, London, **1970**.

30.   (a) Luo, J. D.; Xie, Z. L.; Lam, J. W. Y.; Cheng, L.; Chen, H. Y.; Qiu, C. F.; Kwok, H. S.; Zhan, X. W.; Liu, Y. Q.; Zhu, D. B.; Tang, B. Z. *Chem. Commun.* **2001**, 1740. (b) Hong, Y.; Lam J. W. Y.; Tang, B. Z. *Chem. Soc. Rev.* **2011**, *40*, 5361.

31.   Han, T.; Feng, X.; Tong, B.; Shi, J.; Chen, L.; Zhi, J.; Dong Y. *Chem. Commun.* **2012**, *48*, 416.

32.   Goswami, S.; Chakrabarty, R. *Eur. J. Org. Chem.* **2010**, 3791.

33.   Fang, Z.; Wang, S.; Zhao, L.; Dong, B.; Xu, Z.; Ren, J.; Yang, Q.; *Materials Letters* **2008**, *62*, 1514.

34.   Alfonso, M.; Espinosa, T´arraga, A. A.; Molina, P. *Organic Letters* **2011**, *13*, 2078.

35.   Alfonso, M.; T´arraga, A.; Molina, P. *Dalton Trans.* **2010**, *39*, 8637.

36.   M. Alfonso, A. T´arraga, P. Molina, *J. Org. Chem.* **2011**, *76*, 939.

37.   Hou, C.; Xiong, Y.; Fu, N.; Jacquot, C. C.; Squier, T. C.; Cao, H. *Tetrahedron Letters*, **2011**, *52*, 2692.

38.   Cheng, X.; Li, Q.; Li, C.; Qin, J.; Li, Z. *Chem. Eur. J.* **2011**, *17*, 7276.

39.   Li, J.; Wu, Y.; Song, F.; Wei, G.; Cheng, Y.; Zhu, C. *J. Mater. Chem.* **2012**, *22*, 478.

40.   Yuan, M.; Li, Y.; Li, J.; Li, C.; Liu, X.; Lv, J.; Xu, J.; Liu, H.; Wang, S.; Zhu, D. *Organic Letters* **2007**, *9*, 2313.

41.   Pandey, R.; Gupta, R. K.; Shahid, M.; Maiti, B.; Misra, A.; Pandey, D. S.; *Inorg. Chem.* **2012**, *51*, 298.

42.   Zhang, J. F.; Kim, S.; Han, J. H.; Lee, S. J.; Pradhan, T.; Cao, Q. Y.; Lee, S. J.; Kang, C.; Kim, J. S. *Organic Letters* **2011**, *13*, 5294.

43.   Zhou, Y.; Li, Z. X.; Zang, S. Q.; Zhu, Y. Y.; Zhang, H. Y.; Hou, H. W.; Mak, T. C. W. *Organic Letters* **2012**, *14*, 1214.

44.   Meng, X.; Wang, S.; Li, Y.; Zhu, M.; Guo, Q. *Chem. Commun.* **2012**, *48*, 4196.

45.   Chiang, C. K.; Fincher, C. R.; Park, Y. W.; Heeger, A. J.; Shirakawa, H.; Louis, E. J.; Gau, S. C.; MacDiarmid, A. G. *Phys. Rev. Lett.* **1977**, *39*, 1098.

46. Chiang, C. K.; Druy, M. A.; Gau, S. C.; Heeger, A. J.; Louis, E. J.; MacDiarmid, A. G.; Park, Y. W.; Shirakawa, H. *J. Am. Chem. Soc*. **1978**, *100*, 1013.

47. Burroughes, J. H.; Bradley, D. D. C.; Brown, A. R.; Marks, R. N.; Mackay, K.; Friend, R. H.; Burns, P. L.; Holmes, A. B.; *Nature* **1990**, *347*, 539.

48. Burn, P. L.; Kraft, A.; Baigent, D.; Bradley, D. D. C.; Brown, A. R.; Friend, R. H.; Gymer, R. W.; Holmes, A. B.; Jackson, R. W. *J. Am. Chem. Soc*. **1993**, *115*, 10117.

49. Kraft, A.; Grimsdale, A. C.; Holmes, A. B. *Angew. Chem. Int. Ed*. **1998**, 37, 402.

50. Friend, R. H.; Gymer, R. W.; Holmes, A. B.; Burroughes, J. H.; Marks, R. N.; Taliani, C.; Bradley, D. D. C.; Dos Santos, D. A.; Bredas, J. L.; Logdlund, M.; Salaneck, W. R. Nature, **1999**, 397, 121.

51. Alan, J. H. *Angew. Chem. Int. Ed*. **2001**, *40*, 2591.

52. Arango, A. C.; Johnson, L. R.; Bliznyuk, V. N.; Schlesinger, Z.; Carter, S. A.; Höhold, H. H. *Adv. Mater*. **2000**, *12*, 1689.

53. McDonald, S. A.; Konstantatos, G.; Zhang, S. G.; Cyr, P. W.; Klem, E. J. D.; Levina, L.; Sargent, E. H. *Nat. Mater*. **2005**, *4*, 138-U14.

54. Coakley, K. M.; McGehee, M. D. *Chem. Mater*. **2004**, *16*, 4533.

55. Ramos, A. M.; Rispens, M. T.; van Duren, J. K. J.; Hummelen, J. C.; Janssen, R. A. J. *J. Am. Chem. Soc*. **2001**, *123*, 6714.

56. Jager, E. W. H.; Inganäs, O.; Lundström, I.; Adv. Mater. **2001**, *13*, 76.

57. Burgmayer, P.; Murray, R. W. *J. Am. Chem. Soc*. **1982**, *104*, 6139.

58. Gangopadhyay, R.; De, A. *Chem. Mater*. **2000**, *12*, 608.

59. Meyer, W. H.; *Adv. Mat*er. **1998**, *10*, 439.

60. Dimitrakopoulos, C. D.; Malenfant, P. R. L. *Adv. Mater*. **2002**, *14*, 99.

61. Thomas, S. W.; Joly, G. D.; Swager, T. M. *Chem. Rev*. **2007**, *107*, 1339.

62. Swager, T. M. *Acc. Chem. Res*. **1998**, *31*, 201.

63. McQuade, D.T.; Pullen, A. E.; Swager, T. M. *Chem. Rev*. **2000**, *100*, 2537.

64. Gaylord, B. S.; Massie, M. R.; Feinstein, S. C.; Bazan, G. C.; *Proc. Natl. Acad. Sci. U.S.A.* **2005**, *102*, 34.

65. Kumaraswamy, S.; Bergstedt, T.; Shi, X. B.; Rininsland, F.; Kushon, S.; Xia, W. S.; Ley, K.; Achyuthan, K.; McBranch, D.; Whitten, D.; *Proc. Natl. Acad. Sci. U.S.A.* 2004, *101*, 7511.

66. Petrella, A.; Tamborra, M.; Curri, M. L.; Cosma, P.; Striccoli, M.; Cozzoli, P. D.; Agostiano, A. *J. Phys. Chem. B*, **2005**, *109*, 1554.

67. Dwight, S. J.; Gaylord, B. S.; Hong, J. W.; Bazan, G. C. *J. Am. Chem. Soc*. **2004**, *126*, 16850.

68. Watt, A.; Thomsen, E.; Meredith, P.; Rubinsztein-Dunlop, H. *Chem. Commun*. **2004**, 20, 2334.

69. Ho, H. A.; Leclerc, M. *J. Am. Chem. Soc*. **2004**, *126*, 1384.

70. Ho, H.-A.; Boissinot, M.; Bergeron, M. G.; Corbeil, G.; Dore, K.; Boudreau, D.; Leclerc, M. *Angew. Chem. Int. Ed*. **2002**, *41*, 1548.

71. Li, J.; Pang, Y. *Macromolecules* **1998**, *31*, 5740.

72. Pang, Y.; Li, J.; Hu, B.; Karasz, F. E. *Macromolecules* **1998**, *31*, 6730.

73. Skoheim, T. A.; Elsenbaumer, R. L.; Reynolds, J. R. *Handbook of Conducting Polymers, second ed., Marcel Dekker, New York, NY*, **1998**.

74. Leclerc, M. *Adv. Mater*. **1999**, *11*, 1491.

75. Levesque, I.; Leclerc, M. *Chem. Mater*. **1996**, *8*, 2843.

76. Wang, B.; Wasielewski, M. R. *J. Am. Chem. Soc*., 1997, *11*, 912.

77. Zhou, Q.; Swager, T. M. *J. Am. Chem. Soc*. **1995**, *117*, 12593.

78. Zhou, Q.; Swager, T. M. *J. Am. Chem. Soc*. **1995**, *117*, 7017.

79. (a) Teixidor, F.; Flores, M. A.; Escriche, L.; Vi~nas, C.; Casab_o, J. *Chem. Commun*. **1994**, 963. (b) Chung, S.; Kim, W.; Park, S. B.; Yoon, I.; Lee S. S.; Sung, D. D. *Chem. Commun*. **1997**, 965. (c) Kimura, K.; Yajima, S.; Tatsumi, K.; Yokoyama M.; Oue, M.

Anal. Chem. **2000**, *72*, 5290. (d) Ceresa, A.; Radu, A.; Peper, S.; Bakker, E.; Pretsch, E. *Anal. Chem.* **2002**, *74*, 4027.

80.   (a) Amendola, V.; Fabbrizzi, L.; Licchelli, M.; Mangano, C.; Pallavicini, P.; Parodi, L.; Poggi, A. *Coord. Chem. Rev.* **1999**, *190-192*, 649. (b) Prodi, L.; Bolletta, F.; Montalti, M.; Zaccheroni, N. *Coord. Chem. Rev.* **2000**, *205*, 59. (c) Zhao, Q.; Li, F. Y.; Huang, C. H. *Chem. Soc. Rev.* **2010**, *39*, 3007. (d) Dwivedi, A. K.; Saikia G.; Iyer, P. K. *J. Mater. Chem.* **2011**, *21*, 2502. (e) Chetia, B.; Iyer, P. K. *Tetrahedron Letters* **2008**, *49*, 94.

81.   J. S. Liu-Fu, Lead Poisoning, A Century of Discovery and Rediscovery, in Human Lead Exposure, ed. H. L. Needleman, Lewis Publishing, Boca Raton, FL, 1992.

82.   (a) C. Qin, W. Y. Wong and L. Wang, Macromolecules, 2011, 44, 483; (b) C. Qin, Y. Cheng, L. Wang, X. Jing and F. Wang, Macromolecules, 2008, 41, 7798; (c) M. Dekhtyar, W. Rettig and W. Weigel, Chemical Physics, 2008, 344, 237.

83.   (a) R. Zhou, B. Li, N. Wu, G. Gao, J. You and J. Lan, Chem. Commun., 2011, 47, 6668; (b) Z. -Q. Hu, C. -S. Lin, X. -M. Wang, L. Ding, C.-L. Cui, S. -F. Liu and H. Y. Lu, Chem. Commun., 2010, 46, 3765; (c) X. -L. Ni, S. Wang, X. Zeng, Z. Tao and T.Yamato, Org. Lett., 2011, 13, 552.

84.   Y. Miyake, M. Wu, M. J. Rahman, Y. Kuwatani and M. Iyoda, J Org. Chem., 2006, 16, 6110.

85.   A. Meyer, E. Sigmund, F. Luppertz, G. Schnakenburg, I. Gadaczek, T. Bredow. S. S. Jester and H. Höger, Beilstein J. Org. Chem., 2010, 6, 1180.

86.   S. Sirilaksanapong, M. Sukwattanasinitt and P. Rashatasakhon, Chem. Commun., **2012**, *48*, 293.

87.   (a) Zhang, Z.; Wu, D.; Guo, X.; Qian, X.; Lu, Z.; Xu, Q.; Yang, Y.; Duan, L.; He, Y.; Feng, Z.; *Chem. Res. Toxicol.* **2005**, *18*, 1814; (b) M. Harada, *Crit. Rev. Toxicol.* **1995**, *25*, 1; (c) Renzoni, A.; Zino, F.; Franchi, E. *Environ. Res.* **1998**, *77*, 68. (d) Benoit, J. M.; Fitzgerald, W. F.; Damman, A. W. *Environ. Res.* **1998**, *78*, 118.

135

88. (a) Que, E. L.; Domaille, D. W.; Chang, C. J. *Chem. Rev.* **2008**, *108*, 1517 and references therein. (b) Frederickson, C. J.; Koh, J. Y.; Bush, A. I. *Nat. Rev. Neurosci.* **2005**, *6*, 449. (c) Scrimgeoura, A. G.; Stahl, C. H.; McClung, J. P.; Marchitelli, L. J.; Young, A. J. *J. Nutri. Biol.* **2007**, *18*, 813.

89. (a) Amendola, V.; Fabbrizzi, L.; Forti, F.; Licchelli, M.; Mangano, C.; Pallavicini, P.; Poggi, A.; Sacchi, D.; Taglieti, A. *Coord. Chem. Rev.* **2006**, *250*, 273. (b) Rurack, K.; Resch-Genger, U. *Chem. Soc. Rev.* **2002**, *31*, 116. (c) Mutihac, L.; Lee, J. H.; Kim, J. S.; Vicens, J. *Chem. Soc. Rev.* **2011**, *40*, 2777. (d) Xu, Z.; Singh, N. J.; Lim, J.; Pan, J.; Kim, H. N.; Park, S. S.; Kim, K. S.; Yoon, J. *J. Am. Chem. Soc.* **2009**, *131*, 15528.

90. (a) Xu, Z.; Yoon, J.; Spring, D. R. Chem. Soc. Rev. **2010**, *39*, 1996. (b) Burdette, S. C.; Frederickson, C. J.; Bu, W.; Lippard, S. J. J. Am. Chem. Soc. **2003**, *125*, 1778. (c) Brombosz, S. M.; Zucchero, A. J.; Phillips, R. L.; Vazquez, D.; Wilson, A.; Bunz, U. H. F. Organic Letters **2007**, *9*, 4519. (d) Wong, K. M. C.; Tang, W. S.; Lu, X. X.; Zhu, N.; Yam, V. W. W. Inorg. Chem. **2005**, *44*, 1492. (e) Peng, X.; Xu, Y.; Sun, S.; Wu, Y.; Fan, J. Org. Biomol. Chem. **2007**, *5*, 226. (f) Quang, D. T.; Kim, J. S. Chem. Rev. **2007**, *107*, 3780. (i) Chen, W. H.; Xing, Y.; Pang. Y.; Organic Letters **2011**, *13*, 1362.

91. (a) Rurack, K.; Kollmannsberger, M.; Resch-Genger, U.; Daub, J. *J. Am. Chem. Soc.* **2000**, *122*, 968. (b) McQuade, D. T.; Hegedus, A. H.; Swager, T. M. *J. Am. Chem. Soc.* **2000**, *122*, 12389.

92. (a) Kim, J. S.; Quang, D. T. *Chem. Rev.* **2007**, *107*, 3780. (b) Zhang, J. F.; Lim, C. S.; Bhuniya, S.; Cho, B. R.; Kim, J. S. *Organic Letters* **2011**, *13*, 1190.

93. Yuan, L.; Lin, W.; Chen, B.; Xie. Y.; *Organic Letters* **2012**, *14*, 432.

94. (a) Kaur, P.; Kaur, S.; Singh, K; *Org. Biomol. Chem.* **2012**, *10*, 1497. (b) Yang, M. H.; Thirupathi, P.; Lee, K. H.; Org. Lett. 2011, 13, 5028. (c) Lohani, C. R.; Kim, J. M.; Lee, K. H. Tetrahedron 2011, 67, 4130. (d) Kaur, P.; Kaur, S.; Singh, K.; Sharma, P. R.; Kaur, T.; Dalton Trans., 2011, 40, 10818. (e) Joshi, B. P.; Lohani, C. R.; Lee, K. H. Org. Biomol. Chem. 2010, 8, 3220. (f) Neupane, L. N.; Kim, J. M.; Lohani, C. R.; Lee. K.

H.; J. Mater. Chem. 2012, 22, 4003. (g) Yang, M. H.; Lohani, C. R.; Cho, H.; Lee, K. H. Org. Biomol. Chem. 2011, 9, 2350. (h) M. Kumar, N. Kumar, V. Bhalla, H. Singh, P. R. Sharma, T. Kaur. Org. Lett., 2011, 13, 1422.

95. (a) Y. Xu, Y. Pang. Dalton Trans. 2011, 40, 1503. (b) Y. Xu, Y. Pang. Chem. Commun. **2010**, *46*, 4070. (c) K. Hanaoka,bY. Muramatsu, Y. Urano, T. Terai, T. Nagano. Chem. Eur. J. **2010**, *16*, 568. (d) L. Wang, W. Qin, X.Tang, W. Dou, W. Liu. J. Phys. Chem. A **2011**, *115*, 1609.

96. Barberis, V. P.; Mikroyannidis, J. A. Synthetic Metals **2006**, 156, 1408.

97. (a) Hanif, M.; Lu, P.; Li, M.; Zheng, Y.; Xie, Z.; Ma, Y.; Li, D.; Li, J. Polym. Int. **2007**, *56*, 1507. (b) He, B.; Tian, H.; Geng, Y.; Wang, F.; Muellen, K. Org. Lett. **2008**, *10*, 773.

98. Benesi, H. A.; Hildebrand, J. H. J. Am. Chem. Soc. **1949**, *71*, 2703.

99. (a) Krooswyk, J. D.; Tyrakowski, C. T.; Snee, P. T. *J. Phys. Chem. C*. **2010**, *114,* 21348. (b) Shimkunas, R. A.; Robinson, E.; Lam, R.; Lu, S.; Xu, X.; Zhang, X. Q.; Huang, H.; Osawa, E.; Ho, D. *Biomaterials* **2009**, *30*, 5720. (c) Cui, L.; Zhong, Y.; Zhu, W.; Xu, Y.; Du, Q.; Wang, X.; Qian, X.; Xiao, Y.; *Organic Letters* **2011**, *13*, 928. (d) Liu, Y.; Deng, C.; Tang, L.; A. Qin, R. Hu, J. Z. Sun, B. Z. Tang, *J. Am. Chem. Soc*. **2011**, *133*, 660; (e) Maity, D.; Govindaraju, T.; *Chem. Commun*. **2010**, *46*, 4499. (f) Snee, P. T.; Somers, R. C.; Nair, G.; Zimmer, J. P.; Bawendi, M. G.; Nocera, D. G. *J. Am. Chem. Soc*. **2006**, *128*, 13320. (g) Guo, Z. Q.; Zhu, W. H.; Zhu, M. M.; Wu, X. M.; Tian, H. *Chem. Eur. J*., **2010**, *16*, 14424. (h) Jung, J. H.; Lee, J. H.; Shinkai, S. *Chem. Soc. Rev*. **2011**, *40*, 4464.

100. (a) Myochin, T.; Kiyose, K.; Hanaoka, K.; Kojima, H.; Terai, T.; Nagano, T. *J. Am. Chem. Soc*. **2011**, *133*, 3401. (b) Qian, F.; Zhang, C.; Zhang, Y.; He, W.; Gao, X.; Hu, P.; Guo, Z. *J. Am. Chem. Soc*. **2009**, *131*, 1460. (c) Maity, D.; Govindaraju, T.; *Inorg. Chem*. **2010**, *49*, 7229. (d) Guliyev, R.; Coskun, A.; Akkaya, E. U. *J. Am. Chem. Soc*. **2009**, *13*, 9007. (e) Kim, H. N.; Guo, Z.; Zhu, W.; Yoon, J.; Tian, H. *Chem. Soc. Rev*.

2011, *40*, 79. (f) Park, M.; Seo, S.; Lee, I. S.; Jung, J. H. *Chem. Commun*. **2010**, *46*, 4478. (g) Maity, D.; Manna, A. K.; Karthigeyan, D.; Kundu, T. K.; Pati, S. K.; Govindaraju, T. *Chem. Eur. J*. **2011**, *17*, 11152. (h) Guo, Z. Q.; Zhu, W. H.; Tian, H. *Macromolecules* **2010**, *43*, 739; (i) Maity, D.; Govindaraju, T. *Chem. Eur. J*. **2011**, *17*, 1410. (j) Son, H.; Lee, H. Y.; Lim, J. M.; Kang, D.; Han, W. S.; Lee, S. S.; Jung, J. H. *Chem. Eur. J*. **2010**, *16*, 11549. (k) Lee, H. Y.; Bae, D. R.; Park, J. C.; Song, H.; Han, W. S.; Jung, J. H. *Angew. Chem*. **2009**, *121*, 1265.

101.   (a) Kim, F. S.; Ren, G.; Jenekhe, S. A. *Chem. Mater*. **2011**, *23*, 682. (b) Usta, H.; Facchetti, A.; Marks, T. *Acc. Chem. Res*. **2011**, *44*, 501. (c) Grimsdale, A. C.; Chan, K. L.; Martin, R. E.; Jokisz, P. G.; Holmes, A. B. *Chem. Rev*. **2009**, *109*, 897. (d) Liao, L.; Cirpan, A.; Chu, Q.; Karasz, F.; Pang, Y. *J. Polym. Sci. Part A Polym. Chem.* **2007**, *45*, 2048. (e) Cheng, Y. J.; Yang, S. H.; Hsu, C. S. *Chem. Rev*. **2009**, *109*, 5868. (f) Torrent, M. M.; Rovira, C. *Chem. Rev*. **2011**, *111*, 4833. (g) Shao, B. Y.; Gong, X.; Heeger, A. J.; Liu, M.; Jen, A. K. Y. *Adv. Mater*. **2009**, *21*, 1972. (h) Cho, N.; Yip, H. L.; Davies, J. A.; Kazarinoff, P. D.; Zeigler, D. F.; Durban, M. M.; Segawa, Y.; O'Malley, K. M.; Luscombe, C. K.; Jen, A. K. Y. *Adv. Energy. Mater*. **2011**, *6*, 1148. (i) Huang, F.; Chen, K. S.; Yip, H. L.; Hau, S. K.; Acton, O.; Zhang, Y.; Luo, J.; Jen, A. K. Y. *J. Am. Chem. Soc*. **2009**, *131*, 13886.

102.   (a) Thomas III, S. W.; Joly, G. D.; Swager, T. M. *Chem. Rev*. **2007**, *107*, 1339. (b) Liu, B.; Dai, H.; Bao, Y.; Du, F.; Tian, J.; Bai, R. *Polym. Chem*. **2011**, *2*, 1699. (c) Lee, H.; Lee, J. H.; Kang, S.; Lee, J. Y.; John, G.; Jung, J. H. *Chem. Commun*. **2011**, *47*, 2937. (d) Duan, X.; Liu, L.; Feng, F.; Wang, S.; *Acc. Chem. Res*. **2010**, *43*, 260. (e) Dong, H.; Cao, X.; Li, C. L. *ACS Appl. Mater. Interfaces*. **2009**, *1*, 1599. (f) Lou, X.; Zhang, Y.; Qin, J.; Li, Z. *Chem. Eur. J*. **2011**, *17*, 9691. (g) Li, J.; Wu, Y.; Song, F.; Wei, G.; Cheng, Y.; Zhu, C. *J. Mater. Chem*. **2012**, *22*, 478.

103.   (a) Fana, L. J.; Zhanga, Y.; Murphya, C. B.; Angell, S. E.; Parkera, M. F. L.; Flynna, B. R.; Jones, W. E. J. *Coord. Chem. Rev*. **2009**, *253*, 410. (b) McQuade, D. T.; Pullen, A.

138

E.; Swager, T. M. *Chem Rev*. **2000**, *100*, 2537. (d) Liu, B.; Bao, Y.; Wang, H.; Du, F.; Tian, J.; Li, Q.; Wang, T.; Bai, R. *J. Mater. Chem*. **2012**, *22*, 3555.

104.   (a) Thomas, S. W.; Joly, G. D.; Swager, T. M. *Chem.Rev*. **2007**, *107*, 1339. (c) Hong, S. W.; Ahn, C. H.; Huh, J.; Jo, W. H. *Macromolecules* **2006**, *39*, 7694. (d) Clarke, Y.; Xu, W.; Demas, J. N.; DeGraff, B. *A. Anal. Chem*. **2000**, *72*, 3468. (e) Potyrailo, R. A. *Angew. Chem. Int., Ed.* **2006**, *45*, 702. (h) Kruppa, M.; König, B. *Chem. Rev*. **2006**, *106*, 3520. (f) Bozdemir, O. A.; Buyukcakir, O.; Akkaya, E. U. *Chem. Eur. J*. **2009**, *15*, 3830. (g) Coskun, A.; Akkaya, E. U. *J. Am. Chem. Soc*. **2006**, *128*, 14474. (h) Jiang, J.; Xiao, X.; Zhao, P.; Tian, H. *J. Polym. Sci., Part A: Polym. Chem*. **2010**, *48*, 1551.

105.   (a) Blomberg, M. R. A.; Siegbahn, P. E. M.; Wikstrom, M. *Inorg. Chem*. **2003**, *42*, 5231. (b) Yamamoto, S.; Takeda, H.; Maki, Y.; Hayaishi, O. *J. Bio. Chem*. **1969**, *244*, 2951. (c) Cartwright, G. E.; Gubler, C. J.; Wintrobe, M. M. *J. Bio. Chem*., **1957**, *224*, 533. (d) Shellaiah, M.; Rajan, Y. C.; Lin, H. C. *J. Mater. Chem*. **2012**, *22*, 8976.

106.   (a) Aisen, P.; Resnick, M. W.; Leibold, E. A. *Curr. Opin. Chem. Biol*. **1999**, *3*, 200. (b) Eisenstein, R. S. *Annu. Re V. Nutr.* **2000**, *20*, 627. (c) Neilands, J. B. *Ann Rev Biochem.* **1981**, *50*, 715. (d) Ouchetto, H.; Dias, M.; Mornet, R.; Lesuisse, E.; Camadro, J. M.; *Bioorg. Med. Chem.* **2005**, *13*, 1799. (e) Kalinowski, S. D.; Sharpe, C. P.; Bernhardt, V. P.; Richardson, R. D. *J. Med. Chem*. **2008**, *51*, 331. (f)   Chaud, V. M.; Izumi, C.; Nahaal, Z.; Shuhama, T. D.; Bianchi, L. P. M.; Freitas, O. *J. Agric. Food. Chem*. **2002**, *50*, 871. (g) Zou, Q.; Li, X.; Zhang, J.; Zhou, J.; Sun, B.; Tian, H.; *Chem. Commun*. **2012**, *48*, 2095.

107.   (a) Neilands, J. B. S. *Struct. Bonding* **1984**, *58*, 1. (b) Winkelmann, G.; van der Helm, D.; Neilands, J. B. *Iron Transport in Microbes, Plants, Animals*, VCH Verlagsgesellschaft mbH, D-6940, Weinheim, Germany, **1987**. (c) Matzanke, B. F.; Matzanke, G. M.; Raymond, K. N. *Iron Carriers, Iron Proteins*, VCH Publishers, New York, **1989**, 5. (d) Brugnara, C. *Clin. Chem*., **2003**, *49*, 1573.

108. (a) Ghosh, S.; Dey, C. K.; Manna, R. *Tetrahedron Letters* **2010**, *51*, 3177. (b) Liu, Y.; Miao, Q.; Zhang, S. W.; Huang, X. B.; Zheng, L. F.; Cheng, Y. X. *Macromol. Chem. Phys.* **2008**, *209*, 685. (c) Miao, Q.; Huang, X. B.; Cheng, Y. Q.; Liu, Y.; Zeng, L. L.; Cheng, Y. X. *J Appl Polym Sci.* **2009**, *111*, 3137. (d) Liu, X.; Zhou, X.; Shu, X.; Zhu, J. *Macromolecules* **2009**, *42*, 7634–7637. (e) Zhang, Y.; Murphy, C. B.; Jones, W. E. *Macromolecules* **2002**, *35*, 630. (f) Rabindranath, A. R.; Maier, A.; Schaer, M.; Tieke, B. *Macromol Chem Phys.* **2009**, *210*, 659. (g) Kimura, M.; Horai, T.; Hanabusa, K.; Shirai, H. *Adv. Mater.* **1998**, *10*, 459. (h) Rabindranath, A. M.; Bernd, A. R. T. *Adv. Mater.* **2009**, *21*, 959; (i) Rabindranath, A. M.; Tieke, A. R. B. *Chem. Mater.* **2009**, *21*, 3668. (j) Lin, O. S. J.; Duan, Z. H.; Zhang, C. Y.; Bai, H. T. Z. P. *Chem. Commun.* **2006**, *42*, 4392; (k) Seguchi, W. S.; Yoshida, H.; Kifune, K.; Tadaki, K.; Shiozaki, T. H.; *Tetrahedron Lett*ers **2005**, *46*, 8827. (l) Saikia, G.; Iyer, P. K.; *Macromolecules* **2011**, *44*, 3753. (m) Dwivedi, A. K.; Saikia, G.; Iyer, P. K. *J. Mater. Chem.* **2011**, *21*, 2502.

109. (a) Matuso, S.; Kiyomiya, K.; Kurebe, M. *Arch. Toxicol.* **1998**, *72*, 798. (b) Zhang, S. W.; Swager, T. M. *J. Am. Chem. Soc.* **2003**, *125*, 3420. (c) Laisalmi, M.; Kokki, H.; Soikkeli, A.; Markkanen, H.; Yli-Hankala, A.; Rosenberg, P.; Lindgren, L.; *Acta Anaesthesiol. Scand.* **2006**, *50*, 982. (d) Liu, B.; Tian, H.; *J. Mater. Chem.* **2005**, *15*, 2681. (e) Huang, W.; Li, Y.; Yang, Z.; Lin, H.; Lin, H. *Spectrochimica Acta Part A.* **2011**, *79*, 471. (f) Berryman, O. B.; Sather, A. C.; Jr, J. R. Organic Letters **2011**, *13*, 5232. (g) Tong, H.; Wang, L.; Jing, X.; Wang, F. *Macromolecules* **2003**, *36*, 2584. (h) Zhou, G.; Cheng, Y.; Wang, L.; Jing, X.; Wang, F. *Macromolecules* **2005**, *38*, 2148; (i) Bao, Y.; Liu, B.; Wang, J.; Tian, H. R. Bai, Chem. Commun. 2011, 47, 3957.

110. (a) Denisova, A. S.; Degtyareva, M. B.; Dem'yanchuk, E. M.; Simanova, A. A. *Russian J. Org. Chem.* **2005**, *41*, 1690. (b) Amb, C. M.; Beaujuge, P. M.; Reynolds, J. R. *Adv. Mater.* **2010**, *22*, 724.

111. Beek, R. V.; Zoombelt, A. P.; Jenneskens, L. W.; Walree, C. A.V.; Donega, C. M.; Veldman, D.; Janssen, R. A. J. *Chem. Eur. J.* **2006**, *12*, 8075.

112. (a) Denisova, A. S.; Degtyareva, M. B.; Dem'yanchuk, E. M.; Simanova, A. A.; *Russian J. Org. Chem.* **2005**, *41*, 1690. (b) Edelmann, M. J.; Raimundo, J. M.; Utesch, N. F.; Diederich, F. *Helvetica Chemica Acta.* **2002**, *85*, 2195. (c) Amb, C. M.; Beaujuge, P. M.; Reynolds, J. R. *Adv. Mater.* **2010**, *22*, 724.

113. (a) Chan, S. H.; Chen, C. P.; Chao, T. C.; Ting, C.; Lin, C. S.; Ko, B. T. *Macromolecules* **2008**, *41*, 5519. (b) Jung, I. H.; Yu, J.; Jeong, E.; Kwon, S.; Kong, H.; Lee, K.; Woo, H. Y.; Shim, H. K. *Chem. Eur. J.* **2010**, *16*, 3743. (c) Chen, C. P.; Chan, S. H.; Chao, T. C.; Ting, C.; Ko, B. T. *J. am. Chem. Soc.* **2008**, *130*, 12828. (d) Xu, Y. Pang, Y. *Chem. Commun.* **2010**, *46*, 4070. (e) Atilgan, S.; Ozdemir, T.; Akkaya, E. U. *Organic Letters* **2010**, *12*, 4792. (f) Wu, P. T.; Xin, H.; Kim, F. S.; Ren, G.; Jenekhe, S. A. *Macromolecules.* **2009**, *42*, 8817. (g) Yue, W.; Zhao, Y.; Tian, H.; Song, D.; Xie, Z.; Yan, D.; Geng, Y.; Wang, F. *Macromolecules.* **2009**, *42*, 6510. (h) Liu, X.; Shu, X.; Zhou, X.; Zhang, X.; Zhu, J.; *J. Phys. Chem. A.* **2010**, *114*, 13370.

114. (a) Huang, J. H.; Li, K. C.; Kekuda, D.; Padhy, H. H.; Lin, H. C.; Ho, K. C.; Chu, C. W. *J. Mater. Chem.*, **2010**, *20*, 3295. (b) Kleinhenz, N.; Yang, L.; Zhou, H.; Price, S. C.; You, W. Macromolecules **2011**, *44*, 872. (c) Zou, Y. P.; Gendron, D.; Badrou-Aich, R.; Najari, A.; Tao, Y.; Leclerc, M. *Macromolecules* **2009**, *42*, 2891.

115. (a) Mameli, M.; Aragoni, M. C.; Arca, M.; Caltagirone, C.; Demartin, F.; Farruggia, G.; Filippo, G. D.; Devillanova, F. A.; Garau, A.; Isaia, F.; Lippolis, V.; Murgia, S.; Prodi, L.; Pintus, A.; Zaccheroni, N. *Chem. Eur. J.* **2010**, *16*, 919. (b) Shen, L.; Lu, X.; Tian, H.; Zhu, W. *Macromolecules* **2011**, 44, 5612. (c) Borisov, S. M.; Wolfbeis, O. S.; *Chem. Re*v. **2008**, *108*, 423; (d) Hembury, G. A.; Borovkov, V. V.; Inoue, Y.; *Chem. Rev.* **2008**, *108*, 1.

116. (a) Satapathy, R.; Wu, Y. H.; Lin, H. C. Chem. Commun. **2012**, DOI: 10.1039/C2CC31131C; (b) Yang, P. J.; Chu, H. C.; Chen, T. C.; Lin, H. C. *J. Mater.*

Chem. **2012**, DOI: 10.1039/C2JM31367G; (c) Chu, H. C.; Lee, Y. H.; Hsu, S. J.; Yang, P. J.; Yabushita, A.; Lin, H. C. *J. Phys. Chem. B*, **2011**, *115*, 8845.

117. (a) Erkkila, K. E.; Odom, D. T.; Barton, J. K. *Chem. ReV.* **1999**, *99*, 2777-2795. (b) Barigelletti, F.; Flamigni, L. *Chem. Soc. ReV.* **2000**, *29*, 1-12. (c) Laine´, P.; Bedioui, F.; Amouyal, E.; Albin, V.; Burruyer-Penaud, F. *Chem.-Eur. J.* **2002**, *8*, 3162-3176. (d) Ott, S.; Kritikos, M.; A kermark, B.; Sun, L. *Angew. Chem., Int. Ed.* **2003**, *42*, 3285-3288. (e) Andres, P. R.; Schubert, U. S. *AdV. Mater.* **2004**, *16*, 1043-1068. (f) Hofmeier, H.; Schubert, U. S. *Chem. Soc. ReV.* **2004**, *33*, 373-399. (g) Bianke´, G.; Häner, R. *ChemBioChem* **2004**, *5*, 1063-1068. (h) Schmittel, M.; Kalsani, V.; Kishore, R. S. K.; Cölfen, H.; Bats, J. W. *J. Am. Chem. Soc.* **2005**, *127*, 11544-11545. (i) Schmittel, M.; Kalsani, V.; Mal, P.; Bats, J. W. *Inorg. Chem.* **2006**, *45*, 6370-6377. (j) Hwang, S. H.; Moorefield, C. N.; Dai, L.; Newkome, G. R. *Chem. Mater.* **2006**, *18*, 4019-4022.

118. Gohy, J.-F.; Lohmeijer, B. G. G.; Schubert, U. S. Chem Eur J., 2003, 9, 3472–3479.

119. (a) Lehn, J.-M. *Supramolecular Chemistry, Concept and PerspectiVes*, VCH: Weinheim, **1995**. (b) Newkome, G. R.; He, E.; Moorefield, C. N. *Chem. ReV.* **1999**, *99*, 1689-1746. (c) Schubert, U. S.; Eschbaumer, C. *Angew. Chem., Int. Ed.* **2002**, *41*, 2892-2926. (d) Newkome, G. R.; Wang, P.; Moorefield, C.; Cho, T. J.; Mohapatra, P. P.; Li, S.; Hwang, S.-H.; Lukoyanova, O.; Echegoyen, L.; Palagallo, J. A.; Lancu, V.; Hla, S.-W. *Science* **2006**, *312*, 1782-1785. (e) Flores-Torres, S.; Hutchison, G. R.; Soltzberg, L. J.; Abrun~a, H. D. *J. Am. Chem. Soc.* **2006**, *128*, 1513-1522. (f) Bonnet, S.; Collin, J. P.; Koizumi, M.; Mobian, P.; Sauvage, J. P. *Adv. Mater.* **2006**, *18*, 1239.

120. (a) Cheng, K. W.; Mak, C. S. C.; Chan, W. K.; Ng, A. M. C.; Djurii, A. B.; *J. Polym. Sci., Part A: Polym. Chem.*, **2008**, *46*, 1305. (b) Man, K. K. Y.; Wong, H. L.; Chan, W. K.; Kwong C. Y.; Djurisic, A. B. *Chem. Mater.*, 2004, 16, 365–367; (c) P. D. Vellis, J. A. Mikroyannidis, C. N. Lo and C. S. Hsu, J. Polym. Sci., Part A: Polym. Chem., 2008, 46, 7702. (d) V. Duprez, M. Biancardo, H. Spanggaard and F. C. Krebs, Macromolecules, 2005, 38, 10436–10448; (e) O. Hagemann, M. Jørgensen and F. C.

Krebs, J. Org. Chem., 2006, 71, 5546–5559. (f) K. K. Y. Man, H. L. Wong, W. K. Chan, A. B. Djurisic, E. Beach and S. Rozeveld, Langmuir, 2006, 22, 3368–3375; (g) Y. Pan, B. Tong, J. Shi, W. Zhao, J. Shen, J. Zhi and Y. Dong, J. Phys. Chem. C, 2010, 114, 8040–8047; (h) V. Stepanenko, M. Stocker, P. Müller, M. Büchner and F. Würthner, J. Mater. Chem., 2009, 19, 6816–6826.

121. (a) Vellis, P. D.; Mikroyannidis, J. A.; Lo, C. N.; Hsu, C. S. *J. Polym. Sci. Part A: Polym. Chem.* **2008**, *46*, 7702. (b) Vellis, P. D.; Mikroyannidis, J. A.; Lo, C. N.; Hsu, C. S. *J. Polym. Sci. Part A: Polym. Chem.* **2008**, *46*, 7702. (c) Padhy, H.; Sahu, D.; Chiang, I. H.; Patra, D.; Kekuda, D.; Chu, C. W.; Lin, H. C. J. Mater. Chem. **2011**, 21, 1196. (d) Padhy, H.; Ramesh, M.; Patra, D.; Satapathy, R.; Pola, M. K.; Chu, H. C.; Chu, C. W.; Wei, K. H.; Lin, H. C. Macromolecular Rapid Comm. doi:10.1002/marc.201100752

122. (a) Kline, R. J.; McGehee, M. D.; Kadnikova, E. N.; Liu, J. S.; Fre´chet, J. M. J. *Ad V . Mater*. **2003**, *15*, 1519. (b) Schilinsky, P.; Asawapirom, U.; Scherf, U.; Biele, M.; Brabec, C. J. *Chem. Mater*. **2005**, 17, 2175. (c) Yang, X. N.; Loos, J.; Veenstra, S. C.; Verhees, W. J. H.; Wienk, M. M.; Kroon, J. M.; Michels, M. A. J.; Janssen, R. A. J. Nano Letters **2005**, 5, 579. (d) Kopidakis, N.; Mitchell, W. J.; van de Lagemaat, J.; Ginley, D. S.; Rumbles, G.; Shaheen, S. E.; Rance, W. L. *Appl. Phys. Lett.* **2006**, *89*, 103524.

123. (a) Hasobe, T.; Kashiwagi, Y.; Absalom, M. A.; Sly, J.; Hosomizu, K.; Crossley, M. J.; Imahori, H.; Kamat, P. V.; Fukuzumi, S. *Adv . Mater*. **2004**, *16*, 946. (b) Bettignies, R.; Nicolas, Y.; Blanchard, P.; Levillain, E.; Nunzi, J.-M.; Roncali, J. *Adv. Mater*, **2003**, *15*, 1939. (c) Satoh, N.; Nakashima, T.; Yamamoto, K. *J. Am. Chem. Soc*. **2005**, *127*, 13030.

124. (a) Newkome G. R.; Moorefield C.N.; Vögtle, F. Dendrimers and dendrons: concepts, syntheses, applications. Weinheim: Wiley-VCH; **2001**.(a) Fre´chet J. M. J.; Tomalia D. A. Dendrimers and other dendritic polymers. Chi-chester: Wiley; **2002**. (c) Kawa, M.; Fre´chet, J. M. J.; *Chem Mater* **1998**, *10*, 286. (d) Hawker C. J.; Frechet J. M. J. *J*

Am Chem Soc **1992**,*114*, 8405. (e) Maraval, V.; Laurent, R.; Donnadieu, B.; Mauzac, M.; Caminade, A. M.; Majoral, J. P.; *J Am Chem Soc* **2000**, *122*, 2499.

Curriculam Vitae

PERSONAL DETAILS:

Name   : Rudrakanta Satapathy
E-Mail   : rudrakanta_chem@yahoo.co.in
Date of Birth   : 12th August 1984
Nationality   : Indian
Marital Status : Unmarried

ADDRESS TO COMMUNICATE:

C/O- Rabinarayan Satapathy
At/Po - Chhatia.(Chhatia Champapur Road)
Dist - Jajpur
Pin-   754023
Orissa, India.
Email: rudrakanta_chem@yahoo.co.in, rudrakanta@gmail.com

EDUCATIONAL QUALIFICATION:

Degree	Subject	Institution	Year	Grade
Doctor of Phylosophy (PhD)	Organic Synthesis, Chemosensory and Optoelectronic applications.	National Chiao Tung University (NCTU), Taiwan.	Feb 2008- May 2012	1st Division, 91% (Course-work)
Master of Science (M.Sc.)	Organic, Inorganic, Physical and Analytical Chemistry.	Utkal University,Odisha, India	2004-2006	1st Division
Bachelor of Science (B.Sc.)	Chemistry (Major) Physics and Mathematics (Minor)	Ravenshaw Auto. College, Odisha, India.	2001-2004	1st Division with distinction
+2 Sc	Physics, Chemistry, Mathematics, Biology, English, Odia.	Stewart Science Colege, Cuttack, Odisha, India	1999-2001	1st Division

NATIONAL LEVEL ACHIEVENT:

I have qualified National Eligibility Test (**NET**) held on june 2006 (LS) and 2007 (UGC JRF) by CSIR, INDIA.

ADDITIONAL WORK EXPERIENCE:

Dec-2006 to Feb-2008: Research experience in R &D Sector of Chemgen Pharma International (C.R.O). My work was involved in dealing with different projects of multinational companies, which implicates development of new synthetic methods and synthesis of organic drug molecules via retro synthetic analysis.

LIST OF PUBLICATIONS:

1. **Rudrakanta Satapathy**, Yen-Hsing Wu and Hong-Cheu Lin*, Novel dithieno-benzo-imidazole-based Pb^{2+} sensors: substituent effects on sensitivity and reversibility, *Chem Comm*, DOI: 10.1039/c2cc31131c.

2. **Rudrakanta Satapathy**, Yen-Hsing Wu, and Hong-Cheu Lin*, Novel Thieno-Imidazole-Based Probe for Colorimetric Detection of Hg^{2+} and Fluorescence Turn-on Response of Zn^{2+}, *Organic Letters*. (Just Accepted Manuscript).

3. **Rudrakanta Satapathy**, Harihara Padhy, Yen-Hsing Wu, and Hong-Cheu Lin*, Synthesis and Characterization of Reversible Chemosensory Polymers: Amendment of Sensitivity via Novel Imidazole Pendants. (Manuscript under revision in *Chemistry a European Journal*).

4. **Rudrakanta Satapathy**, Mohan Ramesh, Harihara Padhy, Yen-Hsing Wu, Chih-Wei Chu*, Kung-Hwa Wei, and Hong-Cheu Lin*, Synthesis and Photophysical properties of Supramolecular Ru containing thiophene dendrimers and their photovoltaic applications. (Manuscript ready to communicate in Journal of Materials Chemistry).

5. Harihara Padhy, Mohan Ramesh, Dhananjaya Patra, **Rudrakanta Satapathy**, Murali Krishna Pola, Hsuan-Chih Chu, Chih-Wei Chu*, Kung-Hwa Wei, Hong-Cheu Lin*, Synthesis of Main-Chain Metallo-Copolymers Containing Donor and Acceptor Bis-Terpyridyl Ligands for Photovoltaic Applications, Macromol. Rapid Commun. **2012**, 33, 528−533. DOI: 10.1002/ marc. 201100752.